Université d'Ottawa · University of Ottawa

HYDROCHEMISTRY AND ISOTOPE SYSTEMATICS OF THE INDUS RIVER BASIN

Ajaz Karim

A thesis submitted to the school of Graduate Studies and Research in partial fulfillment of the requirements for the Ph.D. degree in Earth Sciences

Ottawa-Carleton Geoscience Centre

Department of Earth Sciences

University of Ottawa

Ottawa, Canada

Canada

The undersigned hereby recommend to the School of Graduate Studies and Research acceptance of this thesis, submitted by Ajaz Karim in partial fulfillment of the requirements for the Ph.D. degree in Earth Sciences
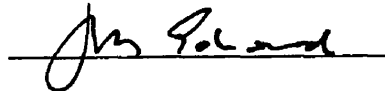
Dr. John Blenkinsop
Department of Earth Sciences
Carleton University
Ottawa, Ontario
Canada
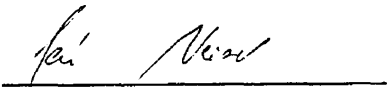
Dr. Eion Cameron
Department of Earth Sciences
University of Ottawa
Ottawa, Ontario
Canada

Dr. Ian Clark
Department of Earth Sciences
University of Ottawa
Ottawa, Ontario
Canada

Dr. John Edmond
Department of E.A.P.S.
Massachusetts Institute of Technology
Cambridge, Massachusetts
U.S.A.

Dr. Jan Veizer
(Thesis Supervisor)
Department of Earth Sciences
University of Ottawa
Ottawa, Ontario
Canada

ABSTRACT

This study presents a complementary geochemical and isotopic database (Ca^{2+}, Mg^{2+}, Na^+, K^+, HCO_3^-, SO_4^{2-}, Cl^-, trace elements and isotopes of H, O, C, S and Sr) for water samples from the Indus River Basin. It encompasses ~3000 km stretch of the Indus main channel and its tributaries, sampled during both high and low water stands and a time series collected at Sukkur barrage, ~500 km upstream from the mouth of the Indus River. These results, as well as published data for precipitation (amount, chemical and isotopic composition), and river discharges were used to address the following aspects of the Indus River Basin: (1) water budget, annual solute fluxes, and denudation rate; (2) whether the summer monsoon or delayed runoff from winter precipitation dominates the discharge of the Indus and where does the water vapor for precipitation originate; (3) what are the sources and processes that control the distribution of solutes; (4) estimate the contribution of major ions to river water from carbonate and silicate weathering.

The long-term mean annual precipitation water flux into the Indus River Basin is 398 km^3. The mean annual water fluxes close to the mouth of the Indus River before and after the construction of two major dams were respectively, 100 and 53 km^3. This constitutes only one-fourth to one-eighth of the precipitation input and the remainder leaves the surface water system by groundwater storage and evapotranspiration. Based on major ion chemistry of rain and snow, the annual precipitation flux of Total Dissolved Solids (TDS) to the Indus River Basin is ~844,400 tons. The Indus River annually transports ~18 million tons of TDS that translates into a chemical denudation rate of 21 tons km^{-2}.

Oxygen and deuterium isotopes in the Indus River at Sukkur barrage for the Water Year March-94 to February-95 define the relationship $\delta D = 7.5\ (\delta^{18}O) + 10$, similar in slope to the Local Meteoric Water Lines at Kabul, and New Delhi, as well as to the Global Meteoric Water Line. This implies that despite aridity, significant evaporative enrichment is limited due to the short residence time of water and due to the minor contribution of runoff from the arid middle and lower parts of the basin. Deuterium excess ($d = \delta D - 8\delta^{18}O$) at Sukkur barrage ranges from 12 to 20‰, with a discharge weighted average of 18‰. These values are distinctly higher than d-excess in monsoon rains in New Delhi (~8) or snow of the Himalayas (~10), east of the Indus River Basin. In the western Himalayas, maximum accumulation of snow occurs during the winter, which corresponds to the rainy season of the eastern Mediterranean region that also has a characteristic d-excess of ~20‰. Isotope balance calculations require that 80% of the total discharge of the Indus must be derived from delayed runoff from snow melt in the headwaters that ultimately owes its origin to moisture that originated in the Mediterranean or other inland seas.

Hydrochemistry of the Indus River is dominated by $Ca^{2+} > Mg^{2+} > (Na^+ + K^+)$ and $HCO_3^- > (SO_4^{2-} + Cl^-) >$ Si. In the lowland tributaries and in some of the Punjab rivers, however, $(Na^+ + K^+)$ and $(SO_4^{2-} + Cl^-)$ predominate. Based on riverine Cl^- concentration, cyclic salts constitute only up to 6% of the TDS, the bulk of these, however, are derived from rock weathering. Sediment weathering is the dominant source for major cations, silicate weathering is important only locally, particularly for $(Na^+ + K^+)$ in the headwaters. In the lower Indus, on average, about 75% of the total $(Ca^{2+} + Mg^{2+})$ is derived from

weathering of sedimentary carbonates. In the same stretch, ~60% of the total ($Na^+ + K^+$) is derived from weathering of halite and the remaining from silicate rocks. Bicarbonate is derived from carbonate and silicate rock weathering under both atmospheric and biogenic CO_2 input. Turbulent flow and low air temperature in the headwaters facilitate mixing of atmospheric gases leading to oxygen supersaturation and equilibration of carbon isotopes. Sulfur isotopic composition of sulfate lies within the range of values reported for sulfide minerals in igneous, metamorphic and sedimentary rocks. This together with oxygen isotope composition of sulfate suggests oxidation of sulfide minerals to sulfate. Three end member compositions control the Sr-isotope systematics of the Indus River. These are: (a) weathering of old silicate (silicic) rocks with high $^{87}Sr/^{86}Sr$ ratios and represented by rivers draining the Precambrian high grade metamorphic rocks of the Nanga Parbat-Haramosh massif and the "Central Crystallines" of the Higher Himalayas; (b) young silicate (mafic) rocks with the lowest $^{87}Sr/^{86}Sr$ ratios of all the Indus tributaries and represented by rivers draining mafic-ultramafic units of the Cretaceous Kohistan-Ladakh arcs; and (c) weathering of sedimentary carbonates with intermediate $^{87}Sr/^{86}Sr$, represented by the lowland tributaries draining sedimentary carbonates and shales of the West Pakistan Fold Belt.

RÉSUMÉ

Cette étude présente une base de données géochimique et isotopique complémentaires (Ca^{2+}, Mg^{2+}, Na^+, K^+, HCO_3^-, SO_4^{2-}, Cl^-, éléments traces et isotopes de D, O, C, S et Sr) pour des échantillons d'eau provenant du bassin de la rivière Indus. L'étude englobe une étendue d'environ 3000 km le long de l'Indus même et de ses tributaires qui fut échantillonnée pendant les périodes des hautes et basses eaux, ainsi qu'une série recueillie au barrage Sukkur, à environ 500 km en amont de l'embouchure de la rivière Indus. Les résultats des analyses couplés aux données publiées de précipitation (quantité, composition chimique et isotopique) et de débits, ont été utilisés afin d'adresser les aspects suivants du bassin de la rivière Indus: (1) budget d'eau, flux annuels de solutés, et taux de dénudation; (2) déterminer si la mousson estivale ou l'écoulement retardé de la précipitation hivernale domine la décharge de l'Indus et détermine la provenance de la vapeur d'eau à l'origine de la précipitation; (3) identifier les sources et processus qui contrôlent la distribution des solutés; (4) estimer la contribution des ions majeurs provenant de l'altération des carbonates et silicates à l'eau de la rivière.

Le flux d'eau de précipitation annuel moyen à long terme entrant dans le bassin de la rivière Indus est de 398 km^3 alors que le flux d'eau annuel moyen près de l'embouchure de la rivière Indus avant et après la construction de deux barrages importants étaient respectivement de 100 et 53 km^3. Ceci ne constitue qu'un quart à un huitième de l'apport par précipitation dans le bassin. Ainsi, la fraction restante se soustrait au système d'eau de surface par le réseau des eaux souterraines et par évapotranspiration. Selon la chimie des ions majeurs de la pluie et de la neige, le flux de précipitation annuel en Solide Total Dissous (STD) au bassin de la rivière Indus est d'environ 844,400 tonnes. Sur une base annuelle, l'Indus transporte 18 millions de tonnes de STD, ce qui représente un taux de dénudation de 21 tonnes km^2.

Les isotopes d'oxygène et de deutérium dans la rivière Indus au barrage Sukkur pour l'année hydrologique (mars-94 à février-95) définissent la relation $\delta D = 7.5$ $(\delta^{18}O) + 10$, dont la pente est similaire aux Lignes d'Eau Météorique Locales à Kabul, et à New Delhi, ainsi qu'à la Ligne d'Eau Météorique Globale. Ceci signifie que malgré l'aridité, l'enrichissement par évaporation est limité dû au temps de résidence restreint de l'eau et aussi à la contribution très minime de l'eau de ruissellement des régions arides centrales et avales du bassin. L'excès de deutérium ($d = \delta D - 8\delta^{18}O$) au barrage Sukkur se situe entre 12 et 20‰, avec une moyenne pondérée par la décharge de 18‰. Ces valeurs sont significativement plus élevées que l'excès-d dans les pluies de mousson de New Delhi (~8) ou de la neige (~10) de l'Himalayas à l'est du bassin de la rivière Indus. Dans l'Himalayas occidental, les accumulations maximales de neige se retrouvent pendant l'hiver qui est la saison des pluies de la région méditerranéenne orientale. Cette dernière a aussi un excès-d caractéristique de ~20‰. Des calculs de bilan isotopique exigent que 80% de la décharge totale de l'Indus doit provenir de l'écoulement retardé de la fonte des neiges dans la région source. Celle-ci provient de l'évaporation des bassins de la Méditerranée ou des autres mers intérieures.

L'hydrochimie de la rivière Indus est dominée par $Ca^{2+} > Mg^{2+} > (Na^+ + K^+)$ et $(SO_4^{2-} + Cl^-)$. Cependant, dans les tributaires avals et certaines des rivières du Punjab, $(Na^+ + K^+)$ et $(SO_4^{2-} + Cl^-)$ prédominent. Selon les concentrations en Cl^- de la rivière, les sels cycliques ne

constituent que 6% auplus des SDT, dont la grande partie, provient de l'altération de la roche mère. La source des cations majeurs provient de l'altération des sédiments. Néanmoins, l'altération des silicates ne joue un rôle important que localement, particuliérement pour $Na^+ + K^+$ dans les eaux dans la région source. Dans le tronçon inférieure de l'Indus, en moyenne près de 75 % du $Ca^{2+} + Mg^{2+}$ total provient de l'altération des carbonates sédimentaires. Dans ce même secteur, ~60 % du $Na^+ + K^+$ total provient de l'altération de l'halite et le reste de roches silicatées. Les bicarbonates proviennent de l'altération sous CO_2 atmosphérique et biogénique de roches carbonatées et silicatées. Le mélange des gaz atmosphériques est facilité dans la région source grâce aux flux turbulent et aux basses témperatures, mènant à une sursaturation en oxygène et à un équilibre des isotopes de carbone. La composition isotopique du soufre des sulfates se situe à l'intérieur de l'étendue de valeurs rapportées pour les minéraux sulfurés des roches ignées, metamorphiques et sédimentaires. Ceci, en plus de la composition isotopique en oxygène des sulfates, suggère une oxidation des minéraux sulfurés en sulfates. Trois compositions extrêmes contrôlent la systématique de l'isotope-Sr dans la rivière Indus. Ceux-ci sont: (a) l'altération de vieilles roches silicatées (silicique) avec des ratios $^{87}Sr/^{86}Sr$ élevés et représenté par des rivières s'écoulant sur les roches métamorphiques "de haut degré" Précambriennes du massif Nanga Parbat-Haramosh et les " Centrales Cristallines " des Hautes Himalayas; (b) des roches silicatées (mafiques) récentes avec les ratios $^{87}Sr/^{86}Sr$ les plus faibles de tous les tributaires de l'Indus et représenté par des rivières s'écoulant sur des unitées mafiques-ultramafiques des arcs Crétacés Kohistan-Ladakh; et (c) l'altération de carbonates sédimentaires avec des ratios $^{87}Sr/^{86}Sr$ intermédiaires et représenté par les tributaires des basses terres qui sécoulent sur des carbonates sédimentaires et des schistes argileux de la Zone Orogénique du Ouest Pakistan.

ACKNOWLEDGEMENTS

DEDICATION

For: Shahrane, Sulaiman and Harris

TABLE OF CONTENTS

CHAPTER 2

GEOLOGY AND TECTONICS 18

CHAPTER 3

FIELD AND LABORATORY METHODS 41

CHAPTER 6

CHAPTER 7

LIST OF FIGURES

xiv

xv

LIST OF TABLES

Chapter 1

Introduction

1.1 Objectives

The major objectives of the present study can be listed as follows:

1. Constrain the water budget of the Indus River Basin and evaluate the relative importance of moisture sources to the total discharge of the Indus River;

2. Examine spatial and temporal variations in hydrochemistry of surface waters of the Indus River Basin and evaluate sources and processes that modify major ions, using complementary geochemical, isotope and environmental data;

3. Characterize the role of weathering regime for water chemistry in the Indus River Basin and evaluate the relative importance of carbonate and silicate weathering; and

4. Investigate anthropogenic impact on water chemistry.

1.2 Previous work

Previous studies on the Indus River Basin are limited to samples collected at its mouth or at isolated locations within the basin. They deal principally with the influence of rock weathering on water chemistry (Goldstein and Jacobsen, 1987; Palmer and Edmond, 1989; Pande et al., 1994), with monitoring the particulates and their fluxes (Ittekkot and Arain, 1987) and with tabulation of data for discharge and major ion chemistry at selected locations (WAPDA, 1976; 1985; 1989a; 1990). Stewart (1990) investigated iodine deficiency in surface waters and related health problems in the Shyok and Shigar valleys.

Other studies focussed on heavy metals in fish (Ashraf and Jaffar, 1990; Tariq et al., 1996).

While these studies provide valuable information on selected aspects of the hydrochemistry and hydrogeology of the Indus River Basin, none addresses spatial and seasonal variations and the environmental factors. Published stable isotope data is scarce for oxygen, deuterium (Kabul, Jhelum and Chenab rivers, Hussain et al., 1991) and carbon (lakes in the Shyok basin, Fontes et al., 1996) and nonexistent for sulfur. The present study reports a complementary geochemical, isotope and environmental database for the entire Indus River Basin in Pakistan, compressed in a unified model, and explores various aspects of the hydrochemistry and isotope geology of the basin.

1.3 Location

The Indus River Basin is located on the northwestern periphery of the Indo-Pakistani subcontinent from latitude 24° to 37°, and from longitude 66° to 81°. It covers an area of about 863,508 km^2, occupying the western half of the Indo-Gangetic plain and sections of the bordering mountain ranges (Fig. 1.1). Most of the Indus River Basin lies within Pakistan but includes also parts of Afghanistan, Tibet and India. It is bound in the east by the Ganges-Brahmaputra basin that drains into the Bay of Bengal. All other rivers sharing a drainage divide with the Indus drain into inland lakes or basins. To the north is the Yarkand River Basin of China and to the northwest are the Amu Darya and Syrdarīya rivers of Tadzhikistan, draining into the Aral "Sea". To the west is the Helmand Basin of Afganistan and Iran. The Indus originates near Mount Kailas (6714 masl) in the Gangdise Range of Tibet. It flows westwards, parallel to the Himalayan and Karakoram mountain

2

ranges, turns abruptly to the south near Nanga Parbat and exits the Himalayas near the

Salt Range. It continues to flow in the south through the monotonous alluvial plain and

drains into the Arabian Sea in the south, covering a total distance of about 3000 km.
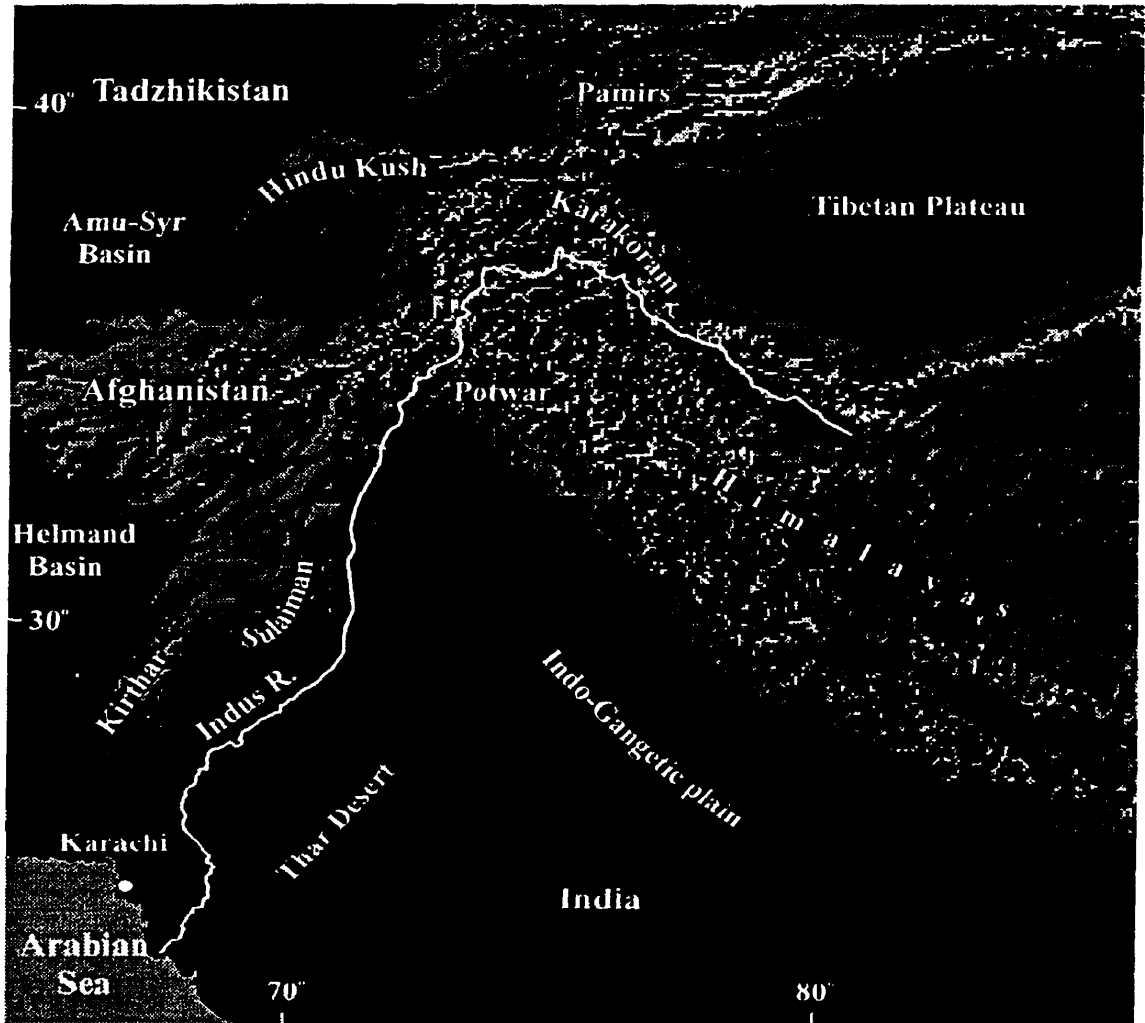
Fig. 1.1. Physiography and regional location of the Indus River Basin.

1.4 Physiography

The Indus River Basin encompasses four major physiographic regions (Fig. 1.1). These include, 1) The northern mountains, 2) The Salt Range and the Potwar Plateau, 3) The western mountains, and 4) The Indus plain.

1.4.1 The northern mountains

The northern mountains include a series of mountain ranges, extending from the Pamirs in the west to Assam in the east. These include the Hindu Kush, the Karakoram and the Himalayan mountain ranges. The Karakoram is characterized by a high concentration of lofty peaks, several between 7000-8000 m. Precipitation is scarce and is mostly in the form of snow. A large part of the stream discharge is derived from glacier basins and many large rivers emerge directly from the snouts of large glaciers.

1.4.2 The Salt Range and the Potwar Plateau

The Salt Range begins in the east near the Jhelum River and continues westwards across the Indus River. It comprises parallel ranges of low flat-topped hills, intermontane valleys and a number of saline lakes. The Salt Range is known for its almost complete stratigraphic section and occurrence of rock salt.

North of the Salt Range is the Potwar Plateau, bound in the east by the Jhelum River and in the west by the Indus River. The Soan River drains the Potwar Plateau, except for its southeastern portion, and discharges into the Jhelum River. Elevations range from 300 to 600 m on a heavily dissected surface of easily erodable sandstone and shale.

4

1.4.3 The western mountains

The Indus Plain is bordered in the west by a series of mountain ranges. South of the Kabul River is the Safed Koh Range, with an average elevation of 3600 m that grades into Waziristan Hills. The Kurram and Tochi rivers drain the latter. Further south and parallel to the Indus River is the seismically active Sulaiman Range. The Kirther Range extends north-south and forms the western boundary of the lower Indus basin.

1.4.4 The Indus plain

Covering the entire area between the Salt Range and the Arabian Sea is the monotonous Indus plain. It varies in width between 50 and 300 km and consists of Tertiary and Quaternary alluvium deposited by the Indus and its tributaries. The general slope of the plain towards the sea is gentle, with an average gradient of one meter per five kilometers. Although the plains are featureless on a large scale, several elements of micro-relief have been recognized. These are: a) Active flood plain, b) Meander flood plain, c) Cover flood plain, d) Scalloped interflues, e) Piedmont plain, f) Hilly sand plain, g) Deltaic flood plain, and h) Tidal delta (Tamburi, 1974; Kureshy, 1991).

a) Active flood plain, locally known as *Bet* or *Khaddar*, is the terrain adjacent to the rivers and is inundated during the summer floods. It is often called 'the summer bed' of rivers. Embankments have been built in many places along its outer margin to protect the surrounding areas from floods. The soils of the active flood plain are coarse-textured sands and silt. Active flood plain is found along all the rivers, except the lower half of the Ravi. Along the Indus it widens from near the Salt Range to its mouth.

b) Meander flood plain is a complex of bars, meander scrolls, levees, and oxbow lakes. It is adjacent to and somewhat higher than the active flood plain. Relief is only a meter or so and is widespread along the Jhelum, Chenab and upper reaches of the Ravi rivers. Along the Indus, it is absent upstream from Panjnad, but widespread further downstream.

c) The cover flood plain is characterized by recent alluvium spread over former riverine features. Due to large variations in the conditions of deposition, the soil textures are highly variable. The cover flood plain deposits are widespread along the lower reaches of the Indus and the Punjab rivers.

d) Scalloped interfluves or bar uplands are terraces common to the "doab" (land between two rivers) regions and separated by river cut scarps, usually six meters or more in height. Soils in these regions are highly fertile and the development of modern irrigation system has turned this once desert region into highly productive croplands.

e) Piedmont plain is the land formed by coalescent alluvial fans at the front of a mountain range. The term is apparently synonymous with "bajada" as used in the American literature. Piedmont soils are well developed in the Punjab, Salt Range, and at the foot of the Sulaiman Range.

f) Hilly sand plain is a desert landscape with transverse and longitudinal sand dunes. Portions of the hilly sand plains are stabilized by sparse, stunted scrub vegetation. The Thar Desert is a prominent feature of southeast Pakistan, bordering the Indus on the east (Fig 1.1).

g) Deltaic flood plain is the region between Thatta, near Karachi and the high tide line near the coast, characterized by abandoned channels of tidal estuaries and river distributaries.

h) Tidal delta is an area of tidal mud flats extending from Karachi to western India, 10-50 km wide. The area is occasionally flooded and is covered with mangroves along the estuaries.

1.5 Land use and population density

About one half of Pakistan's labor force is employed in agriculture, producing ~30% of the nation's gross income. About one-third of the country's foreign exchange is earned by export of agricultural products, mainly cotton (textile yarn and fabrics produce more than one-half of export earnings) and rice (Paasch, 1987). Principal crops include sugarcane, wheat, rice, cotton lint, and corn. A large area of the Indus River Basin, comprised of high mountains, supports only sparse natural vegetation and terrace farming on mountain slopes. Although the plains contain thick soils, agriculture is limited due to scarcity and seasonal nature of precipitation and about three-fourth of the total river flow is used for irrigation (Akram, 1986). Agriculture therefore relies heavily on irrigation, sustained by the world's largest contiguous surface distribution system (Ahmad and Kutcher, 1992).

Environmental problems arising from extensive damming and improper agricultural practices include: 1) Water logging and soil salinization resulting in the loss of some 40,000 ha of arable land every year (Ahmad, 1993; Gilani, 1992); 2) Increased salinities in groundwaters (Beg, 1977); 3) Diminution of sediment load and nutrient-rich

7

river waters to the coastal areas (Milliman et al., 1984); 4) Potential loss of world's fifth or sixth largest coastal mangrove forest (Harrison et al., 1994); and 5) Pollution of freshwater and fish habitat (Tariq et al., 1996).

The population of Pakistan (1996 estimate) is 129,275,660, yielding an average population density of about 162 persons km^2 (Encarta, 1997). The annual population growth rate is approximately 2.7%. Only about 35% of the people live in urban areas. The geographic distribution of population density and land use is given in chapter 7.

1.6 Climate

The climate of the Indus River Basin varies widely from place to place. In the mountain regions of the north and west, temperatures fall below freezing during winter; in the Indus valley, temperatures range between about 32° and 49° C in summer, and the average during winter is about 13° C. Throughout most of Pakistan rainfall is scarce. The Punjab region receives the most precipitation. Regions in the southeast and southwest are arid. Most rain falls in July and August. Thus, a large spatial and temporal variation in weather elements characterizes the region. These are described below.

1.6.1 Temperature

a) The Cold Weather Season (mid December to March) is marked by temperatures below 5° C in the mountainous areas and varies between 10° C in the north and 18° C in the south of the plain areas. This season is occasionally affected by disturbances from the Mediterranean front that reach Pakistan after traveling across Iraq, Iran and Afghanistan.

8

b) The Hot Weather Season (April to June) is characterized by high temperature and aridity. Mean maximum daily temperature varies between 41 and 46° C. Southern and southwestern parts of the basin register higher temperature than the rest. Jacobabad, on the southern periphery of the Sulaiman Range, is the hottest place in the subcontinent with the highest recorded temperature of 53° C.

c) The Monsoon Season (July-September), established as a result of a low pressure system that builds up over most of the subcontinent during the months of May and June. The monsoon has two components, one originating from the Arabian Sea penetrates only the coastal areas of the Indus River Basin. The second, originating along the inter tropical front in the Bay of Bengal, moves over India and enters Pakistan.

d) The Post Monsoon Season is a transitional period between the monsoon and the cold season and is also known as the 'season of retreating monsoon'. In October maximum temperature ranges between 34 and 37° C. November and December are the driest months.

1.6.2 Precipitation and humidity

During the summer season, the Himalayan foothills and the Punjab plains receive abundant rainfall from the monsoon system. These areas receive an average annual rainfall of ~1000 to more than 2000 mm (Fig. 1.2), bulk of which occurs during the summer. The intensity of precipitation declines rapidly southwards and northwards where most of the landscape receives less than 500 mm. The mean annual precipitation over the Indus River Basin is 461 mm that is equivalent to a total water flux of 398 km^3 (see chapter 7).

In the northern mountains, large variations in the amount of precipitation with altitude have been noticed. Mean annual precipitation varies between about 90 mm at Leh in the Ladakh Range to about 1800 mm in Sonamarg, Kashmir in the Higher Himalayas (Holmes, 1993). In the central Karakoram, maximum precipitation (1000-1800 mm water equivalents) occurs at 5000-7000 masl (Shi and Zhang, 1984; Hewitt, 1989). In contrast, below 3000 m arid and semi arid conditions prevail and precipitation varies between 100-200 mm (Whiteman, 1985).

Humidity is generally low throughout the year. It is relatively higher, approaching 60% during the post monsoon and the cold season, declining to ~40% towards the spring and summer (Tamburi, 1974; Ahmad, 1993).
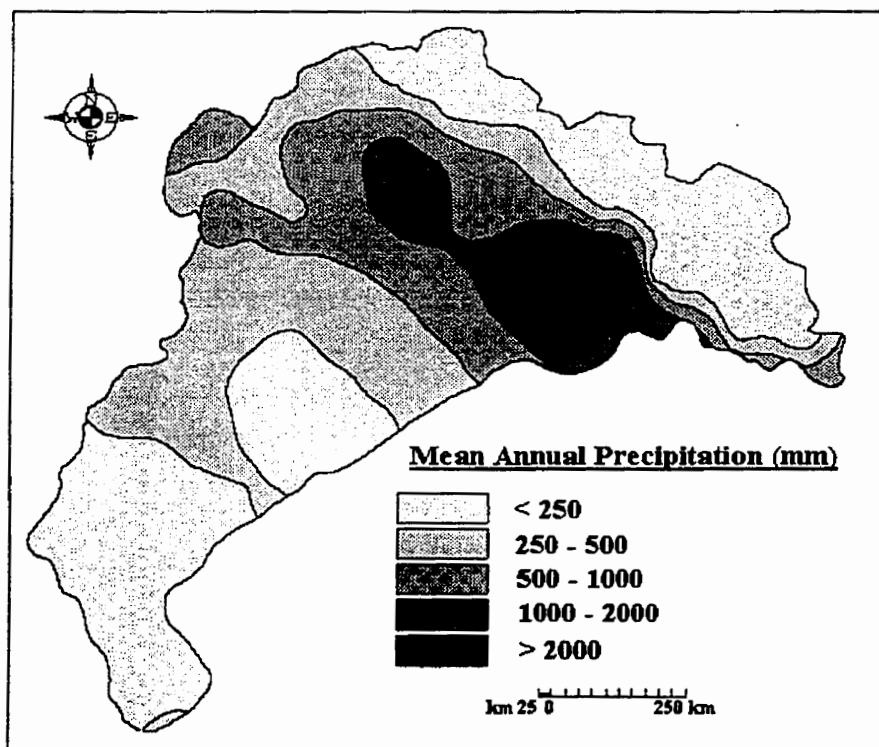
Fig. 1.2. Mean annual precipitation for the Indus River Basin.

1.6.3 Moisture source of precipitation

The Indus River Basin forms a transition zone between the monsoon in the east and the Mediterranean climate in the west. The climate is more 'continental' than that of other parts of the subcontinent which are influenced by a more typical monsoon regime (Kureshy, 1991). The northern mountains are the dominant source regions for the water budget of the Indus. At its mouth about 80% of the total discharge of the Indus is derived from melting of snow (see chapter 4).

In the headwaters, both the winter and summer seasons are thought to be dominated by the westerly air masses from which bulk of the snow fall is derived (Boucher, 1975; Barry and Chorley, 1982). In contrast, Wake (1989a), based on geographic distribution of precipitation, suggested that summer precipitation is mostly due to monsoon, much of the moisture derived from the Arabian Sea, constituting about 30-50% of the snowfall accumulation on the glaciers. These disparate interpretations will be discussed in detail in chapter 4.

1.7 Hydrology

1.7.1 Major rivers

Figure 1.3 shows major and minor tributaries of the Indus River Basin. Among the headwater tributaries the Shingo, Shyok, Shigar, Hunza, Gilgit and Kabul are the major ones. The humid Punjab region (meaning *the land of five rivers*) produces the Jhelum, Chenab, Ravi, Beas and Sutlej. However, the last three are no longer part of the Indus system. Their headwaters have been diverted into India according to the 1960 Indus Basin Treaty. As a result of these diversions, the channel of the Beas River has been completely

abandoned and the Ravi and Sutlej carry insignificant natural discharges except during the monsoon floods. In order to sustain annual irrigation, all Punjab rivers are linked by canals and water from the Indus, Chenab and Jhelum are diverted to the other three rivers.
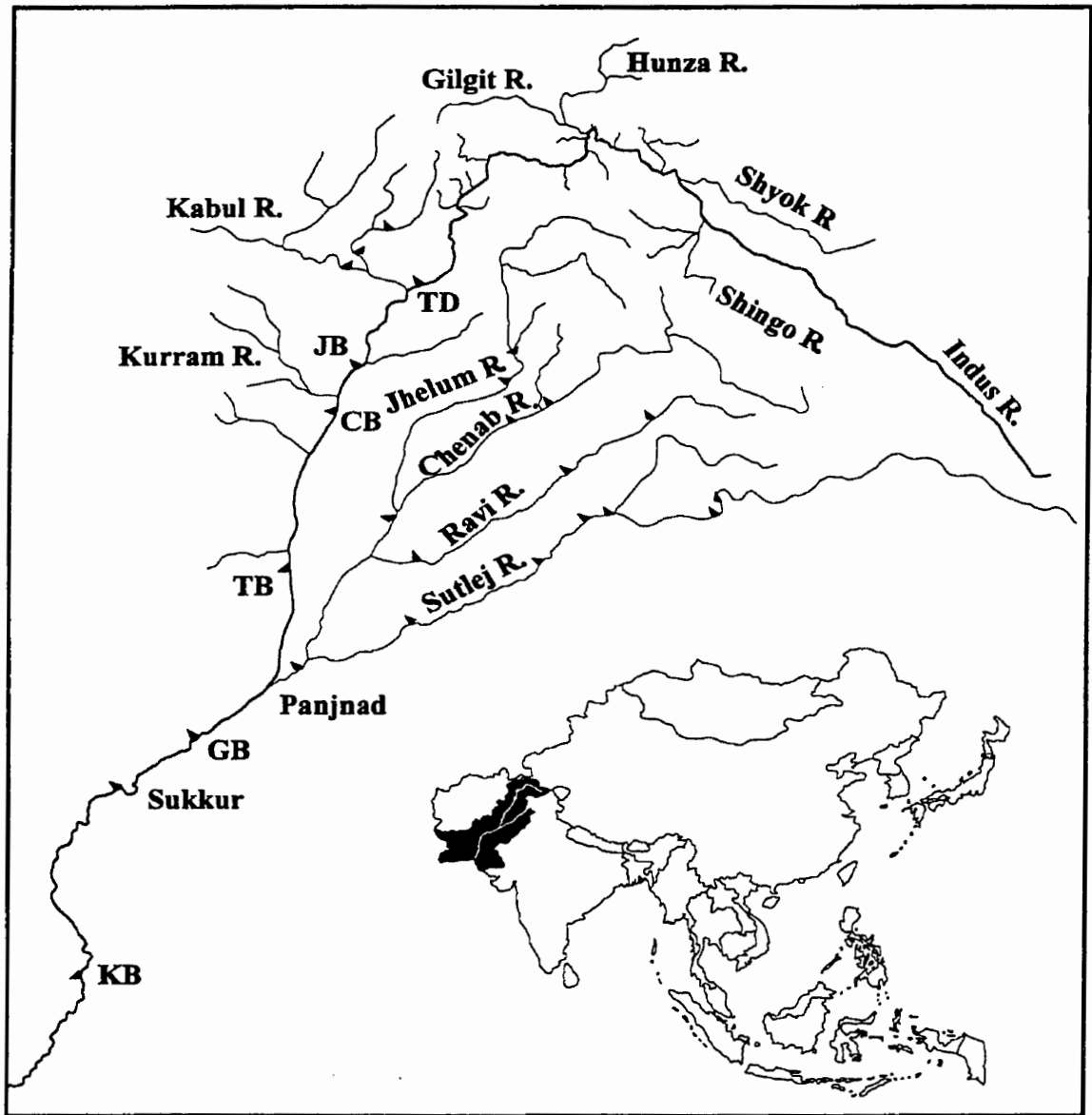
Fig. 1.3. Tributaries and location of major dams and barrages (triangles) of the Indus River Basin. TD, Tarbela Dam; JB, Jinnah Barrage; CB, Chashma Barrage; TB, Taunsa Barrage; GB, Guddu Barrage; KB, Kotri Barrage.

12

Discharge of major rivers within the Indus River Basin starts to rise in April, concomitant with the melting of snow, peaks around August during the summer monsoon and returns to base flow conditions in October (Fig. 1.4). About 90% of the total discharge occurs in the seven-month period from April to October (Table 1.1). Discharge at Panjnad outweighs all other tributary discharge within the Indus River Basin. During low flow it accounts for about one-third of the total tributary discharge to the Indus. Another third is supplied by the Kabul River and the remainder is accounted for by the other tributaries, with the Swat, Gilgit, Shyok, Hunza and Shigar being the most important. During high flow season, the contribution of Panjnad and most of the headwater tributaries increases slightly, while that of the Kabul River and lowland tributaries declines by about a factor of two. For the headwater tributaries, the discharge for a given season varies by a factor of >10 and for the lowland ones by a factor of <5. This seasonal pattern reflects an interplay of two distinct hydrologic regimes, particularly during the low flow season. During this period, the headwater tributaries receive only small contribution from direct runoff or from groundwater. This is due to the fact that direct runoff decreases steeply with the dwindling of snow cover and with the subsequent temperature drop, while groundwater supply is limited by the scarcity of shallow aquifers in the terrain dominated by crystalline rocks and sparsely developed soils. At the same time, in the lowland tributaries, discharge is sustained by sporadic monsoon and by groundwater discharge from thick alluvial aquifers, thus reducing the disparity between discharge extremes.

The mean monthly discharge at the mouth of the Indus is lower than the mean tributary input throughout the year (Table 1.1). The difference is conspicuous during the

13

rising limb of the hydrograph and attenuates during recession (Fig. 1.4). This is due to extensive impoundment (Fig. 1.3) and withdrawal of water along the Indus for irrigation purposes. The filling of reservoirs starts in the spring, concomitant with the melting of snow, and continues until the commencement of monsoon in mid July when the reservoirs attain peak levels. As the season advances, the difference between tributary input and discharge at the mouth of the Indus decreases until the inception of the post monsoon season in October. Complementary to this is water removal during floods by bank storage (Todd, 1995) into extensive alluvial aquifers that border the Indus. However, the steep slope of the falling limb of the hydrograph, typical of flood hydrographs with no bank storage (Freeeze and Cherry, 1979), indicates that these phenomena are of subordinate importance for the Indus water budget.
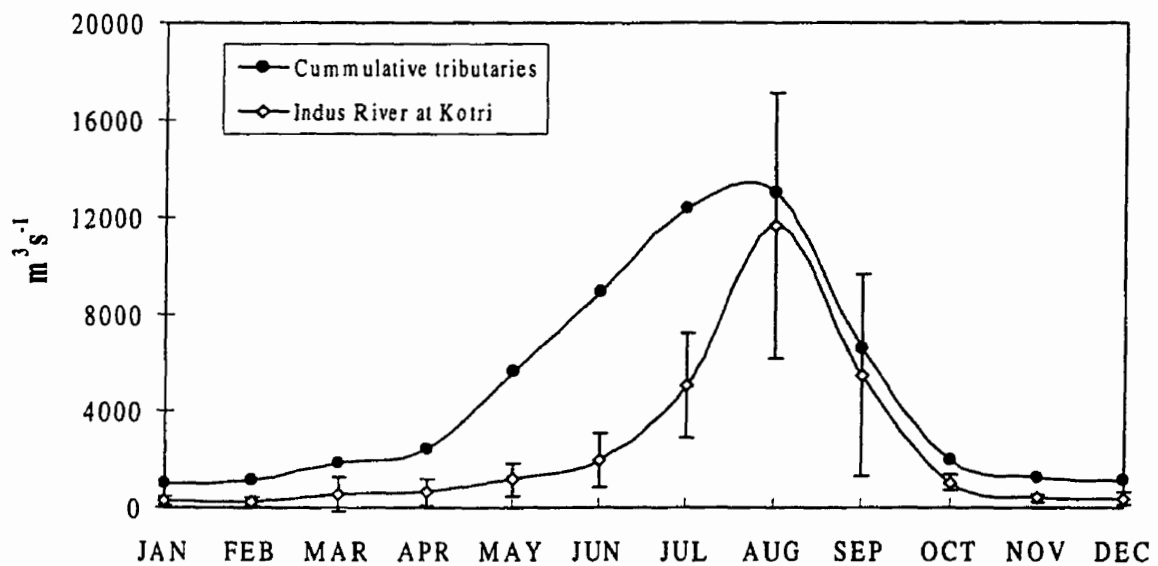
Fig. 1.4. Mean monthly discharge of the Indus River and mean monthly cumulative discharge of its tributaries. The error bars represent standard deviation of the discharge of the Indus. Sources of unpublished data are Global Runoff Data Centre (GRDC) for the Indus and Water and Power Development Authority, Pakistan (WAPDA) for the tributaries.

14

Table 1.1. Average seasonal discharge (m^3s^{-1}) and relative proportions to the cumulative discharge of tributaries of the Indus River Basin (source of data Global Runoff Data Center and WAPDA, 1976; 1985; 1989a; 1990).

River	April - October	November - March	% April - October	% November - March
Shyok	4835	326	9.6	5.1
Shigar	2718	139	5.4	2.2
Hunza	4221	284	8.3	4.5
Gilgit	3052	340	6.0	5.4
Astore	1909	199	3.8	3.1
Gorband	164	93	0.3	1.5
Kabul	8499	1809	16.8	28.5
Swat	2046	434	4.0	6.8
Soan	653	151	1.3	2.4
Haro	385	96	0.8	1.5
Siran	172	114	0.3	1.8
Kurram	110	29	0.2	0.5
Panjnad	21729	2321	42.9	36.5
Indus	26924	1830	93.6	6.4
Total	50617	6349		
Percent			89	11

Historical discharge data for two stations on the Indus (Fig. 1.5) shows that the mean annual discharge has decreased dramatically after the construction of the Guddu and Kotri barrages. This was also accompanied by reduction in sediment discharge (Jorgensen et al., 1993). Kazmi (1984) attributed shrinkage of the modern delta to an 80% reduction in water and sediment load. At the Kotri barrage the mean annual water flux during the pre-dam and post-dam era were, 100 and 53 km^3 respectively. Note that the present day discharge at the Sukkur barrage is similar to the pre-dam discharge at the Kotri barrage. The riverine water flux thus constitutes only one-fourth to one-eighth of the precipitation water flux (398 km^3, chapter 7) and the remainder leaves the surface

15

water system by groundwater storage, evapotranspiration and evaporation. The role of these processes will be further discussed in chapter 4.
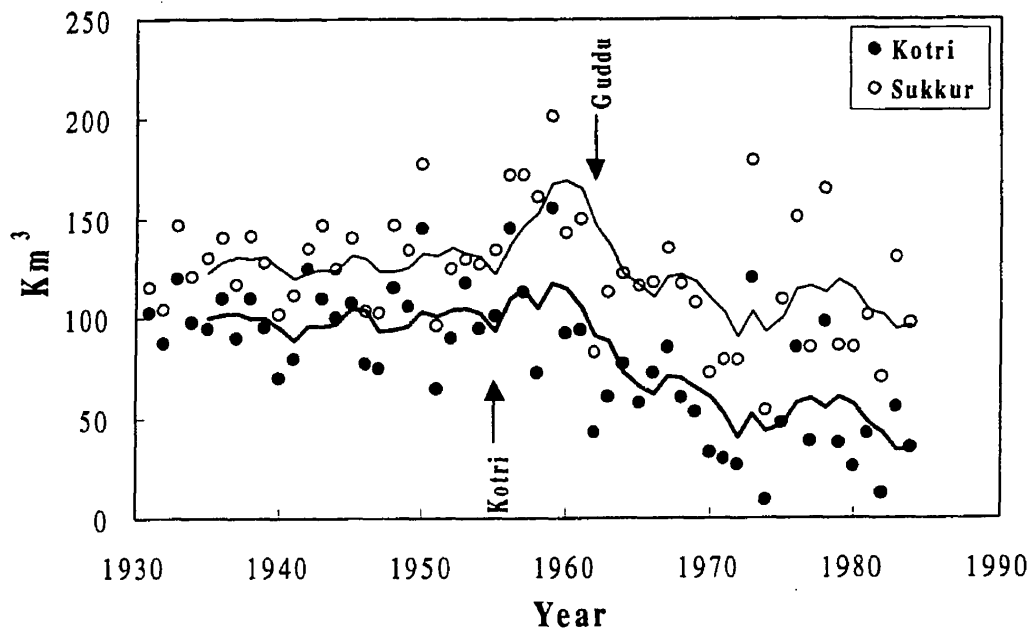
Fig. 1.5. Mean annual discharge for the Indus River at Sukkur and Kotri barrages (modified after Jorgensen et al., 1993). The thin curve is a five point moving average through the Sukkur data and the thick one for the Kotri barrage. The arrows represent the year when the barrages were closed.

1.8 Original Contributions

Original contributions of the present study to the research on the Indus River Basin include but are not limited to:

1. Water sampling of the tributaries and the Indus River along its entire length in Pakistan, on-site measurements and subsequent analyses for a suite of complementary geochemical and isotopic parameters.

2. Construction of an environmental database comprised of geology, topography, precipitation, land use, population density, and watershed boundaries.

3. Estimates of relative proportions in each tributary basin of units of geology, land use and population density. Estimates for mean altitude, precipitation, and geographic coordinates.

4. Quantification of precipitation and riverine flux of solutes and water.

5. Delineation of moisture sources of the Indus River Basin and their relative contribution.

6. Estimates of relative roles of carbonate and silicate weathering within the Indus River Basin.

7. Evaluation of natural and anthropogenic factors that influence hydrochemistry of the Indus River tributaries.

Chapter 2

Geology and Tectonics

The present-day configuration of the Indo-Pakistani subcontinent is the result of mountain building processes which started during the Carboniferous to Early Permian. The breakup of Pangea, about 300-200 Ma ago, and subsequent rifting produced a major new ocean called "Tethys" which separated the Eurasian continent in the north from the Gondanwana continent in the south (Smith et al., 1981). While Eurasia included northern Europe and most of Asia north of the Pamirs and the Tien Shan, Gondawana included Africa, Arabia, Australia and Antartica. In between these two large contintents were numerous small continental fragments (central Iran microcontinent, the Lut and Afghan blocks, the Tarim plate, the Qiantang and Lhasa blocks) consisting of Precambrian crust and Paleozoic cover. Thus, the Tethys Ocean was subdivided into a northern ocean called the Palaeo-Tethys and a southern one called the Neo-Tethys. Rifting continued between the continents and by the late Triassic marine conditions prevailed on the passive margins of drifting continents. This is illustrated by thick carbonate platform sequences in Europe, Iran-Arabia and northern India (Searle, 1991).

The Gondwana continent also fragmented during the Jurassic and early Cretaceous and newly formed ocean floor was accreted to the drifting continents. During the late Cretaceous India began its rapid northward drift across the Indian Ocean. This was accompanied by major ophiolite emplacement in the Zagros suture in Iran, the Oman mountains, the Bela, Muslimbagh and the Zhob ophiolites in Pakistan and the ophiolites south of the Indus suture zone (Searle, 1991). India's continued drift towards the southern

Asian paleomargin lead to the terminal collision at about 40 Ma ago (Molnar & Tapponnier, 1975), with initial collision at about 55 Ma (Klootwijk, 1979). The collision caused metamorphism, thrusting, magmatism and uplift on the edges of the colliding plates and subsequent geomorphic processes resulted in the present landscape.

Geology of the Indus River Basin can be classified into eight lithotectonic units, from north to south these are: (1) The Hindu Kush-Karakoram-western Tibet block; (2) The Main Karakoram Thrust; (3) The Kohistan-Ladakh arcs; (4) The Indus-Zangbo suture zone; (5) The Indian plate sequence; (6) The Lesser and Sub Himalayas; (7) The west Pakistan fold belt (8) The Indus plain.

2.1 The Hindu Kush-Karakoram-western Tibet block (HKT)

The HKT forms an arcuate belt, ~90 km wide, parallel to the northern watershed boundary of the Indus River Basin and represents rocks accreted to the southern paleomargin of the Asian plate (Fig. 2.1). It extends from Pakistan-Afghan border to western Tibet. It is bound in the north by the Pamir-Kun Lun Ranges and to the south by the Shyok suture zone that forms the southern limit of the Eurasian plate. The Kunar River, a major tributary of the Kabul River, drains portion of the Hindu Kush terrain, within the Indus River Basin. Its lithology consists mainly of amphibolite and greenschist facies metapelites, marbles, cherts and sandstones, intruded by granodiorite and granite.

The Karakoram is an area of rugged terrain and four of its peaks exceed 8000 m. Among these is K2, the second highest (8611 m) peak in the world. The range is covered by perennial snow and ice and includes glacially influenced subbasins of Gilgit, Hunza, Shigar and Shyok rivers. The Karakoram Range encompasses a granitic batholith in the

center, flanked in the south by a high-grade metamorphic belt consisting of interbedded pelites, marbles and amphibolites (Searle et al., 1996), and in the north by a sedimentary/metasedimentary zone.

2.1.1 The Northern sedimentary/metasedimentary zone

Gaetani et al. (1990) classified rocks of the upper Hunza valley into three tectonics belts. These are, (a) Northern Belt (Misgar Unit), at least 30-40 km wide and consists of unfossiliferous slates and quartzites that are intruded by granodiorite. The slates show extensive quartz recrystallization and growth of mica, chlorite or biotite. The clastic rocks consist of arkose and quartzarenite. (b) Intermediate Belt (Sost Unit), is a fault bound block, consisting of Permian to Jurassic and possibly Cretaceous marine sediments, and (c) Southern Belt (Gujhal Unit), consisting of thick-bedded dolomites with minor slates and sandstones, ranging in age from Carboniferous to Cretaceous.

2.1.2 The Karakoram Batholith

In Karakoram, the backbone of the main range is made up of an axial composite batholith known as the Karakoram batholith. Occurring as a narrow belt of plutons, about 500 km long and up to 20 km wide, the Karakoram batholith extends from near Pakistan-Afghan border to northwestern Ladakh, with analogs that can be traced for another 2500 km in the southeast (see below).

The granitic rocks of the Karakoram batholith display a wide range of compositional and textural variations. Gneissose biotite-hornblende granodiorite appears to be the dominant rock type (Jan et al., 1981a) but adamellite, quartz diorite, hornblende

diorite, tourmaline granite, aplite, pegmatite and lamprophyre also occur. These are intruded by granitic, aplitic and pegmatitic dikes and contain metasedimentary enclaves. Based on chemical and isotopic data, Debon et al (1987) suggested three phases of magmatism within the Karakoram batholith. (1) a Mid-Cretaceous (110-95 Ma) phase of sub-alkaline and calc-alkaline character, related to the subduction of oceanic crust underneath the Karakoram plate margin; (2) preceeding the second phase of magmatism, between 65 and 59 Ma, was a strong tectonometamorphic event that resulted in gneissification of the Cretaceous intrusives, and was a consequence of the closure of northern Tethys due to collision of the Kohistan arc with the Karakoram plate. The tectonometamorphic event, between 59 and 43 Ma, was followed by a major intrusive stage of sub-alkaline magmatism and emplacement into the welded Karakoram and Kohistan domains; and (3) an Upper Miocene (9 Ma) light-colored subalkaline phase that was related to subduction of Kohistan and Indian continental crust underneath the Karakoram.

Rocks similar in chemistry and age to the Karakoram batholith can be followed along a nearly continuos belt, further southeast that is about 50 km wide and 2500 km long. They are known as the Transhimalaya batholith or the Kangdese belt. The chemistry and ages of the Karakoram and Transhimalaya batholiths are similar (Le Fort et al., 1983; Debon et al., 1987), suggesting that they both belong to the same belt (Le Fort 1988).
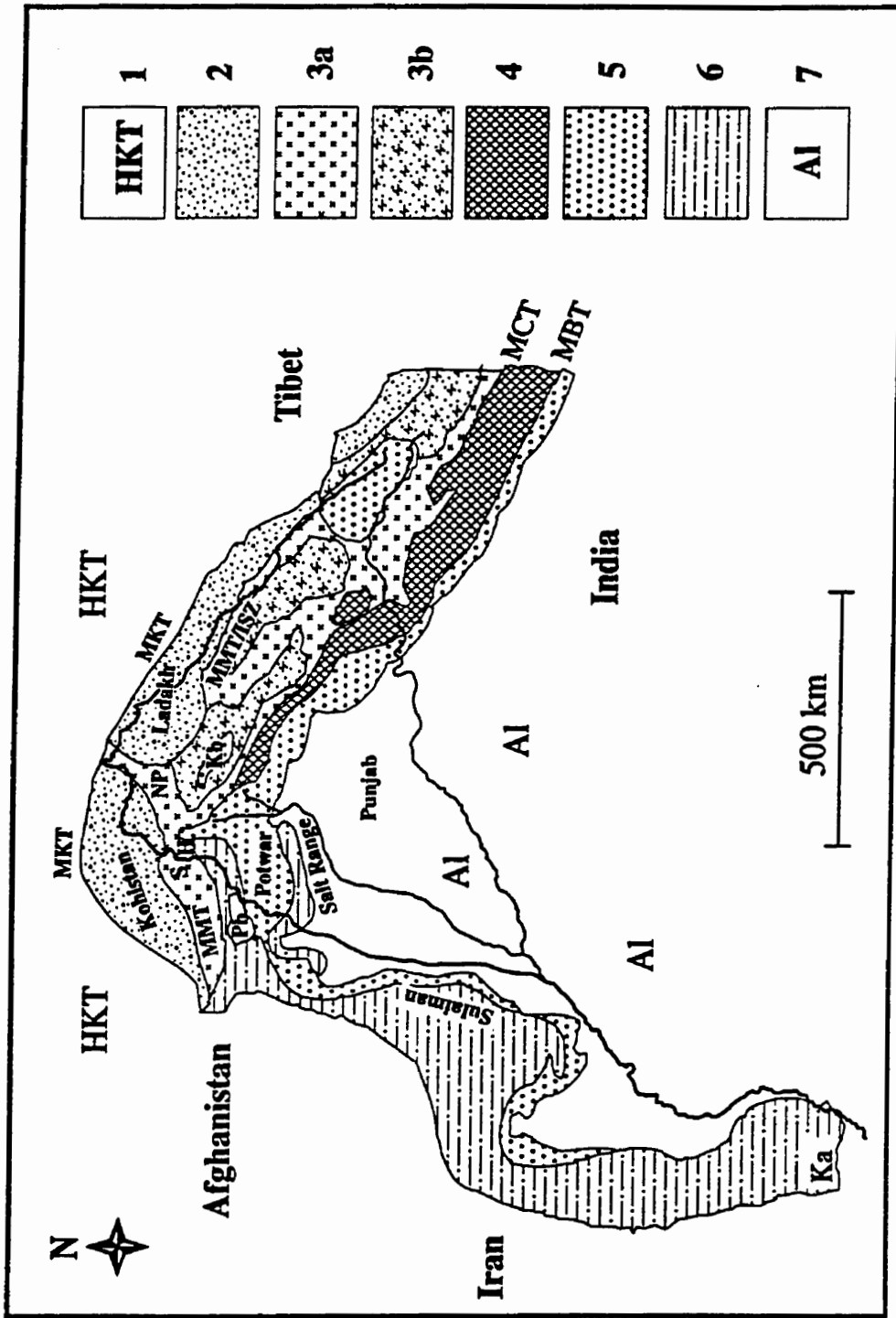
Fig. 2.1. Regional geology of the Indus River Basin. 1, Hindu Kush-Karaokram-western Tibet block; 2, Kohistan-Ladakh arcs and the Trans-Himalayan Batholith; 3a, Higher Himalayas "Central Crystalline"; 3b, Higher Himalayas Tethyan sediments; 4, Lesser Himalayas; 5, Mollase sediments of Sub Himalayas and old river terraces; 6, West Pakistan Fold Belt; 7, Indus Alluvial Plain. ISZ, Indus Suture Zone; H, Hazara; Ka, Karachi; Kb, Kashmir basin; MBT, Main Boundary Thrust; MCT, Main central Thrust; MKT, Main Karakoram Thrust; MMT, Main Mantle Thrust; Pb, Peshawar basin; S, Swat.

22

2.2 The Main Karakoram Thrust (MKT)

Rocks of the Karakoram terrane are joined to the Kohistan-ladakh arc along a suture zone known in Pakistan as the Northern Suture (Pudsey, 1986) the Northern Megashear (Tahirkheli, 1979) or the Main Karakoram Thrust (Tahirkheli, 1982) and in India as the Shyok Suture (Rai, 1982). In northern Pakistan the suture zone is 150 m to 4 km wide and contains blocks of volcanic greenstones, limestones, shales, conglomerates, quartzites and serpentinites in a slate matrix. Limestone and volcanic greenstone are the most common, the former has been dated as Aptian-Albian and attains a size of about 200x50 m (Pudsey, 1986). Based on petrological and structural data, the melange zone associated with the MKT is interpreted to be an olistostrome, formed in a back arc basin (Pudsey et al., 1985; Hanson, 1989). However, a tectonic origin has also been suggested by some workers (Coward et al., 1982a; Windley, 1983).

2.3 The Kohistan-Ladakh island arcs

Kohistan, meaning "the land of mountains" includes most of the area along the Indus valley, between Nanga Parbat in the east and upper Swat valley in the west. Geologically, Kohistan refers to the terrain bound in the north and northwest by the MKT and in the south and southeast by the Main Mantle Thrust (MMT). Trending east-west and dipping steeply north, the Kohistan sequence is composed predominantly of mafic, ultramafic and calc-alkaline layered plutonic and volcanic rocks. This 40 km thick sequence, thought to be the only complete island arc cross-section presently exposed in the world, is sandwiched between the Indian and Eurasian plates (Tahirkheli, 1979). The Kohistan terrain has been divided into six major units, from bottom to top:

23

2.3.1 Jijal-Pattan Complex

Along the Indus River and to the north of the MMT is an isolated outcrop of granulites and ultramafic rocks called the Jijal-Pattan complex (Jan and Howie, 1980). It covers an area of about 150 km^2 and consists of garnet granulites and ultramafic rocks. The granulites have been distinguished as plagioclase bearing, the most extensive rock type, and plagioclase free types (Jan and Howie, 1981). The granulites are composed of garnet, clinopyroxene, and quartz ± plagioclase ± orthopyroxene. The ultramafic rocks comprise diopsidite, dunite, harzburgite, websterite, and podiform chromitite. The protolith of the complex is interpreted to represent either the Tethyan lower crust or magmatic cumulates at the base of the Kohistan arc (Jan, 1985).

2.3.2 Kamila Amphibolite

The Kamila Amphibolite is an extensive belt, about 40 km wide, north of the MMT and extending west of the Nanga Parbat Massif, through Babusar, Indus and Swat valleys to eastern Afghanistan. Amphibolite is the predominant rock type but ultramafic rocks, gabbros, diorites, tonalites, granites and trondhjemites are also present. The amphibolites consist essentially of hornblende, plagioclase ± epidote, ± garnet ± clinopyroxene. Both banded and non-banded amphibolites are present. They are derived from volcanic and plutonic precursors and have calc-alkaline chemical affinities (Jan, 1988). Owing to the scarcity of siliceous rocks, Bard et al. (1980) suggested that the amphibolites represent oceanic crust on which the Kohistan island arc was built. An island arc origin is preferred by others (Coward et al., 1986; Jan, 1988).

2.3.3 Chilas Complex

The Chilas Complex is a mafic-ultramafic stratiform complex. It is more than 10 km thick and extends for about 300 km between Nanga Parbat and western Dir. Gabbronorite is the dominant rock type (with minor pyroxenite and anorthosite layers) and subordinate hypersthene-quartz diorites, collectively referred to as "principal gabbronorite association". They are characterized by a lack of olivine and the presence of plagioclase of andesine to labradorite composition. In contrast, the "ultramafic association", consisting of veins, dikes and lensoidal bodies of ultramafic rocks, gabbronorites, gabbros, anorthosites, chromitite and mafic pegmatites, contains plagioclase of more calcic composition and olivine (Khan et al., 1989; Jan et al., 1989). The rocks have been metamorphosed to medium-pressure granulite grade (Jan and Howie, 1981).

In western Ladakh, mafic rich gabbros, orthopyroxene-bearing norites and hornblende-pyroxene anorthosites occur in the Kargil area (Rai and Pande, 1978) and may be the lateral equivalent of the Chilas complex (Searle, 1991).

2.3.4 Kohistan Batholith

The Kohistan batholith is the northernmost unit of the Kohistan arc and comprises a suite of rocks with an average composition of granodiorite-quartz diorite (Petterson and Windley, 1991). It is an elongated belt (300x60 km) consisting of plutons over 250 km^2 in area and minor stocks, sills and dikes. Three stages of magmatism within the Kohistan batholith have been recognized. These are:

a) Stage 1, typified by the Matum Das pluton, the oldest, deformed rocks, represented by a bimodal suite of a basic-intermediate member (mostly medium-high-K gabbros and diorites) and an acid member (low-K trondhjemites). This stage was dated at 110-90 Ma (Petterson and Windley, 1991).

b) Stage 2, plutons constituting about two third of the Kohistan batholith. They are undeformed and cross-cutting relationsips demonstrate a temporal trend from basic to acidic magmatism. The rocks consist of a series of medium-high-K gabbros, diorites, granodiorites and granites with minor basic dikes. This stage was dated at 85-40 Ma (Petterson and Windley, 1991).

c) Stage 3. Rocks of this stage crop out near the confluence of the Indus and Gilgit-Hunza rivers. They are represented by swarms of leucogranite sheets that constitute only a minor part of the Kohistan batholith. Geochemically, they are different from earlier plutons and represent the final stage of magmatism (~30 Ma) within the Kohistan batholith. Individual sheets have an average thickness of one meter and contain alternating layers of aplite and pegmatite. Important minerals include biotite, quartz, feldspar, tourmaline, garnet and muscovite.

2.3.5 Interbedded volcanics and sediments

Intercalated volcanics and sediments occur at higher stratigraphic levels within the Kohistan island arc. Although common, they constitute only a small component of the island arc. Searle (1991) subdivided the volcanics into post-collision and pre-collision belts. The post-collision volcanics represented by the Dir Volcanic Group range in composition from basalt to rhyolite with abundant pyroclastics. They are intruded by the

Kohistan batholith and are dated as Paleocene to early Eocene. The pre-collision volcanics include the Chalt and Shamran (Ghizar) volcanic groups. The former occur to the south of the MKT, forming a linear belt, about 300 km long, comprised of a deformed and metamorphosed sequence of submarine pillow lavas and volcanogenic sediments. Important rock types are hornblende, pyroxene, plagioclase-phyric andesite, basaltic andesite and basalts, with some high-Mg tholeiitic andesites and boninites. The Chalt volcanics are overlain conformably by slates, turbidites, and shallow marine Tethyan limestones of the Yasin Group. A similar suite of rocks, consisting of basaltic and dacitic flows, pyroclastics and associated pillow lavas and volcano-sedimentary rocks, known as Dras volcanics occurs in the Ladakh area (Honegger, et al., 1982). In both regions, limestones containing mid Cretaceous fossils (Pudsey, 1986; Wadia, 1937) overlie the volcanics. The second member of the pre-collision volcanic belt is the Shamran (Ghizar) Volcanic Group that comprises metamorphosed pyroclastic, calc-alkaline andesites and basaltic andesites and interbedded pelites.

2.4 The Indus-Zangbo Suture Zone (ISZ)

The Kohistan terrain is joined to the Indian plate sequence along a north dipping thrust fault known as the "Main Mantle Thrust" (MMT), the name used by Tahirkheli et al. (1979) to emphasize that it separates mantle-related rocks from crustal rocks. The MMT is the western extension (Jan et al., 1981b) of the roughly 2000 km long Indus-Zangbo suture (ISZ) which defines the collision zone between the Indian plate and the Karakoram-Lhasa block to the north (Gansser, 1964; Allègre et al., 1984). The suture zone is named after the Indus River since the Indus valley follows it for several hundred

kilometers in the Ladakh region. It is possible that the ISZ had a geomorphic control on the course of the river.

In Ladakh the ISZ consists of three major linear thrust belts separated by major fault zones or ophiolitic melange belts (Searle et al., 1988): (1) The Lamayuru complex consisting mainly of shale, sandstone and limestone; (2) The Nindam-Dras Volcanic Group, comprising basalts, andesites, dacites, intercalated volcaniclastics and associated volcano-sedimentary succession of the Nindam Formation; (3) The Indus Group molasse, approximately 2000 m thick, consisting of continental clastic rocks, derived mainly from the Ladakh batholith and the suture zone itself.

In Shangla-Mingora area of northern Pakistan, the ISZ zone consists of thrust bound blocks, but with different rock types. Here too, the suture zone has been divided into three units separated by thrust faults (Kazmi et al., 1984). From south to north these are: (1) The Mingora ophiolite melange, characterized by abundant ophiolite suite rocks and emerald mineralization. Important rock types are serpentinite, talc-dolomite schist, greenstone, greenschist, metagabbro, metasediments and metachert; (2) The Charbagh greenschist melange, charecterized by greenstone, greenschist and minor tectonized metasediments; and (3) The Shangla blueschist melange, composed of dismembered masses (up to 6 km) of metavolcanics and phyllite schist with smaller lensoidal masses of serpentinite, metadolerite, metagraywacke, metachert and marble. Limestone blocks within the suture zone contain Jurassic to middle Cretaceous fossils (Kazmer et al., 1983).

2.5 The Indian plate Sequence

South of the ISZ are the remnants of the Indian continental margin consisting of deformed and metamorphosed late Precambrian to early Paleozoic gneisses, granite gneisses, schists and marbles that have been thrust south over Mesozoic sediments (Tahirkheli et al., 1979; Coward et al., 1982b; Tahirkheli, 1982). Near the confluence of the Indus and Gilgit-Hunza rivers is one of the most striking geological feature of northern Pakistan. The ISZ is folded into a crustal scale antiform (Coward, 1985) forming the Nanga-Parbat Haramosh massif (NPHM). The massif and the adjacent terrain contain some of the highest peaks in the Himalayas. Nanga Parbat (main summit at 8125 m) and the Indus River (at 1300 m, located only 20 km away) define the world's greatest relief. The NPHM has been undergoing high rates of uplift of about 7 mm year^{-1} (Zeitler, 1985) and equally high rates of erosion (Butler and Prior, 1988). Several small and highly turbulent streams drain this region of high topographic relief. The main rock types of the NPHM are a series of biotite augen gneisses derived from an igneous (Butler and Prior, 1988) or metasedimentary (Chaudhry and Ghazanfar, 1990) precursor. The emplacement age of NPHM is not clear. Radiometric ages of 2300 to 2500 Ma and a much younger age of 2.3 Ma has been obtained on these rocks (Zeitler, 1985; Zeitler et al., 1989).

2.5.1 Indian plate sequence east of NPHM

The terrain between the Main Central Thrust (MCT) and the ISZ constitutes the Higher Himalayas that forms the drainage divide between the Indus River and the Punjab and the Ganges-Brahmaputra rivers. The Indian plate sequence consists primarily of gneiss-migmatite-metasedimentary basement that is overlain by Tethyan cover sediments,

both intruded by granitic plutons. Geology of this region can be classified into (a) Higher Himalayas Tethyan sequence (b), Higher Himalayas "Central Crystallines" and (c) Panjal volcanics.

a) The Higher Himalayas Tethyan sequence occurs on both sides of the NPHM as an almost continuous belt (upto 100 km wide) of unmetamorphosed or weakly metamorphosed rocks that stretch along the entire length of the Himalayas. Abundant fossils and a complete Cambrian to Eocene succession, deposited on an intermittently subsiding continental shelf (Gansser, 1964; Gupta and Kumar, 1975) characterize it. The rocks preserve a complete record of tectonic events, commencing with the rifting of the Neo-Tethys during the Permian to final collision of the Indian plate with the Eurasian plate in the Eocene (Garzanti et al., 1986; Searle et al., 1988). The sediments consist mainly of shales, carbonates and quartzites. The Permian-Jurassic sediments are more widespread and consist mainly of carbonates, quartzites and shales (Andrews-Speed and Brookfield, 1982). Details of the geology are given in Gupta and Kumar (1975), Brookfield and Andrews-Speed, (1984) and Garzanti et al. (1986). Two ophiolite complexes have been thrust onto the Tethyan sediments, the Spongtang ophiolite in Zanskar (Frank et al., 1977) and the Jungbwa Amlang La ophiolite (Gansser, 1964), the latter near the origin of the Indus and Sutlej rivers in SW Tibet.

b) The Higher Himalayas "Central Crystallines", about 5 to more than 10 km thick, form the central axis of the Himalayas, and are comprised predominantly of pelitic to psammitic schists and gneisses and minor bands of amphibolite, marble and quartzite of Precambrian to Paleozoic ages (Kundig, 1989). In the Zanskar valley, the complex is bound in the north by a normal fault with a shear zone up to about 7 km wide (Herren,

1987) and in the south by the MCT. The rocks have undergone deformation, polyphase metamorphism and partial melting and display well developed mineral zonation of Barrovian type metamorphism from chlorite to sillimanite (Pêcher and Le Fort, 1986). A characteristic feature of this region is the occurrence of inverted metamorphic zones (Heim and Gansser, 1939): metamorphic grade decreases downwards, as for example seen in the Darjeeling hill where biotite grade rocks occur at the bottom, garnet at the intermediate level and staurolite at the top (Bhattacharya and Das, 1983).

c) The Panjal volcanics are located southeast of the NPHM, along the southern limit of the Higher Himalayas in the Kashmir Basin. They cover an area of about 20,000 km^2 and that is drained by the Jhelum River. Geology of the basin is dominated by a thick succession of volcanics, agglomeratic slates and Quaternary alluvium. The volcanics cover about 60% area of the basin and consist of a thick succession (up to 2500 m) of basaltic-andesitic flows with interbedded tuffs and limestone underlain by agglomeratic slates, grits, pyroclastics, limestone/marble, graphitic schist, pelitic schist and conglomerate (Wadia, 1957; Honegger et al., 1982). The volcanics are variably altered and metamorphosed, epidote, calcite, chalcedony and jasper are common secondary minerals. The agglomeratic slates, as thick as the volcanics, are composed of a fine greywacke-like matrix with fragments of quartzite, porphyry and granite (Wadia, 1957). The Panjal volcanics have a stratigraphic age of late Carboniferous to Triassic, but much of the volcanic activity took place during the Permian (Pareek, 1982; Gupta et al., 1982).

The rocks can be traced further east where they are limited to only a few outcrops in the headwaters of the Ravi River. Westwards, they can be traced near the Hazara-Kashmir Syntaxis (HKS) where they are metamorphosed to eclogite facies (Spencer et al.,

1990). Rocks of similar age and geochemical affinities (Jan and Karim, 1990) occur further west in the Peshawar plain.

2.5.2 Indian Plate Sequence west of NPHM

The Higher Himalayas sequence of the Indian plate continues in the NW and protrudes into the Kohistan-Ladakh arcs. Further west, the belt is squeezed to about 20 % of its width near the HKS, widening again further west. The southern boundary of the Higher Himalayas is based on its position relative to the MCT (Gansser, 1964). The latter is not clear in northern Pakistan and Kashmir. Chaudhry and Ghazanfar (1990) proposed that the Luat-Batal and faults are the western continuation of MCT. Coward et al. (1988), on the other hand, considers the Panjal and the Mansehra thrust structures to be equivalent to, but not necessarily coeval with, the MCT in the Himalayan ranges in the east. In order to overcome these controversies and emphasize geological diversity of the region, the Indian plate sequence in Pakistan is presented here in a greater detail. This terrain has been deeply dissected along major rivers and most studies have focused on these areas. Classical sections of the Indian plate sequence from west to east are along the Swat, Indus and Kaghan valleys.

a) In the Swat valley, south of the MMT, Alpurai Group, Swat Granite Gneisses and Manglaur Schist dominate. The Alpurai Group consists of calcareous schist, marbles and amphibolites (Lawerence et al., 1989) of lower Paleozoic age (Humayun, 1986). The Manglaur crystalline schists are tectonized, non-calcareous, quartz-mica-garnet schists that have three lithologic variants: quartz-feldspar schist; quartz-mica-kyanite schist and quartz-mica-garnet schist (Kazmi et al., 1984). The Swat granite gneisses are sheet-like

intrusives within the Manglaur Schist. The former closely resembles the Mansehra granite in the southeast which has a 516 ± 16 Ma Rb/Sr isochron age (Le Fort et al., 1980). The Mansehra granite intrudes the staurolite to sillimanite grade metasediments of Tanawal Formation of Precambrian age and resembles the Manglaur crystalline schist (Kazmi et al., 1984).

b) The Indus valley exposes Precambrian gneisses of the Besham Group (metasedimentary schists, marbles and amphibolites, Treloar, 1989). The gneisses are imbricated with metasediments of Paleozoic Karora Group, a pelite rich metasedimentary sequence and lesser graphitic, psammitic, and calcarous rocks, metamorphosed at greenschist to amphibolite facies (William, 1989). On lithologic basis, the Indus valley is not very different from the adjacent Swat valley, except for different proportions of rock types. The calcareous rocks of Alpurai Schist predominate in the Swat valley whereas the pelitic rocks predominate in the Indus valley.

The Hazara region forms the drainage divide between the Indus and the Jhelum River. The northern part of the region largely consists of metapelites and metapsammites of the Precambrian Tanawal Formation and of the equally abundant late Cambrian Mansehra granite. In the south, however, in addition to the Tanawal Formation, the Precambrian Salkhala and Hazara formations and the Carboniferous to Triassic Kingriali Formation are also present. The Salkhala Formation consists largely of slates, phyllites, graphitic schists and marbles (Wadia, 1957), it outcrops only locally near Tarbela but extends as a broad belt through Kaghan valley into the Higher Himalayas. The Hazara Formation is predominantly composed of slates, phyllites and minor limestone and graphite. The Kingriali Formation consists mainly of dolomite, quartzite and phyllite

(Calkins et al., 1975) and occurs only locally in the Siran River basin, now mostly inundated by the Tarbela reservoir. Rocks of similar lithology as that of the southern Hazara continue westwards along the southern margin of the Peshawar plain in the Attock-Cherat Range to Khyber Agency near the Pakistan-Afghan border.

On the periphery of the Swat and Hazara regions, the Peshawar plain is a large alluvial intermontane basin that exposes scattered outcrops of alkaline igneous rocks (Kempe and Jan, 1970). The largest body of the suite is represented by the Ambela Granitic Complex that covers an area of about 900 km^2, comprising granites, syenites, carbonatite and dolerite (Rafiq, 1987). Other members of the alkaline suite, the Tarbela Complex being an exception, are volumetrically less significant and do not occur close to major tributaries. The Tarbela Complex stretches over a distance of about 4 km, but many outcrops have been removed or covered during the construction of the dam. It comprises gabbroic rocks, dolerites, albitites, granites, albite-carbonate and carbonatites (Jan et al., 1981c).

At the southern margin of the Peshawar plain, the Attock-Cherat Range consists of three east-west trending fault-bound blocks (Hussain et al., 1989). (1) The northern block consisting of Precambrian metapelites and minor limestone and quartzite, (2) The central block dominated by siltstone, argillite, quartzite and subordinate limestone of Precambrian Dakhner Formation. And finally, (3) the southern block, comprised predominantly of unfossiliferous limestone and dolomite and argillite and quartzite. Overall the Dakhner Formation is the most extensive formation in the Attock-Cherat Range.

c) In contrast to the Indus valley, the Kaghan valley contains extensive Salkhala Formation rocks. Chaudhry and Ghazanfar (1990) subdivided the rocks of Salkhala Formation into: (1) mid-Proterzoic to Archean Sharda Group consisting of (calc-pelitic, pelitic, and graphitic) gneisses, marbles with sheet granites, migmatites and amphibolites. The Sharda Group is bound in the south by the Luat-Batal Fault and continues in the north into the NPHM. Eastwards, in the Swat valley, the Alpurai Group may be correlated with the Sharda group (Treloar, 1989); (2) The late Proterozoic Kaghan Group consists of quartz schists, quartzites, graphitic schists, calc-schists, marbles, gypsum and metaconglomerates. The lateral extent of the Kaghan group is not clear, but the Sharda Group appears to be more extensive, and distinct from the former by its lack of quartzite and metaconglomerate and the presence of migmatites and bedded amphibolites (Chaudhry and Ghazanfar, 1990).

2.6 The Lesser and Sub Himalayas

The Lesser Himalayas are a fault bounded block, between the MCT and the MBT (Main Boundary Thrust), of weakly metamorphosed, late Proterozoic and Paleozoic sediments consisting mainly of carbonates, slates, quartzite, flysh and tillites (Windley, 1988). The terrain between MBT and the alluvial plain in the south constitutes the Sub Himalayas. The most characteristic and widespread rocks of the Sub Himalayas are the Siwaliks, a Neogene molasse sequence, named after Siwalik Hills near Hardwar in India, where the first world-famous vertebrate fossils were discovered (Medlicott, 1864). They extend as a continuos belt (~5 km thick) over a distance of more than 3000 km, from Aassam Ranges near the Brahmaputra River westwards, across the headwaters of the

Punjab rivers into the Kohat-Potwar region where they attain a width of about 140 km. They continue westwards into Afghanistan and Iran and in the south into the West Pakistan Fold Belt (Wadia, 1957; Gansser, 1964). The Siwaliks and the underlying Murree Formation are composed predominantly of Neogene sandstones, siltstones, clays and conglomerate (Wadia, 1957). The Murree Formation, consisting of red shale and sandstone, outcrops as a wedge near the Ravi River and widens up to 40 km in the Jhelum River valley. It continues in the northwest, turns around in the HKS, and continues westwards into Hazara and Kohat-Potwar region.

Lithologically, the bulk of the Siwaliks and Murree Formation closely resembles the modern alluvial deposits of the Indus. Petrographic and geochemical studies of sandstones in the Kohat-Potwar region indicate that the source region of the Siwalik sediments was located in the Kohistan island arc and in the northern margin of the Indian plate (Abbasi and Friend 1989; Cerveny et al., 1989). Thus, the Siwaliks are very similar to the modern alluvial deposits, except that the former are uplifted, indurated and deformed. The lithological similarity and uniform distribution of Siwaliks led several workers to suggest a river flowing through the region, named as Siwalik (Pilgrim, 1919) Indobrahm (Pascoe, 1920) Paleoindus (Behrensmeyer and Tauxe, 1982) or ancestral Indus (Cerveny et al., 1989).

South of the Potwar Plateau is the Salt Range known for its extensive salt deposits. It is an arcuate mountain range and constitutes the drainage divide between the Jhelum and Soan rivers. It is one of the rare regions of the world where marine Permian is followed by marine Triassic rocks and the Permo-Triassic boundary is clearly exposed. The Salt Range is comprised of the saliferous Eocambrian Salt Range Formation at the

base, followed upward by marine sediments of Cambrian age, a complete succession from

Permian to Eocene, and finally of fluviatile and lacustrine clastic sediments of Miocene

age (Gee, 1989). The region is deeply dissected by dried gullies where vegetation and

precipitation are scarce. As such, it contributes very little discharge to the Jhelum or Soan

River.

2.7 The West Pakistan Fold Belt

An almost continuos belt of marine to continental sediments extends from the

western flank of the HKS through Kalachitta and Kohat areas to the Sulaiman Range in

the west. The belt is approximately 15 km wide near Margalla Hills, tapering westwards

and reaches 70 km near the Pakistan-Afghan border. Also, in the upper reaches of the

Punjab rivers, particularly the Jhelum and Chenab, these rocks occur as a fault bound

block, thrust onto the Siwaliks. Kazmi et al. (1982) assigned a Paleocene to Eocene age to

the entire belt. These sediments have been studied in detail in three regions:

(a) In Parachinar, at the headwaters of the Kurram River, Meissner et al. (1975)

identified the following units: the undifferentiated Jurassic rocks (limestone and

interbedded sandstone and shale); the largely Cretaceous Kurram Formation (shale,

limestone and sandstone), and the undifferentiated Lumshiwal and Chichali Formation

(sandstone and shale).

(b) In the Kohat area to the east, the Cretaceous Kawagarh Formation occurs at

the base, followed upwards by Paleocene rocks of the Makarwal Group. The latter is

comprised of the Hangu Formation (sandstones and shales containing some coal beds),

the Lockhart Limestone, the Patala Formation (shales, limestones and sandstones). The

Makarwal Group is overlain by the Eocene Panoba Shale, the Sheikhan Formation (limestones and gypsum), the Kuldana Formation (gypsiferous and arenaceous shales and sandstones) and finally the Kohat Formation (limestone and shale), at the top. Rocks of the Kawagarh Formation and the overlying Makarwal Group, the Kuldana Formation (and the Kohat Formation only in the Potwar area) continue eastwards into the Potwar-Kalachitta and Hazara regions. The Margalla Hill Limestone and the Chor Gali Formation (limestone and shale) represent additional Eocene rocks.

(c) Hunting Survey Corporation (1960) mapped the entire fold belt between the Kurram basin and the mouth of the Indus River. The region has been subdivided into 91 formations whose description is beyond the scope of the present work. However, three main lithological and a structural/tectonic zone have been recognized. These are:

(i) The Axial Belt, a "tectonic fence" dividing the two main basins of sedimentation (Hunting Survey Corporation, 1960) that consists of Eocene to Pliocene or Lower Pleistocene marine to continental sedimentary rocks (Kazmi et al., 1982). In the Sulaiman and northern Kirthar ranges, the Axial Belt forms the drainage divide of the Indus River Basin with the Helmand Basin of Afghanistan, and in the Las Bela and Makran ranges with the Arabian Sea;

(ii) The Calcareous Zone, typified by limestones, but sandstones and shales dominates locally. It is either separated by a narrow band of Siwaliks or in direct contact with the alluvial deposits of the Indus flood plain. The rocks range in age from Triassic to Pleistocene and less commonly Permo-Carboniferous (Hunting Survey, 1960). On purely lithological basis, the Calcareous Zone conforms to the Pliocene-Eocene marine-continental sediments discussed above;

38

(iii) The Arenaceous Zone, comprised of sandstones and shales, mainly of Oligocene and younger ages. However, older rocks, predominantly limestones, crop out adjacent to the Calcareous Zone. This zone conforms broadly with the Siwaliks discussed above; and finally,

(iv) The Eruptive Zone that includes rocks of the Chagai volcanics that lie outside the Indus River Basin.

2.8 The Indus plain

After exiting the Himalayas near the Salt Range, the Indus River flows through a thick monotonous alluvial plain before draining into the Arabian Sea. The plain forms part of the Indo-Gangetic foredeep (Seeber and Armbruster, 1979) consisting of sediments of Tertiary-Holocene age that were derived from uplifted northern and western mountain belts and deposited on the Indian continental margin (Hunting Survey, 1960; Kazmi, 1984). In addition to alluvial sediments, sandy deserts form a significant part of the Indus plain. The eastern portion of the lower Indus plain is bordered by the Thar Desert and the interfluve between the Indus and the Jhelum-Chenab called the Thal Desert. The surface of the desert is a wild maze of sand dunes and sand ridges.

Although the Indus plain is the simplest component of the geology of the basin, it not only outweighs all other rock types but it also has distinct hydrogeological characteristics. The alluvial deposits are mainly sands with minor clays, silts and gravels. Throughout the middle and lower reaches of the Indus and in the Punjab plains they form extensive aquifers with the highest water yields (WAPDA, 1989b). In contrast to the crystalline and consolidated sedimentary rocks, hardly suitable for any agriculture and

39

supporting only sparse natural vegetation, the alluvial plains contain fertile soils and host large areas of croplands.

Surface soils of the middle and lower Indus plain have been derived from loess, old alluvial deposits, mountain outwash and recent stream deposits. The parent material is a mixed calcareous alluvium that is moderately to highly alkaline, with pH ranging between 8.2 and 10.0, and containing less than 0.75 % of organic material (Beg, 1993).

Chapter 3

Field and laboratory methods

3.1 Sampling

The Indus River and its major tributaries were sampled twice, during the winter and summer of 1994-95. Sample locations are shown in Fig. 3.1. Tributaries other than the Punjab rivers were sampled only once, just before their confluence with the Indus main channel. In the headwaters, five samples were collected from perennial springs in close proximity to Indus. The Indus main channel was sampled every month at Sukkur Barrage, for one year during the period March-1994 to February-95.

Sample locations on the Indus main channel were dictated mainly by the availability of bridges in the headwaters and dams and barrages in the plains. The objective was to sample the river along its downstream profile, away from the confluence of major tributaries, at regular intervals of 100 to 150 km. Water samples were collected by lowering 2.5 L, pre-washed, glass bottles in the middle of a river to a depth of about four meters. Figure 3.2 shows the layout for field and laboratory measurements.

3.2 Analyses on unfiltered water

3.2.1 pH and temperature

Immediately after sampling, the water temperature and pH were measured with a HACH One™ combination pH electrode. Buffer solutions of pH 7.00 and 10.00, bracketing the range of values observed in the Indus River, were used for calibration. A

buffer solution of pH 8.00 was measured as unknown before and after each sample. Precision and accuracy are given in Table 3.1.
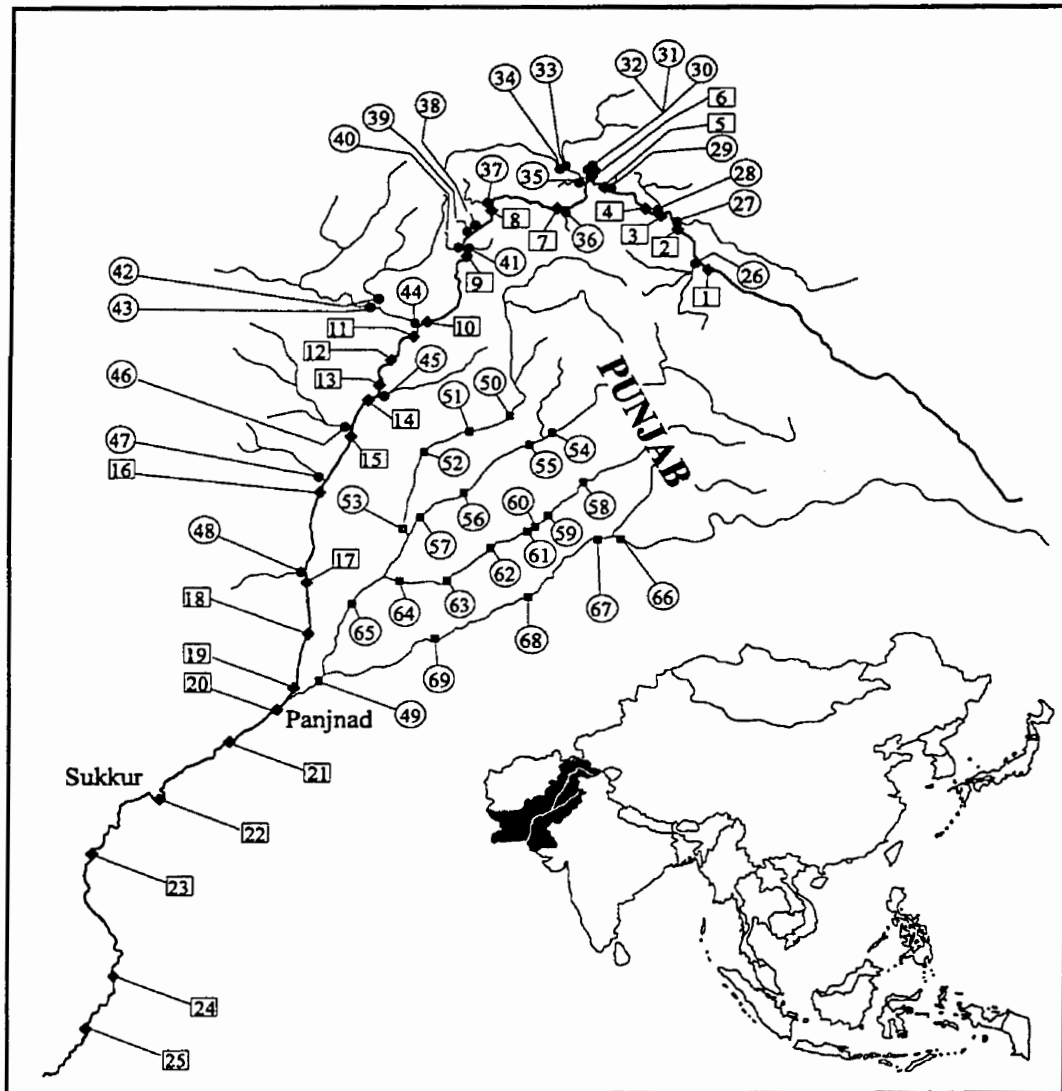
Fig. 3.1. Tributaries of the Indus River Basin and sample locations. Indus River (rhombs) at: Chambar bridge, 1; Humayun bridge, 2; Nar bridge, 3; Skardu bridge, 4; Stak, 5; Ansar Camp, 6; Chilas, 7; Dasu bridge, 8; Thakot bridge, 9; Ghazi, 10; Attock Toi, 11; Khushhal Garh bridge, 12; Makhad, 13; Jinnah Barrage, 14; Chashma Barrage, 15; Darya Khan, 16; Taunsa Barrage, 17; Ghazi Ghat bridge, 18; Sarki, 19; Mithankot, 20; Guddu Barrage, 21; Sukkur Barrage, 22; Dadu-Moro bridge, 23; Kotri Barrage, 24; Thatta bridge, 25. (caption contd. pp 43)

42

Tributaries (circles): Shingo, 26; Shyok, 27; Shigar, 28; Stak, 29; Shahbatot, 30; Sassi, 31; Khaltaro, 32; Hunza, 33; Gilgit, 34; Jaglot, 35; Gonar, 36; Khandian, 37; Kial, 38; Duber, 39; Khan, 40; Allai, 41; Swat, 42; Kabul, 43; Kabul at Kund, 44; Soan, 45; Kurram, 46; Shahur, 47; Sanghar, 48; Panjnad, 49.

Punjab rivers (squares), Jhelum River at: Jhelum, 50; Pind Dadan Khan, 51; Khushab, 52; Kot Shakir, 53. Chenab River at: Wazir Abad, 54; Qadir Abad Headworks, 55; Chiniot, 56; Jhang, 57; Multan, 65. Ravi River at: Syphen, 58; Shahdara, 59; Qila Korka, 60; Baloki, 61; Pindi Sheikh Musa, 62; Chichawatni, 63; Sidhnai Headworks, 64. Sutlej River at: Atari, 66; Sulemanki, 67; Islam Headworks, 68; Bhawalpur, 69.

3.2.2 Electrical conductivity (E.C.)

Electrical conductivity was measured in the field with a HACH Conductivity/TDS meter (model 44600). The instrument was calibrated prior to each test by a KCl standard solution (HACH). Electrical conductivity is reported in $\mu S cm^{-1}$ and total dissolved solids in mgL^{-1}.

3.2.3 Dissolved oxygen

Samples for dissolved oxygen were taken with a Teflon bailer which allows sampling of water from a particular depth and eliminates contact with the atmosphere, prior to measurement. Dissolved oxygen was measured in the field with an Orion (model 97-08) oxygen electrode. The electrode was calibrated in water-saturated air using a correction factor based on the elevation of sampling site. The sample was stirred gently with a magnetic stirrer and concentration of dissolved oxygen was read off the pH meter, connected to the electrode. The results are expressed in mgL^{-1}.

3.3 Analyses on filtered samples

Soon after collection the samples were filtered through 0.45 μm cellulose acetate filter paper, the pore size considered to be a boundary between suspended and dissolved

River Water

Unfiltered

Pressure Filtration

Syringe Filtration

Water Temperature

pH

Dissolved Oxygen

Electrical Conductivity

Alkalinity

Photometry NO_3,NH_3,SO_4 PO_4,SiO_2

Preservation with $HgCl_2$

Acidified with HNO_3

Unacidified

AAS

Ca,Mg,Na,K

ICP-MS Al, As, Ba, Cr, Fe, Mn, Ni, Rb, Sb, Sr, Ti,

Aliquots for $^{87}Sr/^{86}Sr$

HPLC Cl, F

Precipitate $BaSO_4$

Aliquots for δD & $\delta^{18}O$

Mass Spectrometric measurement of $^{87}Sr/^{86}Sr$, $\delta^{34}S$, δD, $\delta^{18}O$, $\delta^{13}C$

Pre-concentration/Extraction

Fig. 3.2. Experimental layout for field and laboratory work.

chemical constituents (Dominico and Schwartz, 1990). The effective pore diameter may be smaller than 0.45 μm in turbid waters of the Indus. In order to facilitate filtration, nitrogen gas pressure was employed on water in a glass column (Telmer, 1997).

3.3.1 Anions

Alkalinity was measured in the field by titration using a HACH digital titrator (model 16900-01) and standardized sulfuric acid. Bromcresol Green-Methyl Red indicator delineated the end-point. Alkalinity was measured as equivalent $CaCO_3$ and is expressed as HCO_3^-, since the latter constitutes over 95% of the dissolved inorganic carbon in the Indus River Basin (see chapter 6).

Sulfate, nitrate, ammonia, phosphate and dissolved silica were measured with a portable HACH spectrophotometer (model DR/2000). Detailed instrumentation is given in HACH (1989). Calibration curves were constructed using HACH standard solution and blanks. For sulfate the samples were diluted to a concentration range such that the steepest part of the calibration curve was used.

Chloride and fluoride were measured with a DIONEX100 High Pressure Liquid Chromatography (HPLC). Calibration curves were constructed using a control blank and DIONEX standard solutions.

Table 3.1. Detection limit, analytical precision and accuracy on standard samples for anions and other parameters measured in the field. Values under "analyzed" are averages for a minimum of five replicate measurements. Precision and accuracy are expressed in percent and the equations are given in section 3.4. E.C. = electrical conductivity; D.O. dissolved oxygen. All ions, SiO_2 and D.O. expressed in mgL^{-1}, E.C. in μScm^{-1}.

	Det. limit	Analyzed	Std. Dev.	Certified	Precision	Accuracy
SO_4^{2-}	1	41	2.08	40	5.1	1.7
HCO_3^-	-	48.3	2.83	-	5.9	-
NO_3^-	0.05	1.53	0.08	1.50	5.0	2.2
NH_3	0.01	0.32	0.00	0.30	1.1	6.1
PO_4^{3-}	0.01	1.10	0.01	1.00	0.9	10.0
SiO_2	0.001	4.700	0.01	5.000	0.2	-6.0
F^-	0.01	20.31	2.46	19.50	12.1	4.1
Cl^-	0.1	30.66	1.81	30.7	5.9	-0.1
pH	-	7.99	0.02	8.00	0.3	-0.1
E.C.	-	1421	4.51	1417	0.3	0.3
D.O.	-	8.07	0.57	-	7.0	-

3.3.2 Cations and trace elements

Samples for cations and trace elements were collected in 50 mL polypropylene containers. The tubes were washed with aqua regia, filled with de-ionized water, carried to the field as such and emptied just before sampling. Prior to sampling, they were thoroughly washed with filtered river water. Samples were acidified in the field with 0.5 mL, 8 M, ultrapure nitric acid.

Ca^{2+}, Mg^{2+}, Na^+ and K^+ were measured with a Perkin Elmer Atomic Absorption Spectrophotometer (AAS). Prior to analyses a Cs/La buffer solution was added to a suitable aliquot of each sample to suppress ionization. Trace elements were measured with a Fisons Inductively Coupled Plasma Mass Spectrometer (ICPMS). Analytical precisions and accuracies are given in Table 3.2.

Table 3.2. Detection limit, standard deviation, analytical precision and accuracy on standard samples for major cations and trace elements. Values under "analyzed" are average of six replicate analyses of a standard sample. Precision and accuracy are expressed in percent and the equations are given in section 3.4. Ca^{2+}, Mg^{2+}, Na^+ and K^+ in $mgL^{-1}$and the trace elements in ppb.

	Det. limit	Analyzed	Std. Dev	Certified	Precision	Accuracy
Ca^{2+}	0.1	8.1	0.10	8.0	1.2	1.3
Mg^{2+}	0.1	2.07	0.06	2.1	2.8	1.6
Na^+	0.1	2.53	0.06	2.5	2.3	1.3
K^+	0.1	0.72	0.02	0.7	2.4	1.4
Li	0.005	0.615	0.04	0.591	6.2	4.1
Al	2	101	4.21	97	4.2	4.0
Ti	0.05	3.07	0.12	2.60	3.9	17.9
Cr	0.1	0.25	0.02	0.2	6.5	23.2
Fe	5	44	1.91	42	4.4	4.5
Mn	0.1	11.5	0.40	10.8	3.5	6.9
Ni	0.2	0.78	0.05	0.8	5.9	2.9
As	0.1	0.67	0.10	0.6	14.4	11.4
Rb	0.05	1.55	0.06	1.52	3.8	1.9
Sr	0.5	66.7	1.82	66.0	2.7	1.0
Sb	0.01	0.067	0.01	0.07	10.4	3.9
Ba	0.2	16.7	0.29	16.9	1.8	0.9
U	0.005	0.026	0.00	0.024	10.7	6.5

3.3.3 Deuterium

For hydrogen and oxygen isotopes in river water, filtered samples were collected in 30 ml Nalgene®, low density, polyethylene bottles. In order to minimize evaporation, the bottles were filled completely, lids tightly closed and kept refrigerated.

Hydrogen gas was prepared by catalytic reduction of water with zinc. About 110 mg of Bloomington® zinc was dried in a breakseal under vacuum, by heating at temperature close to melting of Zn. 3 µL of water was injected into the breakseal and allowed to react at 500° C. Samples were processed in batches of eight, with two

additional internal laboratory standards included to correct for analytical drift. The hydrogen gas was analyzed with an automated double collector VG 602D mass spectrometer. The results are expressed in ‰ with reference to VSMOW and the analytical precision is ±1.7 ‰.

3.3.4 Oxygen

Oxygen-18 was measured by CO_2-water equilibration method of Epstein and Mayeda (1953). Three milliliters of samples were loaded in small vessels on an automated shaker, mounted on a water bath, maintained at 25° C. Carbon dioxide was fed into the vessels and allowed to equilibrate for 12 hours. The equilibrated CO_2 was subsequently analyzed on a triple collector VG SIRA 12 mass spectrometer. The results are expressed in ‰ with reference to VSMOW and the analytical precision is ±0.05 ‰.

Analytical precision for deuterium excess (d) is ±1.7 ‰, calculated as follows,

$$\sigma d \text{ (analyzed)} = \sqrt{(8 \ \sigma\delta^{18}O)^2 + \sigma \ \delta D^2} \qquad \text{(After Gat and Dansgaard, 1972)} \qquad (3.1)$$

3.3.5 Sulfur and oxygen in sulfate

Dissolved sulfate was precipitated in the field as $BaSO_4$ by lowering the pH of water with HCl to about 2 and adding a saturated solution of $BaCl_2$. The precipitate was collected on a 0.45 μm cellulose acetate filter paper, washed profusely with deionized water, dried at 110° C and scraped off the filter paper. The $BaSO_4$ was converted into SO_2 by the method of Coleman and Moor (1978), followed by isotopic analyses on a triple collector VG SIRA 12 mass spectrometer. A mixture of 17.5 mg of $BaSO_4$, 125 mg of CuO and 200 mg of quartz was combusted under vacuum, for about 20 minutes at

1100° C. The SO_2 was purified cryogenically, using ethanol and liquid nitrogen slurry at -80° C and -125° C. Two internal laboratory standards were included with each batch of samples and used subsequently to correct for analytical drift. The results are expressed with reference to ‰ CDT and the analytical precision is ±0.2 ‰.

The oxygen-18 isotopic composition of sulfate was measured on CO_2 prepared by graphite reduction of $BaSO_4$ (Shakur, 1982). Briefly, the $BaSO_4$ was mixed with graphite (1:1) in a platinum boat, heated to below 600° C for 15 to 30 minuets to expel water vapors. The mixture was heated at 900 to 1100° C to release CO, the latter being spark discharged to CO_2 that was analyzed on a VG Micromass 903. The results are expressed in ‰ with reference to VSMOW and the analytical precision is ±0.5 ‰.

3.3.6 Dissolved inorganic carbon (DIC)

Samples for dissolved inorganic carbon were filtered through a 0.45 μm, cellulose acetate, CAMEO® filter, fitted on a syringe. In order to prevent loss of DIC through photosynthesis, bacterial respiration and degassing, brown glass bottles with airtight caps were used and the samples were poisoned with $HgCl_2$.

A known volume of sample was acidified under vacuum with H_3PO_4. Carbon dioxide degassed from water was recovered quantitatively, using liquid nitrogen. The accompanying moisture was subsequently removed by freezing with a slurry of ethanol and liquid nitrogen at -80° C. The CO_2 gas was analyzed on a triple collector VG SIRA 12 mass spectrometer.

Three triplicate water samples, collected at three different locations were analyzed to check for reproducibility of results. The standard deviation for the three sets

range between 0.01 and 0.2 ‰. These estimates cover the reproducibility for the entire procedure from sampling through extraction of CO_2 to analyses on the mass spectrometer.

3.3.7 Strontium

Appropriate volume of water was evaporated to dryness for strontium isotope analyses. The residue was dissolved in ultrapure HCl and strontium extracted on Dowex® AG50-X8 ion exchange resin. The $^{87}Sr/^{86}Sr$ ratio was measured with a Finnigan MAT 261 multicollector thermal ionization mass spectrometer. Procedural blanks for $^{87}Sr/^{86}Sr$ were less than 750 picograms. All samples were corrected for mass fractionation, $^{86}Sr/^{88}Sr = 0.1194$. Fifteen analyses of NBS 987 gave a mean value ($\pm 2\sigma$) of 0.710239 ±0.000014.

3.4 Precision and Accuracy

Analytical precision and accuracy were evaluated using standard samples. The calculations are based on the following equations.

$$\text{Precision} = (\text{Standard deviation/mean concentration}) \cdot 100 \qquad (3.2)$$

$$\text{Accuracy} = \{ (C_{(analyzed)} - C_{(certified)})/C_{(certified)} \} \cdot 100 \qquad (3.3)$$

Standard deviations are based on replicate measurements for a parameter on a standard sample and mean concentration is the average of all these measurements. $C_{(analyzed)}$ is the mean concentration measured during this study and $C_{(certified)}$ is the concentration of the standard sample established by the manufacturer.

In the absence of standard solution for HCO_3^- and dissolved oxygen their analytical accuracy cannot be ascertained directly. Nevertheless, the HCO_3^- concentrations measured in the field compare well with those recalculated from CO_2 yield (Fig. 3.3) in the laboratory (see section 3.3.6).

Recalculated = 0.98 (titration) - 1.36
$r^2 = 0.84$
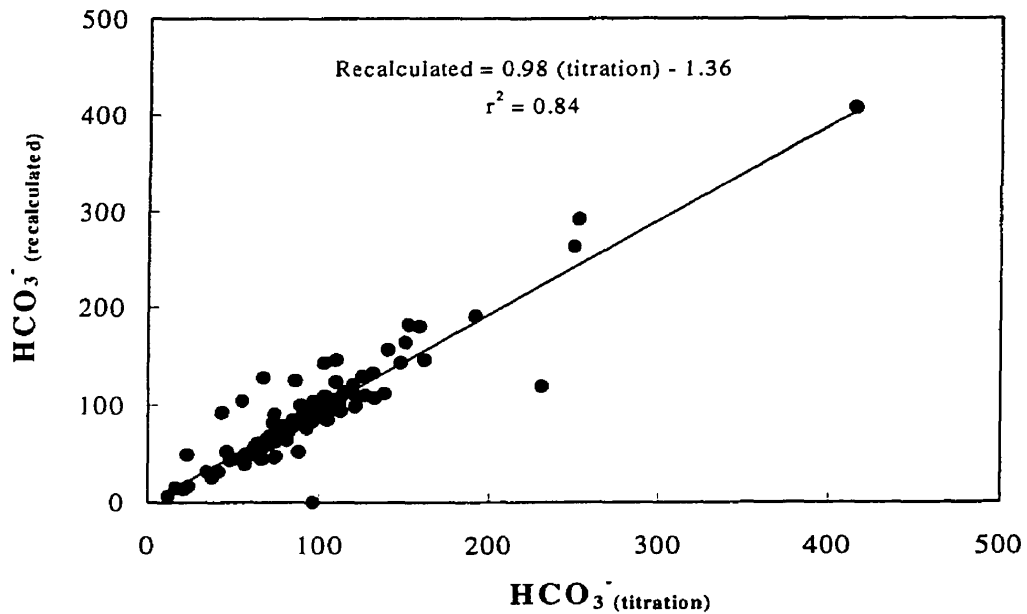
Fig. 3.3. Scatter plot for bicarbonate concentration measured in the field versus recalculated bicarbonate concentration from carbon dioxide yield in the laboratory, both expressed in mgL^{-1}.

3.5 Delta permil notation

Stable isotopes are measured as the ratio of the least abundant isotope to the most abundant isotope of a given element. For example, ^{18}O, the most widespread isotope of oxygen has a terrestrial abundance of about 0.2 %, compared to ^{16}O which represents about 99.8 %, corresponding to an $^{18}O/^{16}O$ ratio of 0.002. Measurement of this true ratio in geological materials is difficult, and since variations in stable isotope

concentration are more important than the actual abundances, isotope ratio is measured relative to a standard. The relative difference is denoted by δ and is defined as:

$$\delta_x = (R_x - R_{std})/ R_{std}$$

$$R_{std} = [(R_x / R_{std}) - 1] \cdot 10^3$$

Where R_x represents isotopic ratios of a sample ($^2H/^1H$, $^{18}O/^{17}O$, $^{34}S/^{32}S$, $^{13}C/^{12}C$) and R_{std} is the isotopic ratio of the corresponding standard: Vienna Standard Mean Ocean water (VSMOW) for $^2H/^1H$ and $^{18}O/^{17}O$; Canon Diablo troilite (CDT) for $^{34}S/^{32}S$; and Pee Dee Bellemnite for (VPDB) $^{13}C/^{12}C$. Variations in isotopic concentrations are not very large, as such the δ–values are expressed in parts per thousand or permil (‰) difference from the reference. A δ-permil value of +10 for oxygen signifies that the sample is 10 ‰ enriched in ^{18}O over the reference. Similarly, a negative value would indicate that the sample is depleted by the same amount over the standard.

All the above laboratory measurements, except for cations, trace elements, Sr isotopes and oxygen-18 of sulfates were performed in the G.G. Hatch Isotope Laboratories of the University of Ottawa. Cations and trace elements were determined at the Geological Survey of Canada and Sr isotopes at Carleton University, both institutions in Ottawa. Oxygen-18 of sulfates was analyzed at the University of Calgary.

Chapter 4

Oxygen and deuterium isotopes

4.1 Overview

The deuterium and oxygen isotopes in precipitation are linearly related and expressed on a global scale by the following empirical relationship:

$$\delta D = 8\delta^{18}O + 10\%o \; VSMOW \qquad (Craig, 1961) \qquad (4.1)$$

This defines the so-called Global Meteoric Water Line (GMWL). On a smaller scale, however, depending on climatic and geographic factors, the isotopic composition of precipitation may deviate from the above relationship in both slope (8±1 to 1.5) and intercept (10±10 to 15), thus producing a series of Local Meteoric Water Lines (LMWL). In general, the isotopic composition of precipitation correlates with air temperature, therefore moving from coastal regions to higher latitudes (the continental effect) or higher altitudes (the altitude effect) precipitation becomes progressively depleted in the heavy isotopes. In addition, factors such as the intensity of precipitation (the amount effect), vapor transport history and the seasonal effects of precipitation may locally control the isotopic composition of precipitation.

Although in-cloud processes of condensation and rain formation are complex, the conversion of vapor to rain seems to maintain isotopic equilibrium, following a line with a slope of 8 (Craig, 1961). However, the slope can decrease due to secondary evaporation following condensation during rainfall (Friedman et al., 1962) or from surface waters (Dincer, 1968; Fontes et al., 1970; Yang et al., 1996).

During primary evaporation at the sea surface, the $\delta^{18}O$ - δD relationship in the resulting precipitation is controlled primarily by relative humidity and sea surface temperature (Ciais and Jouzel, 1994). At low relative humidity, kinetic evaporation dominates and the resulting precipitation is characterized by higher values for the intercept. At the other end, under higher relative humidity the system approaches equilibrium conditions with a lower value for the intercept. Dansgaard (1964) defined the deuterium excess parameter d (d = dD - $8\delta^{18}O$), a property fixed in the atmospheric moisture by air-sea interaction processes (Craig and Gordon, 1965) during primary evaporation. This characteristic feature may however be altered by secondary evaporation during rainfall (Ehhalt et al., 1963; Gat, 1971) or from surface waters (Salati et al., 1979) that lowers the d-excess.

4.2 Deuterium and oxygen isotopes in the Indus River Basin

Sample locations of the studied samples are shown in Fig. 3.1. Analytical procedures for deuterium and oxygen isotopes are given in Chapter 3 and isotope data in Appendix B.

4.2.1 The winter season

Figure 4.1 shows covariation between δD and $\delta^{18}O$ for samples collected during the winter season. The headwater tributaries and the Indus main channel are depleted whereas the lowlands and the lower reaches of the Indus become progressively
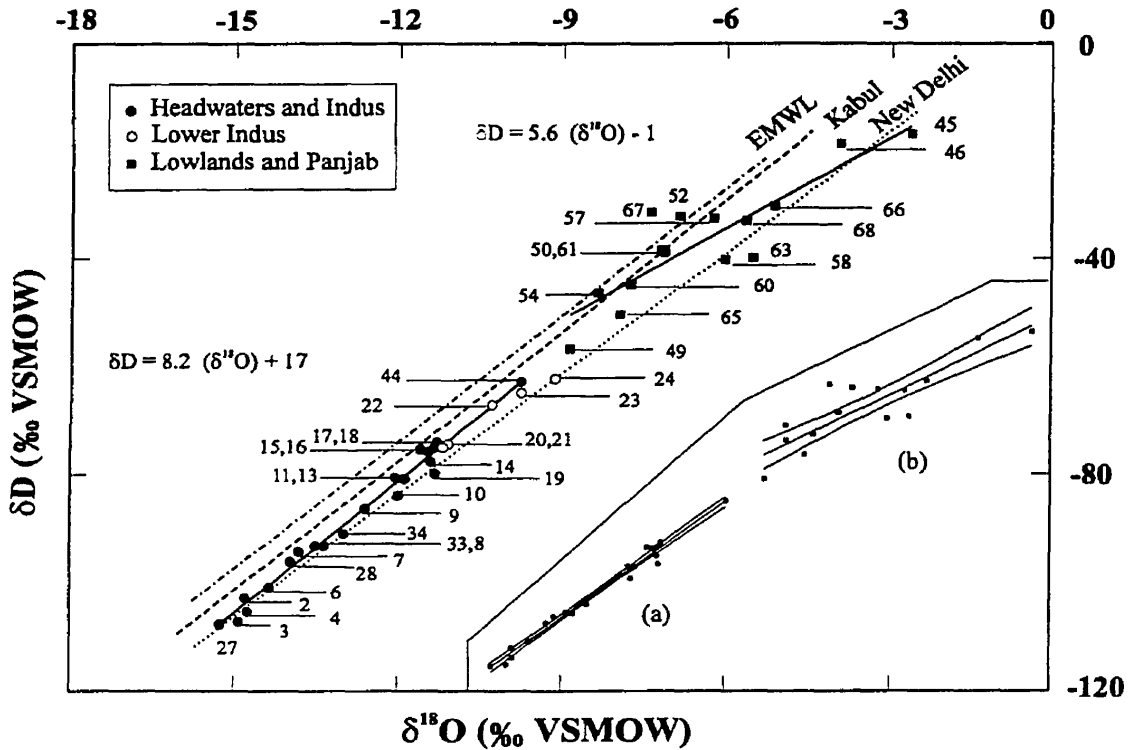
Fig. 4.1. Scatter plot of δD versus $\delta^{18}O$ for water samples collected from the Indus River Basin during the winter season. Dashed lines are Local Meteoric Water Lines: EMWL, Eastern Meteoric Water Line, $\delta D = 8.08\delta^{18}O + 22$ (Gat and Carmi, 1970); Kabul, $\delta D = 8.01\delta^{18}O + 19$; and New Delhi, $\delta D = 7.6\delta^{18}O + 7$ (IAEA-WMO). The lower and upper solid lines are least square fits through the headwaters + the Indus River upstream from Panjnad and the lowland + Punjab respectively. The inset (a) and (b) shows the upper and lower confidence limits at the 95% significance level for the headwaters + Indus and the lowlands + the Punjab, respectively. Confidence limits established following the method described in Payne (1992). The key to sample numbers as in Fig. 3.1.

enriched in the heavy isotopes. Before Panjnad confluence, the Indus main channel and the headwater tributaries evolve along a straight line defined by the following relationship:

$$\delta D = 8.2\ \delta^{18}O + 17 \qquad (4.2)$$

55

The slope is similar but the intercept higher than that of the GMWL. Isotopic enrichment in this part of the basin is caused mainly by decrease in altitude. Here the Indus main channel declines from an altitude of about 4,700 to 400 masl. The lowland and the Punjab rivers as well as the Indus River downstream from the Panjnad confluence show enrichment in the heavy isotopes but along a line with a lower slope (Fig. 4.1). The lowland and the Punjab samples define the following relationship:

$$\delta D = 5.6 \, \delta^{18}O - 1 \qquad (4.3)$$

The Indus River downstream from the Panjnad confluence has a similar relationship ($\delta D = 6.4 \, \delta^{18}O - 3$). The enrichment in heavy isotopes and lower slope on δD - $\delta^{18}O$ diagram for samples from this part of the basin is caused by evaporation from open water bodies, caused by arid climate.

4.2.2 The summer season

In general, isotope variations in the summer are similar to those in the winter season and can be accounted for by processes discussed above. However, there are distinct seasonal differences:

(1) The Indus main channel and the headwater tributaries are depleted in ^{18}O in the summer compared to the winter season (Fig. 4.2). A similar difference exists for δD. This shift in isotopic composition could be due to (a) greater contribution of groundwater during the winter season, the former undergoing evaporative enrichment during summer recharge. If so, river waters should display an evaporative trend. The lowland tributaries and the Indus River downstream from Panjnad are an example of this process (Fig. 4.3). However, for the headwaters, and for the rest of the Indus River, the absence of an

evaporative trend precludes that such a process could be a cause of the isotopic changes. By the same token, evaporation from reservoirs and open surface bodies can also be discounted, since it causes similar isotope effects. (b) Seasonal changes in altitude of snow melting can produce the observed shift in isotopic composition, with melt water generation in valleys during the winter and on peaks and summits during the summer season. Summer transgression of snow line therefore seems to be a likely process for the isotopic shift.
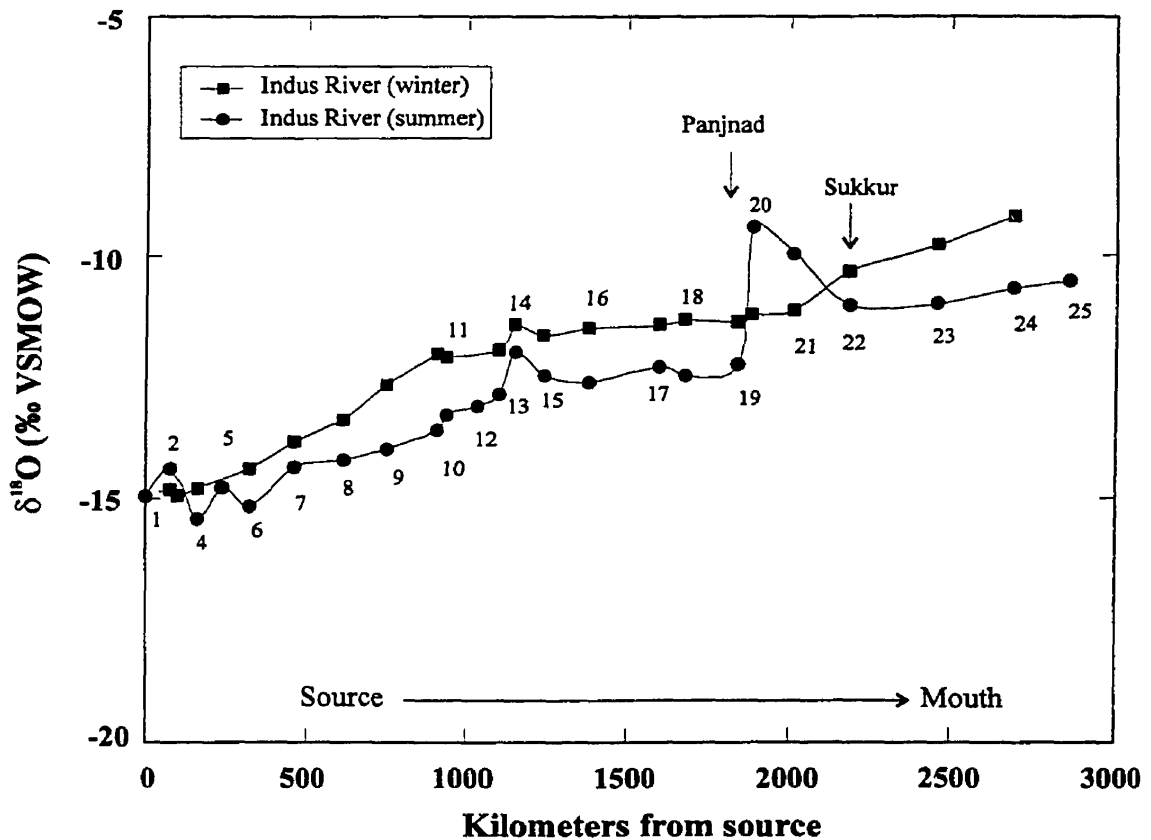
Fig. 4.2. Oxygen isotope ratios of waters from the Indus River plotted as a function of river kilometers from source to mouth. The calculated gradient is 1.5 and 1.9‰ 1000 km⁻¹ for $\delta^{18}O$ for the summer and winter seasons, respectively. The gradient for δD is 14.5 and 13.5‰ 1000 km⁻¹ for the summer and winter seasons, respectively. The arrow points in the direction of flow of the Indus. The key to the sample numbers as in Fig. 3.1.

57

(2) Another peculiar feature of the Indus main channel during the summer season is a 2.8‰ spike in $\delta^{18}O$ after the Panjnad confluence (Fig. 4.2). In this area, the $\delta^{18}O$ of the Indus changes from -12.2‰ before the confluence to -9.4‰ after the confluence. The observed shift is caused by discharge from the Panjnad with a $\delta^{18}O$ of -8.4‰. At Guddu barrage, downstream from the Panjnad confluence, the Indus main channel becomes depleted in the heavy isotopes and the trend continues until Sukkur barrage (Fig. 4.2). In this stretch of the Indus River no major tributary joins the river and discharge of local groundwater can be ruled out since the latter would have the opposite effect. Incomplete mixing with "old depleted water" in the Guddu and Sukkur barrages apparently causes the depletion in heavy isotopes.

Figure 4.3 shows the covariation of $\delta^{18}O$ and δD for the headwater tributaries and the Indus main channel upstream from the Panjnad confluence, defined by the following linear relationship:

$$\delta D = 8.4\delta^{18}O + 23 \qquad (4.4)$$

The lowland tributaries and the Panjnad on the other hand plot along a line with a shallower slope and a smaller value for the intercept given by the following equation:

$$\delta D = 6.7\delta^{18}O + 5 \qquad (4.5)$$

The Indus main channel downstream from Panjnad follows a similar trend given by:

$$\delta D = 6.8\delta^{18}O + 7 \qquad (4.6)$$

$\delta D = 6.7 (\delta^{18}O) + 5$

$\delta D = 8.4 (\delta^{18}O) + 23$

- ● Headwaters and Indus
- ○ Lower Indus
- □ Lowlands and Punjnad

EMWL

Kabul

New Delhi

δD (‰ VSMOW)

$\delta^{18}O$ (‰ VSMOW)
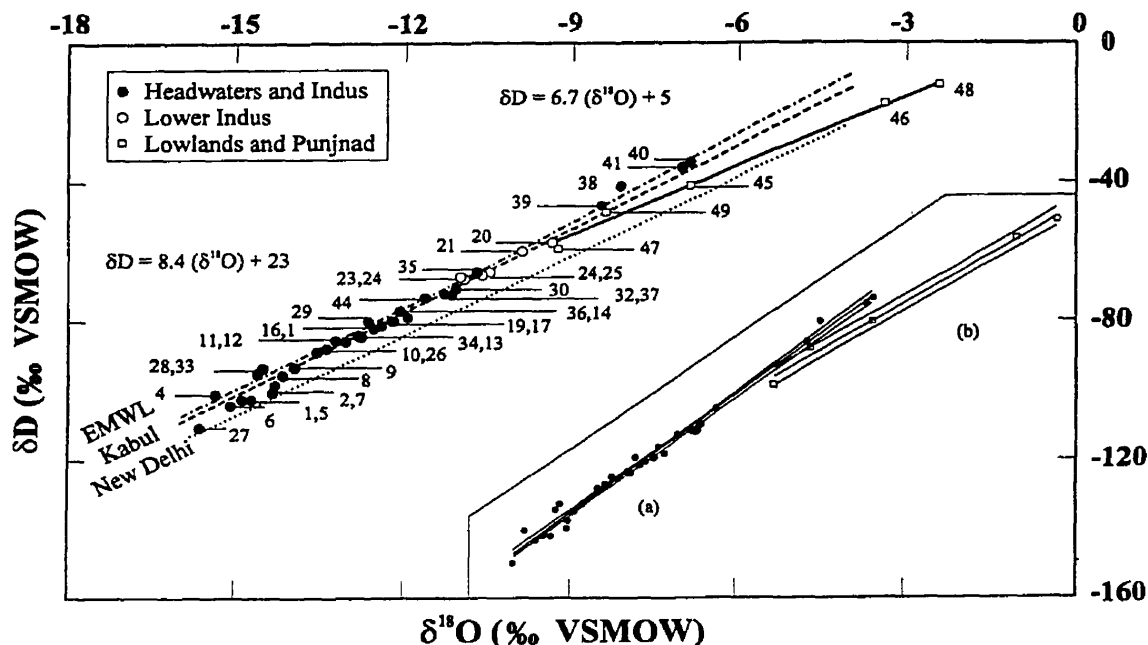
Fig. 4.3. Scatter plot of δD versus $\delta^{18}O$ of water samples collected from the Indus River Basin during the summer. Dashed lines are Local Meteoric Water Lines: EMWL, Eastern Meteoric Water Line, $\delta D = 8.08\delta^{18}O + 22$ (Gat and Carmi, 1970); Kabul, $\delta D = 8.01\delta^{18}O + 19$; and New Delhi, $\delta D = 7.6\delta^{18}O + 7$ (IAEA-WMO). The solid line is a least square fit through the lowland tributaries + the Panjand. Regression line through the headwaters + the Indus has been omitted for clarity. Note that the equation given for the headwaters and the Indus does not include samples downstream from Panjnad. The inset (a) and (b) shows the upper and lower confidence limits at the 95% significance level for the headwaters + Indus and the lowland tributaries + Panjnad respectively. Confidence limits established following the method described in Payne (1992). The Key to the sample numbers as in Fig. 3.1.

4.2.3 Temporal variations

Figure 4.4 shows $\delta^{18}O$ measurements and water discharge at the Sukkur monitoring station. The Indus main channel has a rather uniform composition ranging between -8.2 and -11.9‰ for $\delta^{18}O$ and between -53 and -81‰ for δD, with discharge weighted averages of -11.1 and -70‰, respectively. The gradual increase in $\delta^{18}O$ at Sukkur during the spring probably indicates a greater contribution of the Panjnad. At

Ghazi, a few km downstream from Tarbela dam, the $\delta^{18}O$ of the Indus varies between -4 and -14‰ (D.Dettman, pers. comm., 1996). Within the Indus River Basin, oxygen isotope values higher than -7.0‰ are found only in the lowland tributaries and the anomalously heavy $\delta^{18}O$ values might therefore be due to unmixed local sources.
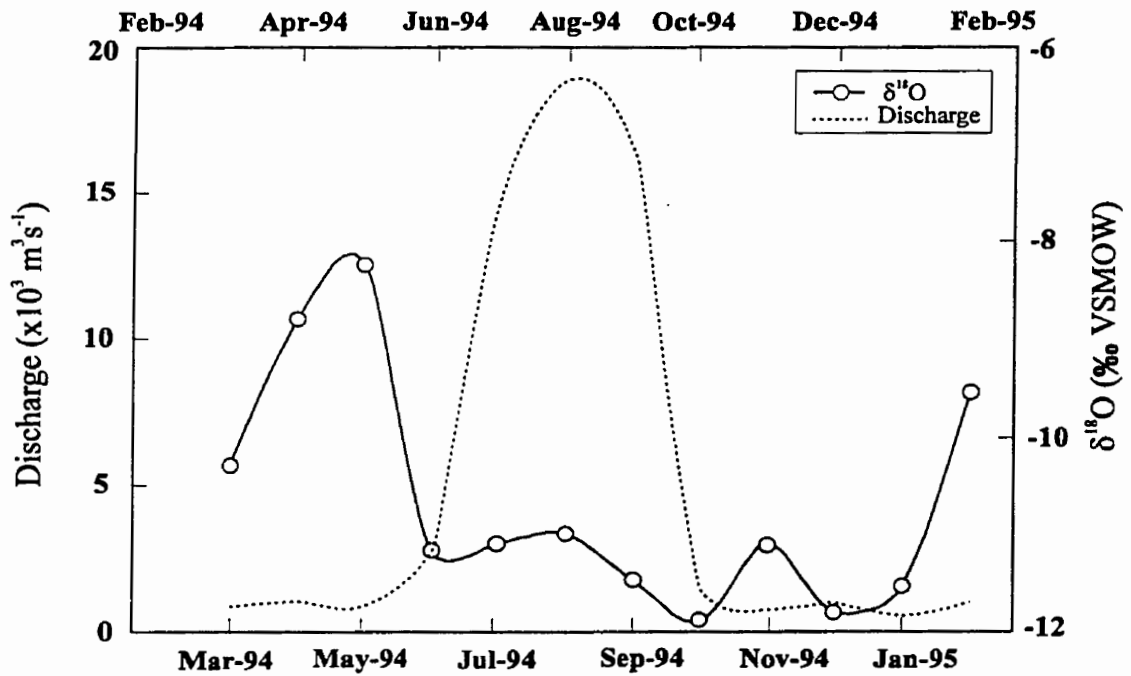
Fig. 4.4. Monthly time series of instantaneous discharge and $\delta^{18}O$ at Sukkur barrage. Discharge data from WAPDA unpublished records.

On a δD vs $\delta^{18}O$ plot (Fig. 4.5) the Indus River at Sukkur defines the following relationship:

$$\delta D = 7.5\delta^{18}O + 10 \qquad (4.7)$$

60

The slope and intercept are similar to that of the GMWL. On a monthly and seasonal basis, however, the deuterium excess varies, ranging from 12 in May to 20‰ in August, with discharge weighted average of 18‰ (Fig. 4.6). This implies that bulk of the discharge in the Indus River is derived not from typical monsoon rains but from melting of snow in the headwaters. Considering that the Indus flows for a significant distance through arid regions, it is interesting to note that isotope data suggest a lack of direct evaporation, at least in comparison with the GMWL. It is therefore imperative to compare the river water data with that of local precipitation.
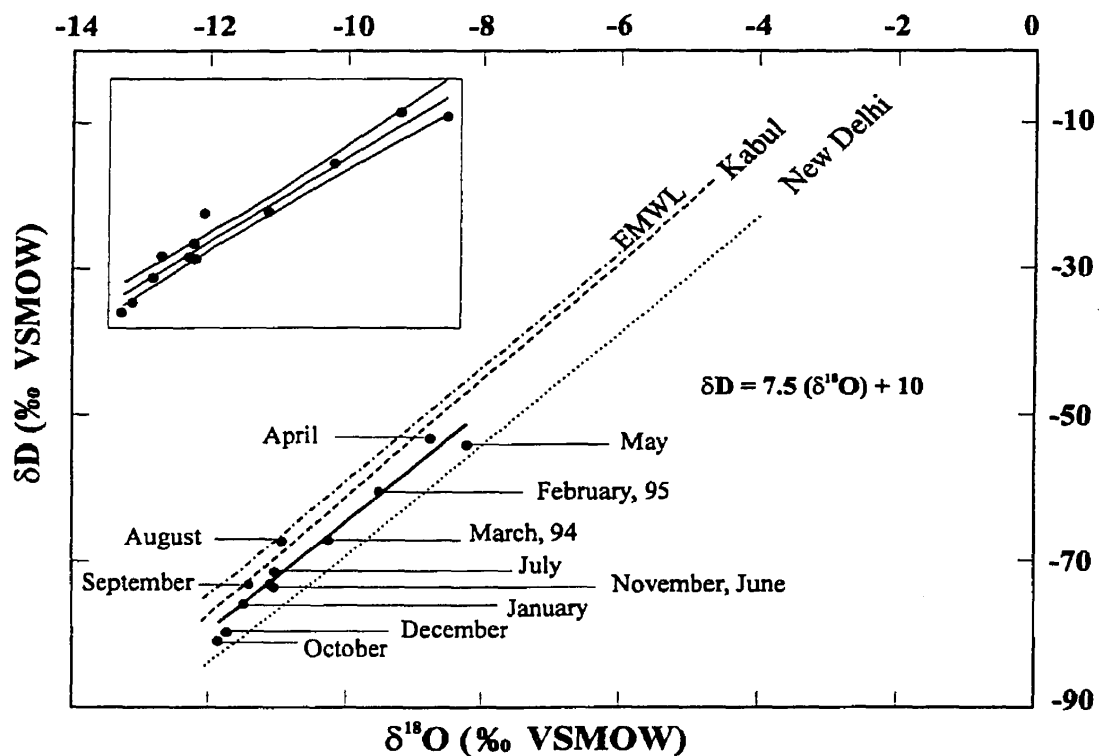
Fig. 4.5. Scatter plot of δD vs $\delta^{18}O$ for time series at the Sukkur barrage. The solid line is regression through the data. Dashed lines are Local Meteoric Water Lines: EMWL, Eastern Meteoric Water Line, $\delta D = 8.08\delta^{18}O + 22$ (Gat and Carmi, 1970); Kabul, $\delta D = 8.01\delta^{18}O + 19$; and New Delhi, $\delta D = 7.6\delta^{18}O + 7$ (IAEA-WMO). The heavy line is a least square fit through the data points. The inset shows the upper and lower confidence limits at the 95% significance level on the regression. Confidence limits established following the method described in Payne (1992).

61

International Atomic Energy Agency (IAEA) and World Meteorological Organization (WMO) have compiled long term isotope data for worldwide precipitation. Two of these stations, Kabul and Karachi, are in the Indus River Basin and New Delhi in close proximity. Karachi is a coastal station, influenced by maritime conditions and is therefore not considered for comparison. The Eastern Meteoric Water Line (EMWL) is characteristic of the Mediterranean climate and New Delhi that of the Indian Monsoon (Fig. 4.5). The Indus River Basin lies in a transitional zone between these climatic extremes. Theoretically, waters that have undergone evaporation, should plot along a line at a shallower slope than the LMWL, intersecting the later at a point representing the unaltered precipitation. It is clear that samples from the Indus do not deviate appreciably in slope from Kabul or New Delhi. Although climatic conditions are conducive to evaporation, the lack of such an isotopic signature suggests the following: (1) The Indus River Basin is a fast flowing system and evaporation is limited due to short residence time of water (~1 year); (2) In the driest parts of the basin if it rains at all, runoff occurs only during extreme events that have little influence on the water budget of the Indus; and 3) River discharge constitutes only about one-fourth to one-eighth of the precipitation flux (see chapter 1 and 7). The missing volume must either be transpired by crops or transmitted to the groundwater reservoir. The former cannot be quantified, because unlike evaporation it does not fractionate isotopes. The relative magnitude of the two processes is therefore difficult to constraint. However, groundwater water table elevations rose up to 27 m in the Indus plains due to irrigation canals (Clark and Fritz, 1997), suggesting that artificial groundwater recharge is indeed responsible for the missing volume of water.
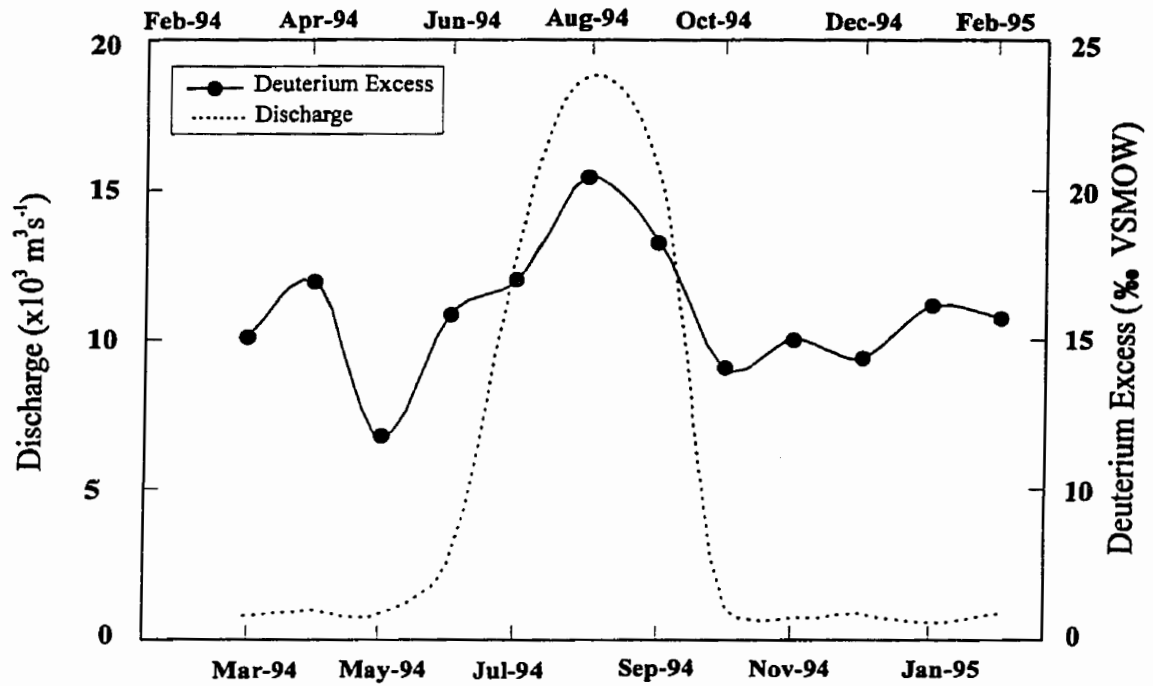
Fig. 4.6. Monthly time series for instantaneous discharge and deuterium excess ($d = \delta D\text{-}8\ (\delta^{18}O)$) at the Sukkur barrage. Discharge data from WAPDA, unpublished records.

4.3. Moisture source of precipitation in the Indus River Basin

The source of water to the upper Indus and its headwater tributaries is mainly melting of snow in the Karakoram, Himalayas and the Hindukush. While the Punjab rivers derive their runoff from both melting of snow and direct rainfall, the lowland tributaries are exclusively rain fed. Potential sources of moisture in the northern mountain ranges are the Indian summer monsoon, originating in the Bay of Bengal and in the Arabian Sea and a westerly source originating in the Mediterranean region during the winter season.

During the summer of 1995, the Punjab rivers upstream from link canals ranged in $\delta^{18}O$ from -10.32‰ for the Jhelum to -12.78‰ for the Chenab, with the Ravi and Sutlej exhibiting intermediate values. In the same year, Panjnad had a $\delta^{18}O$ of -10.56‰. For the entire Punjab basin, during this period, oxygen and deuterium have the following relationship.

$$\delta D = 7.4 \ (\delta^{18}O) + 7 \qquad (4.8)$$

During the summer of 1994, only the Panjnad was sampled and had a $\delta^{18}O$ of -8.39‰. The Punjab plains are heavily influenced by the summer monsoons, their intensity and timing varying from one year to another. The headwaters of the Punjab rivers also derive their runoff from snowmelt in the Himalayas. Published isotopic data on precipitation in the region impose the following constraints for the source of moisture:

1) New Delhi has a long term weighted average $\delta^{18}O$ of -5.9‰ (IAEA-WMO).

Assuming an average $\delta^{18}O$ gradient of -2.0‰ per 1000 km for the Indian monsoon (Krishnamurthy and Bhattacharya, 1991), the $\delta^{18}O$ of precipitation in the Punjab plains should be around -7.0‰. This value is similar to that of the Panjnad in the summer 1994, when the Punjab plains received heavy monsoon rains and is very close to that of the Soan River (-6.9‰, summer 1994), that drains a low altitude basin, where precipitation is exclusively in the form of rain. However, the depleted $\delta^{18}O$ of Panjnad in the summer 1995 reflects snow melting in the headwaters. Furthermore, this value is very similar to that of the Jhelum River at the entrance to the Punjab plains. This implies that the Jhelum River dominated the water balance at Panjnad in the summer 1995 and that there was little contribution from the plains.

2) If precipitation in the headwaters of the Punjab rivers were derived from the Indian monsoons, using the shallowest $\delta^{18}O$ topographic gradient of -0.2‰ per 100 m for low latitude precipitation (Niewodniczanski et al., 1981), the same air mass that precipitates at New Delhi (altitude 200 masl) will over the Punjab headwaters at an average altitude of 3,200 masl, precipitate with a $\delta^{18}O$ of ~ -12.0‰. Using the same topographic gradient and air mass of New Delhi, the Soan River at ~1000 masl should have a $\delta^{18}O$ of about -7.5‰.

Figure 4.7 shows the $\delta^{18}O$ plotted versus mean altitude for all the tributaries of the Indus River Basin sampled during the summer season. Although the Kurram (46) and Sanghar (48) rivers are slightly evaporated, they are at a relatively higher altitude than the Soan River (45), but have more enriched $\delta^{18}O$ than the latter. Similarly, the Shahur River (47) is at a similar altitude as the Soan, but its $\delta^{18}O$ is depleted if compared to the latter. This might suggest that altitude effect is not important and factors other than altitude might control the isotopic composition in monsoon systems. Similar observations (Niewodniczanski et al., 1981; Wake and Stievenard, 1995) have been made elsewhere in the Himalayas. In the headwater tributaries and the upper reaches of the Punjab rivers, however, the $\delta^{18}O$ decreases with altitude (Fig. 4.7). This change in isotope effect from no clear relationship between $\delta^{18}O$ and altitude in the lowlands to a negative correlation in the headwaters occurs on the southern slopes of the Himalayas. This would imply that (1) the altitude effect plays a role only after a certain threshold value and/or (2) the lowlands and the headwaters are distinct systems with separate sources of moisture: a low altitude wind system (monsoon) in which precipitation is modified very little after

condensation due to short residence time in the humid air column; and a high altitude wind system such as the Westerly Jet Stream.
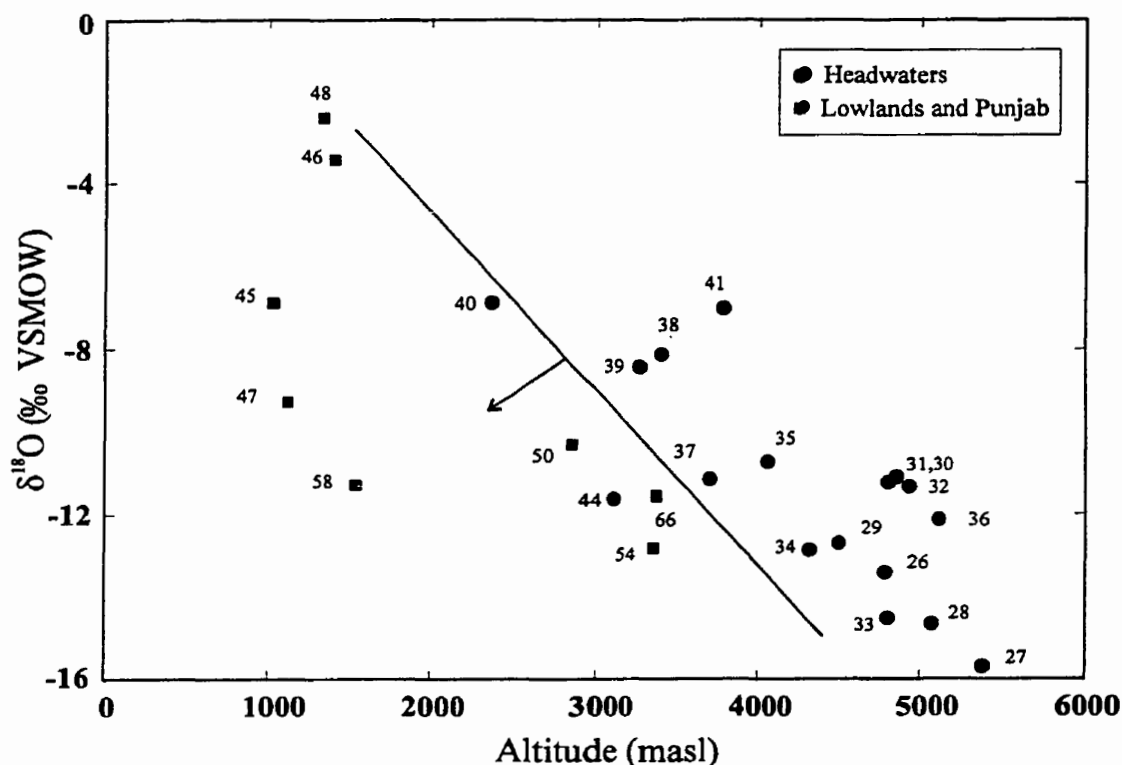
Fig. 4.7. Scatter plot of $\delta^{18}O$ versus mean altitude of sub-basin catchments. The line roughly defines the watershed boundary of the southern slopes of Himalayas and the arrowhead points in the downslope direction. Source of topographic data is NGDC (1988). Numbers as in Fig. 3.1.

The deuterium excess parameter can be used to distinguish between the two regimes. Precipitation in the eastern Mediterranean is characterized by a d-excess of ~20‰ (Gat and Carmi, 1970), while that of the monsoon exemplified by New Delhi is ~8‰ (IAEA, 1992). Although d-excess is considered to reflect physical conditions prevailing at the time of primary evaporation, some studies have shown that other

processes might influence it. Examples of such processes are: (a) Secondary evaporation from open surface waters such as rivers and lakes (Salati et al., 1979; Gat et al., 1994) reduces d-excess of the residual water and results in vapors that on condensation yields precipitation with a high d-excess. The lack of open surface water bodies in the Indus River Basin rules out such process as a cause of the observed increase in d-excess; (b) Change in the form of precipitation from rain to snow results in higher d-excess values in polar snow due to kinetic isotope effects during vapor deposition leading to snow formation (Jouzel and Merlivat, 1984). A direct assessment of the influence of this process is to compare d-excess in snow and that in rain of monsoon regime. Unfortunately, isotopic data exist mainly for $\delta^{18}O$ in ice cores (Wake, 1987; Wake, 1989b; Aizen et al., 1996), but in one study (Niewodniczanski et al., 1981), on the western periphery of the Indus basin, both δD and $\delta^{18}O$ were measured on snow (fresh October snowfall) in the Himalayas. In this study of altitude effect in the South American Andes, the Central Asian Hindus Kush, Mounts Kenya and Kilmanjaro, Africa and the Himalayas, the latter were uniquely devoid of altitude effect at 17 sites between 4400 and ~6000 masl. The d-excess ranged between 8 and 15, with an average of 11‰. This value is only slightly higher than the long term average d-excess of ~8‰ for New Delhi, suggesting that the higher d-excess in the Indus River Basin is not a secondary effect.

Aizen et al. (1996) studied $\delta^{18}O$ in ice cores in the southeastern Tibet, northern Himalayas and central Tien Shan. The latter are about 1000 km NE of the Indus River Basin. Compared to the other two locations, central Tien Shan has a uniform and relatively enriched $\delta^{18}O$ and that was attributed to moisture source that originated over the Caspian or Mediterranean Seas. Nakai et al. (1987) showed that the d-excess for

precipitation in Tibet and southwestern China could be classified into two groups according to the origin of water vapor. The first one, with a d-excess of <10‰ comes from the southern Indian Ocean during the summer monsoon and the second one with d-excess of ~20‰ is derived from the Mediterranean Sea. These two studies, in close proximity to the Indus River Basin, further corroborate my interpretation regarding the moisture source of precipitation. Assuming a d-excess of 10‰ for the Indian monsoon, 20‰ for the Mediterranean Sea, and discharge weighted d-excess of 18‰ in the Indus River, isotope balance requires that 80% of the river water is derived from snow melt that ultimately owes its origin to moisture that originated in the Mediterranean or other inland seas.

In the northern mountain ranges of the Indus River Basin, snowfall begins in October and continues up to May, reaching a maximum in January and February. The winter season is thus the period of accumulation and subsequent months those of melting. In winter, the mid latitude westerlies moving across Iran and Tadzhikistan sweep over the ranges and precipitation comes from the troughs of low pressure in the westerly circulation (Rao, 1981). Snowfall in the Himalayas decreases from west to east and is apparently greater west of 80° E and north of 34° N, the region that is the maximum recharge zone to the Indus. In the monsoon season, however, the intensity of precipitation is reversed, decreasing from east to west (Rao, 1981). In the south, on the windward side, topography drives the monsoon winds (Vesilind and McCurry, 1982) such that the plains and the foothills receive abundant precipitation.

The higher d-excess in the summer season (Fig. 4.6) therefore results from delayed runoff from the northern mountains where snow accumulation occurs in the

winter season, typical rainy season of the Mediterranean region. The prevalence of high *d*-excess during peak discharge that coincides with the monsoon season reflects the subordinate role of the monsoon precipitation for the water budget of the Indus. Such events may increase the discharge locally, on a short time scale, but it is the melt water that constitutes the bulk of the discharge, at least during the water year March 1994-February 1995.

In summary, isotopes in precipitation in the northern mountain ranges of the Indus River Basin contain valuable information concerning the moisture source of precipitation for individual events and complement isotopic data for rivers draining this region. The river data, however, have the advantage in that they integrate all precipitation events into an average signal that allows interpretation of the dominant meteorological regime. Based on combined isotopic and meteorological observations in the region it is suggested that water vapor in the westernmost Himalayas, Karakoram and Hindu Kush is dominantly from inland basins of extreme evaporation such as the Mediterranean, Caspian and Persian Gulf and distinct from the Indo-Gangetic plains and the southern slopes of western Himalayas that receive precipitation from the Indian monsoon.

Chapter 5

Hydrochemistry

5.1. General Characteristics

The field and chemical data together with the ionic charge balance for the Indus

River Basin are listed in Appendix B. Total Dissolved Solids (TDS) in the headwater

tributaries are low and have a bimodal distribution. One group consists of small

tributaries, including the Shahbatot, Jaglot, Khandian, Kial and Duber rivers (stations 30,

35, 37, 38 and 39, respectively), that drain crystalline rocks and have TDS in the range of

30-90 mgL^{-1} (Fig. 5.1). The large headwater tributaries, on the other hand, drain a

mixture of igneous and metamorphic rocks and have TDS of 100-200 mgL^{-1}. Note that

the lowland tributaries in the sedimentary part of the basin reach 300-1000 mgL^{-1}. The

grouping is based on samples collected during the summer season, because of the larger

number of samples in that dataset. Compared to the winter, both the tributaries and the

Indus main channel (Fig. 5.2) are more dilute in the summer.
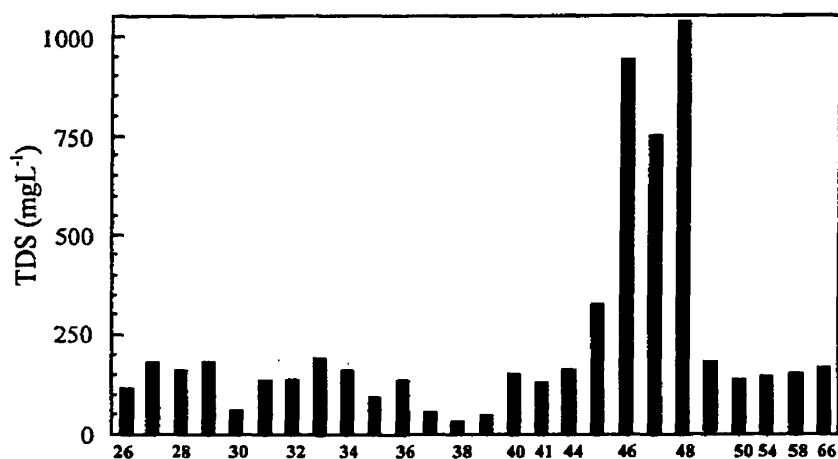
Fig. 5.1. Total Dissolved Solids in the tributaries of the Indus River during the summer season.
The key to the sample numbers as in Fig. 3.1

A conspicuous feature of the Indus main channel is a decline in TDS in the upper Indus and an inversion of this trend in the middle parts of the basin that continues to build up until it drains into the Arabian Sea (Fig. 5.2). Similar shifts occur in major ions and isotopes and reflect a change in weathering regime. The passage from the headwaters to the lowlands is accompanied by a change in lithology, geomorphology, climate, vegetation and land use. In the following sections the major ion characterisics of the Indus River Basin are discussed in relation to their geologic controls, with a comprehensive account of all other factors given in chapter 7.
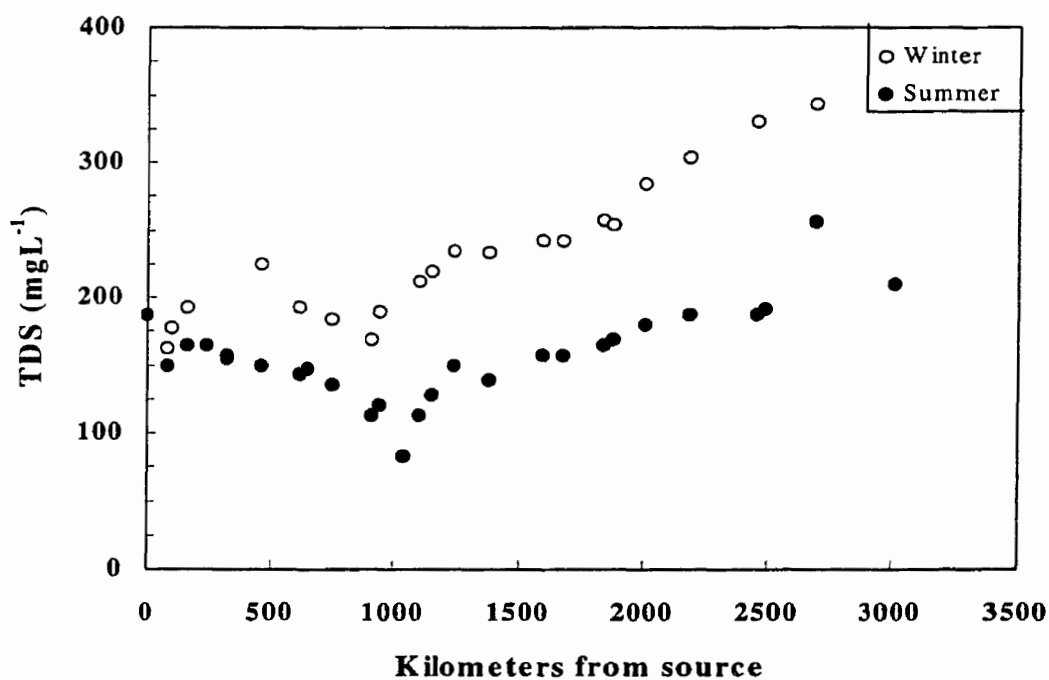
Fig. 5.2. Total Dissolved Solids in the Indus main channel.

The saturation state of the samples with respect to common minerals is given in Appendix B. Figure 5.3 illustrates the saturation index of carbonate minerals in the Indus

71

River Basin during the winter. The Indus main channel waters are undersaturated or approach saturation with respect to aragonite, calcite and dolomite in the upper Indus but become oversaturated in the middle and lower Indus. Water temperatures in the upper Indus during the winter and summer were respectively, ~1 and 12° C, in the lower Indus reaching 24 and 32° C. The solubility of most compound increases with rising temperature, that of calcite however, decreases with increasing temperature and therefore explains the rise in saturation state in the middle and lower Indus. In general, the oversaturation is more pronounced during the winter than in the summer season (Fig. 5.4) and more so for the tributaries in the given stretch than in the main channel.

The ionic charge balance defined in terms of Relative Percent Difference in $meqL^{-1}$ is represented by {(cations-anions)/(cations+anions)}. About 90 percent of the entire dataset has charge imbalance between 0 and 10%, and the remaining between 11 and 15, except two samples that exceed 15 %. The charge imbalances are due to excess positive charge and are in general associated with the summer season. The excess positive charge may result from dissociation of weak acids which produce organic anions (Berner and Berner, 1996), the latter not included in this study.
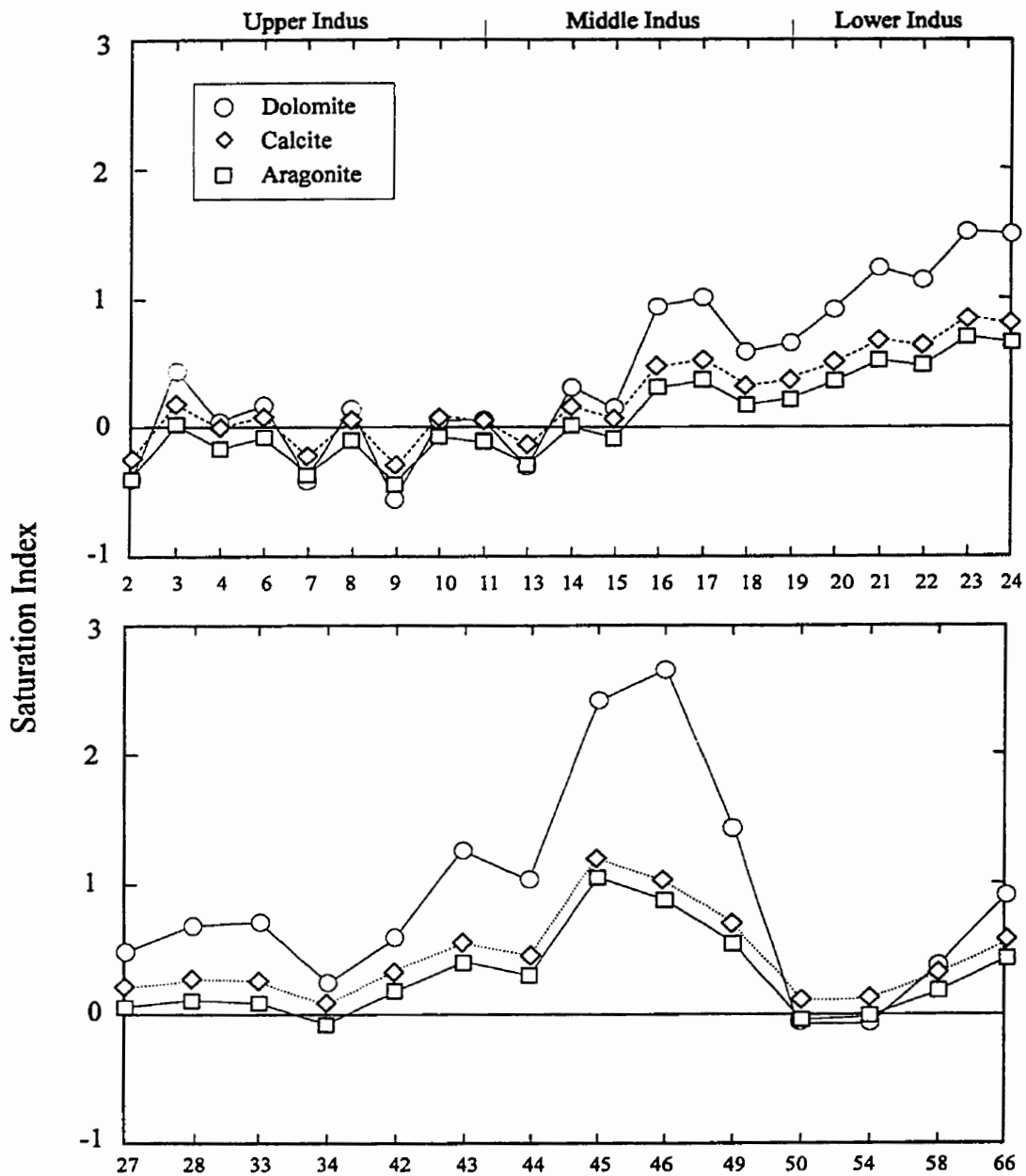
Fig. 5.3. Saturation index for aragonite, calcite and dolomite in the Indus main channel (top) and its tributaries (bottom) during the winter season. The key to the sample numbers is the same as in Fig. 3.1.

73
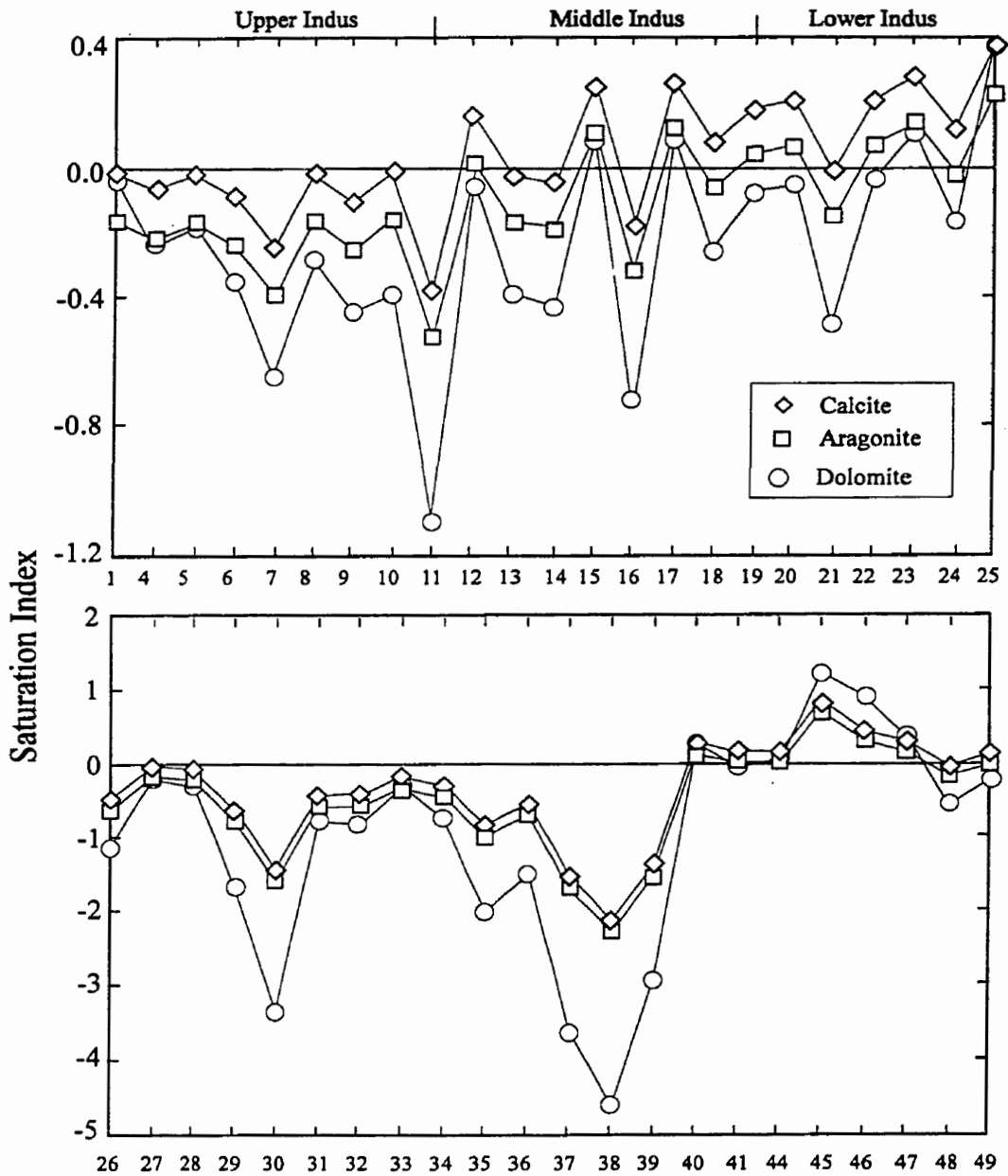
Fig. 5.4. Saturation index for aragonite, calcite and dolomite in the Indus main channel (top) and its tributaries (bottom) during the summer season. The key to the sample numbers as in Fig. 3.1.

74

5.2 Major ions

The major ion chemistry of the Indus River Basin is summarized in Figures 5.5 to 5.10. Ca^{2+} and Mg^{2+} are the dominant cations, with Ca^{2+} alone constituting over half (on equivalent basis) of the total cations in most of the rivers. Exceptions to this are some of the lowland rivers and the lower reaches of the Punjab rivers during winter, when Na^+ and K^+ may dominate. Bicarbonate is the dominant anion and forms over half of the total anion budget in all the rivers but for some of the lowlands and some lower reaches of the Punjab rivers, where SO_4^{2-} and Cl^- dominate. Nitrate, fluoride, silica and phosphate form only a subordinate fraction of the total dissolved constituents.

Figures 5.5 to 5.8 show the downstream evolution of the Indus main channel in terms of its major ion chemistry. The proportion of Ca^{2+} is uniformly high in the upper Indus and decreases gradually throughout the middle and lower Indus. Alkalies (Na^+ and K^+) show the opposite trend with consistently lower values in the upper Indus and progressive increase in the middle Indus. Proportions of Mg^{2+} fluctuates in the upper Indus and declines in the middle parts, rising only slightly in the lower Indus. Silicon is virtually invariant throughout the Indus main channel in the three component system and variations in HCO_3^- are compensated by SO_4^{2-} and Cl^-.
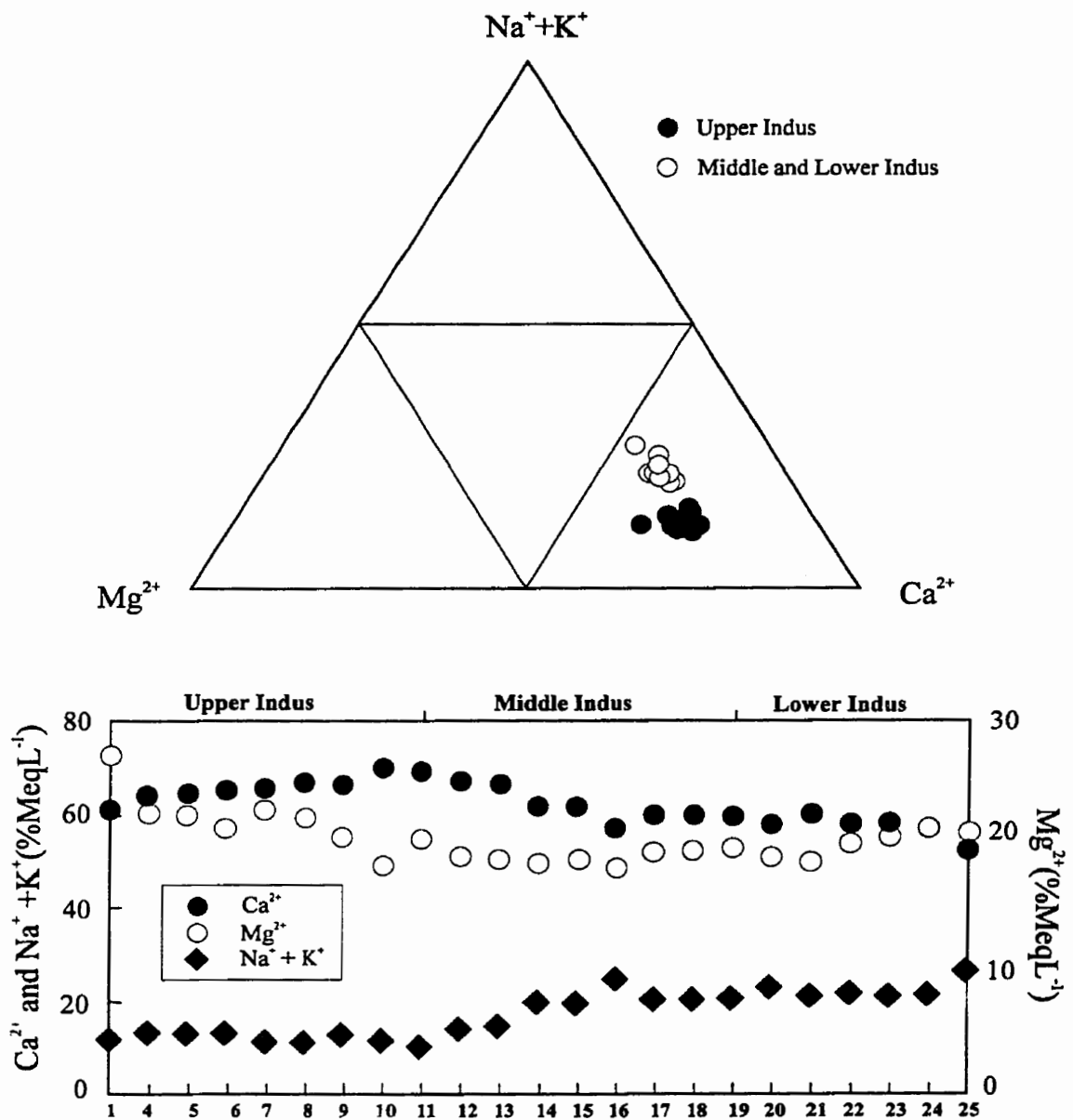
Fig. 5.5. Major cations in percent meqL^{-1} for the Indus main channel during the winter season. The bottom part illustrates how the proportions of cations change in the downstream direction. The key to the sample numbers as in Fig. 3.1.
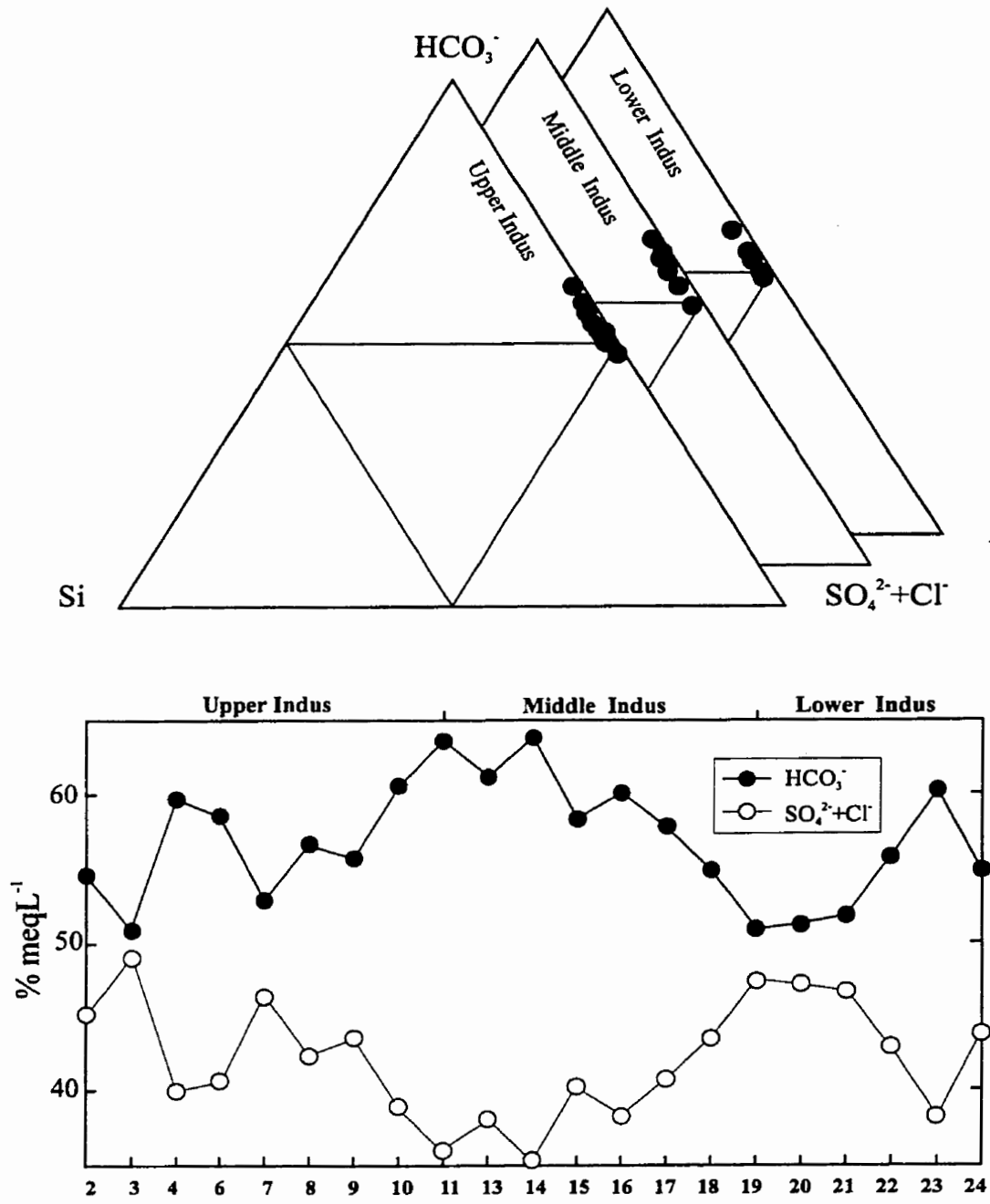
Fig. 5.6. Major anions and dissolved silica concentrations for the Indus main channel during the winter season. All ions expressed in percent meqL^{-1} except for Si that is in mmolesL^{-1}. The key to the sample numbers as in Fig. 3.1

77
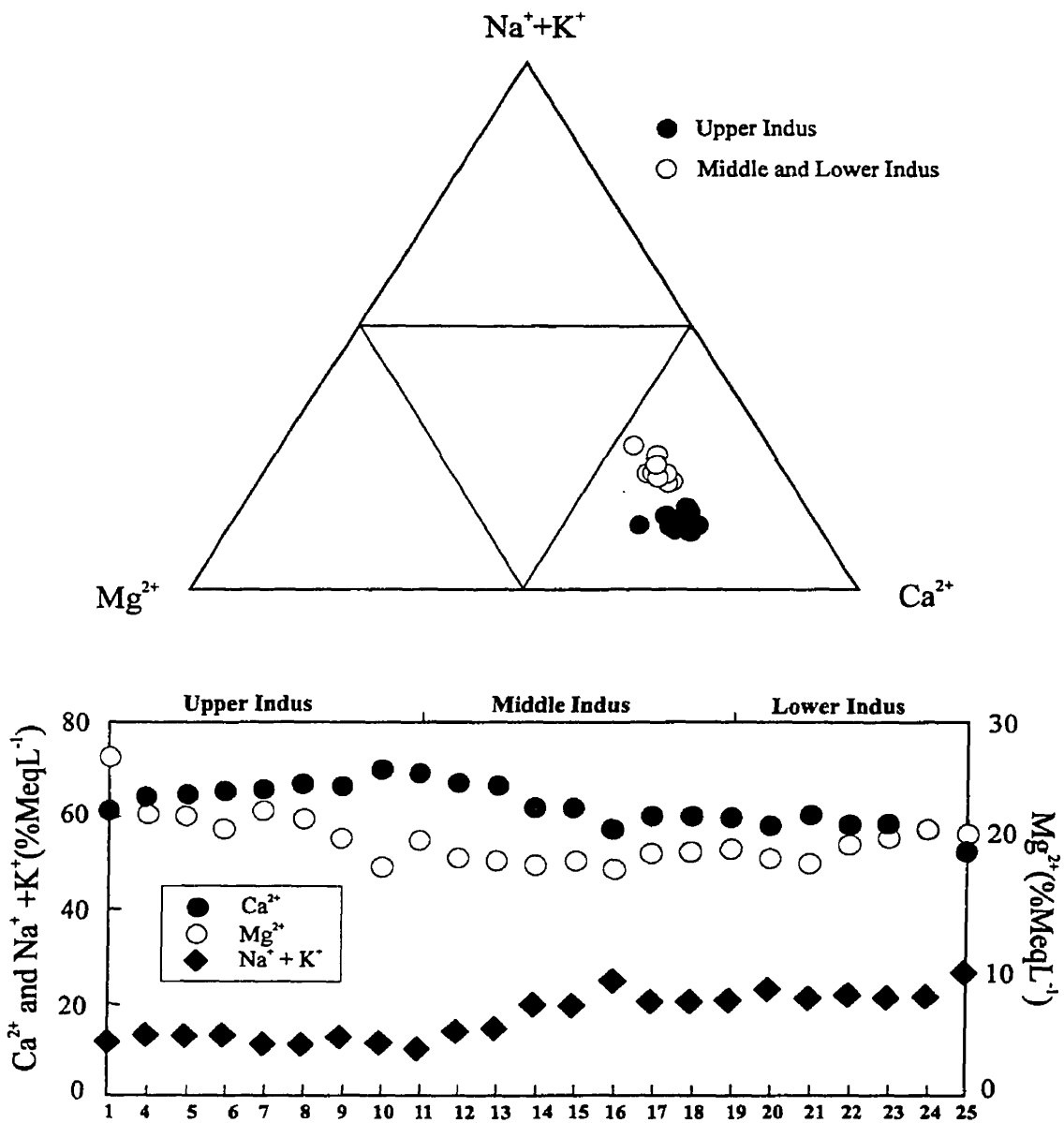
Fig. 5.7. Major cations in the Indus main channel during the summer season. The bottom part illustrates variations in the proportions of the cations in the downstream direction. The key to the sample numbers as in Fig. 3.1
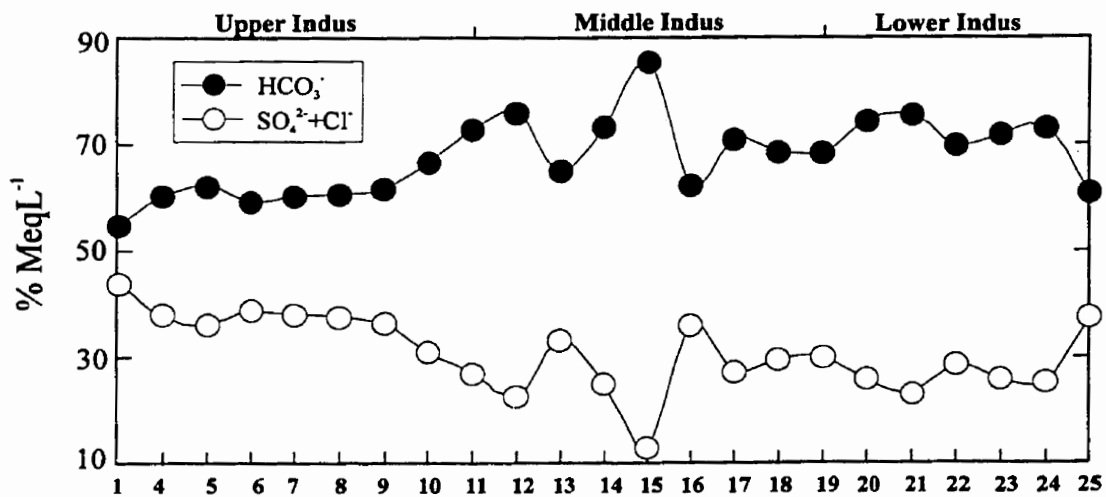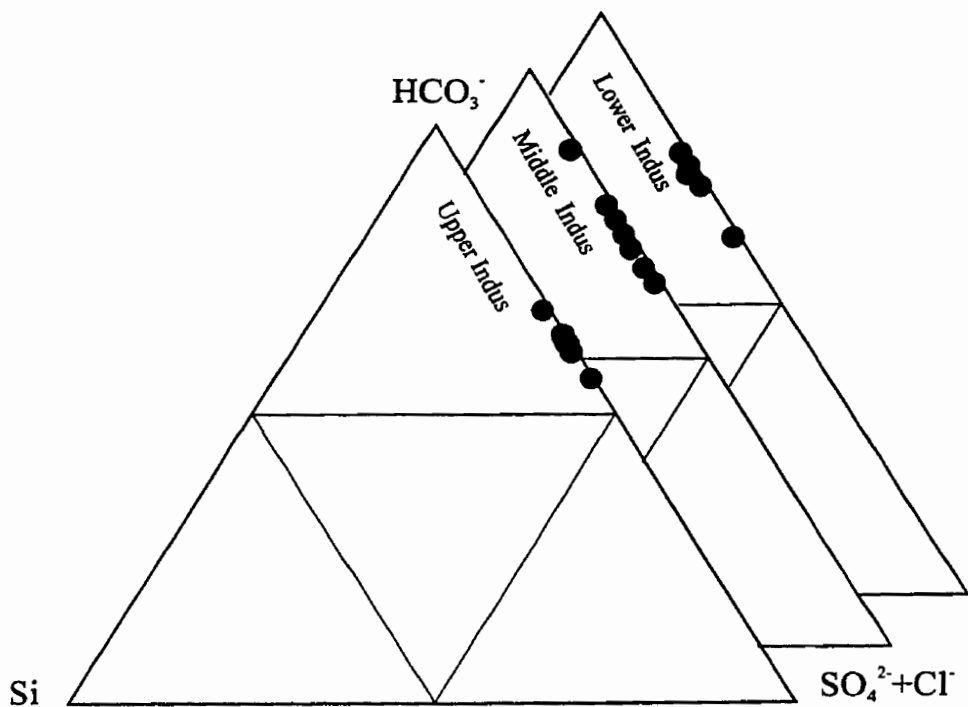
Fig. 5.8. Major anion concentrations and dissolved silica for the Indus main channel during the summer season. All ions expressed in percent $meqL^{-1}$ except for Si that is in $mmolesL^{-1}$. The key to the sample numbers as in Fig. 3.1
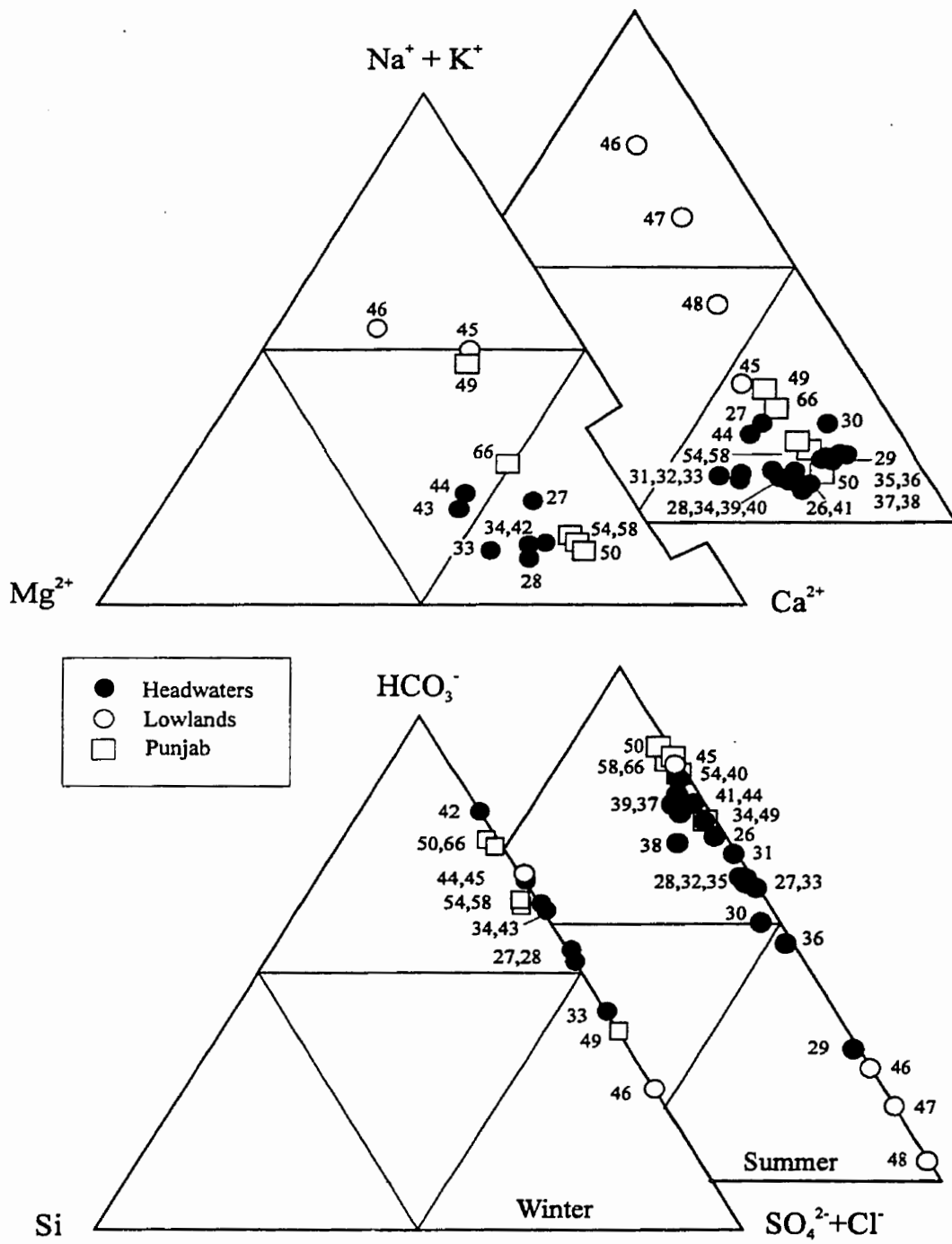
Fig. 5.9. Major ion chemistry of the Indus River tributaries. All ions expressed in percent meqL^{-1} except for Si that is in mmolesL^{-1}. The key to the sample numbers as in Fig. 3.1.
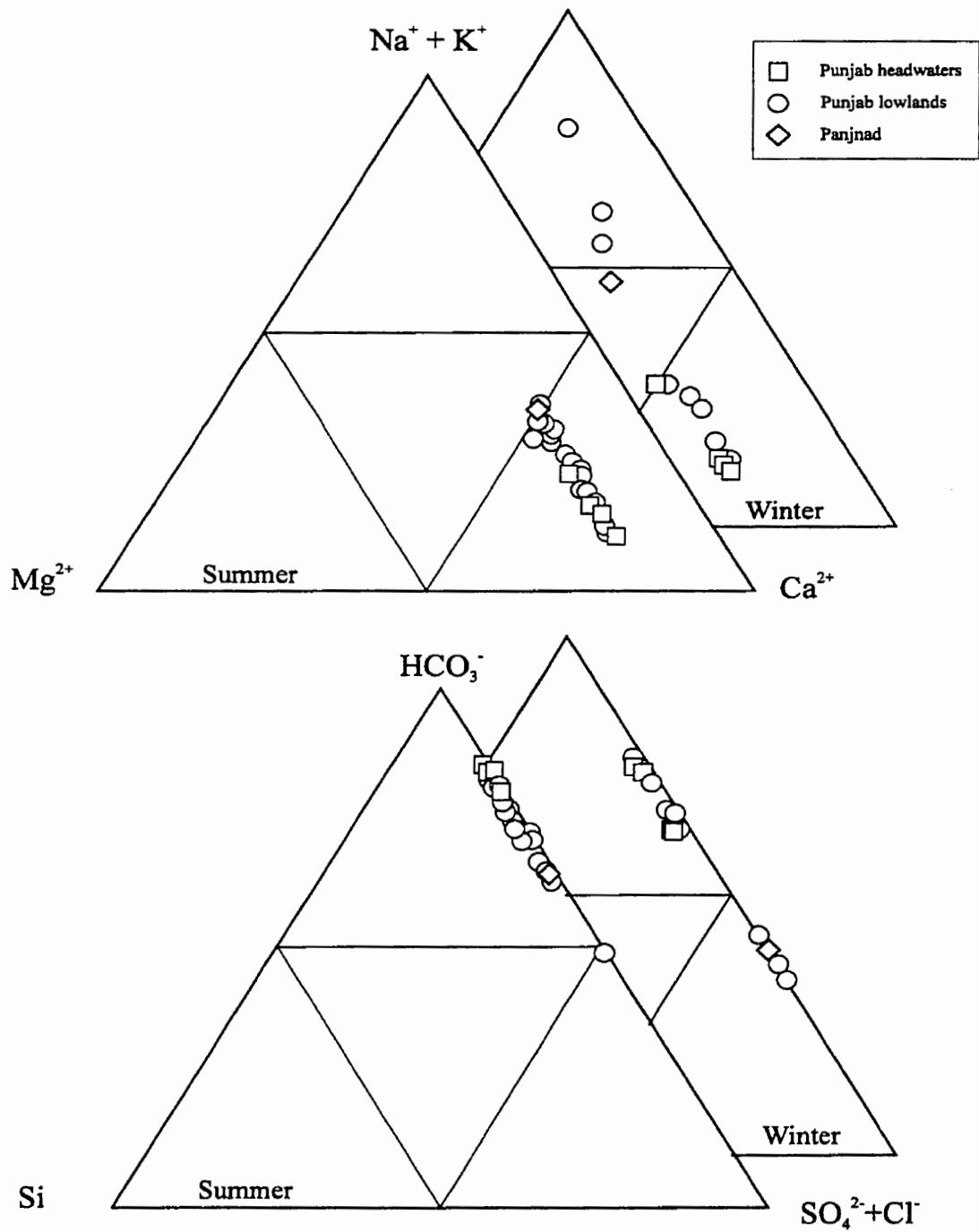
Fig. 5.10. Major ion chemistry of the Punjab rivers. All ions expressed in percent meqL^{-1} except for Si that is in mmolesL^{-1}.

5.3 Sources of ions and weathering reactions

In river water the potential sources of dissolved ions include: 1) atmospheric deposition of cyclic salts, 2) solution of atmospheric gases (mainly carbon dioxide), 3) weathering of rocks, and 4) biogenic processes and pollution. At the outset, it is therefore of interest to estimate the proportions of cyclic salts in the TDS. Assuming that major ions are not heavily fractionated between cyclic salts and seawater (Junge, 1963; MacIntyre, 1974; Hoffman et al., 1980) and that all the Cl^- in river water is derived from cyclic salts, the ion budget of the headwaters for cyclic salts can be constrained. The extent of this process in the lowlands, however, is difficult to quantify due to multiple sources of chloride (halite weathering, pollution).

In the headwaters, chloride concentrations are uniformly low (0.02-0.07, except the Shyok that has 0.141 $mmolesL^{-1}$), indicating a common diffuse source. In these rivers, the largest contribution of cyclic salts is for sodium with ~20 to 40% (and up to 70% in some dilute rivers) of the total Na^+ likely derived from such source (cf. Pande et al., 1994). Similarly, in the upper Indus River, cyclic salts constitute ~30 to 35% of the total Na^+. Nonetheless, the contribution to TDS from cyclic salts does not exceed 6% of the total ion budget in the headwater tributaries and in the upper Indus River. These calculations define an upper limit since small amounts of Cl^- in river water may be derived from weathering of igneous and metamorphic rocks. Ionic/chloride ratios for all samples from the Indus River Basin exceed the complements expected from cyclic salts (cf. Karim and Veizer, submitted) and the bulk of the riverine TDS should therefore originate from rock weathering.

5.3.1 Calcium and Magnesium

Calcium and magnesium are contributed to river water predominantly from rock weathering and only small proportion is derived from pollution and cyclic salts (Berner and Berner, 1996). They are essential constituents of many igneous silicate minerals. Weathering of common Ca and Mg bearing silicate minerals can be represented by the following reactions:

$$CaAl_2Si_2O_8 + 3H_2O + 2CO_2 \rightarrow Al_2Si_2O_5(OH)_4 + Ca^{2+} + 2HCO_3^- \qquad (5.1)$$
(anorthite)   (kaolinite)

$$CaMgSi_2O_6 + 6H_2O + 4CO_2 \rightarrow Ca^{2+} + Mg^{2+} + 4HCO_3^- + 2H_4SiO_4 \qquad (5.2)$$
(pyroxene)

$$Mg_2SiO_4 + 4CO_2 + 4H_2O \rightarrow 2Mg^{2+} + 4HCO_3^- + H_4SiO_4 \qquad (5.3)$$
(olivine)
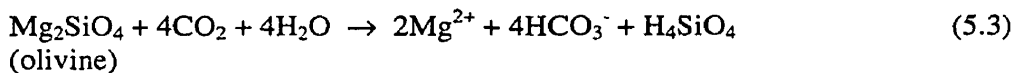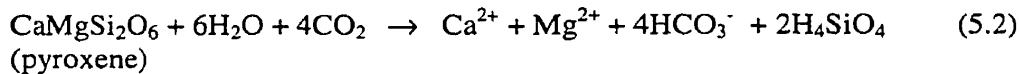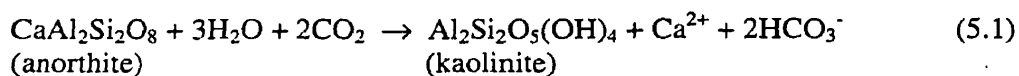
Carbon dioxide in soil or in the atmosphere dissolves in water to form carbonic acid, H_2CO_3. The acidity is neutralized by weathering reactions and ions released into solution. Weathering of carbonate rocks produces Ca^{2+} and HCO_3^- as well as Mg^{2+}, if dolomite is present. Calcium may also be derived from dissolution of gypsum or anhydrite. The weathering reactions can be represented as follows:

$$CaCO_3 + H_2O + CO_2 \rightarrow Ca^{2+} + 2HCO_3^- \qquad (5.4)$$
(calcite or aragonite)

$$CaMg(CO_3)_2 + 2CO_2 + 2H_2O \rightarrow Ca^{2+} + Mg^{2+} + 4HCO_3^- \qquad (5.5)$$
(dolomite)

$$CaSO_4 . 2H_2O \rightarrow Ca^{2+} + SO_4^{2-} + 2H_2O \qquad (5.6)$$
(gypsum)
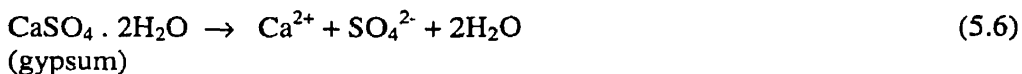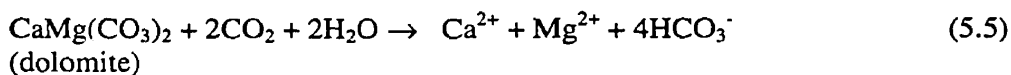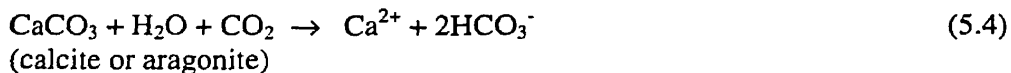
Theoretically, weathering of calcic plagioclase, pyroxene, olivine, and calcite and dolomite by dissolved CO_2 should produce solutions with molar ratios of 1:2 for Ca^{2+} : HCO_3^-, Mg^{2+} : HCO_3^- and $(Ca^{2+} + Mg^{2+})$: HCO_3^-. Note that the minerals included in the above reactions are common rock-forming minerals that represent six of the top nine readily soluble minerals (Table 4.5 in Berner and Berner, 1996). The range of Ca^{2+} : HCO_3^- and $(Ca^{2+} + Mg^{2+})$: HCO_3^- ratios in the Indus River Basin and rivers draining monolithological basins in France (Meybek, 1986) are shown in Table 5.1. It is clear that the range of ionic ratios in the Indus River Basin cannot be explained solely on the basis of above reaction pathways and sources of ions. The differences may be accounted for by: 1) Heterogeneity in natural systems. For example, weathering of plagioclase is commonly represented by the pure Ca-end member, but plagioclase is a solid solution series between the Na and Ca end members. Bicarbonate released by weathering of a granitic rock may be balanced in part by Na^+ and K^+ as well as Mg^{2+}, leading to lower Ca^{2+}/HCO_3^- ratios than that expected from weathering of anorthite alone; 2) Accessory minerals in rocks can weather preferentially and influence the ionic ratios; and 3) The source of acidity may not be CO_2 alone and other sources such as sulfuric acid derived from the oxidation of pyrite may be important, thereby increasing the ionic ratios. This is for example the case for the Sanghar River.

5.3.2 Sodium, Chloride and Potassium

Sodium in river water may be derived from: 1) cyclic salts; 2) weathering of halite; 3) leaching of salts in marine sediments and saline soils; 4) communal and urban discharge and 5) weathering of silicate rocks. While chloride behaves conservatively, sodium may be influenced by cation exchange with clay minerals. It is not possible to

evaluate the significance of cation exchange on the basis of the current dataset. Assuming that NaCl is the dominant source of sodium in communal and urban discharge and in saline soils, all the above five sources can be divided into two main categories, halite and non halite sources. This allows the distinction based on the stoichiometry of dissolution of NaCl.

$$NaCl \rightarrow Na^+ + Cl^- \qquad (5.7)$$

Halite sources release Na^+ and Cl^- in a 1:1 molar ratio, i.e, all the sodium is balanced by chloride.

Table 5.1. Ca^{2+} /HCO_3^- and (Ca^{2+} + Mg^{2+}) /HCO_3^- molar ratios in the Indus River Basin for the summer season and some monolithological river basins in France (Meybek, 1986). The "Range" represents minimum and maximum values, numbers in parentheses are the mean values and n is the number of rivers.

	Ca^{2+} /HCO_3^- Range (mean)	(Ca^{2+} +Mg^{2+})/ HCO_3^- Range (mean)
Indus main channel	0.39 - 0.65 (0.48)	0.52 - 0.85 (0.64)
Headwater tributaries	0.44 - 1.53 (0.66)	0.62 - 1.78 (0.85)
Lowland tributaries	0.31 - 7.52	0.43 - 10.45
Punjab rivers	0.43 - 0.74 (0.50)	0.54 - 0.92 (0.63)
Limestone (n=12)	0.42 - 0.62 (0.46)	0.49 - 0.73 (0.54)
Dolomitic limestone (n=1)	0.29	0.53
Gypsum (n=4)	1.27 - 6.70 (3.36)	1.52 - 7.41 (4.02)
Molasse (n=8)	0.36 - 0.74 (0.47)	0.47 - 0.91 (0.58)
Granite (n=25)	0.09 - 1.74 (0.49)	0.27 - 2.76 (0.58)
Basalt (n=30)	0.20 - 0.32 (0.24)	0.37 - 0.62 (0.45)
Peridotite (n=2)	0.05, 0.6	0.71, 0.85

The non halite sources yield a higher ratio, the part of the sodium that balances chloride is termed "supported" and the residue (Na^+ excess $= Na^+_{(total)} - Cl^-$) is called "unsupported or excess sodium", and must be derived either from weathering of albite in silicate basins or from weathering of carbonates and sulfates of sodium in sedimentary basins.

In the Indus River Basin about 35 - 45% of the total sodium may be derived from halite sources (Table 5.2), but the bulk owes its origin to non halite sources. Some of the headwater tributaries, particularly the dilute ones, derive up to 70% of their sodium from halite sources. This is an upper limit on halite derived sodium because some chloride may also be derived from fluid inclusions in minerals. These rivers are devoid of any known evaporite deposits and are scarcely populated. The halite-derived sodium in these rivers and in the upper Indus is therefore likely from cyclic salts, but excess sodium must originate from weathering of silicate rocks.

Among the lowland tributaries, the Kurram river contains about two-thirds, the Soan and the Shahur about one-third and the Sanghar River only about one-tenth of its sodium from a halite source. The Kurram River, with outcrops of rock salt in the basin (Kruseman and Naqavi, 1988), must derive its sodium predominantly from weathering of halite. All other lowland rivers derive the bulk of their sodium from non-halite sources. Nevertheless, and despite the fact that the lowland tributaries contain sedimentary rocks of Himalayan provenance, the high concentration of excess sodium may not be due solely to silicate weathering, as indicated by Sr-isotopic constraints (see chapter 6). The middle and lower Indus basin contains large areas of waterlogged and saline soils that have high exchangeable sodium and carbonates and sulfates of sodium (Ahmad and Kutcher, 1992).

The high excess sodium in these rivers is therefore likely derived from leaching of saline soils.

The Punjab rivers become progressively saline from their headwaters to their joint confluence, Panjnad (Fig. 5.10). The halite-derived sodium shows a similar pattern. It increases from headwaters (15-33 %) to the Panjnad (50%), reaching 96% locally in the Jhelum River (station 53). The strong increase in the Jhelum River occurs after flowing near the Salt Range. The reason for increase in halite-derived sodium in other Punjab rivers in the plains is more difficult to assess. There are no known evaporites in this stretch, but all these rivers are connected by link canals to the Jhelum River and the water balance at Panjnad is dominated by the Jhelum River. The increase in halite-derived sodium at Panjnad is therefore at least partly due to halite weathering in the Salt Range. The excess sodium that constitutes half of the total sodium at Panjnad is apparently derived from silicate weathering.

Table 5.2. Average concentration of Na^+ and Cl^- (in $mmolesL^{-1}$) and the percentage of sodium derived from halite sources (procedure as described in the text).

	Na^+	Cl^-	% halite Na^+
Upper Indus	0.158	0.062	39
Middle Indus	0.261	0.112	43
Lower Indus	0.461	0.215	46
Headwater tributaries	0.109	0.038	35
Lowland tributaries	5.065	1.857	37
Punjab rivers	0.492	0.203	41

Among the four major cations, potassium is the least abundant constituent of river water (Meybeck, 1984). It is derived predominantly from silicate minerals, K-feldspars and micas, found in igneous, metamorphic and sedimentary rocks. Other sources of potassium are rare evaporite deposits of KCl and pollution from K-fertilizers. Potassium is an important nutrient and is influenced by biological activities. Meybeck (1984) estimates that three fourths of the silicate-derived potassium comes from silicate minerals in sedimentary rocks and only the remainder is derived from igneous and metamorphic rocks. On a worldwide basis, there is little variation in potassium concentration among major rivers, ranging between 0.013-0.102 mmolesL^{-1} (Meybeck, 1980), with the highest concentrations found in high-TDS rivers from arid regions, such as the Nile, Colorado and Rio Grande.

In the Indus River Basin, the highest concentration of K$^+$ are found in the lowland tributaries (0.074-0.149 mmolesL^{-1}) that drain the arid sedimentary part of the basin, the lowest in the headwaters (0.009-0.093 mmolesL^{-1}) and intermediate values in the Punjab rivers (0.047-0.121 mmolesL^{-1}). In the Indus main channel, potassium increases from 0.056 mmolesL^{-1} in the upper Indus through 0.077 in the middle to 0.091 mmolesL^{-1} in the lower Indus. Thus, in terms of K$^+$ abundance, the lowland tributaries are similar to the high-TDS arid rivers and most of them entering the Indus in the sedimentary and alluvial part of the basin.

At the Sukkur barrage, the concentration of potassium varies between 0.082-0.117 mmolesL^{-1}. The discharge-concentration relationship is complex, with K$^+$ concentration decreasing first between March and June concomitant with the melting of snow in the headwaters and dilution of the baseflow. A gradual increase in concentration has been

observed between June and August (rising limb of the hydrograph) followed by a decline between August and November (falling limb of the hydrograph) and then by a rise to the highest concentration during the baseflow. The simultaneous increase in discharge and concentration during the summer season apparently reflects leaching of productive soils as the river inundates its flood plain. A similar feature has been observed in the Central United States, where many streams carry potassium concentrations nearly as high as, or higher than, those at low discharge (Hem, 1985). The decline in concentration during the fall either indicates vanishing supply in the soils or gradual retreat of the river from its flood plain.

5.3.3 Bicarbonate

In river water, bicarbonate is derived almost entirely from rock weathering. Pollution contributes only 2% (Meybeck, 1979) and cyclic salts less than 1% (Berner and Berner, 1996). Weathering related chemical reactions leading to bicarbonate formation are listed above (equations 5.1 – 5.5). Bicarbonate is intimately linked with calcium and magnesium in weathering reactions and the preceding discussion on the two cations is also applicable to its paragenesis. In river water bicarbonate may be grouped into three main categories based on the source of carbon. These are, weathering of carbonate minerals in which half of the carbon is derived from carbonates and the other half from soil CO_2, and weathering of silicate minerals in which all the carbon is derived from soil or atmospheric CO_2. These sources of carbon usually have distinct isotope ratios and can be used to determine their relative importance (Chapter 6). On average, the contribution

of soil CO_2 to the dissolved inorganic carbon in the world rivers is about 67% (Berner et al., 1983; Amiotte Suchet and Probst, 1995).

5.3.4 Sulfate

Sulfate in river water may be derived from several sources: 1) dissolution of gypsum and anhydrite, 2) atmospheric deposition (including acid rain, biogenic sulfur gases and cyclic salts), 3) weathering of pyrite in sediments and in igneous and metamorphic rocks, and 4) pollution resulting from sulfate fertilizers and industrial and municipal wastes.

Within the Indus River Basin, high concentrations of sulfate are found in the lowland tributaries, the Kurram River (1.905 mmolesL^{-1}), Shahur River (3.191 mmolesL^{1}) and Sanghar River (6.247 mmolesL^{-1}). Possible sources of sulfate in these rivers are: 1) The Kurram and Shahur also have high concentrations of Na$^+$, K$^+$ and Cl$^-$ (Fig. 5.9) which may suggest weathering of evaporites. Although this region is known for evaporite occurrences, sulfate in these rivers does not seem to be derived from such a source. The Ca^{2+} /SO_4^{2-} molar ratio of these rivers is ~0.42, with Ca^{2+} less than half of that expected from weathering of gypsum or anhydrite (equation 5.6). In addition, isotopic composition of sulfate precludes such a source (chapter 6). 2) Even if all the chloride in these rivers were derived from cyclic salts, the total contribution of sulfate from cyclic salts would be less than 15% for the Kurram and less than 3%, for the Shahur and Sanghar. 3) Another, more likely, source may be oxidation of pyrite according to the following reaction pathway:

$$4FeS_2 + 15O_2 + 8H_2O \rightarrow 2Fe_2O_3 + 8H_2SO_4 \qquad (5.8)$$

$$H_2SO_4 + 2CaCO_3 \rightarrow 2HCO_3^- + 2Ca^{2+} + SO_4^{2-} \qquad (5.9)$$

$$H_2SO_4 + 9H_2O + 2NaAlSi_3O_8 \rightarrow Al_2Si_2O_5(OH)_4 + 2Na^+ + SO_4^{2-} + 4H_4SiO_4 \quad (5.10)$$
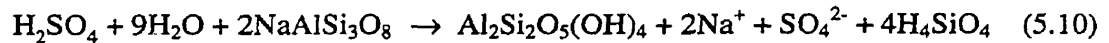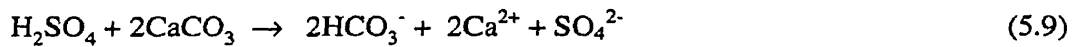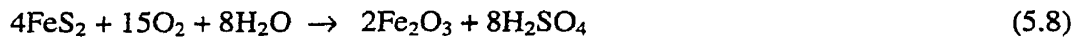
In the absence of H^+ consuming reactions, oxidation of pyrite may lower the pH. The generated acidity may be subsequently neutralized by weathering of silicate or carbonate minerals. The former case can be recognized easily by its low pH, while the latter is difficult to ascertain from general geochemistry. The pH of the three lowland tributaries ranges between 7.99 and 8.21. This, together with isotopic composition of sulfate, suggests sulfide weathering in a mixed terrain. I therefore propose that oxidation of pyrite in shales, sandstones and carbonates of the West Pakistan Fold Belt is the dominant source of sulfate in these rivers. The origin of sulfate in the tributaries and in the Indus main channel will be discussed further in chapter 6.

5.3.5 Silica

Dissolved silica in river water is derived essentially from silicate weathering (Holland, 1978; Meybeck, 1987). Silicate minerals are abundant on the surface of the earth, but on a worldwide basis only very few rivers (cf. Fig. 5.5 in Berner and Berner, 1996) have more than 20% dissolved silica (relative to HCO_3^-, SO_4^{2-}, and Cl^- on equivalent basis). This is apparently due to high solubility of carbonate rocks that overshadows silica released by silicate weathering.

An interesting feature of the major ion chemistry of the Indus River Basin is the relatively low concentration of dissolved silica in all the rivers, even in the headwater silicate basins. (Figs. 5.6 and 5.8 to 5.10). While the lower proportions of silica in the lowland tributaries could be due to the dominance of sediment weathering, those in the headwaters are most likely due to incomplete weathering. The type of weathering products (clays) resulting from silicate weathering depends on lithology and drainage. In general, gibbsite forms due to intense weathering (removing all the cations and silica) in areas of high rainfall and good drainage. Kaolinite forms in regions with less rainfall and adequate drainage (enough to remove all the cations but retain some silica). Low runoff and a hot, dry climate with high evaporation (little removal of cations and silica) favors smectite formation. If volcanic glass is abundant, smectite can form also in humid tropical areas, such as the Amazon (Stallard, 1985).

Information on clay mineralogy in the Indus River Basin is lacking, but stability relations for common clay minerals in equilibrium with water can be used to decipher the nature of the weathering regime. On a log a_{H4SiO4} vs. log (a_{K+}/a_{H+}), water samples from the Indus River Basin straddle the boundary between muscovite (proxy for illite) and kaolinite (Fig. 5.11). The climatic and geomorphic controls on the stability of illites are not clear, but the illite occurs in argillaceous sediments and forms during weathering of feldspars. In sediments the illites may be detrital (silicate weathering) as well as diagenetic (Deer et al., 1982). Illite is found in almost all rivers. In the Danube River it accounts for 75% (of the total clay minerals in the < 2 μm fraction) (Müller and Stoffers, 1974), in the Mackenzie River 66%, and in the Yukon River 41% (Naidu and Mowatt, 1983). Lower concentrations are found in the Amazon and Orinoco River at 20 to 25%

(Irion, 1991) and the Mississippi at 24% (Potter et al., 1975). No illite has been detected in rivers draining the volcano-rich island of Java and in tropical lowland rivers in the Amazon region (Irion, 1987). Relief and climate apparently control the low concentration of silica in the Indus River Basin. In this region, weathering does not proceed to completion due to high rates of exposure of fresh surfaces by strong uplift and erosion.
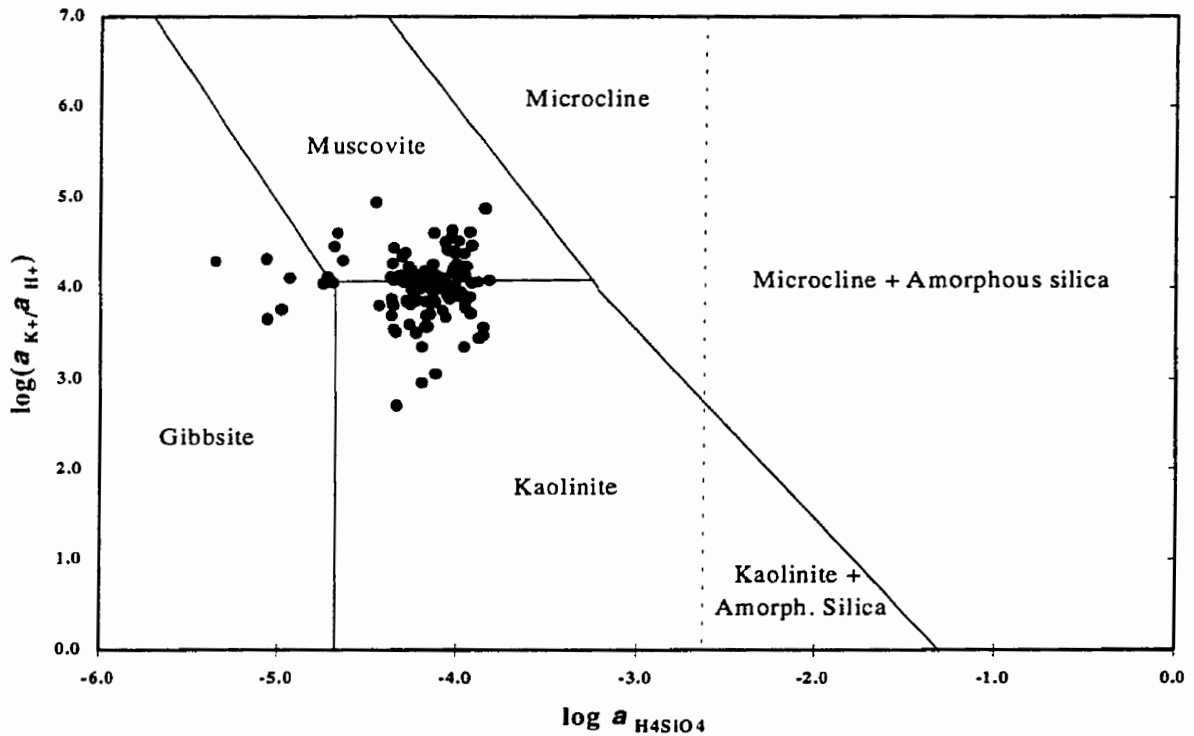
Fig. 5.11. Stability diagram for some minerals in the system K_2O-Al_2O_3-SiO_2-H_2O. The position of field boundaries varies in the literature due to different thermodynamic constants used.

5.4 Temporal variations in major ion chemistry

Another aspect of major ion chemistry of the Indus River at Sukkur barrage is the discharge-concentration relationship. In general, solute concentrations during lean discharge are high, decreasing with increasing discharge due to dilution of baseflow by surface runoff. All the Indus tributaries show higher concentrations in the winter and fall compared to the summer season. This is the commonly observed "dilution trend". However, in the Indus main channel at Sukkur barrage, solute concentrations first decrease, concomitant with the melting of snow in the headwaters, increasing subsequently while still on the rising limb of the hydrograph. At peak discharge, solute concentrations are several orders of magnitude higher than those expected from dilution by "pure water" (Fig. 5.12). The dilution model assumes conservative behavior of solutes in river water and that the surface runoff is pure rain/melt water. The largest discrepancy is shown by K^+ that is ~20 times, followed by Ca^{2+} and HCO_3^- that are about 15 times higher than expected from dilution. The minimum (x5) departure from the dilution trend is shown by chloride. All other ions fall between these extremes.

Two processes apparently cause the departure from classical dilution trend at peak discharge in the Indus River: 1) Leaching of solutes from the flood plain. In the summer season, large areas of the Indus Plains are frequently inundated by floodwater. Surface soils accumulate salts and organic matter during the dry seasons that are leached by the encroaching river during floods; 2) High concentration of solutes build up in soils and groundwater during the dry season that may be flushed out during the rainy season, leading to elevated concentration of solutes at higher discharge, the process known as hysteresis (Schlesinger, 1991). Based on the summer and winter sampling, none of the
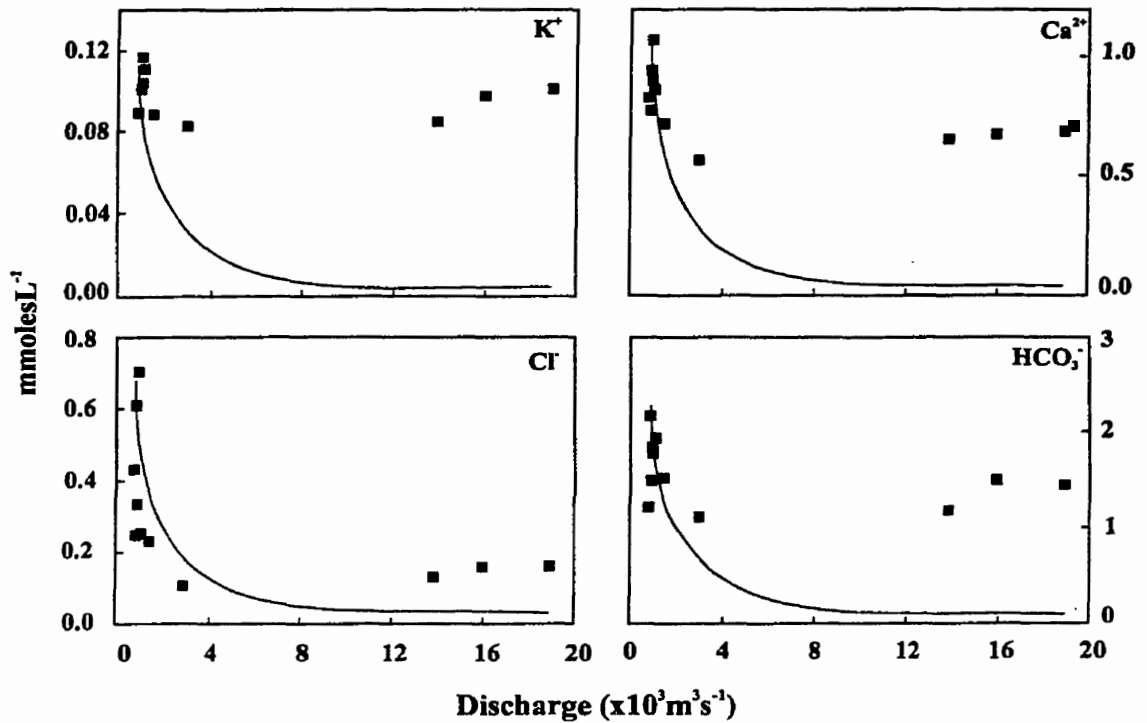
Fig. 5.12. Discharge–concentration relationship of dissolved ions in the Indus main channel at Sukkur barrage The curves represent theoretical mixtures of base flow diluted by increasing volumes of "pure water".

Indus tributaries had solute concentrations at high discharge equal to or higher than those observed at lean discharge. In addition, hydrologic conditions favorable to hysteresis (such as thick soils and shallow aquifers discharging into rivers) are rarely met in the headwaters. Thus leaching of solutes from the flood plains seems to have been the most likely process controlling the higher concentrations at peak discharge.

5.5 Fluxes of dissolved ions

The Indus River Basin has a total area of 863,508 km^2 with an average annual precipitation of ~460 mm (both estimates obtained in this study, chapters 1 and 7). This yields an annual precipitation flux of 398 km^3. Based on average chemical data on precipitation (Sequeira and Kelkar, 1978; Nijampurkar et al., 1993) in the headwaters of the Punjab rivers, the calculated flux of TDS to the Indus River Basin from precipitation is ~844,400 tons $year^{-1}$ (Table 5.3). The riverine TDS flux at Sukkur barrage, based on mean annual discharge for the post-dam era (1963-84), is ~18 million tons per year. This value is expected to be similar to the pre-dam flux at the mouth of the Indus (Fig. 1.5). The calculated precipitation flux of TDS is therefore ~5% of the riverine flux.

Based on the above estimates a chemical denudation rate of 21 tons $km^{-2} year^{-1}$ is obtained. Assuming a value of 9.7 for the ratio of mechanical to chemical denudation for Asia (Garrels and Mackenzie, 1971), the total annual denudation rate of the Indus River Basin is about 200 tons km^{-2}. This certainly represents a lower limit on denudation since discharge of the Indus River has decreased considerably due to withdrawal of water for irrigation during the past few decades.

Table 5.3. Major ion concentration in precipitation from the headwaters of the Punjab rivers, Gulmarg, (Sequeira and Kelkar, 1978) and Spitti (Nijampurkar et al., 1993). Concentrations at Sukkur barrage are discharge-weighted averages based on this study. Precipitation flux is based on area weighted average precipitation data (DAAC-GSFC, 1996). Water discharge of the Indus River is from Jorgensen et al. (1993).

	Ca^{2+}	Mg^{2+}	Na^+	K^+	SO_4^{2-}	Cl^-	HCO_3^-	Si	Sr^{2+}
Gulmarg (μmolesL^{-1})	22.2	6.6	19.6	3.1	3.5	8.7			
Spitti (μmolesL^{-1})	5.7	4.2	17.5	7.2	2.2	21.2			
Average (μmolesL^{-1})	13.9	5.4	18.5	5.1	2.9	15			
Sukkur (mmolesL^{-1})	0.693	0.247	0.429	0.094	0.255	0.180	1.416	0.093	0.003
Annual precipitation flux (x 10^3 tons)	222.4	52.2	169.5	79.6	109.4	211.3			
Annual riverine flux (x 10^4 tons)	299.3	64.7	106.2	39.7	264.2	68.9	931.2	28.3	2.5

Chapter 6
Isotope Geochemistry

6.1 The carbon cycle and aqueous carbonate system

Rivers transport products of erosion and terrestrial primary production to the oceans and represent a major link in the global carbon cycle (Kempe, 1979). The riverine carbon cycle begins with the formation of carbonic acid in the atmosphere but the direct impact commences in the soil zone. The generated acidity is neutralized by chemical reactions in the weathering zone with an attendant release of ions into solution. Products of continental weathering are transported to the oceans where carbon is partly removed by precipitation of carbonates and the remainder returns to the atmosphere in the form of CO_2. Rock weathering, silicate lithologies in particular, may constitute an important sink for atmospheric CO_2 and it has been postulated that intense weathering of the Himalayas during the Cenozoic have been responsible for global climatic cooling (Raymo et al., 1988). It is therefore instructive to characterize the present day weathering regime in the Himalayas and evaluate the relative importance of silicate and carbonate weathering in major rivers draining this region.

Another important aspect of the carbon cycle is its dominant control on acid-base reactions in aquatic systems. Carbon is a nutrient and microbiological activities play an important role in redox conditions. It determines the pH and therefore speciation of elements and state of mineral saturation. The source of carbon in natural waters is carbon dioxide and weathering of carbonate minerals. The dissolution of CO_2 in water continues until equilibrium is reached. At equilibrium, the activity (or concentration since the two

are equal in dilute waters) of dissolved CO_2 is proportional to the partial pressure of CO_2 in the gas phase. The aqueous carbonate system is governed by equilibrium reactions, listed below with dissociation constants at 25° C:

$$CO_{2(g)} + H_2O \Leftrightarrow H_2CO_3 \tag{6.1}$$
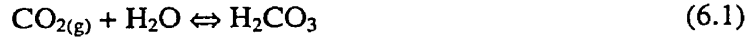
$$K_{CO2} = \frac{H_2CO_3}{pCO_2} = 10^{-1.47} \tag{6.2}$$

$$H_2CO_3 \Leftrightarrow H^+ + HCO_3^- \tag{6.3}$$

$$K_1 = \frac{H^+ . HCO_3^-}{H_2CO_3} = 10^{-6.35} \tag{6.4}$$

$$HCO_3^- \Leftrightarrow H^+ + CO_3^{2-} \tag{6.5}$$

$$K_2 = \frac{H^+ . CO_3^{2-}}{HCO_3^-} = 10^{-10.33} \tag{6.6}$$

The formation of carbonic acid from CO_2 gas involves an intermediate step in which $CO_{2(gas)}$ is hydrated to form dissolved CO_2 (denoted by $CO_{2(aq)}$), which in turn transforms into H_2CO_3. Conventionally, however, $CO_{2(aq)}$ and H_2CO_3 are both referred to as H_2CO_3 and an overall equilibrium constant K_{CO2} is used. The sum of concentration of the three aqueous carbonate speices, H_2CO_3, HCO_3^- and CO_3^{2-} make up the dissolved inorganic carbon (DIC). The relative proportions of these species are controlled by pH and can be calculated using the above equations. Carbonic acid dominates at low, HCO_3^- at higher pH and CO_3^{2-} under highly alkaline conditions. In the Indus waters, over 95% of the DIC is in the form of HCO_3^-.

The $^{13}C/^{12}C$ isotope ratios can be used to trace the evolution of DIC and sources of carbon in water. The dissolution of CO_2 in water and redistribution of aqueous

carbonate species is accompanied by different isotope fractionation factors. These are temperature dependent and are given by the following relationships:

$$\bullet \quad CO2_{(aq)} - CO2_{(g)} = (0.0049 \pm 0.0015) \, T \, (^{\circ}C) - (1.31 \pm 0.05) \qquad (6.7)$$

$$\bullet \quad HCO3 - CO2_{(g)} = -(0.114 \pm 0.003) \, T \, (^{\circ}C) + (10 \pm 0.04) \qquad (6.8)$$

$$\bullet \quad CO3 - CO2_{(g)} = -(0.052 \pm 0.021) \, T \, (^{\circ}C) + (7.22 \pm 0.38) \qquad (6.9)$$

(after Zhang et al., 1995)

6.2 Sources of carbon in the Indus River Basin

In the Indus River Basin possible sources of carbon are: 1) atmospheric carbon dioxide, 2) vegetation and soil carbon dioxide, and 3) carbonate rocks.

Atmospheric CO_2 dissolves in rainwater to form DIC. The concentration of DIC in rainwater depends on the partial pressure of CO_2 and ambient air temperature (equation 6.1). The partial pressure of CO_2 decreases with increasing altitude, represented by the following relationship:

$$P_z = P_0 \exp(-Z/H) \qquad (6.10)$$

where P_z is pressure at altitude z, P_0 the pressure at sea level and H, the scale height (~8.4 km in the lower troposphere). As a result, atmospheric pCO_2 in the upper Indus area at a mean altitude of 4.2 km would be $\sim 10^{-3.7}$ atmosphere or 218 ppmv. Assuming maximum air temperature of 0° C and pH of 5 for precipitation (Mayewski et al., 1983; Mayewski et al., 1984; Wake et al., 1992), rain water in equilibrium with atmospheric CO_2 in the upper Indus would have DIC (over 97% in the form of H_2CO_3) concentration of $\sim 10^{-1.8}$ mmolesL^{-1}, close to the range $(10^{-2} - 5 \times 10^{-2})$ commonly observed in rain water (Stumm

and Morgan, 1996). It implies that despite lower pCO_2, comparable DIC concentrations may be attained even in high altitude basins. Temperature has the overriding effect. Calculated DIC in rain water for the same altitude at 25° C is less than one half of that estimated above.

Assuming a $\delta^{13}C$ of -7.6‰ (Zhang, et al., 1995) for atmospheric CO_2 and a 1.2‰ depletion in $\delta^{13}C$ due to conversion of $CO_{2(gas)}$ to $CO_{2(aq)}$, the isotopic composition of DIC in unaltered rainwater would be about -8.8‰. The acidity may be neutralized by weathering reactions with a concomitant rise in DIC and a redistribution of aqueous carbonate species. Low concentrations (0.15 - 0.40 mmolesL^{-1}) of DIC are found in the dilute headwater tributaries (Fig. 6.1). These concentrations are about 10 to 25 times higher than that of rainwater. In addition, their pH values (7.6-7.9) are higher and $\delta^{13}C$ more enriched compared to rain water (i.e. -8.8‰). All this suggests that rainwater is not the direct source and that rock weathering plays an important role in pH buffering and generation of DIC.

6.2.1 Weathering of silicate rocks

In silicate basins the source of DIC in river water may be soil CO_2 and/or atmospheric CO_2, the former referred to as biogenic CO_2. In areas where soils are poorly developed, such as steep hill slopes, atmospheric CO_2 is the dominant source of DIC and the isotopic composition of resulting DIC is a function of pH (controls the proportions of aqueous carbonate species) and temperature. Since HCO_3^- is the dominant species in all samples and mean water temperatures in the headwaters is ~15° C, DIC in river water will be enriched by ~9‰ relative to atmospheric CO_2. Thus the headwaters weathering

silicate lithologies under atmospheric CO_2 should have a $\delta^{13}C$ around 1.4‰. The amount of DIC formed is a function of the residence time of water in the watershed as well as the
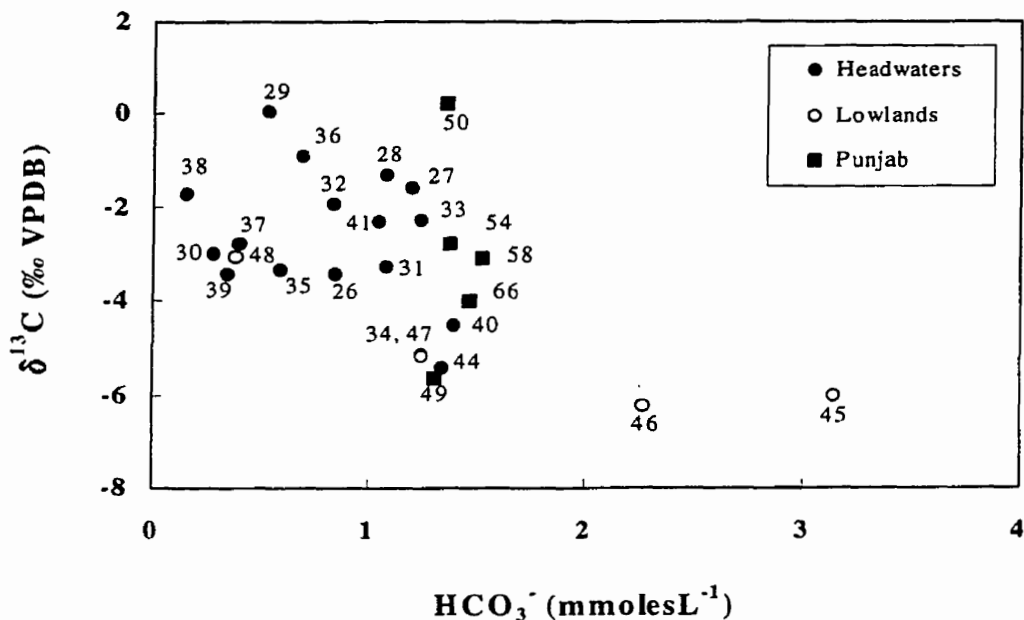
Fig. 6.1. Bicarbonate concentration and its isotopic composition for the Indus tributaries during the summer season. The key to the tributaries (26-66) as in Fig. 3.1.

type of silicate lithology. The latter influences resistance to weathering. The Kial River (38) draining mafic-ultramafic rocks, has the lowest concentration of HCO_3^- among all the Indus basin samples, has $\delta^{13}C$ of -1.7‰ (Fig. 6.1) and has pCO_2 half of that expected from atmospheric equilibrium. The Stak River (29), on the other hand, drains predominantly volcanic rocks and minor granite gneisses, derives 77% of its calcium and magnesium and 88% of its sodium and potassium from silicate weathering (see section 6.7), has pCO_2 close to atmospheric equilibrium (after correction for altitude), HCO_3^- concentration 0.5 mmolesL^{-1} and has $\delta^{13}C$ 0‰. Both rivers are undersaturated with respect to carbonate minerals (Fig. 5.4). Although, the Kial River shows some biogenic

102

influence, these two rivers broadly reflect weathering of silicate rocks under atmospheric conditions.

In regions with well developed soils, biogenic CO_2 constitutes the largest pool of DIC. The isotopic composition of CO_2 is similar to that of the decaying organics that in turns depends on the type of vegetation. Natural vegetation in temperate and high latitude regions is almost entirely C_3. Included in this group are most crops such as wheat, rye and cotton, with $\delta^{13}C$ ranging from -24 to -30‰, with an average of -27‰. Although rare, C_4 plants dominate in hot open ecosystems, such as tropical and temperate grasslands (Ehleringer et al., 1991) and also includes agricultural plants, such as sugar cane and corn, with $\delta^{13}C$ ranging between -10 and -16‰ and an average of -12.5‰ (Vogel, 1993).

The exact ratio of C_3 to C_4 in the Indus basin is not known. The vegetation is considered "mixed" throughout the basin except in the Himalayan foothills where it is dominantly C_4 (Quade et al., 1989; Cerling and Quade, 1993). Assuming a 1:1 ratio in the headwaters, DIC resulting from weathering of silicates by soil CO_2 will have $\delta^{13}C$ of about -11‰. Depleted isotopic compositions resembling this end member do not occur in any of the headwater silicate basins. However, perennial streams in the same area with analogous lithology, range between -8 and -9.6‰. This implies that weathering of silicate rocks by soil CO_2 is important only locally where groundwater passes a considerable distance through the organic-rich soil zone and that the occurrence of such waters is limited due to climatic and geomorphic factors, such as 1) low precipitation 2) sparsely developed soils and therefore 3) scanty vegetation.

6.2.2 Weathering of carbonate rocks

Weathering of carbonates rocks may occur by carbonic acid as well as by sulfuric acid derived from oxidation of sulfide minerals. The SO_4^{2-}/HCO_3^- molar ratio of all samples within the Indus River Basin is ~0.3, except for the lowlands where it ranges between < 0.1 for the Soan to ~17 for the Sanghar River, with the Kurram and Shahur rivers falling in between. This implies that although SO_4^{2-} in the Indus River Basin is derived mainly from oxidation of sulfides (see section 6.4), CO_2 remains the largest source of acidity in all but some of the lowland rivers. The isotopic composition of DIC derived from carbonate weathering will therefore depend also on the relative contribution of carbonic versus sulfuric acid. The Sanghar River, with low concentration of HCO_3^- (0.4 mmolesL^{-1}), pCO$_2$ below atmospheric equilibrium, pH of 8.0, saturation state below equilibrium with carbonate minerals, low Ca^{+2}/SO_4^{2-} (0.5) and high SO_4^{2-}/HCO_3^- molar ratios, together with isotopic composition of SO_4^{2-}, reflects carbonate weathering by sulfuric acid.

Like silicate weathering, CO$_2$ during carbonate weathering may be derived from the soil as well as from the atmosphere. The latter may, however, be constrained by kinetic processes that limits HCO_3^- concentration up to ~0.20 mmolesL^{-1} (Fairchild et al., 1994) and its isotopic composition to 0.7‰, assuming a $\delta^{13}C$ of 0‰ for marine carbonates and isotope enrichment factor of 9‰ at 15° C.

Weathering of carbonate rocks is most pronounced in calcareous terrains overlain by thick soils. Although, the $\delta^{13}C$ of the final DIC may be influenced by the degree of "openness" of the system to soil CO$_2$, at saturation it can account for up to 3‰ variation in $\delta^{13}C$ for the pCO$_2$ range (Clark and Fritz, 1997) observed in the lowland basins. Since

these rivers are calcite saturated at relatively lower pH, their pCO_2 and DIC concentrations require that dissolution of limestone be under open system conditions. Again, it is the $\delta^{13}C$ of decaying vegetation that exerts the dominant influence. Dissolution of carbonates under soil respired C_3 and C_4 vegetation will release DIC with $\delta^{13}C$ -10 and -2.8‰ respectively. Among the lowland rivers the Soan River has the highest concentration of DIC (3.0 mmolesL^{-1}), $\delta^{13}C$ -6‰, is oversaturated with respect to carbonate minerals, pCO_2 ~4 times higher than atmospheric equilibrium and low SO_4^2/HCO_3^- (0.1) molar ratio. These chemical and isotopic characteristics suggest: (1) sulfuric acid weathering plays a subordinate role in acid generation, (2) carbonate weathering proceeds under biogenic CO_2, and (3) the somewhat enriched $\delta^{13}C$ reflects contribution of C_4 vegetation.

6.2.3. End members and mixing relationships

The lowland rivers thus range from typical carbonate weathering under biogenic CO_2 (Soan River) to those undergoing sulfuric acid weathering (Sanghar River). Other lowland rivers represent varying mixtures of these two end members (Fig. 6.1). Therefore, at the scale of the entire Indus River Basin, two silicate end members (Kial and Stak rivers) and two carbonate end members (Soan and Sanghar rivers) can be identified. Using these constraints, the sources of DIC in the Indus main channel can be assessed.

The middle and lower Indus plot along mixing lines that join Kial-Stak-Soan end members (Fig. 6.2). Weathering of carbonates by sulfuric acid can be important locally, but remains unsubstantial in the Indus main channel. The distribution of data points

105

clearly demonstrates the downstream evolution of the Indus with increasing importance of carbonate weathering by biogenic CO_2.

The upper Indus, however, falls outside the mixing domain. Possible reasons for this includes:

1) Photosynthetic enrichment in $\delta^{13}C$, although this process is an unlikely explanation because no living plant, such as algae or other aquatic plants, were seen on filtered residue or in clear waters. Turbulent flow, low nutrients and moderate turbidity apparently limit aquatic flora;
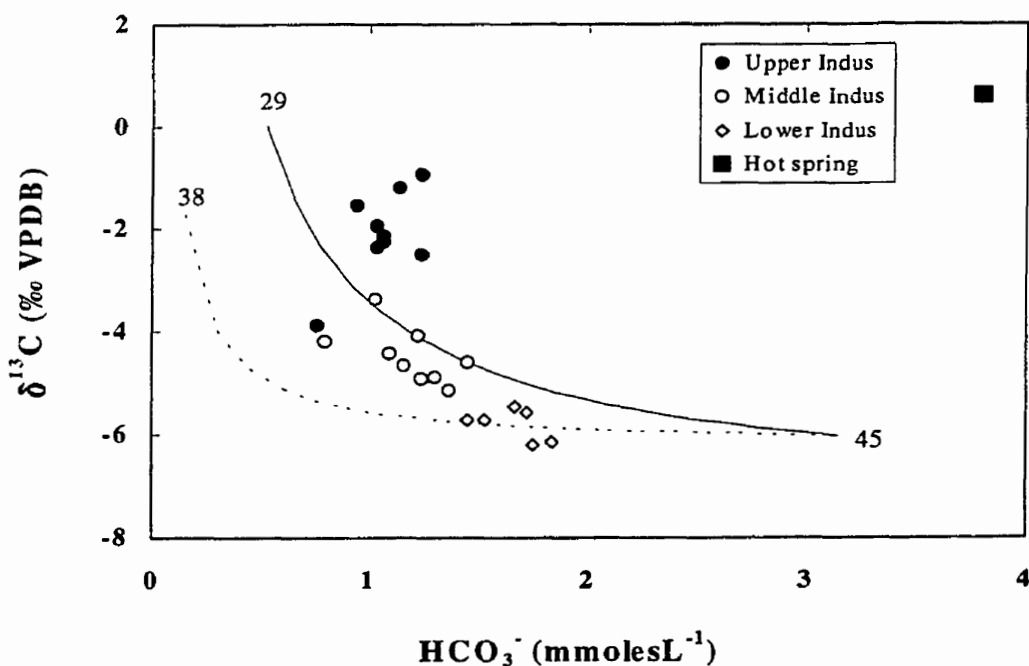
Fig.6.2. Bicarbonate concentration and its isotopic composition for the Indus main channel in the summer season. The curves represent two-component mixtures of the two silicate end members (38 and 29) and a carbonate end member (45) shown in Fig. 6.1.

2) Exchange with atmospheric CO_2. Enriched $\delta^{13}C$, up to 0.7‰, have been reported from the Great Lakes basin (Yang et al., 1993; 1996). These have been

106

attributed to atmospheric equilibration due to long residence time of water in the lakes. In the upper Indus, although the residence time of water is expected to be very short due to steep topography (and therefore hydraulic gradient), physical conditions such as turbulent flow and low temperature would be conducive to dissolution of atmospheric gases. This is demonstrated in the upper Indus by dissolved oxygen supersaturation (Fig. 6.3A) and pCO_2 levels close to or slightly higher than atmospheric equilibrium during the summer season (Fig. 6.3B).

3) Fontes et al. (1996) reported isotope data on closed lakes and inflowing tributaries of the Bangong system, Shyok basin. These range in $\delta^{13}C$ from -4.28 to -14.99‰, locally reaching 2.7‰, and the amount of DIC is between 1.6 and 5.6 mmolesL^{-1}. The lake surface water had DIC with ~67 and 49% modern carbon. These isotopic characteristics were attributed to influx along faults of CO_2 of deep crustal origin. $\delta^{13}C$ values up to 3‰ occur locally in parts of the Ganges-Brahmaputra basin (Galy and France-Lanord, submitted). These occur in the vicinity of thermal springs that contain HCO$_3^-$ concentrations up to 30 mmolesL^{-1} with $\delta^{13}C$ 13.5‰, and their origin is ascribed to metamorphic decarbonation at depth.

Thermal springs are known along the Indus Suture with somewhat greater concentration in the Nanga Parbat region (between stations 5 and 35, Fig. 3.1) and in the lower Indus, ~300 km north of its mouth (Shuja, 1986). The Tata Pani hot spring, Nanga Parbat, was sampled during this study and gave HCO$_3^-$ concentration of 3.8 mmolesL^{-1} and $\delta^{13}C$ 0.6‰. Contributions from such a source (minor, as can be viewed graphically) could explain departure of the upper Indus from the mixing trend on Figure 6.2. If so, this would imply a greater role of weathering of silicates by atmospheric CO_2 (points shifted

diagonally). On the other hand, if exchange with atmospheric CO_2 caused the observed shift it would indicate a greater role of carbonate weathering by biogenic CO_2 (points shifted along the y-axis).
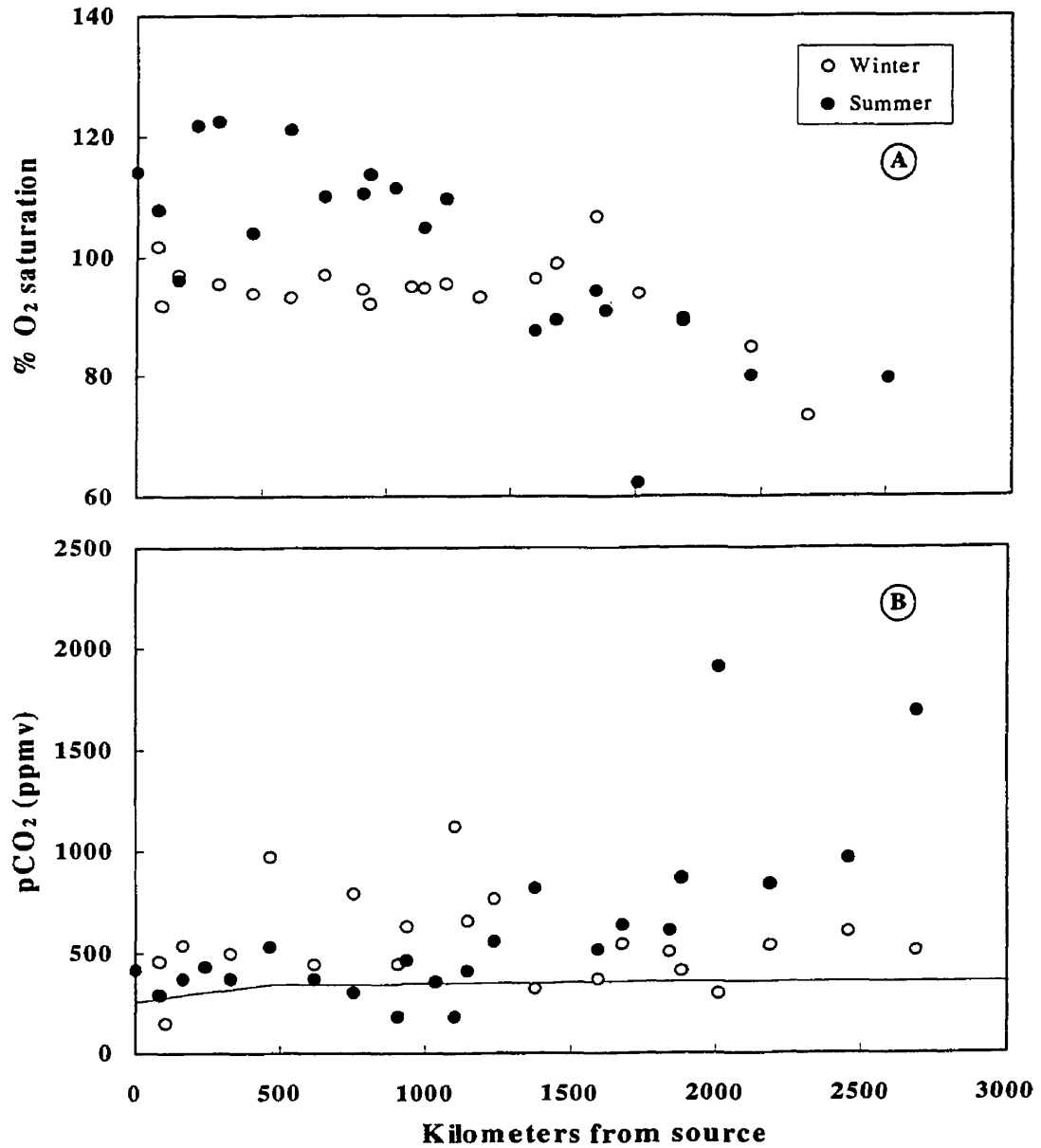
Fig. 6.3. (A) Dissolved oxygen saturation along the length of the Indus main channel. Saturation values take into account altitude of sample locations, explained in the text. (B) pCO_2 in equilibrium with the DIC, the curve represents pCO_2 of the atmosphere at given altitudes.

Seasonally, the Indus main channel at Sukkur barrage varies between -3.63 and -5.88‰ for $\delta^{13}C$ and 1.12 and 2.17 mmolesL^{-1} for HCO$_3^-$ (Fig. 6.4A), with discharge weighted averages of 1.4 mmolesL^{-1} and -5.3‰ respectively. In terms of end members and mixing, bulk of the data plots along mixing curves defined by the three end members (Fig. 6.4B). Samples collected during the base flow depart from the mixing trend due to higher HCO$_3^-$ concentrations and enriched $\delta^{13}C$. This can occur under the following scenarios.

1) The difference in $\delta^{13}C$ between base flow and peak discharge is ~2‰. Theoretically, lower water temperatures during baseflow could account for up to 1‰ enrichment in $\delta^{13}C$ (Eq. 6.8) as well as for enhanced solubility of carbonates and therefore higher concentration of HCO$_3^-$.

2) Exchange with the atmosphere may occur due to long residence time (~1 year) of water in reservoirs. Large water bodies require about two months for establishment of equilibria with the atmosphere (Mook, 1970). At Sukkur barrage, pCO$_2$ levels are mostly higher than atmospheric equilibrium. Exchange of carbon may occur by molecular or eddy diffusion, albeit the net flux of CO$_2$ is from the river to the atmosphere (Fontes et al., 1996).

3) While the higher concentration of HCO$_3^-$ during base flow is a common feature, groundwater should impart a more depleted (rather than the observed enriched) isotopic signature, provided that the source of biogenic CO$_2$ throughout the hydrograph remains the same. The data suggest that this last condition is not met and that there is greater contribution of C$_4$ vegetation during the baseflow. This period in the Indus basin

coincides with the harvesting of corn and sugarcane (both belonging to the C_4 vegetation) during the fall and winter seasons respectively.
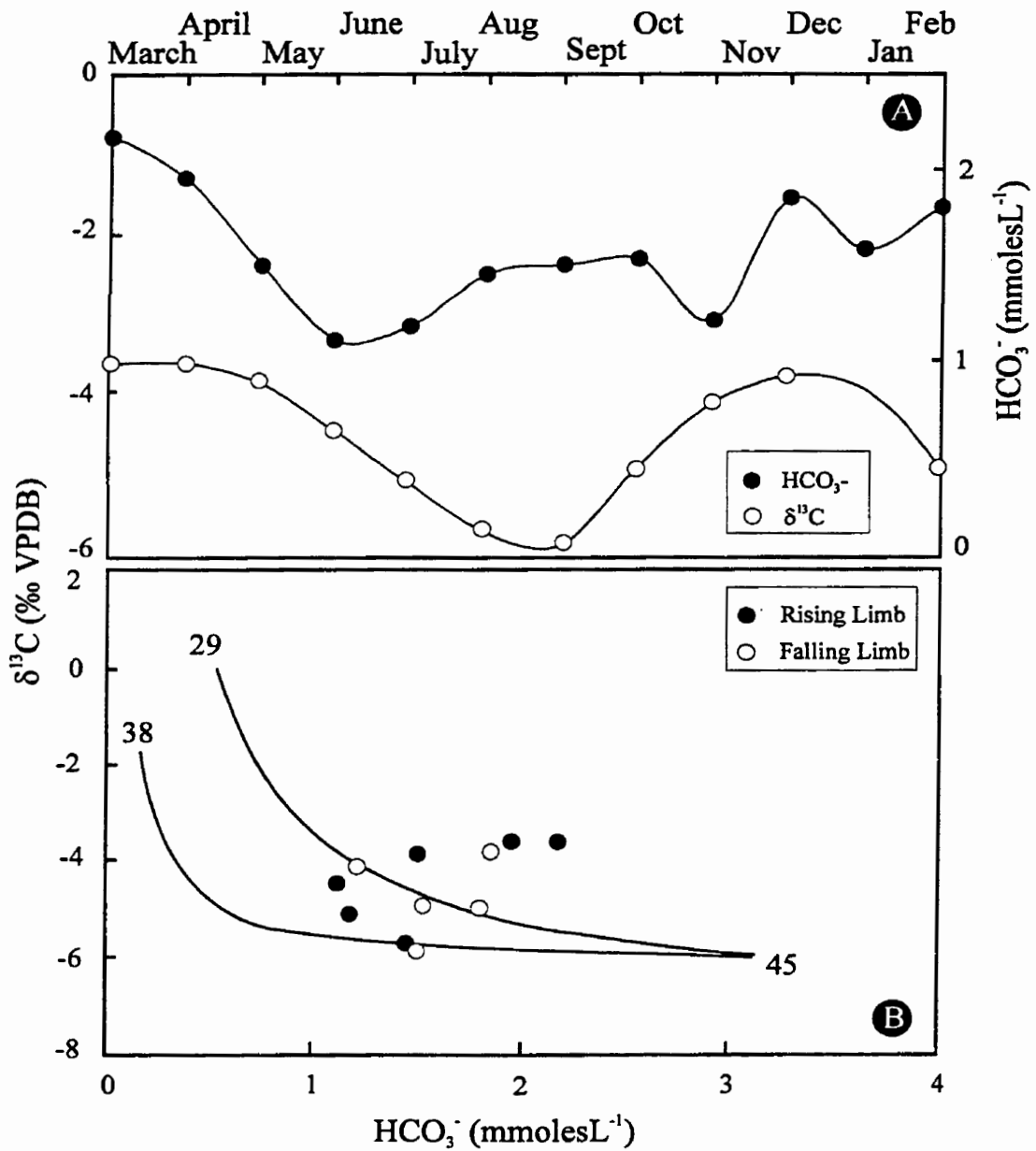
Fig. 6.4. (A). Bicarbonate concentration and its isotopic composition for the time series on the Indus main channel at Sukkur barrage. (B) Two-component mixing curves based on HCO_3^- and $\delta^{13}C$. End members as in Figures 6.1 and 6.2.

6.3 Biogeochemistry

Respiration and photosynthesis are the key biogeochemical processes in aquatic systems that control water chemistry. All photosynthetic plants absorb CO_2 (or HCO_3^-) and water that are transformed into organic matter in the presence of sunlight.

$$CO_2 + H_2O \rightarrow CH_2O + O_2 \qquad (6.11)$$
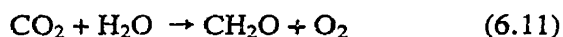
CH_2O is the generalized formula for carbohydrate organic matter. In water bodies dominated by photosynthesis, this process leads to draw down of pCO_2 in the water column, decline in nutrient concentration, enrichment of ^{13}C in the residual DIC due to preferential uptake of ^{12}C, and oxygen supersaturation. Respiration on the other hand drives equation (11) in the opposite direction leading to inversion of chemical and isotopic trends.

6.3.1 Carbon dioxide and oxygen

Figure 6.3B shows pCO_2 variations along the length of the Indus main channel. On average, the highest levels occur in the lower Indus during the summer season followed by intermediate values in the middle reaches. In the upper Indus, pCO_2 levels are close to or slightly above atmospheric equilibrium and more so during the winter season. Dissolved oxygen is close to saturation in the upper and middle Indus during the winter season but supersaturated during the summer (Fig. 6.3A), declining rapidly to undersaturation in the lower Indus, irrespective of the season. The tributaries from headwaters to the mouth of the Indus roughly define similar trends.

In addition to biological processes, altitude and temperature influence dissolved oxygen in water. Partial pressure of oxygen in the atmosphere at a given altitude is given

by equation (6.10). Available topographic data had insufficient resolution, therefore altitude at sample locations were extrapolated from hypsographic curve (Fig. 6.5).

The Henry's law gives equilibrium concentration of oxygen in water. The temperature dependence of Henry's law constant is given by:

$$K_H = H_o . \exp[-\Delta H/R . (1/T - 1/T_o)] \qquad (6.12)$$

Where K_H is Henry's law constant, $H_o = 1.3E\text{-}3$ moles atm^{-1}, $\Delta H/R = 1500K$ (Wilhelm et al., 1977; Lide and Frederikse, 1995), T= temperature in °K, T_o= 298.15. Regression of K_H and temperature (°C) gives

$$K_H = [(3E\text{-}07T^2) - (4E\text{-}05T)] + 2.1E\text{-}3 \qquad (6.13)$$
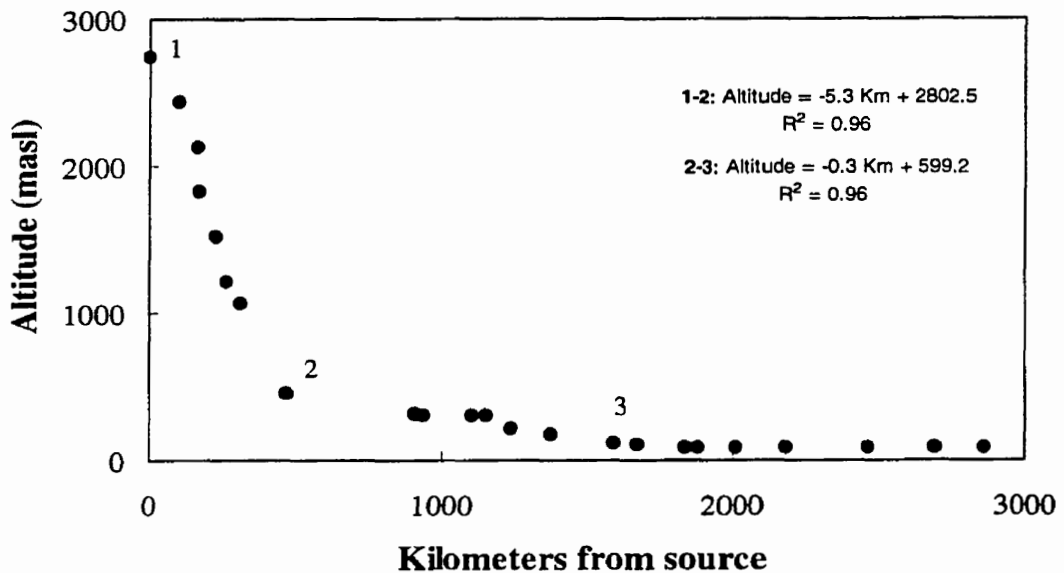
Fig.6.5. Hypsographic curve for the Indus River. Source of data is DMA (1995) for locations between 1 and 3 and NGDC (1988) for locations beyond 3. Polynomial fit for all the data points gave unrealistic values at the lower and upper end of the curve, therefore two linear fits were employed between 1 - 2 and 2 – 3. Beyond location 3, altitude at sample location were available and used for calculations.

112

Thus dissolved oxygen levels in the upper and middle Indus are higher than those predicted by equilibrium relationships and must be therefore controlled by kinetic processes. Most likely, physical entrapment of atmospheric oxygen due to turbulent flow is responsible. Photosynthesis could lead to oxygen supersaturation (Pawellek and Veizer, 1992; Flintrop et al., 1996) but this is not likely the case for reasons discussed above. As a whole, pCO_2 tends to covary negatively with dissolved oxygen (Fig. 6.6A). The Punjab, the lowlands and the lower Indus have CO_2 overpressures and dissolved oxygen deficit. This reflects consumption of oxygen by respiration (of organics) and concomitant release of free CO_2.

6.3.2 Carbon isotopes

The $^{13}C/^{12}C$ ratio together with pCO_2 and dissolved oxygen can be used to asses qualitatively the prevalence of photosynthesis/respiration. In the Indus River Basin, like other rivers (Amazon, Rhine, and Danube), $\delta^{13}C$ declines with rising pCO_2 (Fig. 6.6B). The Punjab rivers during the winter season, the lowlands and the lower Indus have high pCO_2 and depleted $\delta^{13}C$ compared to the headwaters. During the summer season, the middle reaches of the Punjab rivers, however, have enriched $\delta^{13}C$ as well as high pCO_2. The high pCO_2 are a consequence of low pH (Fig. 6.7) caused by acid rain or direct release from industries. Sulfur isotope data (see below) fall within the range of atmospheric or industrial sources.
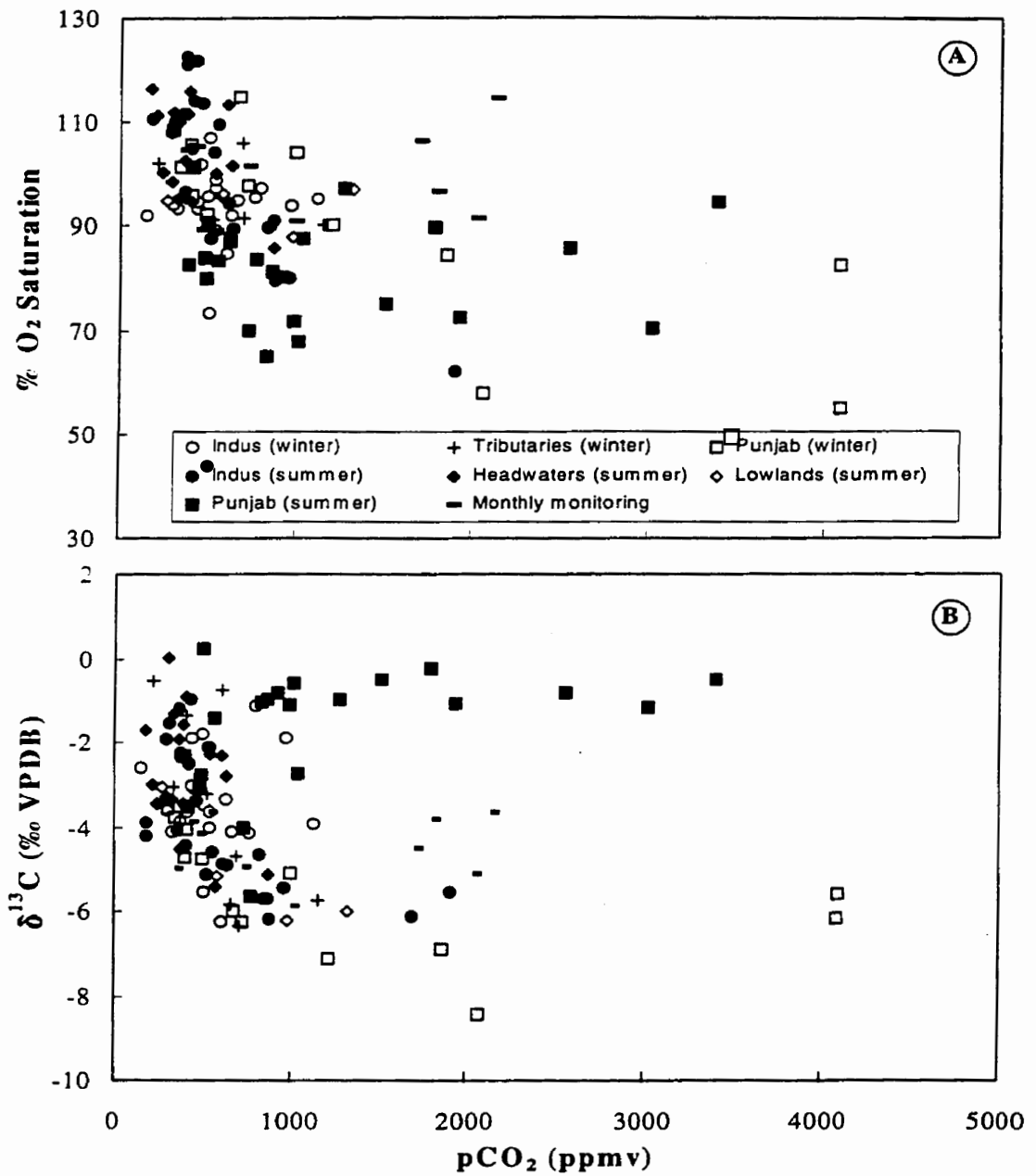
Fig.6.6. Percent oxygen saturation (A) and $\delta^{13}C$ of DIC (B) versus pCO$_2$ for the Indus River Basin.

114

4000

3000

pCO₂ (ppmv)

2000

1000

0

$pCO_2 = -3113.7\ pH + 26140.9$

$R^2 = 0.93$

7.2   7.4   7.6   7.8   8   8.2   ъ.4

pH
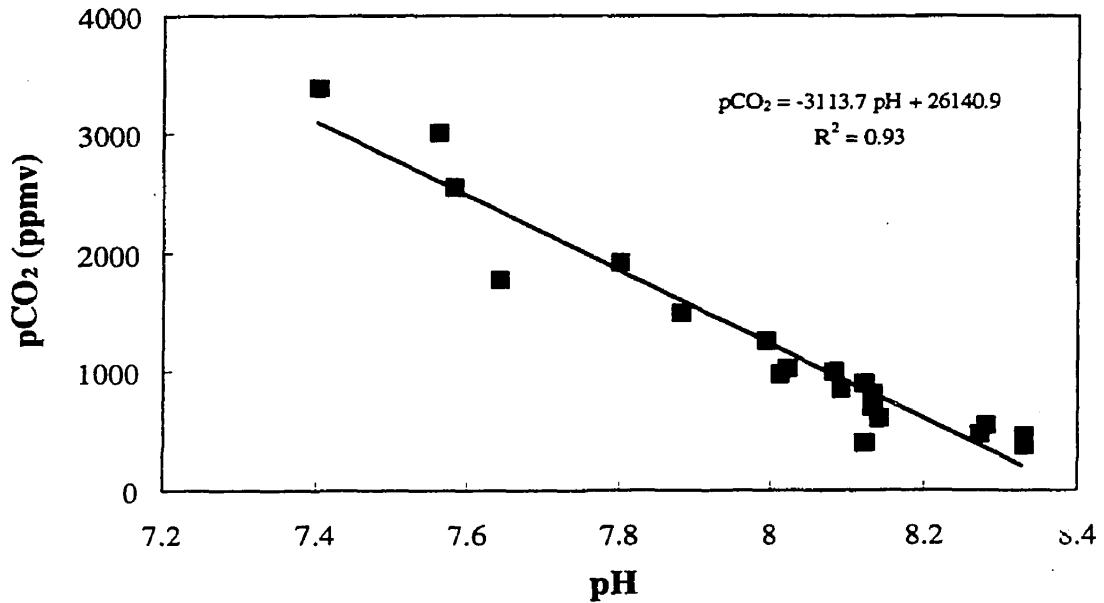
Fig. 6.7. pCO₂ versus pH for the Punjab rivers sampled during the summer season.

6.3.3 Ammonia, Nitrate and Phosphate

Ammonia concentrations in the Indus main channel during both seasons were below detection limits, with measureable concentrations only during the winter season in the Swat and Kurram rivers (3 $\mu molesL^{-1}$), and in the Punjab rivers. The latter range between 4 and 83 $\mu molesL^{-1}$, reaching 395 $\mu molesL^{-1}$ in the Ravi River (station 63).

Nitrate concentrations are lower in the headwaters than they are in the lowlands and in the Punjab. In the Indus main channel during the winter it rises in the downstream direction and peaks just before the confluence with the Panjnad (Fig. 6.8). However, no systematic trend was observed during the summer season. As a whole, the relationship of nitrate with pCO₂ (Fig. 6.9A) and with dissolved oxygen is complex (Fig. 6.9B). Nonetheless, in the tributaries during the summer season nitrate tends to increase with oxygen undersaturation and with rising pCO₂, reflecting respiration of organic matter.

115

This is in contrast to rivers of the North Rhine-Westphalia, where nitrate concentrations decrease with rising pCO_2 and with declining oxygen, both trends caused by nitrate reduction (Flintrop et al., 1996). The Punjab rivers during the summer season appear to
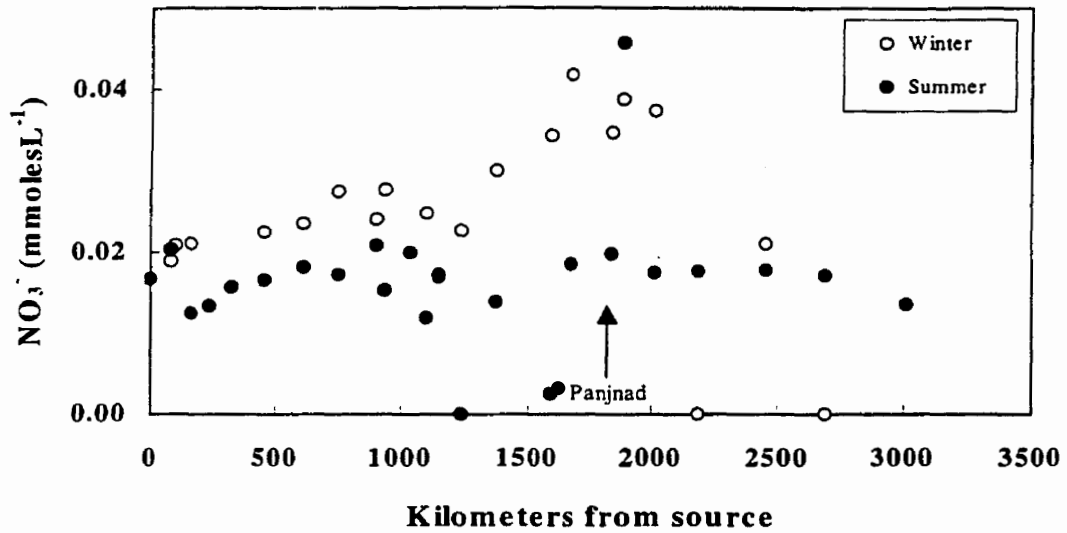
Fig.6.8. Nitrate concentrations along the length of the Indus main channel.

conform to such a trend but the geographic location of samples does not agree with denitrification or nitrate reduction (i.e. the decrease in concentration of nitrate and oxygen undersaturation are not in the downstream direction). Mixing of different water masses (by link canals) and release of nitrate from point sources is more likely to cause this trend.
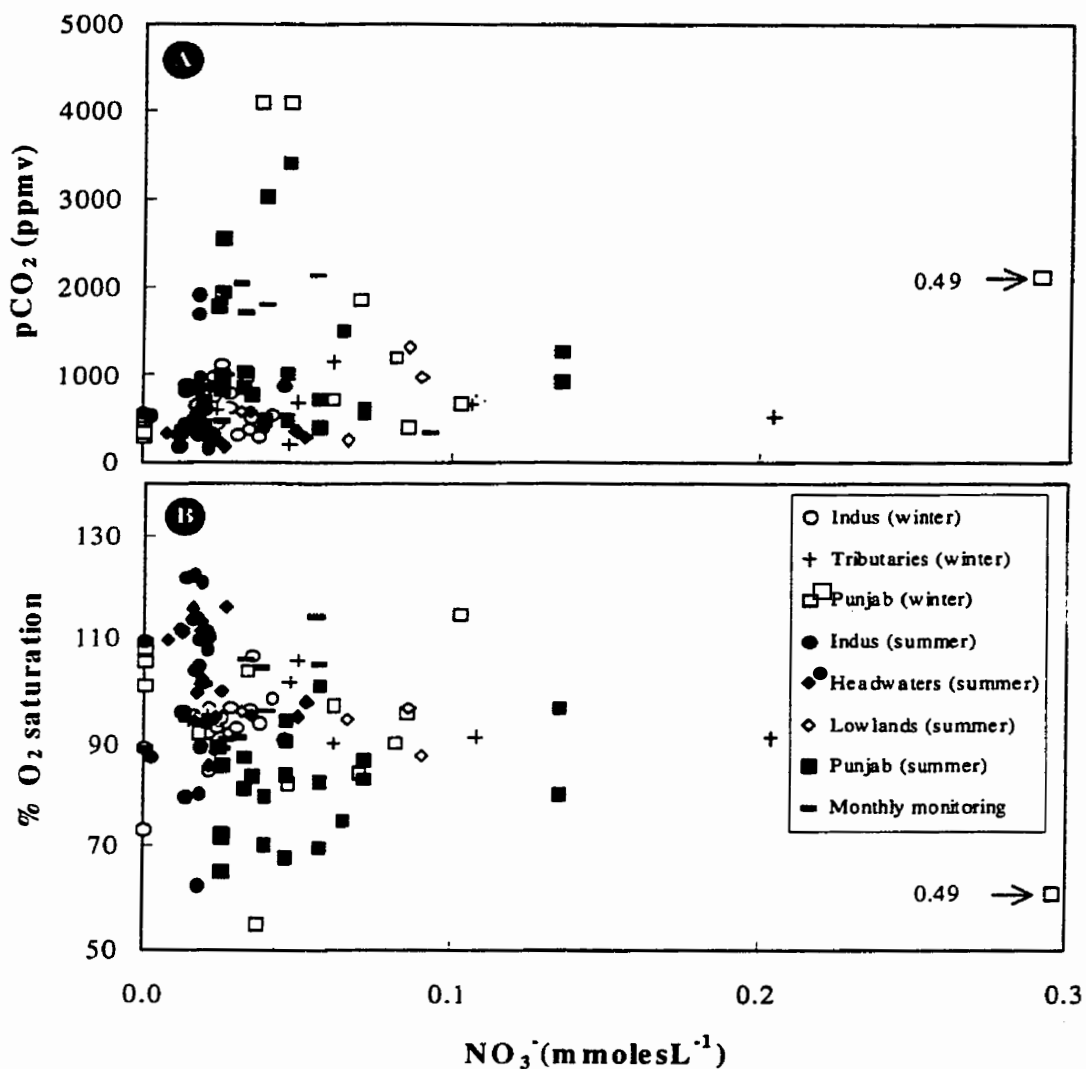
Fig. 6.9. pCO$_2$ (A) and percent oxygen saturation (B) versus nitrate concentration for the Indus River Basin.

The distribution of phosphorous concentration in the Indus River Basin has a similar pattern as the other nutrients. The Punjab, the lowlands and the middle and lower Indus have higher concentrations than the headwaters and more so during the summer compared to the winter (Fig. 6.10 and Appendix B). However, in the Indus River at Sukkur barrage, no clear trends related to discharge or other nutrients are discernible. A

117

similar behavior of phosphorous was observed in the Amazon basin by Devol et al. (1995).
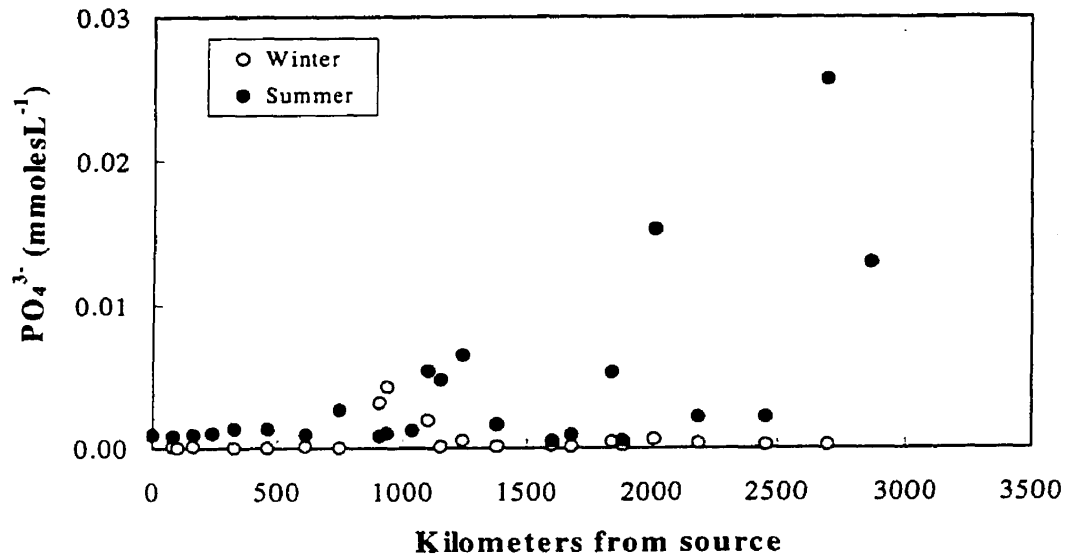
Fig. 6.10. Dissolved phosphorous concentration in the Indus main channel.

In summary, the Indus River Basin has two major ecosystems, the headwaters dominated by geogenic, and the lowlands and the Punjab region by biogenic sources. Scarcity of soils and sparse vegetation combined with aridity and lower temperatures support only limited biological activity in the headwaters. On the other hand, the plains contain thick soils and supports natural vegetation as well as crops. These areas also host the bulk of the population in the basin. Biological decay of organics in these regions plays an important role in modifying water chemistry. The Indus River integrates the two ecosystems and forms a continuum from its source to the mouth.

6.4. The sulfur cycle and sulfur isotope

Sulfur is widely distributed in the lithosphere, biosphere, hydrosphere, and atmosphere. It is a major constituent of sea water as well as marine sediments and is an important nutrient for plants. The biological cycle of sulfur is in part characterized by the activity of sulfur oxidizing and reducing bacteria which together account for the bulk of contemporary turnover rates in the biosphere (Baas-Becking, 1925; Postgate, 1959; Alexander, 1971). In addition to natural sources, sulfur may enter the atmosphere from anthropogenic sources, such as fossil fuel burning, fertilizers and mining and mineral processing. It is actively exchanged between these reservoirs and defines the Global Sulfur Cycle. Rivers annually transport 213×10^{12} g S (Schlesinger, 1991) to the world oceans. This is almost double the amount in the preindustrial age (Ivanov et al., 1983). Similarly, Berner and Berner (1996) estimated that 54% of the riverine sulfate is due to pollution and the remainder from natural sources including rock weathering. Thus it is of interest to examine sulfur in surface waters and in precipitation and to evaluate its sources.

Sources of SO_4^{2-} in river water include: 1) dissolution of gypsum, 2) oxidation of igneous sulfide minerals, 3) oxidation of sedimentary sulfides, 4) atmospheric deposition as dimethyl sulfide, 5) atmospheric deposition of sea spray, and 6) local atmospheric precipitation from biogenic/anthropogenic pollution sources. These alternative sources are usually characterized by different S (and oxygen) isotopic composition, a property that enables their differentiation. The $\delta^{34}S$ of source (1) depends on its age of formation and has varied during the Phanerozoic between ~ +10 and +30‰ (Claypool et al., 1980).

The source (2) is characterized by $\delta^{34}S$ of $0 \pm 3‰$ if mantle-derived (Chaussidon and Lorand, 1990), ~0 to +8‰ for island arc basalts and andesites, and ~ -7 to +11 if granite derived (Rollinson, 1993), with an average for all igneous rocks of 0‰ (Thode, 1991). The $\delta^{34}S$ of sulfate from oxidation of sulfides is mostly only marginally depleted from the original sulfide (Clark and Fritz, 1997), but for biologically-mediated oxidation of base-metal sulfides, the sulfate is depleted in $\delta^{34}S$ by 2 to 5‰ (Toran and Harris, 1989). The source (3), oxidation of sedimentary sulfides yields usually negative $\delta^{34}S$ values and is due to the major isotope fractionation in the sedimentary cycle that accompanies bacterial reduction of sea water sulfate to H_2S and subsequent fixation as FeS and FeS_2. The sulfide minerals may be depleted in ^{34}S relative to sea water by up to 70‰ (SCOPE 19, 1983). The source (4), atmospheric deposition as dimethyl sulfide, has $\delta^{34}S$ of 15.6 $\pm 3.1‰$ (Calhoun et al., 1991). The source (5), atmospheric deposition of sea spray has $\delta^{34}S$ similar to that of modern sea water (+21‰; Rees, 1978). Finally, the source (6), precipitation from biogenic anthropogenic sources is influenced strongly by local sources, but has $\delta^{34}S$ mostly between +4 and +6‰ (Caron et al., 1986; Mcardle and Liss, 1995; Wadleigh et al., 1996).

6.4.1 Sources of sulfate in the Indus River Basin: the tributaries

In the Indus River Basin, sulfate concentrations in all the headwater tributaries are delimited by the Stak and Shahbatot rivers that contain 0.77 and 0.125 mmolesL^{-1} respectively (Fig 6.11). Their $\delta^{34}S$ lies roughly in the range of 0 to +10‰, except for the Shingo and Hunza rivers that have negative values. The lowlands on the other hand reach 6.25 mmolesL^{-1} and $\delta^{34}S$ of about -5.5‰. Among the Punjab rivers the Sutlej has the

lowest and the Panjnad the highest concentration of sulfate, but all have uniform isotopic compositions (+5 ± 1‰). Based on combined field, geochemical and isotopic data the following origin(s) are suggested for sulfate in the Indus River Basin.

1) The headwaters with $\delta^{34}S$ in excess of 0 ‰ derive their SO_4^{2-} from oxidation of igneous sulfides. The range of values in $\delta^{34}S$ apparently reflects natural variations in the oxidizing sulfide minerals, since some of the headwaters with $\delta^{34}S$ around +10 ‰ do not have any known evaporite deposits, such as gypsum. Their lithologies, comprised entirely of igneous and metamorphic rocks, however, may harbour traces of evaporite minerals, and this is seemingly supported by high concentration of SO_4^{2-} and $\delta^{34}S$ in the Stak River (Fig. 6.11, station 29). Some of the headwater rivers appear to plot along a line with negative slope terminating at Jaglot and Kabul rivers (samples 35 and 44) at the lower end. This line intersects the $\delta^{34}S$ axis at ~ +14‰, giving an impression of mixing from an evaporite end member (at +14‰) and an average igneous sulfide (0 ‰). On the other hand, the Shahbatot River (station 30) that has only slightly lower $\delta^{34}S$, has SO_4^{2-} concentration six times lower than the Stak River. This clearly suggests that variations in the amount and isotopic composition of sulfate are due to heterogeneities in the weathered rocks, a proposition supported by the below discussed oxygen isotopes.

2) The Sanghar, Shahur, and Kurram rivers in the lowlands, and the Shingo (and possibly Hunza) river among the headwaters, derive their SO_4^{2-} from oxidation of reduced sedimentary sulfides, such as pyrite in shales and carbonate rocks. Major ion chemistry and carbon isotopes support the role of sulfuric acid in weathering of carbonates in these lowland tributaries. In the lowlands, marine carbonates and shales

121

crop out in the West Pakistan Fold Belt in the headwaters in the Indus Suture Zone and in the Tethyan sequence.

3) The Punjab rivers with their low SO_4^{2-} and $\delta^{34}S$ between +4 and +6‰ load on the biogenic anthropogenic factor (see chapter 7) and most likely derive their sulfur from atmospheric or industrial sources, such as those listed under (6) above.
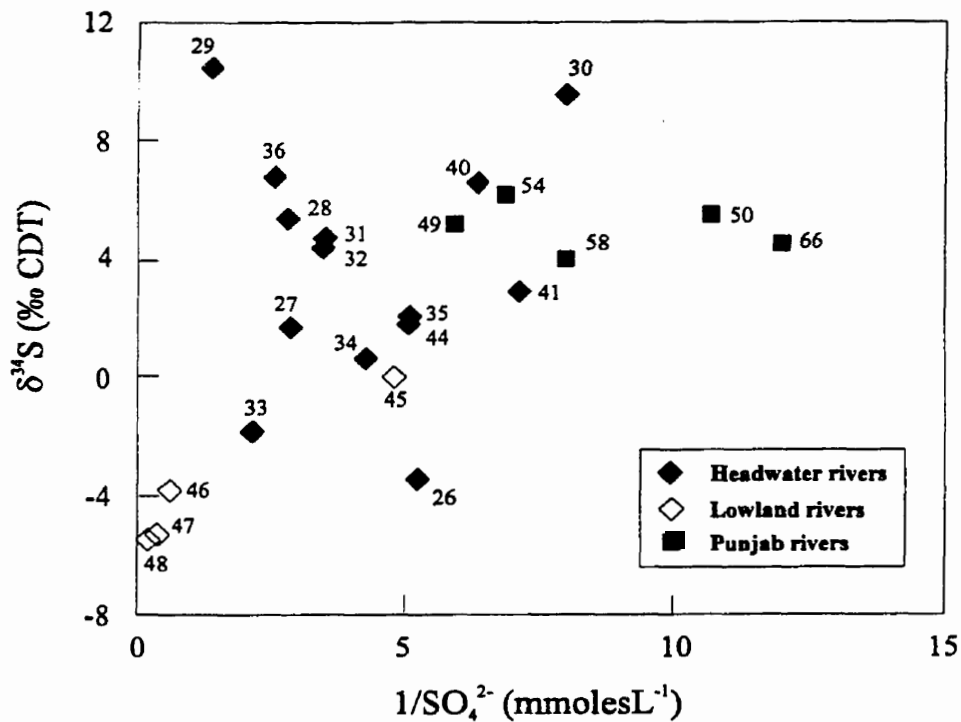
Fig. 6.11. Scatter diagram of $\delta^{34}S$ vs the reciprocal of concentration of sulfate for the tributaries of the Indus River, sampled during the summer season. The key to the tributaries (26-66) as in Fig. 3.1.

A narrow belt of Late Proterozoic to Early Cambrian evaporites, salt and gypsum, can be traced from northwestern Iran through Pakistan into India (Strauss, 1993). In

Pakistan, the Salt Range crops out on the eastern bank of the Jhelum River, extending westwards into the West Pakistan Fold Belt (Gansser, 1964). The $\delta^{34}S$ of gypsum and anhydrite from southern Iran ranges between +21 and +32‰ (Houghton, 1980; Strauss, 1993). Enriched isotopic compositions resembling these values are not found in any rivers in the vicinity of the Salt Range. The absence of such an isotopic signature in the middle and lower Indus basin is apparently due to arid climate of the region and to internal drainage. Apparently, the discharge from these areas does not reach major rivers.

6.4.2 Sulfate in the Indus main channel

Figure (6.12) shows the variation of SO_4^{2-} and its isotopic composition along the downstream profile of the Indus main channel. Analogous to most of the tributaries, both concentration and $\delta^{34}S$ are higher in the winter compared to the summer season. The higher $\delta^{34}S$ during the baseflow are apparently due to contribution from residual sulfates in soils, undergoing bacterial sulfate reduction. The nascent Indus has isotopic signature similar to oxidation of sedimentary sulfides in shales and carbonates, the latter common in the Indus suture zone and the Tethyan sequence. During both seasons, $\delta^{34}S$ rises sharply in the upper Indus and is accompanied by decline in sulfate concentration, particularly pronounced during the summer season. These together reflect subsequent inputs from weathering of igneous and metamorphic rocks.

In the middle Indus, sulfate concentration rises while the $\delta^{34}S$ is more or less uniform during the winter season. In the same stretch during the summer season, the pattern of $\delta^{34}S$ is erratic. Nonetheless, the major peak in concentration coincides with the trough in $\delta^{34}S$. The two spikes in $\delta^{34}S$ at the same locations are also noticeable in $\delta^{18}O$, a

feature attributed to incomplete mixing with tributary and "old" water in the reservoirs (see chapter 4).
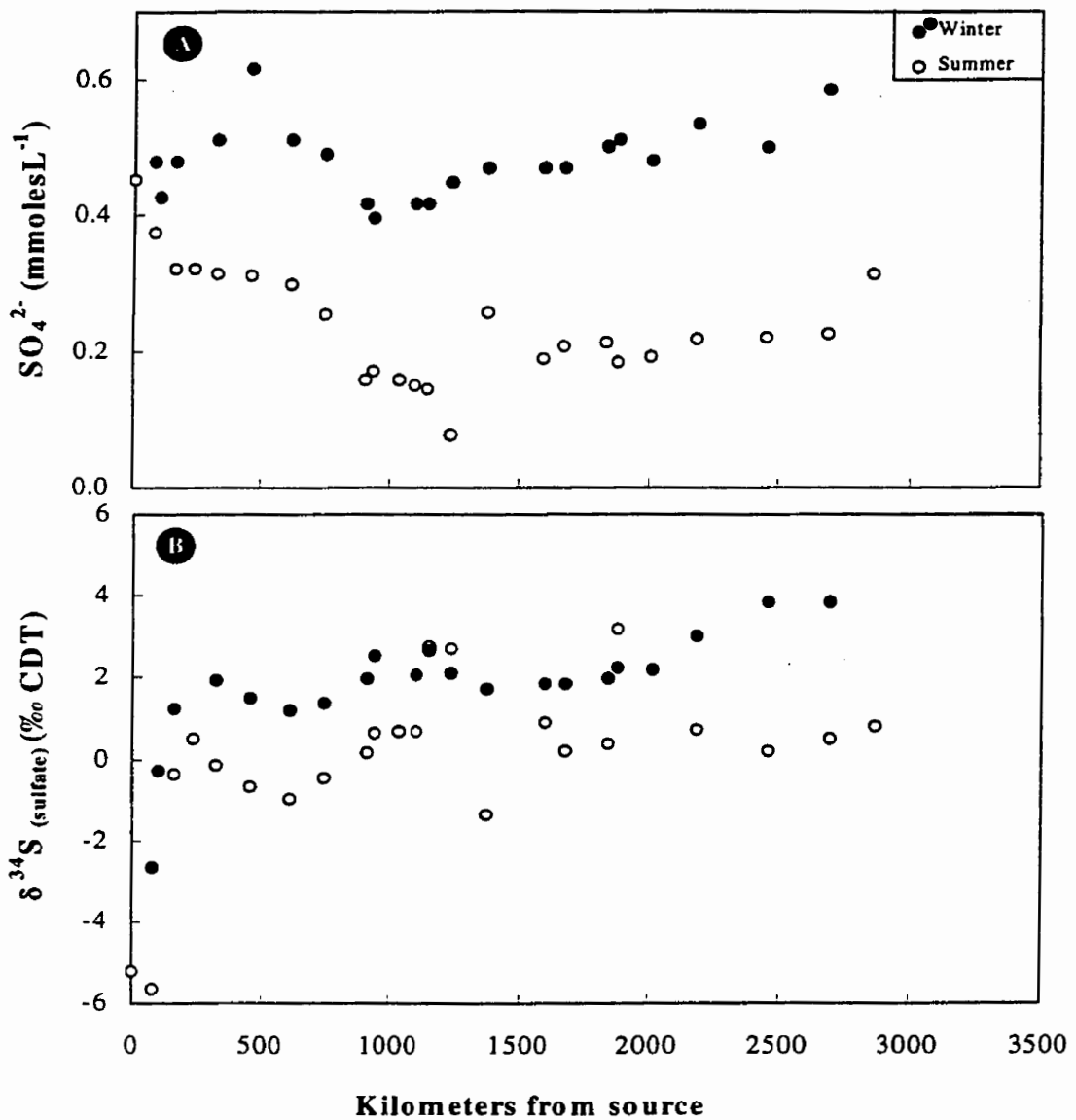
Fig. 6.12. Sulfate concentration (A) and its sulfur isotopic composition (B) for the Indus River along its longitudinal profile.

124

In the lower Indus during the baseflow, SO_4^{2-} continues to rise with increasing $\delta^{34}S$. This is the driest part of the basin where no perennial tributary joins the Indus. The increase in concentration is from ~0.5 to 0.6 mmolesL^{-1} accompanied by a shift in $\delta^{34}S$ from +2 to +4‰. An isotopic mass balance calculation reveals that the unknown source has a $\delta^{34}S$ of +13.8‰. This clearly rules out sea spray, as a cause (see pp. 119-120). Shallow ground waters may cause the observed trend by contributing high concentration of residual sulfate enriched in ^{34}S.

6.4.3 Environment of sulfate formation: oxygen isotopes in sulfate

Oxygen isotopes are uniquely applicable to the study of mechanism of formation of sulfate. This information together with sulfur isotopes can be used to identify the sources of sulfate. The basis for its application as tracer are: 1) once formed, the rate of oxygen isotope exchange between sulfate and environmental water under typical temperature and pH of rain, surface and ground waters is extremely low (Lloyd, 1967; Kusakabe and Robinson, 1977; Chiba and Sakai, 1985). For example, at pH 4.0 the half-time of oxygen exchange between sulfate and water is of the order of 1000 years (Lloyd, 1967) and at normal groundwater temperatures about 10 million years (Chiba and Sakai, 1985); 2) The $\delta^{18}O$ of sulfate is not appreciably affected during analytical procedures (Holt et al., 1978); and 3) Large difference in $\delta^{18}O$ of atmospheric oxygen (+23‰; Horibe et al., 1973) and that of surface/groundwater (function of geographic location but mostly negative values) and sea water (varied between +9 and +23‰ in the past with a present day value of +9.5‰; Claypool et al., 1980; Fritz et al., 1988; Longinelli, 1989), allows discrimination between these sources.

125

In aqueous systems, however, the $\delta^{18}O$ of sulfate formed by oxidation of sulfide is complicated due to contribution of oxygen from both the atmosphere and the water molecule. The relative proportion of the two sources of oxygen varies according to the enzymes involved in the biological pathway (Clark and Fritz, 1997). The incorporation of oxygen from each of these sources involves fractionation effects (Krouse 1980; Longinelli, 1989; Toran and Harris, 1989). The $\varepsilon^{18}O_{SO4-O2}$ during oxidation by Fe^{3+} reduction range between -8.7‰ (Lloyd, 1967) and -11.4‰ (Taylor et al., 1984). On the other hand, $\varepsilon^{18}O_{SO4-H2O}$ is about +2 to +4‰ (Toran and Harris, 1989). With these constraints it is possible to reconstruct the $\delta^{18}O$ of sulfate formed by oxidation of sulfide under different proportions of atmospheric and water derived oxygen.

Table 6.1 lists $\delta^{18}O$ of water and $\delta^{34}S$ together with $\delta^{18}O$ of sulfate of selected samples from the Indus River Basin. The Stak River with the highest $\delta^{34}S$ in the basin, has $\delta^{18}O$ of sulfate +2.4‰, much depleted compared to $\delta^{18}O$ of sulfate of marine origin. The tributaries become progressively enriched in ^{18}O of sulfate as river water $\delta^{18}O$ rises (Fig. 6.13). Two samples from the Indus main channel collected near the source and its mouth follow the same trend. Such a trend clearly reflects the involvement of ambient river or precipitation water in the formation of sulfate. Isotopic mass balance calculations show that ~40 to 60% of oxygen in sulfate is being derived from the ambient river water and the remaining from the atmosphere (Fig. 6.13). The close correspondence between $\delta^{18}O$ of sulfate and $\delta^{18}O$ of river water therefore provides an indirect evidence of the source of sulfates and supports the conclusions based on sulfur isotopes and major ion chemistry.

Table 6.1. Isotopic composition of sulfate and water for selected samples of the Indus River Basin. The location numbers refer to Fig. 3.1.

River	Location	$\delta^{34}S_{(sulfate)}$	$\delta^{18}O_{(sulfate)}$	$\delta^{18}O_{(water)}$
Shyok	27	1.7	-1.8	-15.7
Stak	29	10.4	2.4	-12.7
Gilgit	34	0.6	1.7	-12.9
Gonar	36	6.8	5.6	-12.1
Khan	40	6.6	8.8	-6.9
Sanghar	48	-5.5	8.8	-2.4
Panjnad	49	5.2	6.1	-8.4
Indus (source)	1	-5.2	0.1	-14.9
Indus (mouth)	25	0.8	4.2	-10.5
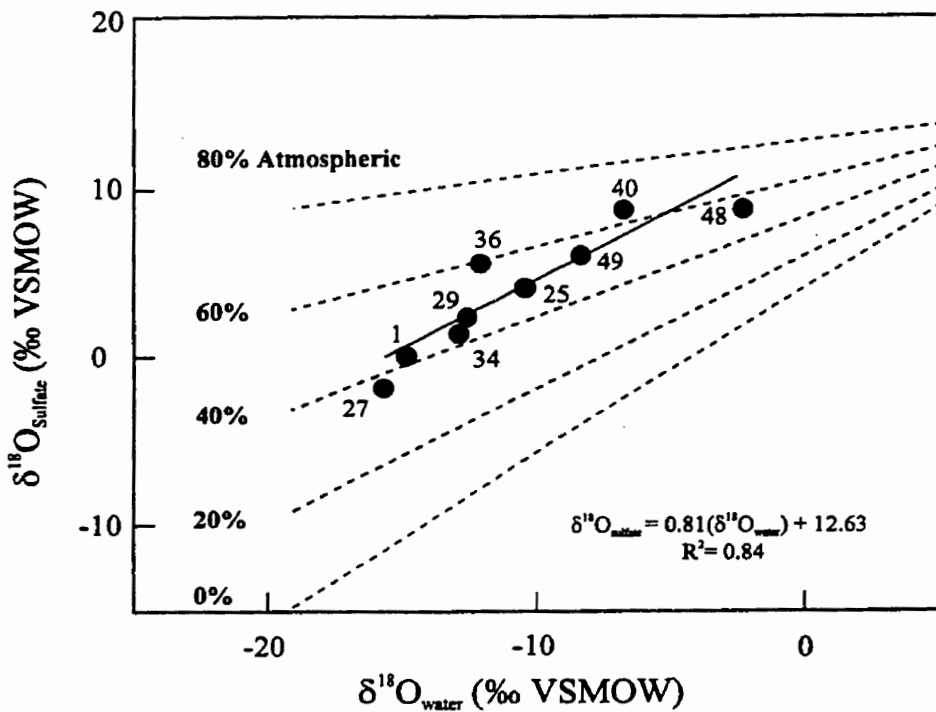
Fig. 6.13. Oxygen isotopic composition of dissolved sulfate and $\delta^{18}O$ of river water of selected samples from the Indus River Basin. The curves are based on isotopic mass balance calculations, assuming a 4.1 ‰ fractionation of $\delta^{18}O$ between sulfate and water and -8.7‰ between sulfate and atmospheric oxygen. The key to the sample numbers as in Fig. 3.1.

127

6.5 Strontium isotopes

6.5.1 Why strontium isotopes in rivers?

Rivers provide the major flux of strontium to the oceans and, therefore, play a major role in defining the marine $^{87}Sr/^{86}Sr$ (Palmer and Edmond, 1992). Modern sea water has $^{87}Sr/^{86}Sr$ = 0.709 (Faure, 1986). This ratio has varied throughout the Phanerozoic and reflects the relative contributions of strontium to the ocean from continental weathering and from hydrothermal activity along mid ocean ridges (Veizer, 1989). Old crustal rocks are characterized by high $^{87}Sr/^{86}Sr$ ratios (> 0.71) while marine carbonates (0.706 – 0.709) and young volcanics by still lower ratios, the latter depending on their age and Rb/Sr ratios. Of particular interest in variations of Phanerozoic sea water $^{87}Sr/^{86}Sr$ is its steady increase during the last 40 Ma, which coincides with the uplift of the Himalayas and with the global climatic cooling. This parallelism led to the hypothesis that intense weathering of silicate rocks in the Himalayas caused the late Cenozoic drawdown of atmospheric carbon dioxide and global climatic cooling (Raymo et al., 1988). Thus it is instructive to examine water chemistry and strontium isotopes of the major rivers draining the Himalayas to elucidate their role in carbon dioxide consumption.

The discharge weighted average river water has been estimated as $^{87}Sr/^{86}Sr$ = 0.7101 or 0.7117; Sr = 708 or 923 nmolesL^{-1} (Wadleigh et al., 1985; Goldstein and Jacobsen, 1987; Palmer and Edmond, 1989). On a global scale, mixing of strontium from two distinct reservoirs controls the isotope systematics of river water (Fig. 6.14). One with high concentration of strontium and low $^{87}Sr/^{86}Sr$ is defined by marine carbonates and evaporites and the other with low strontium concentration but high $^{87}Sr/^{86}Sr$ ratios

represented by old igneous and metamorphic rocks. Departures from a linear trend arise due to rivers draining young island arcs and continental margin materials, such as Japan, Philippines, and Australia. Particularly striking however, are rivers draining the Himalayas. They have high concentrations of strontium as well as high $^{87}Sr/^{86}Sr$, an observation confirmed by other studies (Pande et al., 1994; Trivedi et al., 1995; Harris et al., 1998; Singh et al., 1998).
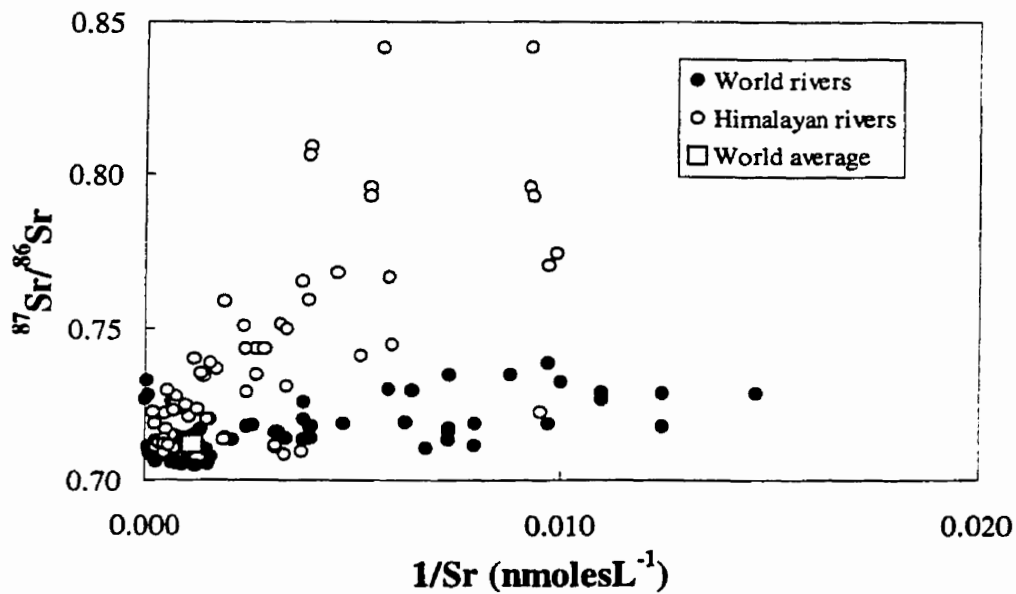
Fig. 6.14. Scatter diagram of reciprocal of strontium concentration versus $^{87}Sr/^{86}Sr$ for major world rivers. Data sources: major world rivers and the world average, Palmer and Edmond (1989), Himalayan rivers, Blum et al. (1998), Harris et al. (1998), Pande et al. (1994), Singh et al. (1998), Trivedi et al. (1995).

6.5.2 Sources of strontium in Himalayan rivers

The source of highly radiogenic strontium in Himalayan rivers remains equivocal.

1) Palmer and Edmond (1992) suggested that it is being derived from carbonates within the High Himalayan Crystalline Series that have been enriched in radiogenic strontium

129

:

during metamorphism, or 2) Metamorphism of silicate lithologies redistributed strontium with high $^{87}Sr/^{86}Sr$ ratios from Rb-rich silicate minerals into more readily weatherable silicates such as plagioclase. 3) Alternatively, weathering of metasedimentary silicates with high proportions of easily weathered radiogenic biotite was the source (Harris, 1995).

The first direct support for Palmer and Edmond's hypothesis came from Sarkar et al. (1996), who reported strontium isotope data from ~2 km thick carbonate-argillite sequence at the Precambrian-Cambrian boundary, exposed along the southern margin of the Himalayas. The $^{87}Sr/^{86}Sr$ ranged between 0.70976 and 0.72918, much more radiogenic compared to the coeval sea water (Veizer, 1989). Fossil shells, paleosol and detrital carbonates from ancestral Himalayan river sediments also show strong similarity and have $^{87}Sr/^{86}Sr$ between 0.7083 and 0.755 (Quade et al., 1997). Singh et al. (1998), analyzed Precambrian carbonates from the Lesser Himalayas and the headwaters of the Ganges, Ghaghara and a tributary of the Indus River and reported still higher $^{87}Sr/^{86}Sr$ for the carbonates (0.7064 and 0.8935). They estimated an upper limit for carbonate derived Sr, based on Sr/Ca ratio in river water, to be between 6 and 43%. However, based on Ca/Na, Sr/Na ratios and $^{87}Sr/^{86}Sr$, they predicted 33 to 89% of Sr in most of the rivers to be derived from silicate rocks. From these observations, Singh et al. concluded that "although some of the carbonates of the Lesser Himalayas can serve as a source for high radiogenic Sr to the streams on regional scale, on average they are unlikely to be a major contributor to the high $^{87}Sr/^{86}Sr$ of the source waters on a basinwide scale". Contrasting results were obtained by Harris et al. (1998) on Bhote Kosi, a small tributary (~120 km long) of the Ganges River in the Higher Himalayas. They attributed less than 10% of the

dissolved strontium to be derived from silicate rocks, with $^{87}Sr/^{86}Sr$ between 0.75 and 1.0, and the remainder from carbonates with $^{87}Sr/^{86}Sr$ up to 0.8. Blum et al. (1998), analyzed carbonate and silicate fractions of rocks and riverbed sand of a small tributary (200 km^2) of the Indus in the Higher Himalayas. The average $^{87}Sr/^{86}Sr$ of the carbonate and silicate fractions of the riverbed sand are respectively 0.73 and 0.86. Based on stoichiometry of weathering of some silicate minerals, they calculated 82% of the bicarbonate flux to be derived from weathering of carbonate and the rest from silicate weathering.

6.6 Strontium in the Indus River Basin

6.6.1 Tributaries and end member compositions

Strontium concentration and its isotopic composition for the Indus River, tributaries and the monthly monitoring station are given in Appendix B. The headwater tributaries range between 109 and 2135 nmolesL^{-1} for strontium and between 0.7083 and 0.8224 for $^{87}Sr/^{86}Sr$. The lowlands, on the other hand, have higher concentrations of strontium, in the range of 5291 and 44528 nmolesL^{-1}, with a rather restricted range of $^{87}Sr/^{86}Sr$ between 0.7082 and 0.7096. Among the Punjab rivers the Jhelum River has the highest concentration but least radiogenic strontium, 2062 nmolesL^{-1} and 0.7127 respectively. The Ravi River is the other extreme with 1326 nmolesL^{-1} strontium and $^{87}Sr/^{86}Sr$ of 0.7291, other Punjab rivers having intermediate values.

Figure 6.15 shows the $^{87}Sr/^{86}Sr$ versus the reciprocal of strontium concentration for all the tributaries sampled during this study and those reported in Pande et al. (1994). Both data sets cover the summer season. At least three end member compositions are required to explain the pattern of strontium and $^{87}Sr/^{86}Sr$ distribution. These are:

131

1) weathering of old silicate (silicic) rocks represented by rivers draining the Precambrian high grade metamorphic rocks of the Nanga Parbat-Haramosh massif and the "Central Crystallines" of the Higher Himalayas, with the Shahbatot River having the highest $^{87}Sr/^{86}Sr$ (0.8224) ratios of all the tributaries. The isotopic composition of this end member is within the range (0.82-0.89) reported for the Nanga Parbat gneisses and their constituent minerals (Gazis et al., 1995).
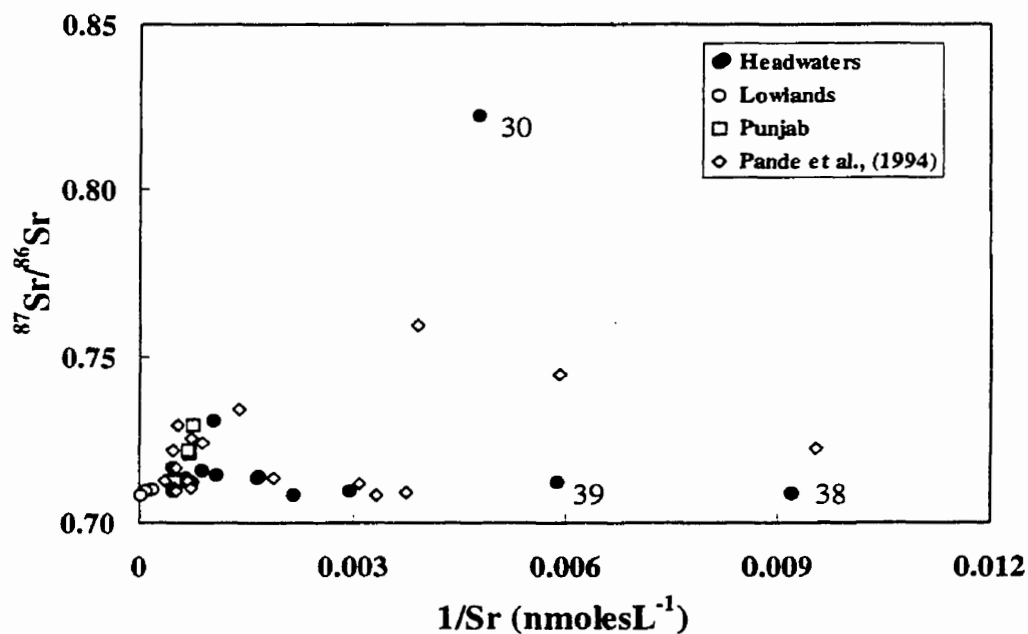
Fig. 6.15. Scatter diagram of reciprocal of strontium concentration versus $^{87}Sr/^{86}Sr$ for tributaries of the Indus River sampled during the summer. Note that data for the tributaries in Pande et al. (1994) is for the same season as the present study. Out of eighteen tributary samples in Pande et al. (1994), fifteen are from upper reaches of four tributaries. In the present study, these were sampled only at their mouths. The key to the sample numbers as in Fig. 3.1.

2) Young silicate (mafic) rocks with low $^{87}Sr/^{86}Sr$ ratios and low strontium concentrations. The Kial River with $^{87}Sr/^{86}Sr$ ratio of 0.7089, draining equal proportions of mafic-ultramafic Jijal Complex and Kamila Amphibolites of the Kohistan-Ladakh arcs, is an example. The present-day $^{87}Sr/^{86}Sr$ ratios for the Kohistan-Ladakh rocks range between 0.7037 and 0.7068 (Sano et al., 1996; Khan et al., 1997). The slightly higher values for the Kial River are apparently due to minor contributions from glacial materials derived from rocks discussed under 1.

3) The lowland tributaries with the highest concentrations of strontium and lower $^{87}Sr/^{86}Sr$ represent weathering of sedimentary carbonates. Note that the measurements reported in Pande et al. (1994) lie approximately within a mixing triangle defined by samples from the present study.

6.6.2 Mixing relationship of end members in the Indus main channel

Figure 6.16 illustrates the $^{87}Sr/^{86}Sr$ vs reciprocal of strontium concentration for the Indus main channel. The upper Indus evolves along a steep slope to higher $^{87}Sr/^{86}Sr$ due to inputs from weathering of silicate rocks represented by end member 1. Unfortunately, mixing relations are complicated due to the fact that most of the small headwater tributaries used in delineating end member compositions were sampled only during the summer season and enough water for isotope analysis for the main channel was available only from samples collected during the winter season. Nonetheless, based on chemical and isotopic data for three headwater tributaries, the relative importance of end members can be ascertained. The Shyok, Shigar and Hunza rivers contain 1.5 to 2.0 times higher Sr concentrations during the winter, but their $^{87}Sr/^{86}Sr$ differ by only up to 0.0005 (in

absolute values). Assuming that all other tributaries behaved in the same way, the concentration of strontium for a given season can be calculated. Assuming an average concentration factor of 1.7 for the Shahbatot River (end member 1), its mixing with the first sample on the Indus is shown in Figure 6.17. The Nascent Indus (Sr concentration data recalculated from Pande et al., 1994) and samples downstream from Chilas require some input from the end member 2, represented by the Kial River (station 38). In these parts of the river, where it flows through the Kohistan-Ladakh island arc, the rise in $^{87}Sr/^{86}Sr$ and decline in strontium concentration is along a much shallower slope compared to samples from upstream of Chilas (Fig. 6.16, station 7), reflecting mixing of water from the Kohistan-Ladakh arc and the Higher Himalayas.
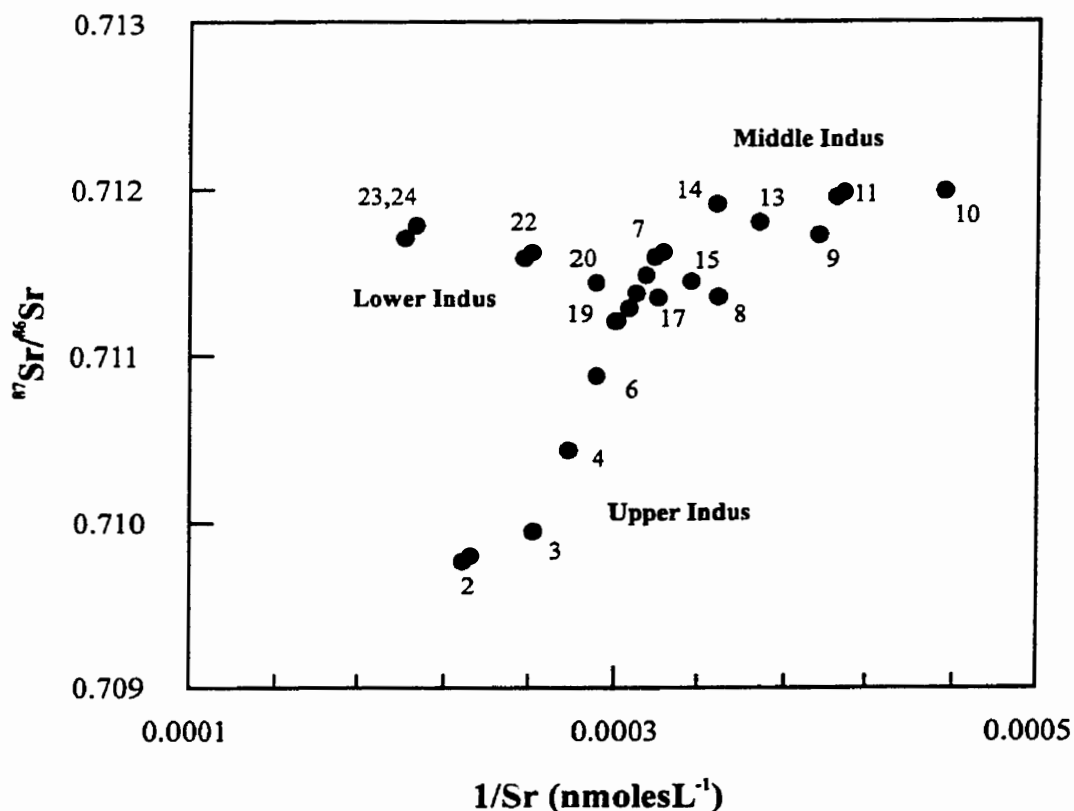
Fig. 6.16. Scatter diagram of reciprocal of strontium concentration versus $^{87}Sr/^{86}Sr$ for the Indus main channel. The key to the sample numbers as in Fig. 3.1

134

In the middle Indus (Fig. 6.16) strontium concentrations increase downriver with an attendant slight decrease in $^{87}Sr/^{86}Sr$ and reflects inputs from weathering of carbonates in the West Pakistan Fold Belt. Strontium continues to increase in the lower Indus, but the $^{87}Sr/^{86}Sr$ increases. This is a feature of some of the Punjab rivers, The Ravi River in particular. The lower Indus hosts three irrigation reservoirs that retain increasing proportions (towards its mouth) of "old water" and could explain the observed trend.
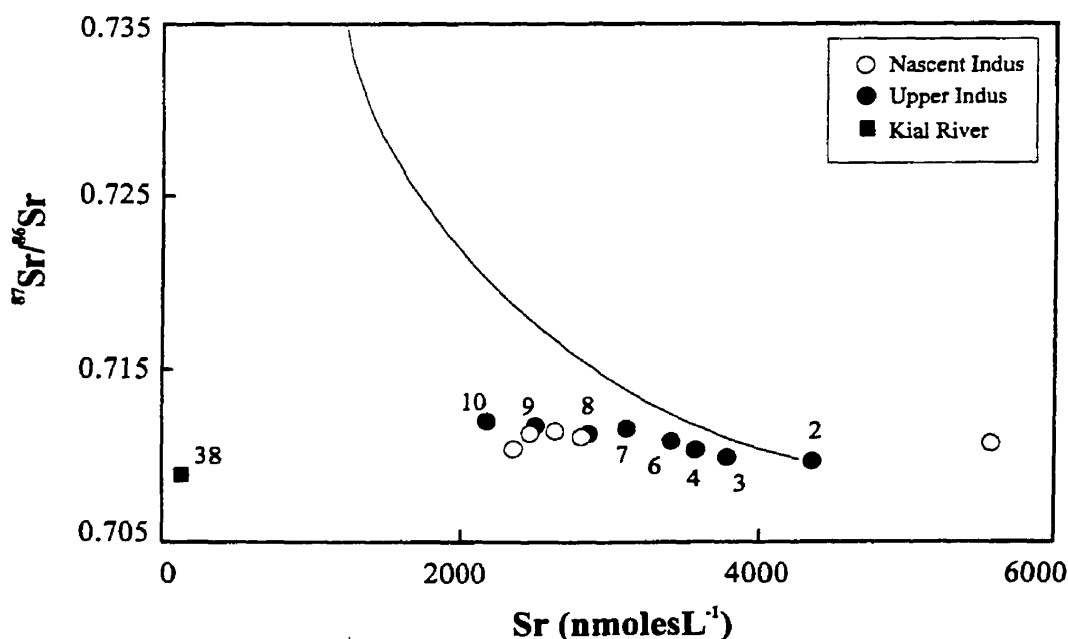
Fig. 6.17. Strontium concentration versus $^{87}Sr/^{86}Sr$ for the nascent and the upper Indus. The curve represents conservative mixing of the silicate end member (station 30, off scale at $^{87}Sr/^{86}Sr$ = 0.82) with the Indus River (station 2). Data for the nascent Indus from Pande et al. (1994). Strontium concentration for the nascent Indus and for the silicate end member recalculated to their equivalent concentration during the winter by a procedure described in the text. The key to the sample numbers as in Fig. 3.1.

The discharge-weighted average concentration of strontium in the Indus main channel at Sukkur barrage is 2670 nmolesL^{-1} with $^{87}Sr/^{86}Sr$ of 0.7118. The isotopic composition is similar to the global average river water and to the earlier measurements on the Indus River (0.7112, Goldstein and Jacobsen, 1987; 0.7111, Pande et al., 1994).

6.7 Carbonate versus silicate weathering

It is clear from the foregoing discussion that two major lithologies, sedimentary carbonates and igneous and metamorphic rocks control the strontium isotope systematics of the Indus River Basin. The influence of evaporite deposits, although present as isolated outcrops in the middle Indus, on water chemistry of the tributaries or the Indus main channel is not supported by major ions and isotopes of sulfate. This reduces one major uncertainty in constraining the relative role of silicate versus carbonate weathering in releasing major cations, permitting the use of simple charge balance equations. All the "supported" alkalies are attributed to a halite source (includes cyclic salts, halite crystals and brines trapped in sediments) and the remainder to silicate weathering, $(Na^+ + K^+)_{sil}$. The proportions of Ca^{2+} and Mg^{2+} derived from carbonate weathering are equal to the concentration (on equivalent basis) of HCO_3^-. The remainder is attributed to silicate weathering, $(Ca^{2+} + Mg^{2+})_{sil}$.

In the upper Indus $(Na^+ + K^+)_{sil}$ reaches about three-fourth of their total concentrations and is accompanied by a sharp increase in $^{87}Sr/^{86}Sr$ ratios (Fig. 6.18). This trend is inverted in the middle Indus, where contribution of $(Na^+ + K^+)_{sil}$ reduces to less than 40%. Finally, in the lower Indus both, the $^{87}Sr/^{86}Sr$ and the silicate-derived alkalies
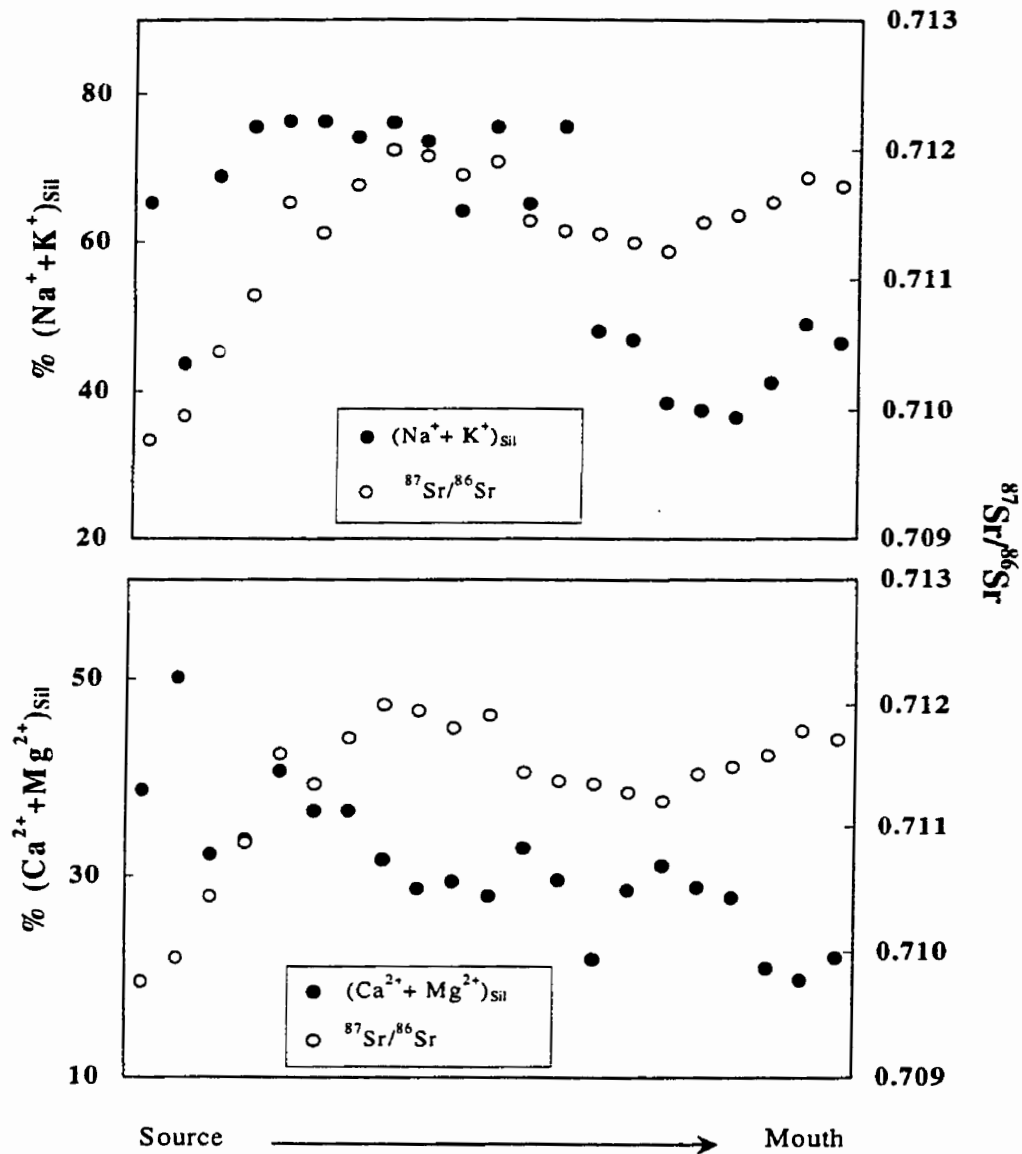
Fig. 6.18. Percent silicate derived $Na^+ + K^+$ and $^{87}Sr/^{86}Sr$ (top), percent silicate derived $Ca^{2+} + Mg^{2+}$ and $^{87}Sr/^{86}Sr$ (bottom) for the Indus main channel during the winter. The arrow points in the direction of the flow of Indus.

rise due to mixing with Panjnad and to increasing proportions of "old water" in reservoirs. In contrast, most of the Ca^{2+} and Mg^{2+} are derived from carbonate weathering. Contribution of the latter is, on average, about two-thirds in the upper Indus, increasing in

137

the downstream direction to about three-fourth in the lower Indus (Fig.6.18). Since Ca^{2+} and Mg^{2+} constitute bulk of the dissolved cations, it is not surprising to note that the Indus River at its mouth is dominated by carbonate weathering.

Chemical and Sr-isotope variation of the tributaries are complex, but not unexpected. The silicate-derived alkalies tend to increase with rising $^{87}Sr/^{86}Sr$ with a considerable scatter towards higher values (Fig. 6.19). This evidently reflects heterogeneity of the silicate end member, for example mafic versus silicic and for the latter younger versus older rocks. Variations of $(Ca^{2+}+Mg^{2+})_{sil}$ with $^{87}Sr/^{86}Sr$ have a slightly forked pattern (Fig. 6.20). Variable mixtures of the three end members (cf. Fig. 6.15) could account for these variations. The only exceptions are the Ravi River (station 58), and Beas and Samdoh rivers of Pande et al. (1994), all draining variable mixtures of rocks of the Higher and Lesser Himalayas. Their low $(Ca^{2+}+Mg^{2+})_{sil}$ characterizes them as typical carbonate rivers, but their $^{87}Sr/^{86}Sr$ ratios are much higher, a feature not uncommon for some previously studied Himalayan rivers (p. 130).

In summary, major ion chemistry and strontium isotopes suggest that in the headwaters of the Indus River, alkalies are derived primarily from weathering of silicate rocks. In contrast, calcium and magnesium, results mainly from weathering of sedimentary carbonates. Conformable with the geology of the basin, the passage from the headwaters to the lowlands is accompanied by increase in proportions of cations derived from weathering of sediments. Overall, silicate weathering may dominate in some tributaries, carbonate weathering, however, overshadows its importance to the total ion budget in the Indus main channel.
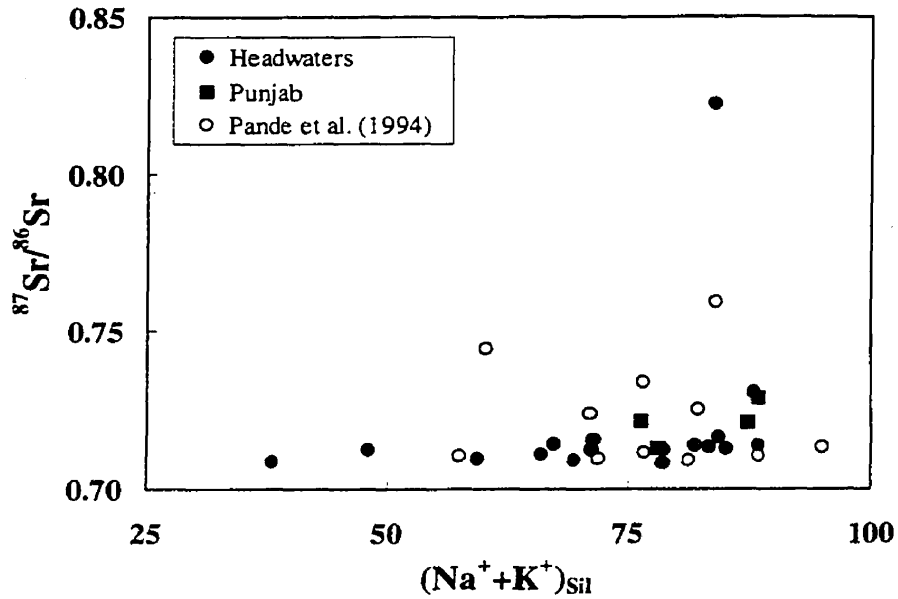
Fig. 6.19. Scatter plot of $(Na^+ + K^+)_{Sil}$ versus $^{87}Sr/^{86}Sr$ for the headwater tributaries and the Punjab rivers of the Indus River Basin during the summer. Note that only the lower order headwater tributaries in Pande et al. (1994), not sampled during the present study, are shown.
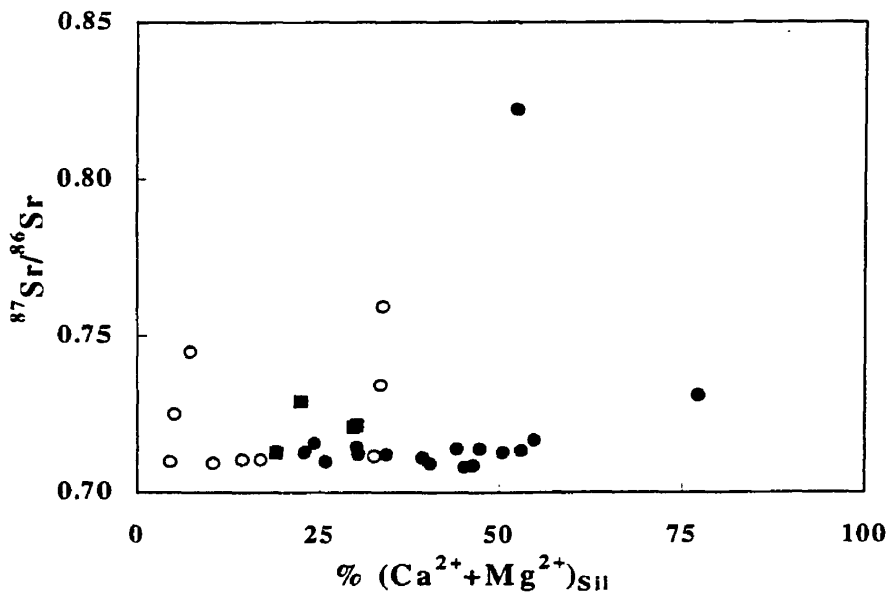
Fig. 6.20. Scatter plot of $(Ca^{2+} + Mg^{2+})_{Sil}$ versus $^{87}Sr/^{86}Sr$ for the headwater tributaries and the Punjab rivers of the Indus River Basin during the summer. Note that only the lower order headwater tributaries in Pande et al. (1994), not sampled during the present study, are shown. In the former study, two samples with negative charge balance have been excluded. The key to the samples as in Fig. 6.19.

Chapter 7
Controls on water chemistry

In the preceding chapters it was demonstrated how physical and chemical processes influenced individual chemical and isotopic parameters. For example, topographic, climatic and geographic controls play a key role in determining oxygen and deuterium isotope variations. Rock weathering influences the amount as well as the type of solutes in water. Equally important are biological controls on the availability of nutrients and on dissolved oxygen. It is therefore of interest to summarize the dominant controls and illustrate how they are distributed within the Indus River Basin. In order to accomplish this a three-step procedure was adopted. The first step involves area analysis of some of the environmental parameters (see for example Gibbs, 1967; Telmer, 1996) of the watershed. Secondly, variables in the geochemical database are reduced to a smaller number of variables using factor analysis. Finally, the environmental and geochemical databases are merged together and relationships between the two studied by performing a second factor analysis.

7.1 The Environmental database

The following maps, unless otherwise stated, were digitized manually from published maps. Digitizing was done in TYDIG (TYDAC Technologies Inc., 1995) and the files imported into SPANS Geographic Information Systems (TYDAC Research Inc., 1997) where they were reclassified and spatial analysis performed.

7.1.1 Watershed boundaries

The watershed boundary (Fig. 7.1) for each tributary was delineated by joining the first order streams by a smooth line. The southern boundary of the Punjab rivers was taken half a kilometer upstream from the link canals. The mean latitudes and longitudes of the tributaries were determined from a "geometric centroid" in each of the basins. The total area of the Indus River basin computed during this study is 863,508 km^2 and that for each tributary is given in Appendix C. The area estimated for the Indus basin reported in the literature is 970,000 km^2 (Meybeck, 1979; Berner and Berner 1996), and apparently includes deserts and endoeric basins in the lower Indus.

7.1.2 Bedrock Geology

The bedrock geology (Fig. 7.2) for the Indus River Basin was digitized and simplified mainly from Gansser (1964) and Kazmi et al. (1982). The purpose of simplifying original detailed maps was to avoid local correlations. A detail of the rock types is given in chapter 2. The exact lithology of parts of the Kabul River basin in Afghanistan and that of the nascent Indus in Tibet is not known. The lack of data from these two areas have little or no influence on the overall conclusions since the Kabul River was excluded from the factor analysis for all the geological variables. For the nascent Indus area none of the sampled rivers lie in this region.

7.1.3 Land Use and Population Density

Land use and population density maps (Fig. 7.3 and 7.4) were digitized and simplified from United States Central Intelligence Agency (1973). Although these maps

are old and considering that Pakistan has a present day population of about 130 million, with population growth rate one of the highest in the region at 2.7%, it is assumed that the relative distribution of population density has remained more or less uniform. Similarly, most of the croplands are in the Punjab and in the lower Indus, where agriculture developed after the completion of major canals in the late 60's (Ahmed and Chaudhry, 1990).
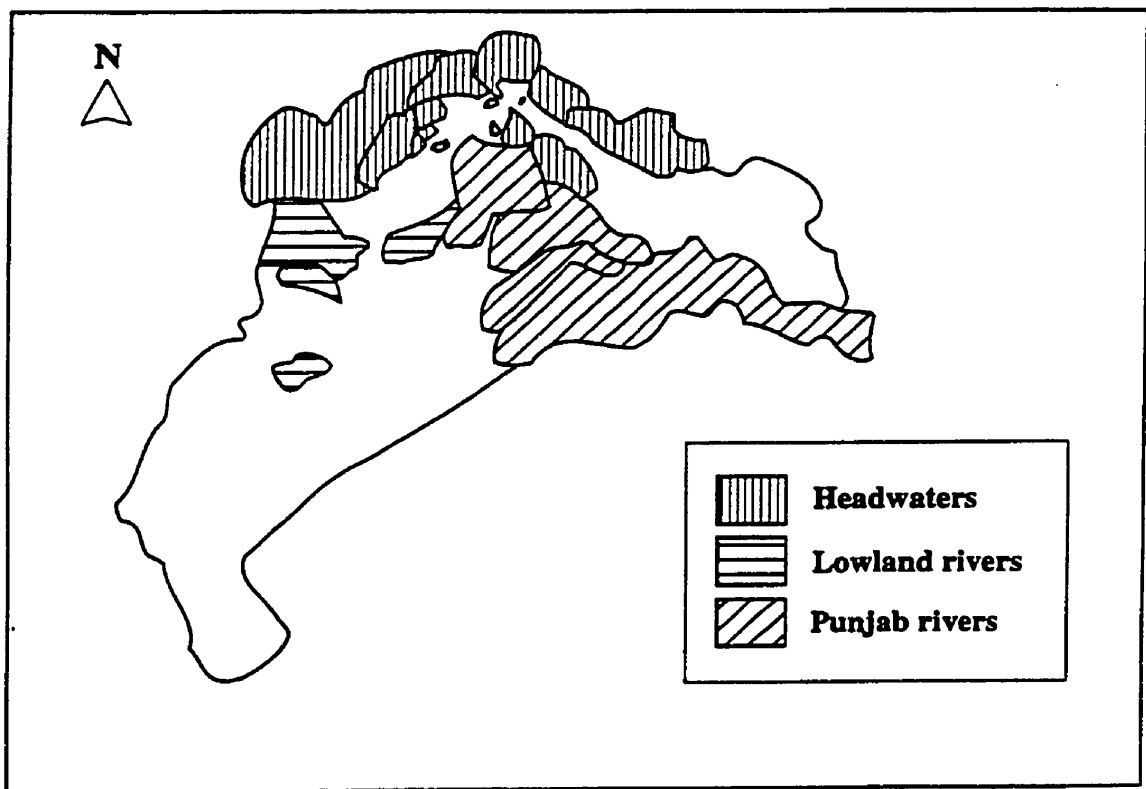
Fig. 7.1. Tributary basins of the Indus River. The southwestern watershed boundaries of the Punjab rivers have been modified to rectify the influence of canals that link all these rivers.
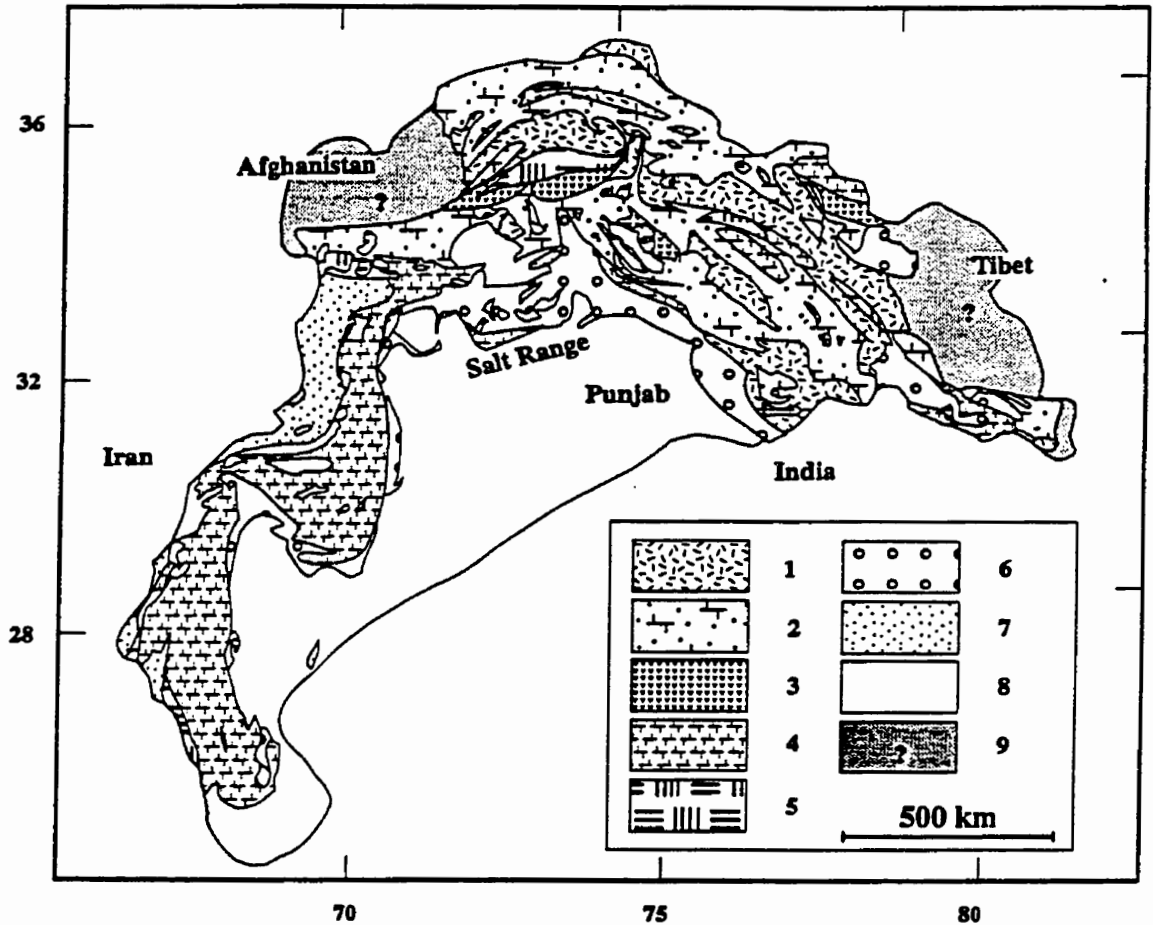
Fig.7. 2. Geological map of the Indus River Basin. 1, Granites; 2, Metasediments; 3, Metabasalts; 4, Sedimentary carbonates; 5, Mafic-ultramafic complexes; 6, Sandstones and siltstones; 7, Shales; 8, Recent alluvium; 9, No data.

143
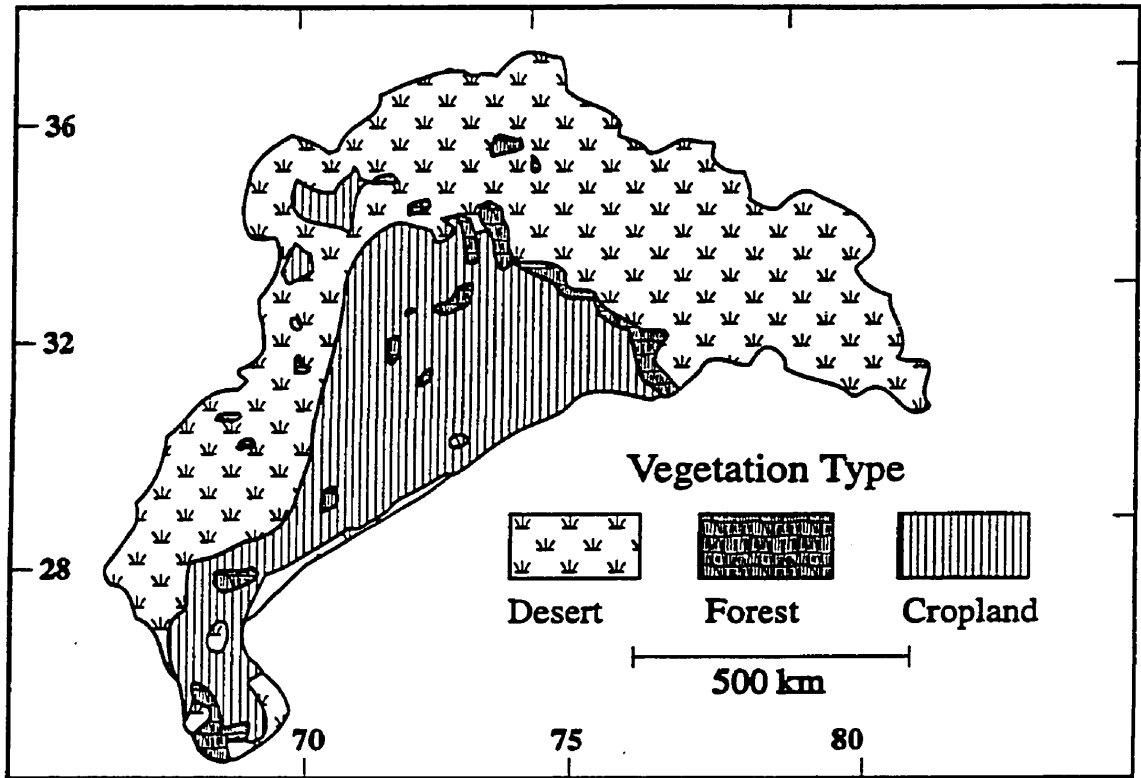
Fig. 7.3. Natural vegetation and croplands within the Indus River Basin.
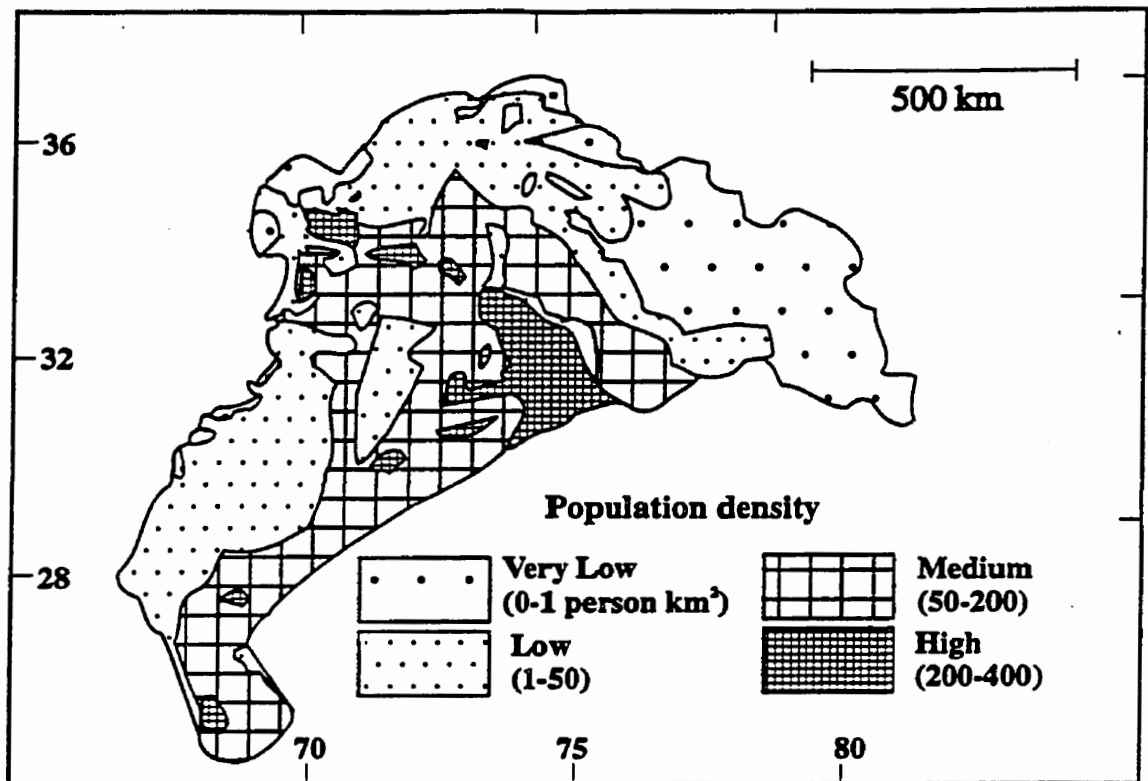
Fig. 7.4. Population density map for the Indus River Basin.

7.1.4 Topography

The topographic map for the Indus River Basin is shown in Figure 7.5, mean altitude for each tributary basin is presented in Appendix C, and a detailed description of physiographic features is given in chapter 1. The contours were generated from a 0.5-minute-latitude/longitude global digital elevation database published by National Geophysical Data Center, NGDC (1988). Mean altitude represents area-weighted average altitude based on a 20-class topographic contour map.

145
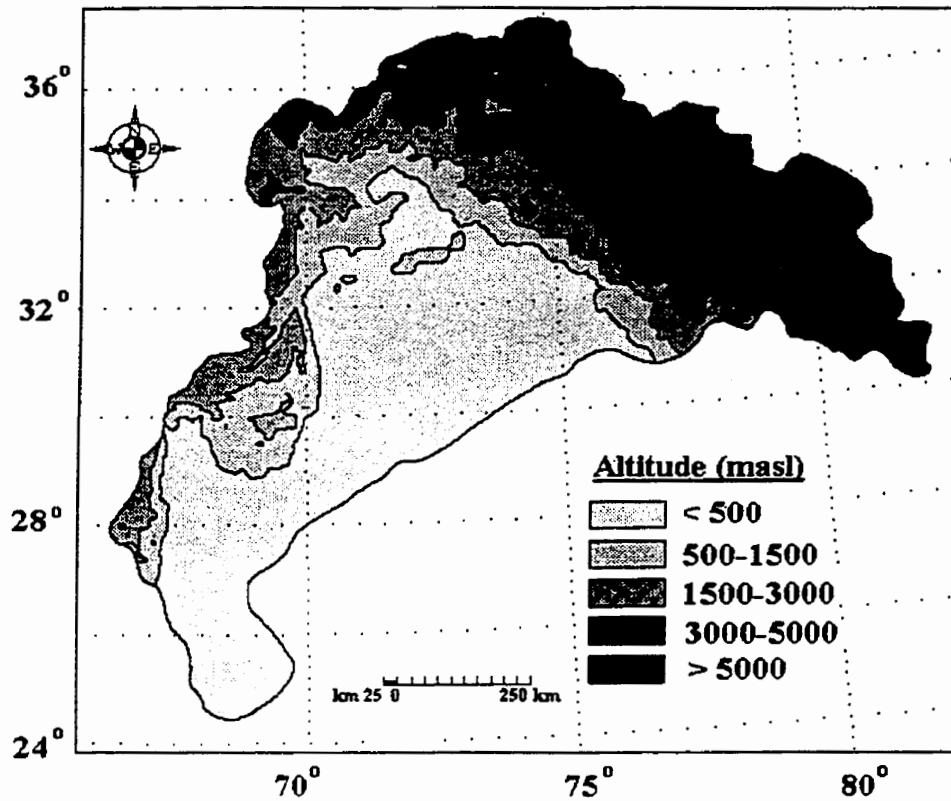
Fig. 7.5. Topographic map for the Indus River Basin.

7.1.5 Precipitation

Mean Annual precipitation map of the Indus River Basin (Fig. 7.6) was created from digital global precipitation data released by Distributed Active Archive Center at Goddard Space Flight Center, DAAC-GSFC (1996). The precipitation data is based on traditional gauge measurements spanning the period from 1920 to 1980, corrected for systematic errors (caused by wind, wetting on the interior walls of the gauge and evaporation from the gauge) before interpolation to a 0.5-minute-latitude/longitude grid.

146

The mean annual water flux to the Indus River Basin is calculated to be 398 km^3. This estimate is based on total area of 863,508 km^2 of the Indus River Basin and average precipitation depth of 461 mm yr^{-1}. Note that the precipitation depth is area-weighted average precipitation depth calculated from a 15-class precipitation map.
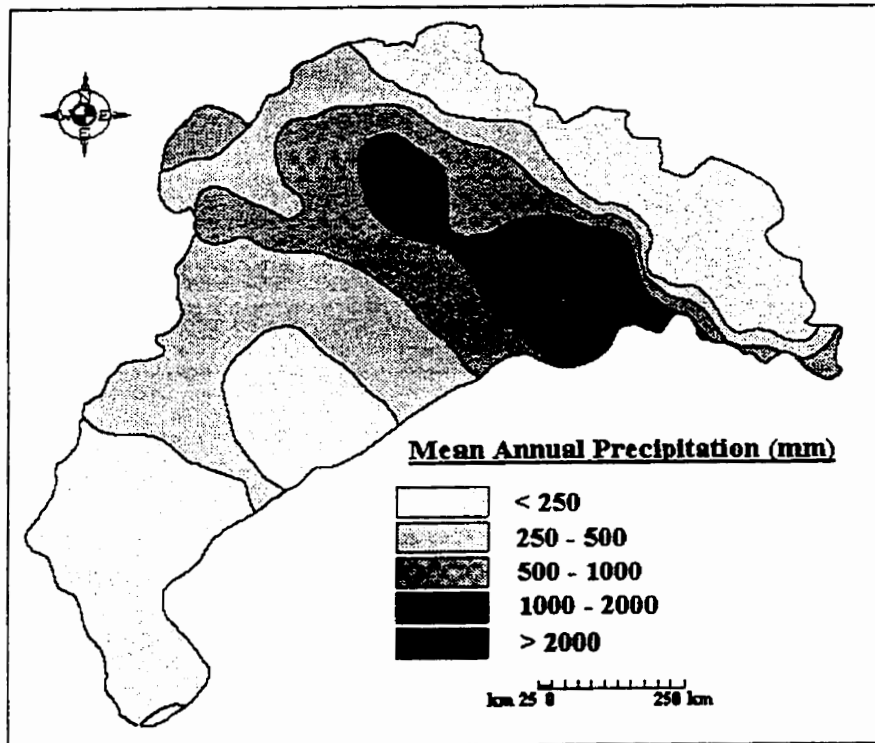
Fig. 7.6. Mean annual precipitation map for the Indus River Basin.

7.2 Area Analysis

The percentage of each environmental class or spatial entity (e.g. rock-type, land use and population density classes) in each tributary basin was obtained in SPANS by performing area-cross tabulation. Conceptually, it means superimposing the watershed boundaries map on each of the environmental parameters maps and measuring the areas of the latter occupying the former. Results of this analysis together with average altitude, mean latitude and longitude are given in Appendix C. Due to the fact that oxygen and deuterium in water behave in a predictable manner only the former was selected, and since it depends strongly on geographic factors such as altitude and latitude, it was included in the environmental data set. The environmental data was then appended to the geochemical database such that row represent samples and columns the variables.

7.3 Factor Analysis

Large geochemical data sets may be difficult to analyze for major trends or clusters. For example, in the present study, relationship between individual chemical species themselves and between environmental parameters are difficult to comprehend from cross-plots alone. Furthermore, variations of trace elements, not addressed in the previous chapters, add further complexity for discerning overall trends. Statistical methods such as factor analysis are helpful in summarizing major trends in a large multivariate data set. Details of factor analysis are given in Jöreskog et al. (1976) and Davis (1986). It can be simply regarded as a technique for reducing the number of variables into a new smaller number of uncorrelated variables. The new variables called components (or factors), are a linear combination of the original ones such that they

148

contain the same amount of information. In the present study factors are interpreted as indicating a common source or a similar concentration process for solutes within the Indus River Basin.

Factor analysis was performed using the software package SYSTAT (SYSTAT Inc., 1993) on 26 tributary samples collected during the summer season. This subset of the database is best suited for performing factor analysis for the following reasons: 1) it represents the largest number of tributary samples with contrasting chemistry; 2) all these samples were collected during maximum discharge; and therefore 3) provides an average chemical signal from the whole watershed as opposed to the winter season where water chemistry may be influenced by local sources.

Due to the fact that most of the major and trace elements have a markedly skewed distribution, all the data except pH and isotope ratios were transformed into log values. A correlation matrix was factored and the reference axes rotated using a varimax method. The results of factor analysis are shown in Table 7.1. A three factor model explains ~66% of the total variance for the 29 chemical and isotopic variables, with additional factors yielding no further insights.

7.3.1 Weathering of sedimentary rocks

About 28% of the total variance is characterized by factor 1, with high to moderate positive loadings for SO_4^{2-}, TDS, Mg^{2+}, Sr^{2+}, Ca^{2+}, Na^+, Li, K^+, Cl', low for Ba and SiO_2 and low negative ones for $\delta^{34}S$ and dissolved oxygen. The lowland tributaries, including the Kurram, Shahur and Sanghar score high on this factor (Fig. 7.7). The origin of all these chemical and isotopic parameters, except Li and Ba, has been discussed in

149

Chapters 5 and 6. Compared to Na^+ and K^+, Li is a rare alkali element, found in Li-bearing minerals in pegmatites as well as in evaporites and brines (Hem, 1985). The lowland tributaries with high concentration of Li can thus be a reflection of the presence of saline waters in their basins. The hydrochemical and environmental associations enables this factor to be interpreted as geogenic, resulting from weathering of sedimentary rocks such as sedimentary carbonates and shales. These lithologies crop out in the West Pakistan Fold Belt, drained by the lowland tributaries.

In general, factor 1 reflects a trend from weathering of igneous and metamorphic rocks at high altitude to weathering of sediments in lowland basins, the latter contributing the greatest weight to this factor. It is therefore not surprising that environmental or spatial variables such as the mean elevation, latitude, and $\delta^{18}O$ and the abundance of carbonates and shales also load on this factor. Moving down Indus, elevation and latitude decline, precipitation becomes more enriched in the heavy isotope of oxygen and sediments dominate the geology.

7.3.2 Weathering of igneous and metamorphic rocks

The second factor, of almost equal statistical importance as the first one, and with high positive loadings for Al, F, Ti, Fe, and U, moderate for Mn, Rb, Ni and As, low for Cr, Li and $\delta^{34}S$ and a low negative one for NO_3^- (Table 7.1), is interpreted as geogenic, caused by weathering of igneous and metamorphic rocks. Eight headwater tributaries, five of them highly, score positive on this factor (Fig. 7.7). The factor loadings include trace elements that are derived from weathering of both silicic rocks and mafic, all abundantly represented in differing proportions in the headwater catchments (cf.

150

Appendix C). This factor coincides with the distribution of granites but conflicts with that of mafic-ultramafic rocks, the latter cannot be explained unequivocally.

Since, in contrast to factor 1, this type of environment is predominant in the elevated mountainous regions, it is not unexpected that environmental variables load on this factor with opposing signs as well. Thus mean elevation increases northward, while at the same time population density declines and precipitation becomes depleted in ^{18}O.

Detailed discussion on the behavior of trace elements in river water is given in Goldstein and Jacobsen (1988), Elderfield et al. (1990), Sholkovitz (1995), Dupré et al. (1996) and Gaillardet et al. (1997). Conclusions from some of these studies are that dissolved load is a mixture of true dissolved fraction and a colloidal fraction (<0.2 or <0.5μm). The latter is closely associated with dissolved organic carbon (DOC) and is believed to enhance the solubility of trace elements. It is not possible to evaluate the role of colloids on trace element concentrations in the headwaters of the Indus River based on the present data. Nevertheless, it is clear that trace element data complements conclusions based on major ions and isotopes, discussed in the previous chapters.

7.3.3 Biogenic and anthropogenic impact

The last major factor, that explains about 14% of the total variance, is marked by positive loadings for Ba, Sb, HCO_3^-, NO_3^-, pH and negative ones for dissolved oxygen and $\delta^{13}C$ (Table 7.1). It is interpreted to be of biogenic and anthropogenic origin, because the population density and land use load highly on this factor. In addition, drainage area loads positive, which could be related to the residence time of water in the watershed. These processes dominate the lowland "alluvial" tributaries, including the Soan, Kurram,

Ravi, Sutlej and Panjnad rivers (Fig. 7.7). The parameters loading on this factor (except Sb and Si) are linked together by the riverine carbon and nitrogen cycles,
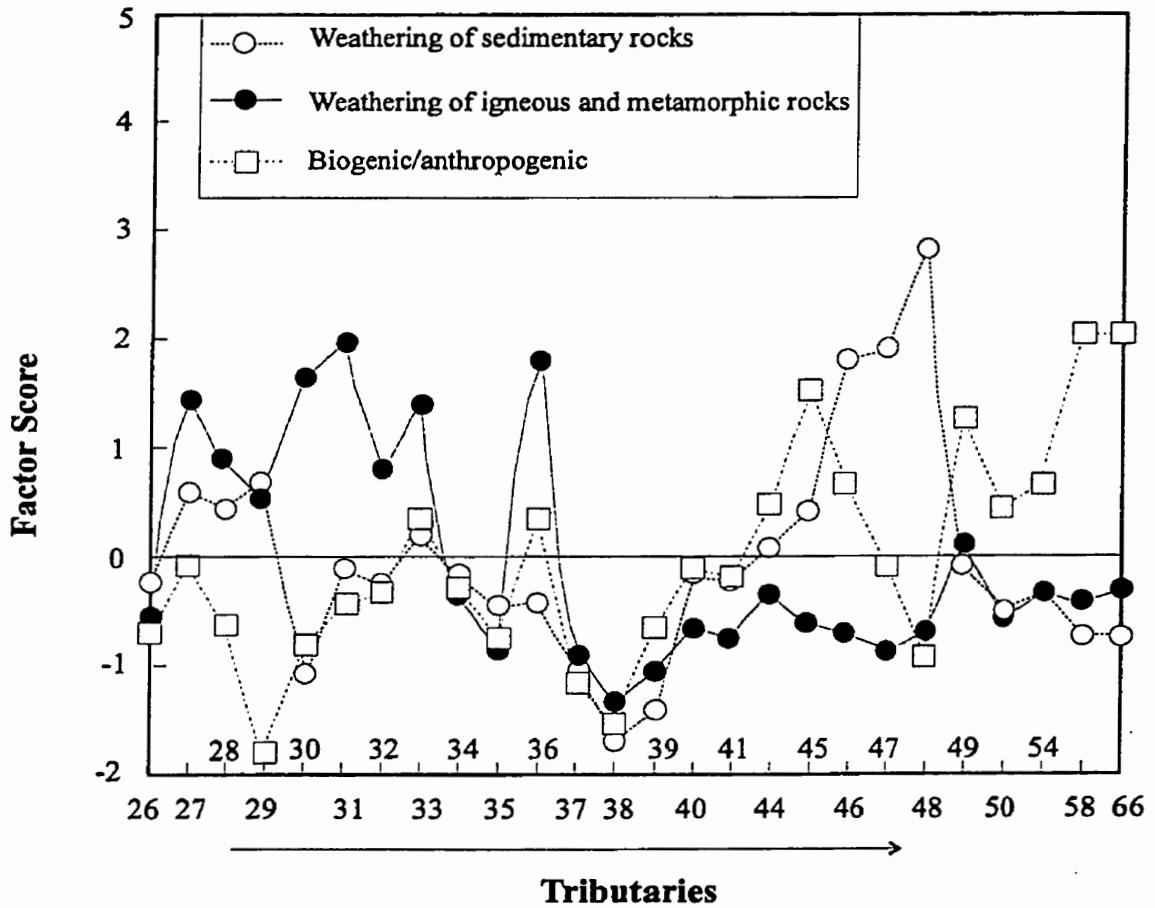
Fig. 7.7. Factor score plot for the tributaries of the Indus River. The arrow points in the direction of the flow of the Indus River, from source to its mouth. The key to the tributaries as in Figure 3.1.

perturbed to varying degrees by pollution from urban discharge as exemplified by some German rivers (Pawellek and Veizer, 1994; Flintrop et al., 1996).

Only two Ba minerals, barite ($BaSO_4$) and witherite ($BaCO_3$) can control the Ba content of natural waters (Puchelt, 1972). The former is the least soluble but the most abundant Ba mineral in the earth's crust. The solubility of witherite depends largely on

pCO$_2$ of the atmosphere. At 25° C and 1 atm. pressure of CO$_2$, the dissociation constant for witherite is $10^{-8.64}$ (Garrels et al., 1960). The lowland and Punjab rivers contain, on average, ~400 nmolesL^{-1} Ba compared to 85 nmolesL^{-1} in the headwaters, perhaps reflecting the high pCO$_2$ of these waters.

Although some of the chemical traits of Sb are similar to those of As, antimony appears to be only one-tenth as abundant in rocks (Hem, 1985). The headwaters contain, on average, 0.7 nmolesL^{-1}, about twice as much in the lowlands, with the highest concentration (up to 4.0 nmolesL^{-1}) in the Punjab rivers. The behavior of Sb during weathering processes is not well known, but Sb is apparently concentrated in soils and shales compared to igneous rocks (Onishi, 1969). This is consistent with the Sb concentrations observed within the Indus River Basin where most of it enters surface waters from the sedimentary and alluvial parts of the basin.

In summary, the Indus River Basin exhibits large areas of immense environmental diversity. The headwaters and the lowlands are mirror images for their geomorphological, lithological, and hydrochemical aspects. The Indus main channel combines these two environments and is reflected in its chemistry along its longitudinal profile. Rock weathering exerts the predominant control on the amount and nature of solutes while biogenic and anthropogenic processes influence nutrients and dissolved oxygen. Topography and geographic location determines the oxygen and deuterium isotopic composition of precipitation within the Indus River Basin in a way similar to the global pattern.

Table 7.1. Factor loadings for the tributaries of the Indus River Basin. Loadings for the environmental variables are from a second factor analysis explained in the text.

Variables	Weathering of sed. rocks	Weathering of ign. and met. rocks	Biogenic and/or anthropogenic
SO_4^{2-}	0.97		
TDS	0.95		
Mg^{2+}	0.89		
Sr^{2+}	0.89		
Ca^{2+}	0.85		
Na^+	0.83		
Li	0.80	0.44	
K^+	0.77		
Cl^-	0.75		
Al		0.92	
F		0.89	
Ti		0.86	
Fe		0.82	
U		0.8·	
Mn		0.6·	
Rb		0.6·	
Ni		0.61	
As		0.60	
NO_3^-		-0.55	0.56
Cr		0.51	
Ba			0.76
Sb			0.75
D.O.			-0.75
HCO_3^-			0.72
PH			0.50
$\delta^{13}C$			-0.42
$\delta^{34}S$	-0.49		
SiO_2	0.42		
Percent of total variance explained	28.1	24.1	14.4
Spatial variables			
Mean elevation	-0.43	0.72	-0.46
Mean latitude	-0.46	0.40	-0.60
$\delta^{18}O$	0.44	-0.69	
Drainage area			0.66
Geology			
Mafic-ultramafic rocks	-0.43	-0.56	-0.40
Carbonates	0.82		
Shales	0.59		
Granites		0.44	
Alluvium			0.78
Sandstones & siltstones			0.58
Metabasalts			-0.41
Land use and vegetation			
Deserts			-0.83
Croplands			0.79
Forests			0.60
Population density (persons/km^2)			
Very Low (0-1)		0.75	
Medium (50-200)		-0.59	
High (200-400)			0.71

Chapter 8
Conclusions

8.1 Hydrology

- The mean annual water flux from precipitation to the Indus river Basin is 398 km^3. The mean annual discharge of the Indus River at its mouth before and after the completion of two major barrages are respectively 100 and 53 km^3. Therefore, bulk of the rainwater leaves the system by groundwater storage and evapotranspiration and only about one-fourth to one-eighth of the volume of rainwater flows as surface runoff.

- Seasonal variations in the discharge result from interplay of two distinct hydrologic regimes, particularly pronounced during the low flow. In the headwaters, discharge declines abruptly due to temperature drop, dwindling of snow cover and scarcity of shallow aquifers. In contrast, in the lowland tributaries, sporadic winter precipitation and groundwater discharge from shallow alluvial aquifers sustain discharge.

8.2 Oxygen and deuterium isotopes

- Oxygen and deuterium isotopes in the Indus River Basin are linearly related and have slope similar to that of the Global Meteoric Water Line. The only exceptions are the lowland tributaries and the lower Indus that depart from this trend due to secondary evaporation.

- The water budget of the Indus River is dominated by melting of snow and ice in the western Himalayas and the Karakoram mountains. The lowland tributaries play a subordinate role in the water budget of the Indus.

155

- Two distinct regions source water vapor for precipitation in the Indus River Basin. One that originates in the Mediterranean or other inland seas constitutes about 80% of the volume of water in the Indus River, with the remainder derived from the Indian monsoon originating in the Bay of Bengal or in the Arabian Sea.

8.3 Hydrochemistry

- Major ion chemistry of the Indus River Basin is dominated by $Ca^{2+} > Mg^{2+} > (Na^+ + K^+)$ and $HCO_3^- > (SO_4^{2-} + Cl^-) >$ Si. In the lowland tributaries and some of the Punjab rivers, however, $(Na^+ + K^+)$ and $(SO_4^{2-} + Cl^-)$ predominate.

- Cyclic salts constitute only up to 6% (of which sodium constitutes ~20 to 40%) of the total ion budget of the Indus River.

- The mean annual precipitation TDS flux to the Indus basin is ~844, 400 tons and that of the Indus River at Sukkur barrage is ~18×10^6 tons. The annual denudation rate is 21 tons km^{-2}.

- Major ion concentrations in the Indus River at Sukkur barrage during peak discharge are 5 to 20 times higher than those expected from dilution of baseflow. Leaching of solutes from the flood plain causes this discrepancy.

8.4 Isotope geochemistry

- Dissolved inorganic carbon in the Indus River is derived from weathering of carbonate and silicate rocks under atmospheric and biogenic carbon dioxide. Turbulent flow and low air temperature in the upper Indus facilitate mixing of

156

atmospheric gases causing supersaturation of dissolved oxygen and equilibration of carbon isotopes.

- Sulfate is derived exclusively from oxidation of sulfide minerals in igneous, metamorphic and sedimentary rocks.

- Strontium in the Indus River Basin is controlled by three end member compositions. These are weathering of old silicic rocks, young mafic rocks and sedimentary carbonates. Discharge weighted average concentration of Sr and its isotopic composition, respectively 2670 nmolesL^{-1} and 0.7118 are similar to the global average river water.

- Weathering of silicate rocks is important locally. At the mouth of the Indus however, sediment weathering predominates. In the headwaters over half of the Ca^{2+} and Mg^{2+} is derived from sedimentary carbonates, rising to about 80% at the mouth of the Indus. In contrast, about 75% of the total alkalies in the upper Indus are derived from silicate weathering, their contribution declining to less than half at the mouth.

8.5 Controls on water chemistry

- Weathering of sedimentary rocks in the lowland tributaries explains about 28% of the total variance and controls the distribution of SO_4^{2-}, TDS, Mg^{2+}, Sr^{2+}, Ca^{2+}, Na^+, Li, K^+, Cl$^-$, sulfur isotopes, dissolved oxygen, Si and Ba .

- Weathering of igneous and metamorphic rocks in some of the headwater tributaries is of similar statistical significance as that of sediment weathering. Trace elements such as Al, F, Ti, Fe, U, Mn, Rb, Ni, As, NO_3^- and Cr, together with sulfur isotopes characterizes this factor.

157

- Biogenic and anthropogenic processes in the lowlands explains about 14% of the total variance and control the distribution of Ba, Sb, HCO_3^-, NO_3^-, pH, dissolved oxygen and isotopes of carbon.

List of References

Abbasi, I.A. and Friend, P.F., 1989. Uplift and evolution of the Himalayan orogenic belts as recorded in the foredeep molasse sediments. In: E. Derbyshire and A.Owen (editors), Quaternary of the Karakoram and Himalaya, 75-88, Gebrüder Borntraeger, Berlin Stuttgart.

Ahmad, M. and Kutcher, G.P., 1992. Irrigation Planning with Environmental Considerations: A case study of Pakistan's Indus Basin. World Bank Technical Paper.

Ahmad, N. and Chaudhry, G.R., 1990. Summaries of Irrigated Agriculture of Pakistan. Shahzad Nazir, Lahore, Pakistan.

Ahmad, N., 1993. Water Resources of Pakistan. Shahzad Nazir, Lahore, Pakistan.

Aizen, V., Aizen, E., Melack, J. and Martma, T., 1996. Isotopic measurements of precipitation on central Asian glaciers (southeastern Tibet, northern Himalayas, central Tien Shan). Journal of Geophysical Research, 101: 9185-9196.

Akram, M., 1986. Pakistan at a glance. Proceedings of the XII International Forum on Soil Taxonomy and Agrotechnology Transfer, Lahore, Pakistan.

Alexander, M., 1971. Microbial Ecology, John Wiley and Sons Inc.

Allègre, C.J., Courtillot, V., Tapponnier, P., Hirn, A., Mattauer, M., Coulon, C., Jaeger, J. J., Achache, J., Schaerer, U., Marcoux, J., Burg, J. P., Girardeau, J., Armijo, R., Gariepy, C., Goepel, C., Li, Tindong, Xiao, Xuchang, Chang, Chenfa, Li, Guanggin, Lin, Baoyu, Teng, Ji, Wen, Wang, Naiwen, Chen, Guoming, Han, Tonglin, Wang, Xibin, Den, Wanming, Sheng, Huaibin, Cao, Yougong, Zhou, Ji, Qiu, Hongrong, Bao, Peisheng, Wang, Songchan, Wang, Bixiang, Zhou, Yaoxiu, Ronghua, Xu., 1984. Structure and evolution of the Himalaya-Tibet orogenic belt. Nature, 307: 17-22.

Amiotte Suchet, P. and Probst, J.L., 1995. A global model for present day atmospheric/soil CO_2 consumption by chemical erosion of continental rocks (GEM CO_2). Tellus, 47B: 273-280.

Andrews-Speed, C.P. and Brookfield, M.E., 1982. Middle Paleozoic to Cenozoic geology and tectonic evolution of the northwestern Himalayas. Tectonophysics, 82: 253-275.

Ashraf, M. and Jaffar, M., 1990. Contents of selected macronutrients in selected local freshwater fish. Pakistan Journal of Scientific and Industrial Research, 33: 278-280.

Baas-Becking, L.G.M., 1925. Studies on sulphur bacteria. Annals Botany, 39: 613-650.

Bard, J.P., Maluski, H., Matte, P. and Proust, F., 1980. The Kohistan Sequence: crust and mantle of an obducted island arc. Geological Bulletin, University of Peshawar, 13: 87-94.

Barry, R.G. and Chorley, R.J., 1982. Atmosphere, Weather, and Climate. Methuen, New York.

Beg, M.A.A., 1977. The Indus River Basin and risk assessment of the irrigation System. International Working Seminar on Environmental Risk Assessment in an International Context. Tihanyi, Hungary.

Beg, M.A.A., 1993. Surface soils and Indus River sediments. In: J.F. Shroder Jr. (editor), Himalaya to the Sea. Routledge, New York, 251-264.

Behrensmeyer, A.K. and Tauxe, L., 1982. Isochronous fluvial systems in Miocene deposits of northern Pakistan. Sedimentology, 29: 331-52.

Berner, E.K. and Berner, R.A., 1996. Global Environment: Water, Air, and Geochemical Cycles. Prentice Hall, New Jersey.

Berner, R.A., Lasaga, A.C. and Garrels, R.M., 1983. The carbonate-silicate geochemical cycle and its effect on atmospheric carbon dioxide over the past 100 million years. American Journal of Science, 283: 641-643.

Bhattacharya, D.S. and Das, K.K., 1983. Inversion of metamorphic zones in the Lower Himalayas at Gangtok, Sikkim, India. Journal of Geology, 91: 98-102.

Blum, J. D., Gazis, C.A., Jacobson, A. and Chamberlain, C.P., 1998. Carbonate versus silicate weathering on the Raikhot watershed within the High Himalayan Crystalline Series. Geology, 26: 411-414.

Boucher, K., 1975. Global Climates. John Wiley and Sons Inc, New York.

Brookfield, M.E. and Andrews-Speed, C.P., 1984. Sedimentation in a high-altitude intermontane basin - the Wakka Chu molasse (mid-Tertiary, northwestern India). Bulletin Geological Association of India, 17: 175-193.

Butler, W.H. and Prior, D.J., 1988. Tectonic controls on the uplift of the Nanga Parbat massif, Pakistan Himalayas. Nature, 333: 247-250.

Calhoun, J., Bate, T. and Carlson, R., 1991. Sulphur isotope measurements of submicrometer sulphate aerosol particles over the Pacific Ocean. Geophysical Research Letters, 18: 1877-1880.

Calkins, J.A., Offield, T.W., Abdullah, S.K.M. and Ali, S.T., 1975. Geology of the Southern Himalaya in Hazara, Pakistan, and Adjacent Areas. United States Geological Survey, Professional Paper 716-C.

160

Caron, F., Tessier, A., Kramer, J.R., Schwarcz, H.P. and Rees, C.E., 1986. Sulphur and oxygen isotopes of sulfate in precipitation and lake water, Quebec. Applied Geochemistry, 1: 601-606.

Cerling, T. and Quade, J., 1993. Stable Carbon and Oxygen Isotopes in Soil Carbonates. In: P.K. Swart, K.C. Lohmann, J. McKenzie and S. Savin (editors), Climate Change in Continental Isotopic Records. American Geophysical Union, Geophysical Monograph 78: 217-231.

Cerveny, P.F., Johnson, N.M., Tahirkheli, R.A.K. and Bonis, N.R., 1989. Tectonic and geomorphic implications of Siwalik Group heavy minerals, Potwar Plateau, Pakistan. Geological Society of America Special Paper, 232: 129-136.

Chaudhry, M.N. and Ghazanfar, M., 1990. Position of the Main Central Thrust in the tectonic framework of Western Himalaya. Tectonophysics, 174: 321-329.

Chaussidon, M. and Lorand, J.P., 1990. Sulphur isotope composition of orogenic spinel lherzolite massif from Ariege (N.E. Pyrenees, France): An ion microprobe study. Geochimica et Cosmochimica Acta, 54: 2835-2846.

Chiba, H. and Sakai, H., 1985. Oxygen isotope exchange between dissolved sulfate and water at hydrothermal temperatures. Geochimica et Cosmochimica Acta, 49: 993-1000.

Ciais, P. and Jouzel, J., 1994. Deuterium and oxygen 18 in precipitation: Isotopic model, including mixed cloud processes. Journal of Geophysical Research 99: 16793-16803.

Coleman, M.L. and Moor, M.P. 1978. Direct reduction of sulphate to sulphur dioxide for isotope analysis. Analytical Chemistry, 50: 1594-1595.

Clark, I.D. and Fritz, P., 1997. Environmental Isotopes in Hydrogeology. Lewis Publishers, New York.

Claypool, G.E., Holser, W.T., Kaplan, I.R., Sakai, H. and Zak, I., 1980. The age curve of sulfur and oxygen isotopes in marine sulfates and their mutual interpretation. Chemical Geology, 28: 199-260.

Coward, M.P., Jan , M.Q., Rex, D., Taney, J., Thirwal, M. and Windley, B.F. 1982a. Geo-tectonic framework of the Himalaya of N.Pakistan. Journal of the Geological Society of London, 139: 299-308.

Coward, M.P., Jan, M.Q., Rex, D., Tarney, J., Thirwall, M. and Windley, B.F., 1982b. Structural evolution of a crustal section in the western Himalayas. Nature, 295: 22-24.

Coward, M.P., 1985. A section through the Nanga Parbat Syntaxis, Indus Valley, Kohistan. Geological Bulletin University of Peshawar, 18: 147-152.

Coward, M.P., Windley, B.F., Broughton, R., Luff, I.F., Petterson, M.G., Pudsey, C., Rex, D. and Khan, M.A., 1986. Collision Tectonics in NW Himalayas. In: M.P. Coward and A.C. Ries (editors) Collision Tectonics, Geological society of London, Special Publication, 19: 203-219.

Coward, M.P., Butler, R.W.H., Chambers, A.F., Graham, R.H., Izatt, Khan, M.A., Knipe, R.J., Prior, D.J., Treloar, P.J. and Williams, M.P., 1988. Folding and Imbrication of the Indian crust during the Himalayan collision. Philosophical Transactions of the Royal Society of London 326: 89-116.

Craig, H., 1961. Standard for reporting concentrations of deuterium and oxygen-18 in natural waters. Science, 133: 1833-1834.

Craig, H., and Gordon, L., 1965. Deuterium and oxygen-18 variations in the ocean and marine atmosphere. In E. Tongiogi (editor), Stable Isotopes in Oceanographic Studies and Paleotemperatures. Spoleto 1965: 9-130.

DAAC-GSFC, 1996. Global climatology and mean monthly precipitation data, 1920-1980. Interpolated resolution 0.5 degree longitude x 0.5 degree latitude. Distributed Active Archive Center, Goddard Space Flight Center, USA. <ftp://daac.gsfc.nasa.gov/data/hydrology/precip/legates/>.

Dansgaard, W., 1964. Stable isotopes in precipitation. Tellus, 16: 434-468.

Davis, J.C., 1986. Statistics and Data Analysis in Geology. John Wiley and Sons Inc, New York.

Debon, F., Le Fort, P., Dautel, D., Sonet, J. And Zimmermann, J.L., 1987. Granites of western and northern Kohistan (Pakistan): A composite Mid-Cretaceous to Upper Cenozoic magmatism. Lithos, 20: 19-40.

Deer, W.A., Howie, R.A. and Zussman, J., 1982. An Introduction to the Rock Forming Minerals. Longman Group Limited.

Dettman, D. 1996. Re: $\delta^{18}O$ variations in the Indus and Kabul River. E-mail communication, Department of Geosciences, University of Arizona.

Devol, A.H., Forsberg, B.R., Richey, J.E. and Pimentel, T.P., 1995. Seasonal variation in chemical distributions in the Amazon (Solimoes) River: A multiyear time series. Global Biogeochemical Cycles, 9: 307-328.

Dincer, T., 1968. The use of oxygen-18 and deuterium concentrations in the water balance of lakes. Water Resources Research, 4: 1289-1305.

DMA, 1995. United States Defense Mapping Agency, Tactical Pilotage Charts. Fairfax, VA. Scale 1:500, 000.

Elderfield, H., Upstill-Goddard, R. and Sholkovitz, E.R., 1990. The rare earth elements in rivers, estuaries, and coastal seas and their significance to the composition of ocean water. Geochimica et Cosmochimica Acta, 54: 971-991.

Encarta, 1997. Microsoft Encarta Encyclopedia.

Ehhalt, D., Knott, K., Nagel, J.F. and Vogel, J.C., 1963. Deuterium and oxygen-18 in rainwater. Journal of Geophysical Research, 68: 3775-3780.

Ehleringer, J.R., Sage, R.F., Flanagan, L.B. and Pearcy, R.W., 1991. Climatic change and the evolution of C_4 photosynthesis. Trends in Ecology and Evolution, 6: 95-99.

Epstein, S. and Mayeda, T., 1953. Varaition of oxygen-18 content of waters from natural sources. Geochimica et Cosmochimica Acta, 4: 213-244.

Fairchild, I.J. and Bradby, L., 1994. Hydrochemistry of carbonate terrains in alpine glacial settings. Earth Surface Processes and Landforms, 19: 33-54.

Faure, G., 1986. Principles of Isoptope Geology, second edition, John Wiley and Sons Inc, New York.

Flintrop, C., Hohlmann, B., Jasper, T., Korte, C., Podlaha, O. G., Scheele, S. and Veizer, J., 1996. Anatomy of pollution: Rivers of North Rhine-Westphalia, Germany. American Journal of Science, 296: 58-98.

Fontes, J.Ch., Gonfiantini, R. and Roche, M.A., 1970. Deuterium et oxygene-18 dans les eaux du lac Tchad. In: Isotope Hydrology 1970, IAEA Symposium 129, March 1970, Vienna: 387-404.

Fontes, J.-Ch., Gasse, F. and Gibert, E., 1996. Holocene environmental changes in Lake Bangong basin (Western Tibet). Part1: Chronology and stable isotopes of carbonates of a Holocene lacustrine core. Palaeogeography, Palaeoclimatology and Palaeoecology, 120: 25-47.

Frank, W., Gansser, A. and Trommsdorff, V., 1977. Geological observations in the Ladakh area (Himalayas). A preliminary report. Suisse mineral. Pertog. 57: 89-113.

Fritz, P., Lapcevic, A., Miles, .M., Frape, S.K., Lawson, D.E. and O'Shea, K.J., 1988. Stable isotopes in sulfate minerals from Salina Formation in southwestern Ontario. Canadian Journal of Earth Sciences, 25: 195-205.

Freeze, R. A., and Cherry, J.A., 1979. Groundwater. Prentice Hall, Englewood, Cliffs, New Jersey.

Friedman, I., Machta, L. and Soller, R., 1962. Water vapour exchange between a water droplet and its environment. Journal of Geophysical Research, 67: 2761-2766.

Gaetani, M., Garzanti, E., Jadoul, F., Nicora, A., Tintori, A., Pasini, M. and Khan, K.S.A., 1990. The north Karakorum side of the Central Asia geopuzzle. Geological Society of America Bulletin, 102: 54-62.

Gaillardet, J., Dupré, B., Allègre, C.J., Négrel, P., 1997. Chemical and physical denudation in the Amazon River Basin. Chemical Geology, 142: 141-173.

Galy, A. and France-Lanord, C., 1998. Processes of the weathering in the Ganges-Brahmaputra and the riverine alkalinity budget. Chemical Geology (Special Issue).

Gansser, A., 1964. Geology of the Himalayas. John Wiley Interscience Publishers, London.

Garrels, R.M. and Mackenzie, F.T., 1971. Evolution of Sedimentary Rocks (second edition). W.W. Norton and Company, Inc. New York.

Garrels, R.M., Thompson, M.E. and Siever, R., 1960. Stability of some carbonates at 25° C and one atmosphere total pressure. American Journal of Science, 258: 402-418.

Garzanti, E., Casnedi, R. and Jouzel, F., 1986. Sedimentary evidence of a Cambro-Ordivician orogenic event in the northwestern Himalayas. Sedimentary Geology, 48: 237-265.

Gat, J.R. and Carmi, I., 1970. Evolution of the Isotopic Composition of Atmospheric Waters in the Mediterranean Sea Area. Journal of Geophysical Research, 75: 3039-3048.

Gat, J.R., 1971. Comments on the stable isotope method in regional groundwater investigations. Water Resources Research, 7: 980.

Gat, J. R. and Dansgaard, W., 1972. Stable isotope survey of the fresh water occurrences in Israel and the northern Jordan rift valley. Journal of Hydrology, 16: 177-212.

Gat, J.R., Bowser, C.J. and Kendall. 1994. The contribution of evaporation from the Great Lakes to the continental atmosphere: estimates based on stable isotope data. Journal of Geophysical Research, 21: 557-560.

Gazis, C.A., Blum, J.D. and Chamberlain, C.P., 1995. The effect of hydrothermal activity on the Sr isotope systematics of gneisses from the Nanga Parbat-Haramosh Massif (Northwest Himalaya, Pakistan), EOS (Transactions, American Geophysical Union), 76: F704.

Gee, E.R., 1989. Overview of the geology and structure of the Salt Range, with observations on related areas of northern Pakistan. Geological Society of America Special Paper, 232: 95-112.

Gibbs, R.J., 1967. The Geochemistry of the Amazon River System: Part I. The Factors that Control the salinity and the Composition and Concentration of the Suspended Solids. Geological Society of America Bulletin, 78: 1203-1232.

Gilani, M.A., 1992. Future Scope: Environmentalism and Sustainability. National Book Foundation, Islamabad, Pakistan.

Goldstein, S.J. and Jacobsen, S, B., 1987. The Nd and Sr isotopic systematics of river-water dissolved material: Implications for the sources of Nd and Sr in seawater. Chemical Geology (Isotope Geoscience Section), 66: 245-272.

Goldstein, S.J. and Jacobsen, S.B., 1988. Rare earth elements in river waters. Earth and Planetary Science Letters, 89: 35-47.

GRDC, 1996. Global Runoff Data Centre, Federal Institute of Hydrology, Koblenz Germany.

Gupta, K.R., Gergan, J.T., Kumar, S., 1982. Geochemistry of the volcanic rocks of the northwestern Himalaya and its bearing on tectonics-A review. In: A.K.Sinha (editor), Contemporary Geoscientific Researches in the Himalaya, Dehra Dun India 2: 9-17.

Gupta, V.J. and Kumar, S., 1975. Geology of Ladakh and Spiti regions of Himalaya with special reference to the stratigraphic position of flysch deposits. Geolgische Rundschau, 64: 540-562.

HACH, 1989. Water Analysis Handbook. HACH Company, Loveland Colorado.

Hanson, C.A., 1989. The northern suture in the Shigar valley, Baltistan, northern Pakistan. Geological Society of America Special Paper, 232: 203-215.

Harris, N.B.W., 1995. Significance of weathering Himalayan metasedimentary rocks and leucogranites for the Sr isotope evolution of seawater during the early Miocene. Geology, 23: 795-798.

Harris, N., Bickle, M., Chapman, H., Fairchild, I. and Bunbury, J., 1998. The significance of Himalayan rivers for silicate weathering rates: evidence from Bhote Kosi tributary. Chemical Geology, 144: 205-220.

Harrison, P.J., Snedaker, S.C., Ahmed, S.I. and Azam, F., 1994. Primary Producers of the Arid Climate Mangrove Ecosystem of the Indus River delta, Pakistan: An Overview. Tropical Ecology, 35: 155-184.

Heim, A. and Gansser, A. 1939. Central Himalaya. Geological observations of the Swiss expedition 1936. Hindustan Publishing corporation Delhi.

Hem, J.D., 1985. Study and Interpretation of the Chemical Characteristics of Natural Water. United States Geological Survey Water-Supply Paper 2254.

Herren, E., 1987. Zanskar shear zone: Northeast-southwest extension within the Higher Himalayas (Ladakh, India). Geology, 15: 409-413.

Hewitt, K., 1989. The altitudinal organisation of Karakoram geomorphic processes and depositional environments. In: E. Derbyshire and A. Owen (editors), Quaternary of the Karakoram and Himalaya, 9-32.

Hoffman, E.J., Hoffman, G.L. and Duce, R.A., 1980. Particle size dependence of alkali and alkaline earth metal enrichment in marine aerosols from Bermuda. Journal of Geophysical Research, 85: 5499-5502.

Holland, H., 1978. The chemistry of the atmosphere and oceans. John Wiley and Sons Inc.

Holmes, J., 1993. Present and past patterns of glaciation in the northwest Himalaya: Climatic, tectonic and topographic controls. In: J.F.Shroder, Jr. (editor), Himalaya to the Sea. Routledge, New York 72-90.

Holt, B.D., Cunningham, P.T. and Engelkemeir, A.G., 1978. Application of the oxygen-18 to the study of atmospheric sulphate formation. In Robinson, B.W. (editor), Stable Isotopes in the Earth Sciences, New Zealand DSIR Bulletin, 105-109.

Honegger, K., Dietrich, V., Frank, W., Gansser, A., Thöni, M. and Trommsdorff, V., 1982. Magmatism and metamorphism in the Ladakh Himalayas (the Indus-Tsangpo suture zone). Earth and Planetary Science Letters, 60, 253-292.

Horibe, Y., Shigehara, K. and Takakuwa, Y., 1973. Isotope separation factors of carbon dioxide-water system and isotopic composition of atmospheric oxygen. Journal Geophysical Research, 78: 2625-2629.

Houghton, M.L., 1980. Geochemistry of the Proterozoic Hormuz Evaporites, Southern Iran. M.Sc. thesis, University of Oregon.

Humayun, M., 1986. Petrology of the Swat Amphibolites and the development of a "Lesser Himalayan" Basin. Geological Bulletin University of Peshawar, 19: 83-100.

Hunting Survey Corporation Limited., 1960. Reconnaissance Geology of part of west Pakistan. A Colombo Plan Cooperative Project, Toronto, Canada.

Hussain, A., Yeats, R.S. and Pogue, K., 1989. Stratigraphic and structural events around the southern margin of Peshawar Basin. Geological Bulletin University of Peshawar, 22: 45-54.

Hussain, S.D., Sajjad, M.I., Ahmad, M., Tasneem, M.A., Yurtsever, Y. and Akram, W., 1991. Isotopic investigation of the interrelationship between surface water and groundwater in the Mardan and Chaj Doab areas in Pakistan. Symposium Proceedings, IAEA-SM-319/23 International Atomic Energy Agency.

IAEA, 1992. Statistical Treatment of data on Environmental Isotopes in Precipitation. Technical Report Series no. 331.

IAEA-WMO. Global Network of Isotopes in Precipitation (GNIP) and its associated database. <http://www.iaea.or.at/programs/ri/gnip/gnipmain.htm>.

Irion, G., 1987. Die Tonmineralvergesellschaftung in Fluß sedimenten der Feuchten Tropen (Amazonas-Becken, West Papua Neuguinea) als Ausdruck der Verwitterung im Einzugsgebiet. Habilitationsschrift, Universität Heidelberg.

Irion, G., 1991. Minerals in Rivers. In E.T. Degens, S. Kempe and J. Richey (editors), Biogeochemistry of Major World Rivers (SCOPE 42). International Council of Scientific Unions , Scientific Committee on Problems of the Environment. John Wiley and Sons Inc New York.

Ittekkot, V. and Arain, R., 1986. Nature of particulate organic matter in the river Indus, Pakistan. Geochimica et Cosmochimica Acta, 50: 1643-1653.

Ivanov, M.V., Grinenko, Y.A. and Rabinovich, A.P., 1983. Sulfur flux from continents to oceans. In: M.V. Ivanov and J.R. Freney (editors), The Global Biogeochemical Sulphur Cycle. John Wiley and Sons Inc, New York.

Jan, M.Q., 1985. High-P rocks along the suture zones around the Indo-Pakistan plate and phase chemistry of blueschist from eastern Ladakh. Geological Bulletin University of Peshawar, 18, 1-40.

Jan, M.Q., 1988. Geochemistry of amphibolites from the southern part of the Kohistan arc, N.Pakistan. Mineralogical Magazine, 52: 147-159.

Jan, M.Q and Howie, R.A., 1980. Ortho- and clinopyroxenes from the pyroxene granulites of Swat Kohistan, northern Pakistan. Mineralogical Magazine, 43: 715-726.

Jan, M.Q., Asif, M. Tahirkheli, T. and Kamal, M., 1981a. Tectonic subdivision of granitic rocks of north Pakistan. Geological Bulletin University of Peshawar 14: 159-182.

Jan, M.Q., Kamal, M. and Khan, M.I., 1981b. Tectonic control over emerald mineralization in Swat. Geological Bulletin University of Peshawar, 14: 101-109.

Jan, M.Q., Asif, M. and Tahirkheli, T., 1981c. The Geology and petrography of the Tarbela 'Alkaline' Complex. Geological Bulletin University of Peshawar, 14: 1-28.

Jan, M.Q and Howie, R.A., 1981. The Mineralogy and Geochemistry of the Metamorphosed Basic and Ultrabasic Rocks of the Jijal Complex. Journal of Petrology, 22: 85-126.

Jan, M.Q., Khan, A. and Windley, B.F., 1989. Mineral chemistry of the Chilas mafic-ultramafic complex, Kohistan island arc, N. Pakistan: Oxide phases. Geological Bulletin University of Peshawar, 22: 217-239.

Jan, M.Q. and Karim, A., 1990. Continental magmatism related to late Palaeozoic-early Mesozoic rifting in north Pakistan and Kashmir. Geological Bulletin University of Peshawar 23: 1-25.

Jöreskog, K.G., Kloven, J.E. and Reyment, R.A., 1976. Geological Factor Analysis. Elsevier, Amsterdam.

Jorgensen, D.W., Harvey, M.D., Schumm, S.A. and Flam, L., 1993. Morphology and dynamics of the Indus River: Implications for the Mohen Jo Daro site. In: J.F. Shroder Jr. (editor), Himalaya to the Sea. Routledge, New York, 288-326.

Jouzel, J. and Merlivat, L. 1984. Deuterium and Oxygen-18 in Precipitation: Modeling of the Isotopic effects During Snow Formation. Journal of Geophysical Research, 89: 11749-11757.

Junge, C.E., 1963. Air Chemistry and Radioactivity. Academic Press, New York.

Karim, A. and Veizer, J. (1998) Hydrochemistry of the Indus River tributaries. Chemical Geology (Special Issue).

Kazmer, C., Hussain, S.S. and Lawerence, R.D., 1983. The Kohistan-Indian plate suture zone at Jawan Pass, Swat, Pakistan. Geological Society of America Abstractswith Programs, 15: 609.

Kazmi, A.H., 1984. Geology of the Indus delta. In: B.U. Haq and J.D. Milliman (editor), Marine Geology and Oceanography of Arabian Sea and Coastal Pakistan. Von Nostrand Reinhold, New York, 71-84.

Kazmi, A.H. and Rana, R.A., 1982. Tectonic Map of Pakistan, Scale 1:2000,000. Geological Survey of Pakistan, Government of Pakistan.

Kazmi, AH., Lawrence, R.D., Dawood, H., Snee, L.W. and Hussain, S.S., 1984. Geology of the Indus suture zone in the Mingora-Shangla area of Swat, N. Pakistan. Geological Bulletin University of Peshawar, 17: 127-144.

Kempe, D.R.C. and Jan, M.Q., 1970. An Alkaline Igneous Province in the NW Frontier Province, West Pakistan. Geological Magazine, 107: 395-398.

Kempe, S., 1979. Carbon in the rock cycle. In: E.T. Degens, S. Kempe, and P.Ketner (editors), The Global Carbon Cycle, SCOPE 13, John Wiley and Sons Inc, New York, 343-377.

Khan, M.A., Windley, B.F., Tarney, J. and Thirlwall, M., 1989. The Chilas mafic-ultramafic igneous complex: The root of the Kohistan island arc in the Himalaya of northern Pakistan. Geological Society of America Special paper, 232: 75-94.

Khan, M.A., Stern, R.J., Gribble, R.F. and Windley, B.F., 1997. Isotopic composition of Sr, Nd, and Pb in the Kohistan Intra-Oceanic Arc Terrane of Northern Pakistan. Journal Geological Society of London, 154: 935-946.

Klootwijk, C.T., 1979. A review of the Palaeomagnetic data from the Indo-Pakistani fragment of Gondwanaland. In: A. Farah and K.A. DeJong (editors), Geodynamics of Pakistan, Geological Survey of Pakistan, 41-80.

Krishnamurthy, R.V. and Bhattacharya, S.K., 1991. Stable oxygen and hydrogen isotope ratios in shallow ground waters from India and a study of the role of evapotranspiration in the Indian monsoon. In: J.R. O'Neil and I.R. Kaplan (editors), Stable Isotope Geochemistry: A Tribute to Samuel Epstein, The Geochemical Society Special Publication, 3: 1-7.

Krouse, H.R., 1980. Sulphur isotopes in our environment. In: P.Fritz and J.-Ch Fontes (editors), Handbook of Environmental Isotope Goechemistry, volume 1, The Terrestrial Environmental, A. Elsevier, Amsterdam, The Netherlands: 219-256.

Kruseman, G.P. and Naqavi, S.A.H., 1988. Hydrogeology and groundwater resources of the North-West Frontier Province, Pakistan. WAPDA, Peshawar, Pakistan and Institute of Applied Geoscience, Delft, The Netherlands.

Kundig, R., 1989. Domal structures and high-grade metamorphism in the Higher Himalayan Crystalline, Zanskar Region, northwest Himalaya, India. Journal of Metamorphic Geology, 7: 43-55.

Kureshy, K.U., 1991. Geography of Pakistan. National Book Service, Lahore, Pakistan.

Kusakabe, M. and Robinson, B.W., 1977. Oxygen and sulphur isotopic equilibria in the $BaSO_4$-HSO_4^--H_2O system from 110-350 °C and applications. Geochimica et Cosmochimica Acta, 41: 1033-1040.

Lawerence, R.D. and 15 others, 1989. Tectonics south of the suture, northern Pakistan. 28th International Geological Congress, washington, Abstract 2: 265.

Le Fort, P., 1988. Granites in the tectonic evolution of the Himalaya, Karakoram and southern Tibet. Philosophical Transactions of the Royal society of London, A326: 281-299.

Le Fort, P., Debon, F. and Sonet, J., 1980. The 'Lesser Himalayan' corderite granite belt: Typology and age of the pluton of Mansehra, Pakistan. Geological Bulletin University of Peshawar, 13: 51-61.

Le Fort, P., Michard, A., Sonet, J. and Zimmermann, J.L., 1983. Petrography, geochemistry and geochronology of some samples from the Karakoram axial batholith (northern Pakistan). In: F.A. Shams (editor), Granites of Himalayas, Karakoram and Hindu Kush. Institute of Geology, Punjab University, Lahore, Pakistan, 377-387.

Lide, D.R. and Frederikse, H.P.R. 1995. CRC Handbook of Chemistry and Physics, 76th Edition. CRC Press, Florida.

Lloyd, R.M., 1967. Oxygan-18 composition of oceanic sulphate. Science, 156: 1228-1231.

Longinelli, A., 1989. Oxygen-18 and sulphur-34 in dissolved oceanic sulphate and phosphate. In: P.Fritz and J.-Ch Fontes (editors), Handbook of Environmental Isotope Goechemistry, volume 3, The Marine Environmental, A. Elsevier, Amsterdam, The Netherlands: 435-472.

MacIntyre, F., 1974. The top millimeter of the ocean. Scientific American, 230: 62-77.

Mayewski, P.A. and Lyons, W.B., 1983. Chemical composition of a high altitude fresh snowfall in the Ladakh Himalayas. Geophysical Research Letters, 10: 105-108.

Mayewski, P.A. Lyons, W.B., Ahmed, N., Smith, G. and Pourchet, M., 1984. Interpretation of the chemical and physical time-series retrieved from Sentik glacier, Ladakh Himalaya, India. Journal Glaciology, 30: 66-76.

Mcardle, N. C. and Liss, P.S., 1995. Isotopes and atmospheric sulphur. Atmospheric Environment, 29: 2553-2556.

Medlicott, H.B., 1864. On the geological structure and relations of the southern portion of the Himalayan ranges between the river Ganges and the Ravee. Memoir Geological Survey of India, 3: 1-212.

Meissner, C.R., Hussain, M., Rashid, M.A. and Sethi, U.B., 1975. Geology of the Parachinar Quadrangle, Pakistan. United States Geological Survey Professionl Paper, 716-F.

170

Meybeck, M., 1979. Concentrations des eaux fluviales en èlèments majeurs et apports en solution aux ocèans, Rev. Gèogr. Phys. 21(3): 215-246.

Meybeck, M., 1980. Pathways of major elements from land to oceans through rivers. In: J.M. Martin, J.D. Burton, And D. Eisma (editors), Review and Workshop on River Inputs to Ocean-Systems, 18-30, Rome: FAO.

Meybeck, M., 1984. Les fleuves et le cycle gèochimique des èlèments. Thèse Doctorat (no. 8435), Ecole Normal Supèrieure, Laboratoire de Gèologie, universitè Pierre et Marie Curie, Paris 6, France.

Meybeck, M., 1986. Composition chimique des ruisseaux non pollués de France. Science Géologie Bulletin, 39: 1-3.

Meybeck, M., 1987. Global chemical weathering of surficial rocks estimated from river dissolved loads. American Journal of Science, 287: 401-428.

Milliman, J.D., Quraishee, G.S. and Beg., M.A.A., 1984. Sediment Discharge from the Indus River to the Ocean: Past, Present and Future. In: B. Haq and J.D. Milliman (editors), Marine Geology and Oceanography of Arabian Sea and Coastal Pakistan, 65-70.

Molnar, P. & Tapponnier, P., 1975. Cenozoic tectonics of Asia: effects of a continental collision. Science, 189: 419-426.

Mook, W.G., 1970. Stable carbon and oxygen isotopes of natural water in the Netherlands: In: W.G. Mook (editor), Isotope Hydrology, International Atomic Energy Agency, Vienna, 163-190.

Müller, G. and Stoffers, P., 1974. Mineralogy and petrology of Black Sea basin sediments. In: E.T. Degens and A. Ross (editors), The Black Sea: Geology, Chemistry and Biology, American Association of Petroleum Geologists Memoirs, 20: 200-248.

Naidu, A.S. and Mowatt, T.C., 1983. Sources and dispersal patterns of clay minerals in surface sediments from the western continental shelf areas of Alaska, Geological Society of America Bullettin, 94: 841-854.

Nakai, N., Mizutani, Y. and Kiyosumi, Y., 1987. Study on the origin of groundwater and water in the Tibet area by using ratios of stable isotopes. In: I. Kayane (editor), Comparative Study of river Basins, 69-81.

NGDC, 1988. Data Announcement 88-MGG-02, Digital relief of the surface of the Earth. National Geophysical Data Center, Boulder Colorado.
<http://www.ngdc.noaa.gov/mgg/global/>

Niewodniczanski, J., Grabczak., Baranski, L. and Rzepka, J., 1981. The altitude effect on the isotopic composition of snow in high mountains. Journal of Glaciology, 27: 99-111.

Nijampurkar, V.N., Sarin, M.M. and Rao. K.D., 1993. Chemical composition of snow and ice from Chhota Shigri glacier, central Himalaya. Journal of Hydrology, 151: 19-34.

Onishi, H., 1969. Antimony. In: K.H. Wedepohl (editor), Handbook of Geochemistry. Springer-Verlag, 51:G-1, I-1.

Paasch, F.R., 1987. International Commission on Irrigation and Drainage (ICID), Executivrat in Pakistan. Deutscher Verband fÜr. Wasserwirtschaft und Kulturbau (DVKW) Nachrichten, Hamburg, Berlin. 1: 89.

Palmer, M.R. and Edmond, J.M., 1989. The strontium isotope budget of the modern ocean. Earth and Planetary Science Letters, 92: 11-26.

Palmer, M.R. and Edmond, J.M., 1992. Controls over the strontium isotope composition of river water. Geochimica et Cosmochimica Acta, 56: 2099-2111.

Pande, K., Sarin, M.M., Trivedi, S., Krishnaswami, K.K. and Sharma K.K., 1994. The Indus river system (India-Pakistan): Major-ion chemistry, uranium and strontium isotopes. Chemical Geology, 116: 245-259.

Pareek, H.S., 1982. The Himachal Panjal Traps-A geochemical appraisal. In: A.K.Sinha (editor), Contemporary Geoscientific Researches in the Himalaya, Dehra Dun India 2: 1-7.

Pande, K., Sarin, M.M., Trivedi, S., Krishnaswami, K.K. and Sharma K.K., 1994. The Indus river system (India-Pakistan): Major-ion chemistry, uranium and strontium isotopes. Chemical Geology, 116: 245-259.

Pascoe, E.H., 1920. The early history of the Indus, Brahmaputra and Ganges. Quarterly Journal Geological Society of London, 75: 138-155.

Pawellek, F. and Veizer, J., 1994. Carbon cycle in the upper Danube and its tributaries: $\delta^{13}C_{(DIC)}$constraints. Israel Journal of Earth Sciences, 43: 187-194.

Payne, B.R., 1992 . On the statistical treatment of environmental isotope data in hydrology. International Atomic Energy Agency Report, 319/36: 273-290.

Pêcher, A. and Le Fort, P., 1986. The metamorphism in central Himalaya, its relation with the thrust tectonics. In: P. Le Fort, M.Colchen and C.Montenat (editors), Evolution des domaines orogeniqué d' Asie méidionale (de la Turquie àl 'Indonésie). Sciences de la Terre, Nancy, mémoir, 47: 285-309.

Petterson, M.G. and Windley, B.F., 1991. Changing source regions of magmas and crustal growth in the Trans-Himalayas: evidence from the chalt volcanics and Kohistan batholith, Kohistan, northern Pakistan. Earth and Planetary Science Letters, 102, 326-341.

Pilgrim, G.E., 1919. Suggestions concerning the history of drainage of northern India. Journal of Asiatic Society of Bengal, N.S. 15: 81-89.

Postgate, J.R., 1959. Sulphate reduction by bacteria. Annual Reviews in Microbiology, 13: 505-520.

Potter, P.E., Heling, D., Shimp, M.F. and Wie, W. van., 1975. Clay mineralogy of modern alluvial muds of the Mississippi river basin. Bullettin Ctr Rech Pau. SNPA9: 353-89.

Pudsey, C.J., 1986. The Northern Suture, Pakistan: margin of a Cretaceous island arc. Geological Magazine, 123: 405-423.

Pudsey, C.J., Coward, M.P., Luff, I.W., Schackleton, R.M., Windley, B.F. and Jan, M.Q., 1985. Collission zone between the Kohistan arc and the Asian plate in the NW Pakistan. Transactions of the Royal Society of Edinburgh, 76: 463-479.

Puchelt, H., 1972. Barium. In: K.H. Wedepohl (editor), Handbook of Geochemistry. Springer-Verlag, 11-1: 56.H-1, H3.

Quade, J., Thure, E. and Bowman, J.R., 1989. Development of Asian monsoon revealed by marked ecological shift during the latest Miocene in northern Pakistan. Nature, 342: 163-166.

Quade J., Roe, L., DeCelles, P.G. and Ojha, T.P., 1997. The Late Neogene $^{87}Sr/^{86}Sr$ Record of Lowland Himalayan Rivers. Science, 276: 1828-1831.

Rafiq, M., 1987. Petrology and geochemistry of the Ambela granitic complex, N.W.F.P. Pakistan. Ph.D. thesis, University of Peshawar.

Rai, H. and Pande, I.C., 1978. Geology of the Kargil igneous complex, Ladakh, Jammu and Kashmir, India. Geological Survey of India, Records, 5: 219-288.

Rao, Y.P., 1981. The climate of the Indian subcontinent. In: K. Takahashi and H. Arakawa (editors), Climates of Southern and Western Asia. Elsevier, Amsterdam.

Raymo, M.E., Ruddiman, W.F. and Froelich, P.N., 1988. Influence of late Cenozoic mountain building on ocean geochemical cycles. Geology, 16: 649-653.

Rees, C.E. 1978. Sulphur isotope measurements using SO_2 and SF_6. Geochimica et Cosmochimica Acta, 42: 283-289.

Rollinson, H.R., 1993. Using Geochemical Data: Evaluation, Presentation, Interpretation. Longman Group Limited, UK.

Salati, E., Dall'Olio, A., Matsui, E. and Gat, R., 1979. Recycling of Water in the Amazon Basin: An Isotopic Study. Water Resources Research, 15: 1250-1258.

Sano, S., Nakajima, T. and Rahim, S., 1996. Sr and Nd isotopic composition of Lower Crustal Material of Kohistan Paleo-Arc. Geological Society of Japan, Annual meeting, 199 368.

Sarkar, A., Roy, A., Ghatak, G.S. and Bhattacharya, S.K., 1996. Strontium Isotope Study of Krol-Tal Carbonates: Implication to the Strontium Isotope Flux of Himalayan Rivers. Indian Journal of Geology, 68: 255-262.

Schlesinger, W.H., 1991. Biogeochemistry: An Analysis of Global Change. Academic Press.

SCOPE 19, 1983. The Global Biogeochemical Sulphur Cycle and Influence on it of Human Activity. In: M.V. Ivanov and J.R. Freney (editors), John Wiley and Sons Inc.

Searle, M.P., 1991. Geology and Tectonics of the Karakoram Mountains. John Wiley and Sons Inc.

Searle, M.P., Cooper, D.J.W. and Rex, A.J., 1988. Collision tectonics of the Ladakh-Zanskar Himalaya. Transactions of the Royal Society of Edinburgh, 117-150.

Searle, M.P., Khan., M.A., Jan M.Q., Dipietro., J.A., Pogue, K.R., Pivnik, D.A., Sercombe, W.J., Izatt, C.N., Blisniuk, P.M., Treloar, P.J., Gaetani, M. and Zanchi, A., 1996. Geological Map of North Pakistan and adjacent areas of northern Ladakh and western Tibet, Scale 1: 650, 000.

Seeber, L. and Armbruster, J.G., 1979. Seismicity of the Hazara arc in northern Pakistan: decollement vs. Basement faulting. In: A.Farah and K.A. DeJong (editors), Geodynamics of Pakistan, Geological Survey of Pakistan, Quetta, 131-332.

Sequeira, R. and Kelkar, D., 1978. Geochemical Implications of Summer Monsoon Rainwater Composition over India. Journal of Applied Meteorology, 17: 1390-1396.

Shakur, A., 1982. δ34S and d18O variations in Terrestrial Sulfates. Ph.D. thesis, University of Calgary.

Shi Yafeng and Zhang Xiangsong, 1984. Some studies of the Batura Glacier in the Karakoram Mountains. In K.J.Miller (editor), The International Karakoram Project 1 Cambridge: Cambridge University Press, 51-63.

Sholkovitz, E.R., 1995. The aquatic chemistry of rare earth elements in rivers and estuaries. Aquatic Geochemistry, 1: 1-34.

Shuja, T.A., 1986. Geothermal Areas in Pakistan. Geothermics, 15: 719-723.

Singh, S.K., Trivedi, J.R., Pande, K., Ramesh, R. and Krishnaswami, S., 1998. Chemical and strontium, oxygen, and carbon isotopic composition of carbonates from the Lesser Himalaya: Implications to the strontium isotope composition of source waters of the Ganga, Ghaghara, and the Indus rivers. Geochimica et Cosmochimica Acta, 62: 773-755.

Smith, A.G., Hurley A.M. and Briden, J.C., 1981. Phanerozoic Palaeocontinental World Maps. Cambridge University Press, Cambridge.

Spencer, D.A., Ramsay, J.G., Spencer-Cervato, C., Pognante, U., Ghazanfar, M. and Chaudhry, M.N., 1990. High pressure (eclogite facies) metamorphism in the Indian plate, NW, Himalaya, , Pakistan. Geological Bulletin, University of Peshawar, 23: 87-100.

Stallard, R.F. 1985. River chemistry, geology, geomorphology, and soils in the Amazon and Orinoco Basins. In: J.I. Drever (editor), The Chemistry of Weathering, 293-316. D. Reidel , Boston.

Stewart, A.G., 1990. For debate: Drifting continents and endemic goitre in northern Pakistan. British Medical Journal, 300: 1507-1512.

Strauss, H., 1993. The sulfur isotopic record of Precambrian sulfates: new data and a critical evaluation of the existing record. Precambrian Research, 63: 225-246.

Stumm, W. and Morgan, J.J., 1996. Aquatic Chemistry: Chemical Equilibria and Rates in Natural Waters. John Wiley and Sons Inc, New York.

SYSTAT Inc., 1993. SYSTAT 5.02. SYSTAT Inc. Evanston, Illinois.

Tahirkheli, R.A.K., 1979. Geology of Kohistan and adjoining Eurasian and Indo-Pakistan continents, Pakistan. Special Issue Geological Bulletin University of Peshawar 11: 1-30.

Tahirkheli, R.A.K., 1982. Geology of the Himalaya, Karakoram and Hindu Kush in Pakistan. Geological Bulletin University of Peshawar, special issue, 15, 51.

Tamburi, A., 1974. Geology and water resource system of the Indus Plains. Ph.D. Thesis, Colorado State University, Colorado.

Tariq, J., Ashraf, M. and Afzal, M., 1996. Pollution status of the Indus River, Pakistan, through heavy metal and macronutrient contents of fish, sediment and water. Water Resource Research, 30: 1337-1344.

Taylor, B.E., Wheeler, M.C. and Nordstorm, D.K., 1984. Stable isotope geochemistry of acid mine drainage: experimental oxidation of pyrite. Geochimica et Cosmochimica Acta, 48: 2669-2678.

Telmer, K.H., 1997. Biogeochemistry and water balance of the Ottawa River Basin. Ph.D. thesis, University of Ottawa.

Thode, H.G., 1991. Sulfur Isotopes in Nature and the Environment: An Overview. In: H.R. Krouse and V.A. Grinenko (editors), Stable Isotopes: Natural and Anthropogenic Sulphur in the Environment. SCOPE 43: 1-26, John Wiley and Sons Inc.

Toran, L. and Harris, R.F., 1989. Interpretation of sulphur and oxygen isotopes in biological and abiological sulphide oxidation. Geochimica et Cosmochimica Acta, 53: 2341-2348.

Treloar, P.J., 1989. Imbrication and unroofing of the Himalayan thrust stak of the north Indian plate, north Pakistan. Geological Bullettin University of Peshawar, 22: 25-44.

Trivedi, J.R., Pande, K., Krishnaswami, S. and Sarin, M.M., 1995. Sr isotopes in rivers of India and Pakistan: A reconnaissance study. Current Science, 69: 171-178.

Todd, K., 1955. Ground-water in relation to a flooding stream. Proceedings American Society of Civil Engineers, 81: 1-20.

TYDAC Technologies Inc., 1995. TYDIG, version 1.1. TYDAC Technologies Inc. Ottawa, Canada.

TYDAC Research Inc., 1997. SPANS EXPLORER, version 7.0. TYDAC Research Inc. Ottawa, Canada.

United States Central Intelligence Agency, 1973. Agriculture, Ethnology, Land Use, Population, Industrial, Mining and Power Centers. Scale 1: 4 050 000. Washington.

Veizer, J., 1989. Strontium isotopes in seawater through time. Annual Reviews, Earth and Planetary Sciences, 17: 141-167.

Veselind, P. and McCurry, S., 1984. Life breath of half of the world: Monsoons. National Geographic, National Geographic Society, Washington D.C. 166: 712-747.

Vogel, J.C., 1993. Variability of carbon isotope fractionation during photosynthesis. In: J.R. Ehleringer, A.E. Hall and G.D. Farquhar (editors), Stable Isotopes and Plant carbon-Water Relations. Academic Press, San Diego.

Wadia, D.N., 1937. The Cretaceous volcanic series of Astor, Deosai, Kashmir, and its intrusions. Records Geological Survey of India, 72/2: 151-161.

Wadia, D.N., 1957. Geology of India. Macmillan and Company London.

Wadleigh, M.A., Schwarcz, H.P. and Kramer, J.R., 1996. Isotopic evidence for the origin of sulfate in coastal rain. Tellus, 48B: 44-59.

Wadleigh, M.A., Veizer, J. and Brooks, C., 1985. Strontium and its isotopic composition in Canadian rivers: fluxes and global implications. Geochimica et Cosmochimica Acta, 49: 1727-1736.

Wake, C., 1987. Snow accumulation studies in the central Karakoram, Pakistan. Proceedings of the 44th Annual Snow Conference, Fredericton, New Brunswick, 19-33.

Wake, C., 1989a. The influence of summertime precipitation events on the meltwater production in the Karakoram, northern Pakistan. Proceedings of the forty-sixth Annual Eastern Snow Conference. Quebec City, Quebec.

Wake, C., 1989b. Geochemical investigations as a tool for determining the spatial and seasonal variation of snow accumulation in the central Karakoram, northern Pakistan. Annals of Glaciology, 13: 279-284.

Wake, C.P., Mayewski, P.A., Ping, W., Qinzhao. Y., Jiankang, H. and Zichu, X., 1992. Anthropogenic sulfate and Asian dust signals in snow from Tien Shan, northwest China. Annals of Glaciology, 16: 45-52.

Wake, C. and Stievenard, M., 1995. The amount effect and oxygen isotope ratios recorded in Himalayan snow. Proceedings of the IGBBP-PAGES/PEPII Nagoya (Japan) Symposium, 1-5.

WAPDA (Water and Power Development Authority), 1976. Annual Report of River and Climatological Data of Pakistan. Hydrology and System Analysis Organization, Surface Water Hydrology Project, Lahore, Pakistan.

WAPDA, 1985. Annual Report of River and Climatological Data of Pakistan. Surface Water Hydrology Project, Hydrology and Water Management Organization Planning Division WAPDA in collaboration with German Agency for Technical Cooperation.

WAPDA, 1989a. Annual Report of River and Climatological Data of Pakistan. Surface Water Hydrology Project, Hydrology and Water Management Organization Planning Division WAPDA in collaboration with German Agency for Technical Cooperation.

WAPDA,1989b. Hydrogeological Map of Pakistan, Scale 1:2, 000, 000.

WAPDA, 1990. Annual Report of River and Climatological Data of Pakistan. Surface Water Hydrology Project, Hydrology and Water Management Organization Planning Division WAPDA in collaboration with German Agency for Technical Cooperation.

Wilhelm, E., Battino, R. and Wilcock, R.J., 1977. Low pressure solubility of gases in liquid water. Chemical Reviews, 77: 219-262.

Whiteman, P.T.S., 1985. Mountain Oasis: A technical Report of Agricultural Studies (1982-84) in Gilgit District, Northern Areas , Pakistan. U.N. Food and Agriculture Programme, Pak/80/009.

William, M.P., 1989. The Geology of the Besham area, north Pakistan: Deformation and imbrication in the footwall of the Main Mantle Thrust. Geological Bullettin University of Peshawar, 22: 65-82.

Windley, B.F., 1983. Metamorphism and tectonics of the Himalayas. Journal of the Geological Society of London. 140: 849-866.

Windley, B.F., 1988. Tectonic framework of the Himalaya, Karakoram and Tibet, and problems of their evolution. Philosophical Transactions of the Royal Society of London, A326: 3-16.

Yang, C., Telmer, K. and Veizer, J., 1993. Isotopic Signature of Inorganic Carbon in the "St. Lawerence" System. Proceedings CSCE-ASCE National Conference on Environmental Engineering, Montreal, Quebec.

Yang, C., Telmer, K. and Veizer, J., 1996. Chemical dynamics of the "St. Lawerence" River System: δD_{H2O}, $\delta^{18}O_{H2O}$, $\delta^{13}C_{DIC}$, $\delta^{34}S_{sulfate}$ and dissolved $^{87}Sr/^{86}Sr$. Geochimica et Cosmochimica Acta, 60, 851-861.

Zhang, J., Quay, P.D. and Wilbour, D.O., 1995. Carbon isotope fractionation during gas-water exchange and dissolution of CO2. Geochimica et Cosmochimica Acta, 59: 107-114.

Zeitler, P.K., 1985. Cooling history of the NW Himalaya, Pakistan. Tectonics, 4: 127-151.

Zeitler, P.K., Sutter, J.F., Williams, I.F., Zartman, L.S. and Tahirkheli, R.A.K., 1989. Geochronology and temperature history of the Nanga Parbat Haramosh massif, Pakistan. Geological Society of America Special Paper, 232: 1-22.

Appendix A

Discharge data

Table A1. Discharge of the Indus River at Kotri and Sukkur barrages.

Year	Kotri Km^3yr^{-1}	Sukkur	Year	Kotri Km^3yr^{-1}	Sukkur	Sukkur	m^3s^{-1}
1931	103	115	1958	73	161	March-94	901
1932	88	104	1959	155	201	April-94	1083
1933	120	147	1960	93	143	May-94	920
1934	98	121	1961	94	150	June-94	3013
1935	95	130	1962	43	83	July-94	13904
1936	110	140	1963	61	113	August-94	18977
1937	90	117	1964	78	123	September-94	15983
1938	110	141	1965	58	116	October-94	1503
1939	96	128	1966	73	118	November-94	809
1940	70	102	1967	85	135	December-94	972
1941	80	111	1968	60	117	January-95	596
1942	125	135	1969	53	108	February-95	972
1943	110	147	1970	33	73		
1944	100	125	1971	29	79		
1945	108	140	1972	26	79		
1946	78	103	1973	120	179		
1947	75	102	1974	9	54		
1948	115	147	1975	48	109		
1949	106	134	1976	85	151		
1950	145	178	1977	38	85		
1951	65	96	1978	98	165		
1952	90	125	1979	37	86		
1953	118	129	1980	25	85		
1954	95	127	1981	42	101		
1955	101	134	1982	12	70		
1956	145	172	1983	55	130		
1957	113	172	1984	35	97		

179

Appendix B

Chemical and isotope data

Table B1. Chemical analyses for the Indus River and its tributaries. No. refers to sample locations on Fig. 3.1, and CB to ionic charge balance.

River	No.	Season	T °C	pH	TDS	D.O mgL⁻¹	HCO₃⁻	SO₄²⁻	Cl⁻	PO₄³⁻	NO₃⁻	Si	Ca²⁺	Mg²⁺	Na⁺	K⁺	CB %
			°C		I	mgL⁻¹	I				mmolesL⁻¹					I	%
Indus	1	Summer	11.8	8.21	188	9.15	1.234	0.453	0.087	0.001	0.017	0.068	0.727	0.325	0.246	0.030	2.9
Indus	2	Summer	11.8	8.29	150	9.08	1.031	0.375	-	0.001	0.020	0.064	-	-	-	-	-
Indus	4	Summer	11.5	8.23	165	8.59	1.139	0.320	0.079	0.001	0.012	0.064	0.659	0.232	0.211	0.063	4.6
Indus	5	Summer	13.4	8.21	165	10.99	1.239	0.320	0.081	0.001	0.013	0.060	0.655	0.228	0.204	0.061	1.3
Indus	6	Summer	13.9	8.21	158	11.54	1.060	0.313	0.073	0.002	0.016	0.072	0.637	0.210	0.191	0.068	4.7
Indus	7	Summer	14.2	8.06	150	10.50	1.065	0.310	0.055	0.002	0.017	0.058	0.614	0.214	0.148	0.063	2.9
Indus	8	Summer	19.4	8.24	143	11.09	1.037	0.297	0.051	0.001	0.018	0.060	0.585	0.195	0.133	0.059	1.4
Indus	9	Summer	16.4	8.26	135	10.74	0.939	0.254	0.049	0.003	0.017	0.056	0.550	0.171	0.144	0.069	4.1
Indus	10	Summer	20.5	8.42	113	10.01	0.759	0.159	0.038	0.001	0.021	0.054	0.495	0.130	0.096	0.065	10.7
Indus	11	Summer	21.0	8.15	120	10.20	1.029	0.171	0.043	0.001	0.015	-	0.278	0.082	0.052	0.029	-28.2
Indus	12	Summer	22.8	8.35	83	9.69	1.219	0.158	0.048	0.001	0.020	0.055	0.506	0.144	0.139	0.069	-3.2
Indus	13	Summer	21.0	8.45	113	-	0.795	0.150	0.109	0.006	0.012	0.045	0.423	0.119	0.120	0.065	1.4
Indus	14	Summer	22.1	8.24	128	9.28	1.095	0.145	0.086	0.006	0.017	0.050	0.458	0.138	0.226	0.066	-0.7
Indus	15	Summer	27.3	8.25	150	8.79	1.447	0.077	0.063	0.008	0.000	0.073	0.570	0.175	0.276	0.080	4.5
Indus	16	Summer	25.5	7.98	139	-	1.159	0.255	0.163	0.002	0.014	0.060	0.536	0.171	0.389	0.077	0.8
Indus	17	Summer	29.4	8.26	158	6.83	1.359	0.189	0.148	0.001	0.002	0.067	0.581	0.189	0.312	0.085	1.2
Indus	18	Summer	29.1	8.13	158	7.04	1.239	0.205	0.128	0.001	0.019	0.075	0.571	0.187	0.300	0.088	2.8
Indus	19	Summer	30.9	8.17	165	7.19	1.298	0.211	0.147	0.006	0.020	0.069	0.599	0.199	0.322	0.090	2.6
Indus	20	Summer	31.4	8.09	169	6.87	1.529	0.182	0.167	0.001	0.046	-	0.637	0.210	0.422	0.085	2.2
Indus	21	Summer	30.6	7.80	180	4.77	1.724	0.190	0.148	0.018	0.017	0.082	0.694	0.216	0.391	0.090	-0.5
Indus	22	Summer	32.3	8.08	188	6.65	1.449	0.217	0.161	0.003	0.018	0.077	0.682	0.237	0.409	0.101	6.3
Indus	23	Summer	32.6	8.08	188	5.92	1.662	0.220	0.161	0.003	0.018	0.122	0.694	0.247	0.407	0.094	2.1
Indus	24	Summer	30.9	7.88	256	-	1.834	0.225	0.192	0.031	0.017	0.091	0.730	0.271	0.444	0.100	-0.8
Indus	25	Summer	30.0	8.14	210	6.17	1.747	0.312	0.458	0.016	0.014	0.100	0.787	0.313	0.692	0.106	1.8
Tributary	26	Summer	9.9	8.06	113	9.66	0.835	0.191	0.024	-	0.015	0.059	0.506	0.146	0.050	0.027	4.8
Tributary	27	Summer	11.5	8.23	180	9.48	1.195	0.354	0.141	-	0.018	0.076	0.674	0.235	0.335	0.081	4.0
Tributary	28	Summer	10.1	8.24	158	9.80	1.078	0.360	0.022	-	0.008	0.096	0.720	0.210	0.098	0.093	5.7

Table B1. Chemical analyses for the Indus River and its tributaries.

River	No.	Season	T °C	pH	TDS	D.O mgL⁻¹	HCO₃⁻	SO₄²⁻	Cl⁻	PO₄³⁻	NO₃⁻	Si	Ca²⁺	Mg²⁺	Na⁺	K⁺	CB %

Table header units: T in °C; D.O in mgL^{-1}; ions (HCO_3^-, SO_4^{2-}, Cl^-, PO_4^{3-}, NO_3^-, Si, Ca^{2+}, Mg^{2+}, Na^+, K^+) in $mmolesL^{-1}$; CB in %.

River	No.	Season	T °C	pH	TDS	D.O	HCO₃⁻	SO₄²⁻	Cl⁻	PO₄³⁻	NO₃⁻	Si	Ca²⁺	Mg²⁺	Na⁺	K⁺	CB %
Tributary	29	Summer	9.6	7.97	180	10.90	0.521	0.770	0.032	-	0.012	0.052	0.798	0.130	0.194	0.076	0.5
Tributary	30	Summer	11.7	7.86	60	10.70	0.279	0.125	0.020	-	0.012	0.044	0.236	0.037	0.076	0.048	8.9
Tributary	31	Summer	12.4	7.98	135	10.80	1.039	0.287	0.027	-	0.019	0.043	0.524	0.290	0.070	0.079	3.4
Tributary	32	Summer	12.2	8.10	135	9.84	0.831	0.288	0.024	-	0.019	0.073	0.511	0.239	0.067	0.079	6.3
Tributary	33	Summer	9.6	8.09	188	11.00	1.237	0.472	0.027	0.002	0.017	0.047	0.727	0.346	0.109	0.073	2.2
Tributary	34	Summer	13.9	7.91	158	8.67	1.249	0.236	0.053	-	0.021	0.070	0.656	0.234	0.124	0.063	4.6
Tributary	35	Summer	7.97	7.97	90	10.80	0.580	0.197	0.029	0.002	0.023	0.043	0.412	0.082	0.083	0.054	4.3
Tributary	36	Summer	13.5	7.98	135	9.65	0.685	0.396	0.028	0.001	0.016	0.055	0.583	0.109	0.109	0.068	1.1
Tributary	37	Summer	15.1	7.56	53	10.10	0.395	0.051	0.030	0.002	0.018	0.063	0.228	0.033	0.050	0.025	4.1
Tributary	38	Summer	14.5	7.70	30	11.77	0.151	0.020	0.022	0.001	0.026	0.046	0.109	0.023	0.026	0.009	10.3
Tributary	39	Summer	12.9	7.91	45	10.45	0.344	0.041	0.021	0.002	0.025	0.059	0.175	0.060	0.030	0.011	3.0
Tributary	40	Summer	18	8.36	150	9.00	1.395	0.157	0.041	0.001	0.050	0.088	0.672	0.214	0.096	0.048	3.0
Tributary	41	Summer	21.8	8.38	128	8.62	1.078	0.140	0.036	0.002	0.053	0.119	0.586	0.154	0.076	0.033	4.6
Tributary	44	Summer	26.2	8.20	158	7.75	1.339	0.197	0.070	0.001	0.034	0.095	0.595	0.239	0.261	0.067	4.0
Tributary	45	Summer	33.4	8.22	323	6.90	3.145	0.209	0.315	0.002	0.086	0.152	0.982	0.372	0.948	0.074	-3.1
Tributary	46	Summer	32.8	8.21	938	6.35	2.270	1.905	4.730	0.002	0.090	0.114	0.765	0.751	8.178	0.109	1.8
Tributary	47	Summer	28.3	8.17	750	7.60	1.249	3.191	1.653	0.023	0.031	0.074	1.275	0.629	5.437	0.124	-0.1
Tributary	48	Summer	36.4	7.99	1035	6.50	0.375	6.247	0.730	0.001	0.066	0.095	2.823	1.100	5.698	0.149	0.1
Tributary	49	Summer	30.6	8.07	180	6.42	1.301	0.169	0.187	0.003	0.035	0.084	0.672	0.204	0.537	0.089	12.0
Tributary	49	Summer	28	7.88	233	6.06	1.660	0.250	0.432	0.008	0.065	0.090	0.757	0.241	0.863	0.103	5.0
Tributary	50	Summer	26.5	8.27	135	7.51	1.355	0.094	0.037	0.007	0.046	0.057	0.637	0.140	0.120	0.051	2.4
Tributary	51	Summer	28	7.40	143	7.60	1.239	0.094	0.059	0.009	0.046	0.075	0.680	0.162	0.181	0.047	10.1
Tributary	52	Summer	29.4	8.14	150	6.82	1.239	0.104	0.145	0.001	0.071	0.068	0.709	0.172	0.296	0.051	11.7
Tributary	53	Summer	31.5	7.58	218	6.47	1.391	0.229	0.998	0.000	0.025	0.063	0.763	0.239	1.035	0.060	3.8
Tributary	54	Summer	24.5	8.27	143	6.90	1.369	0.146	0.042	0.003	0.039	0.065	0.669	0.169	0.254	0.073	6.7
Tributary	55	Summer	28.5	8.12	120	8.07	0.797	0.146	0.019	0.011	0.057	0.062	0.594	0.143	0.098	0.073	15.7
Tributary	56	Summer	29.3	7.64	158	7.03	1.125	0.177	0.065	0.001	0.024	0.067	0.635	0.160	0.283	0.086	11.0

Table B1. Chemical analyses for the Indus River and its tributaries. No. for the springs refer to the closest location of river sample on Fig. 3.1.

River	No.	Season	T °C	pH	TDS	D.O mgL⁻¹	HCO_3^-	SO_4^{2-}	Cl^-	PO_4^{3-}	NO_3^-	Si	Ca^{2+}	Mg^{2+}	Na^+	K^+	CB %
										mmolesL⁻¹							
Tributary	57	Summer	30.2	8.33	173	6.39	1.209	0.198	0.075	0.013	0.057	0.024	0.657	0.172	0.300	0.096	7.3
Tributary	58	Summer	26	8.33	150	7.03	1.521	0.125	0.034	0.002	0.046	0.057	0.696	0.162	0.217	0.074	3.9
Tributary	59	Summer	28.5	8.01	146	5.72	1.463	0.125	0.064	0.001	0.025	0.088	0.714	0.174	0.265	0.082	8.0
Tributary	60	Summer	28	8.08	165	5.47	1.768	0.146	0.107	0.002	0.046	0.062	0.775	0.188	0.483	0.091	5.9
Tributary	61	Summer	28	8.28	173	6.71	1.549	0.156	0.099	0.004	0.071	0.098	0.735	0.182	0.431	0.089	7.0
Tributary	62	Summer	23.2	8.13	210	5.75	1.710	0.177	0.143	0.003	0.025	0.104	0.757	0.195	0.531	0.097	6.1
Tributary	63	Summer	26.2	7.80	195	6.05	1.796	0.198	0.181	0.039	0.025	0.112	0.772	0.211	0.596	0.096	2.8
Tributary	64	Summer	32.1	7.99	218	7.24	1.778	0.239	0.251	0.013	0.136	0.059	0.811	0.233	0.803	0.121	5.8
Tributary	65	Summer	31.2	8.02	210	6.63	1.554	0.229	0.437	0.015	0.032	0.106	0.740	0.221	0.746	0.086	4.3
Tributary	66	Summer	25	8.13	165	5.97	1.463	0.083	0.120	0.004	0.057	0.012	0.686	0.193	0.413	0.094	11.0
Tributary	67	Summer	25	7.56	180	6.01	1.636	0.167	0.241	0.004	0.039	0.138	0.700	0.212	0.629	0.102	6.0
Tributary	68	Summer	26	8.09	308	6.81	1.566	0.219	0.323	0.009	0.032	0.112	0.697	0.237	0.800	0.113	7.6
Tributary	69	Summer	29.4	8.12	225	6.29	1.748	0.260	0.399	0.004	0.136	0.100	0.753	0.247	0.950	0.116	4.3
Spring	G1	Summer	10.8	7.58	-	-	1.139	0.245	0.045	-	0.018	-	-	-	-	-	-
Spring	G4	Summer	12.6	8.20	180	-	1.239	0.268	0.060	-	0.025	-	0.760	0.245	0.191	0.115	10.9
Hot Spring	G36	Summer	54.5	8.73	780	-	3.792	1.757	1.139	-	0.000	0.876	0.061	0.016	9.656	0.118	8.1
Spring	G7	Summer	18.1	7.97	218	-	2.057	0.111	0.083	-	0.205	-	0.928	0.362	0.226	0.072	5.7
Spring	G9	Summer	21.7	8.41	270	-	2.498	0.273	0.106	-	0.061	-	1.084	0.432	0.431	0.117	5.4
Indus	2	Winter	1.3	8.14	162	10.51	1.271	0.479	0.093	0.000	0.019	0.009	0.734	0.304	0.235	0.033	0.1
Indus	3	Winter	1.9	8.57	177	9.52	1.124	0.427	0.231	0.000	0.021	-	0.798	0.329	0.352	0.056	8.9
Indus	4	Winter	3.5	8.18	193	10.13	1.617	0.479	0.126	0.000	0.021	0.018	0.843	0.350	0.331	0.074	1.2
Indus	6	Winter	5.6	8.22	155	10.58	1.614	0.510	0.101	0.000	0.016	0.042	0.876	0.341	0.335	0.079	1.7
Indus	7	Winter	8	7.91	225	10.70	1.509	0.614	0.093	0.000	0.023	0.043	0.886	0.387	0.309	0.082	1.4
Indus	8	Winter	6.7	8.24	192	10.96	1.481	0.510	0.088	0.000	0.024	0.048	0.823	0.346	0.291	0.079	1.8
Indus	9	Winter	7.5	7.95	184	11.28	1.360	0.489	0.086	0.000	0.028	0.036	0.756	0.317	0.261	0.072	0.5
Indus	10	Winter	11.6	8.24	169	10.20	1.398	0.416	0.068	0.004	0.024	0.019	0.751	0.271	0.211	0.076	-0.1
Indus	11	Winter	11.4	8.14	190	9.98	1.584	0.396	0.104	0.005	0.028	0.020	0.783	0.327	0.313	0.081	1.8

Table B1. Chemical analyses for the Indus River and its tributaries.

River	No.	Season	T °C	pH	TDS	D.O	HCO$_3^-$	SO$_4^{2-}$	Cl$^-$	PO$_4^{3-}$	NO$_3^-$	Si	Ca^{2+}	Mg^{2+}	Na$^+$	K$^+$	CB
						mgL^{-1}					mmolesL^{-1}						%
Indus	13	Winter	12.3	7.91	212	10.19	1.648	0.416	0.193	0.002	0.025	0.044	0.813	0.356	0.461	0.080	3.1
Indus	14	Winter	13	8.17	220	10.03	1.741	0.416	0.130	0.000	0.017	0.053	0.828	0.380	0.448	0.084	4.0
Indus	15	Winter	12.2	8.09	235	10.29	1.695	0.448	0.274	0.001	0.023	0.086	0.847	0.413	0.700	0.086	6.7
Indus	16	Winter	12.4	8.48	233	10.07	1.742	0.468	0.175	0.000	0.030	0.099	0.838	0.399	0.631	0.085	5.0
Indus	17	Winter	14.9	8.47	242	9.98	1.894	0.468	0.396	0.000	0.034	0.089	0.821	0.389	0.672	0.089	-1.3
Indus	18	Winter	16.9	8.28	242	9.86	1.733	0.468	0.439	0.000	0.042	0.103	0.822	0.391	0.735	0.091	1.6
Indus	19	Winter	17.9	8.31	257	10.47	1.697	0.500	0.581	0.001	0.035	0.101	0.835	0.397	0.850	0.093	1.4
Indus	20	Winter	19.1	8.42	254	-	1.753	0.510	0.595	0.000	0.039	0.098	0.836	0.397	0.857	0.094	0.1
Indus	21	Winter	18.2	8.57	284	9.15	1.818	0.479	0.681	0.001	0.037	0.096	0.861	0.399	0.974	0.096	1.3
Indus	22	Winter	19.6	8.4	303	8.45	2.173	0.531	0.612	0.000	0.000	0.098	0.939	0.432	0.940	0.101	-0.8
Indus	23	Winter	23.9	8.44	330	7.39	2.528	0.500	0.606	0.000	0.021	0.124	1.068	0.506	1.083	0.107	2.1
Indus	24	Winter	21.5	8.48	343	6.69	2.394	0.583	0.749	0.000	0.000	0.106	1.013	0.518	1.288	0.109	1.7
Tributary	27	Winter	2.9	8.48	224	10.25	1.317	0.583	0.043	0.000	0.047	0.044	0.893	0.358	0.535	0.092	9.7
Tributary	28	Winter	1.8	8.24	270	9.28	2.107	0.822	0.143	-	0.023	0.020	1.248	0.568	0.291	0.164	2.1
Tributary	33	Winter	5.8	8.31	272	10.60	1.617	1.072	0.050	-	0.014	0.049	1.128	0.691	0.304	0.110	2.9
Tributary	34	Winter	6.4	8.34	157	10.59	1.406	0.385	0.048	-	0.020	0.044	0.729	0.341	0.139	0.056	2.0
Tributary	43	Winter	14.9	8.31	300	10.71	2.436	0.562	0.359	0.003	0.050	0.004	1.020	0.761	0.698	0.096	4.6
Tributary	42	Winter	13	8.21	203	9.60	2.027	0.177	0.113	0.000	0.108	0.010	0.937	0.372	0.311	0.035	6.5
Tributary	44	Winter	15.6	8.15	292	9.00	2.783	0.479	0.369	0.000	0.061	0.044	1.008	0.720	0.848	0.092	2.6
Tributary	45	Winter	15.6	8.67	512	9.16	4.202	0.448	1.011	0.017	0.204	0.036	1.169	0.665	3.422	0.189	6.7
Tributary	46	Winter	12.6	8.58	1223	-	4.467	2.873	6.070	-	0.107	0.121	1.340	2.591	9.091	0.111	2.0
Tributary	49	Winter	17.3	8.6	449	10.75	1.978	0.645	1.717	0.000	0.000	0.022	0.847	0.516	2.440	0.103	2.7
Tributary	50	Winter	17.3	7.97	203	8.95	1.876	0.219	0.079	0.001	0.082	0.086	0.908	0.261	0.213	0.051	2.5
Tributary	52	Winter	22.4	8.23	188	8.76	1.896	0.198	0.125	0.001	0.061	0.101	0.841	0.237	0.259	0.049	-0.4
Tributary	54	Winter	22.4	8.26	158	8.60	1.151	0.271	0.041	0.001	0.086	0.098	0.666	0.208	0.152	0.059	3.7
Tributary	57	Winter	31.2	8.43	540	8.71	2.581	0.531	2.421	0.001	0.103	0.097	0.830	0.514	3.915	0.162	4.6
Tributary	58	Winter	20.7	8.3	184	8.56	1.555	0.364	0.075	0.002	0.018	0.131	0.770	0.237	0.237	0.059	-1.5

183

Table B1. Chemical analyses for the Indus River and its tributaries.

River	No.	Season/month	T °C	pH	TDS	D.O	HCO$_3^-$	SO$_4^{2-}$	Cl$^-$	PO$_4^{3-}$	NO$_3^-$	Si	Ca^{2+}	Mg^{2+}	Na$^+$	K$^+$	CB %
					mgL^{-1}					mmolesL^{-1}							
Tributary	60	Winter	23.7	7.44	225	4.83	1.710	0.354	0.242	0.004	0.037	0.131	0.786	0.269	0.576	0.103	1.5
Tributary	61	Winter	20.6	7.48	218	7.68	1.954	0.281	0.155	0.002	0.047	0.109	0.888	0.269	0.361	0.073	0.5
Tributary	63	Winter	23.2	8.33	1433	5.14	6.729	2.457	6.515	0.152	0.494	0.144	1.030	1.111	13.767	0.356	-1.9
Tributary	65	Winter	24.4	8.53	461	8.74	1.740	0.718	1.949	0.001	0.000	0.077	0.798	0.524	3.001	0.119	5.9
Tributary	66	Winter	25.6	8.48	195	8.91	1.797	0.115	0.313	0.001	0.000	0.053	0.619	0.280	0.581	0.081	2.4
Tributary	67	Winter	23.5	7.81	229	7.42	1.824	0.323	0.215	0.000	0.070	0.119	0.871	0.276	0.570	0.082	3.3
Tributary	68	Winter	31	8.14	236	7.92	1.974	0.354	0.269	0.001	0.033	0.084	0.780	0.323	0.720	0.093	0.5
Indus	22	Mar-94	19.6	8.40	303	8.45	2.173	0.531	0.612	0.000	0.000	0.098	0.939	0.432	0.940	0.101	-0.8
Indus	22	Apr-94	29.1	7.80	263	9.02	1.949	0.370	0.253	0.002	0.055	0.111	0.860	0.398	0.760	0.111	6.0
Indus	22	May-94	29.5	8.38	216	8.24	1.498	0.378	0.250	0.001	0.056	0.114	0.775	0.346	0.559	0.100	6.2
Indus	22	Jun-94	31.1	7.66	164	8.07	1.118	0.214	0.106	0.007	0.032	0.068	0.564	0.218	0.359	0.082	8.1
Indus	22	Jul-94	20	7.56	142	8.6	1.180	0.293	0.130	0.002	0.030	0.138	0.651	0.228	0.328	0.084	5.8
Indus	22	Aug-94	32.3	8.08	188	6.65	1.449	0.217	0.161	0.003	0.018	0.077	0.682	0.237	0.409	0.101	6.3
Indus	22	Sep-94	31.6	8.02	180	6.84	1.498	0.217	0.158	0.001	0.026	0.080	0.674	0.239	0.418	0.097	4.9
Indus	22	Oct-94	28.7	8.16	203	8.06	1.531	0.300	0.231	0.001	0.019	0.081	0.719	0.257	0.502	0.088	3.2
Indus	22	Nov-94	22.5	8.22	248	7.99	1.213	0.375	0.432	0.002	0.025	0.103	0.828	0.325	0.748	0.089	12.9
Indus	22	Dec-94	16.2	7.78	233	9.78	1.850	0.375	0.333	0.004	0.039	0.074	0.899	0.358	0.624	0.117	4.4
Indus	22	Jan-95	16.3	8.40	240	10.58	1.578	0.302	0.432	0.000	0.038	0.046	1.160	0.047	0.083	0.013	-2.8
Indus	22	Feb-95	17	8.49	311	-	1.799	0.396	0.707	0.002	0.093	0.087	1.068	0.429	1.316	0.104	13.0

* - not measured

184

Table B2. Saturation indices, pCO_2, and oxygen saturation for the Indus River Basin.

River	No.	Season	Calcite	Aragonite	Dolomite	Barite	Anhydrite	Witherite	Magnesite	Gypsum	pCO_2 ppmv	O_2 sat. %
Indus	1	Summer	-0.01	-0.17	-0.04	-0.41	-2.42	-3.68	-0.97	-2.16	419	114
Indus	2	Summer	-	-	-	-	-	-	-	-	291	108
Indus	4	Summer	-0.06	-0.22	-0.24	-0.54	-2.59	-3.69	-1.13	-2.33	368	96
Indus	5	Summer	-0.02	-0.17	-0.18	-0.58	-2.59	-3.66	-1.06	-2.34	431	122
Indus	6	Summer	-0.09	-0.24	-0.35	-0.56	-2.60	-3.70	-1.15	-2.35	372	122
Indus	7	Summer	-0.25	-0.40	-0.65	-0.51	-2.62	-3.78	-1.28	-2.37	530	104
Indus	8	Summer	-0.02	-0.16	-0.28	-0.74	-2.65	-3.71	-1.00	-2.41	370	121
Indus	9	Summer	-0.11	-0.26	-0.45	-0.75	-2.74	-3.74	-1.16	-2.49	305	110
Indus	10	Summer	-0.01	-0.16	-0.39	-1.04	-2.96	-3.68	-1.08	-2.72	182	110
Indus	11	Summer	-0.38	-0.53	-1.10	-1.19	-3.15	-4.00	-1.40	-2.91	463	114
Indus	12	Summer	0.16	0.02	-0.05	-0.81	-2.95	-3.25	-0.85	-2.73	355	111
Indus	13	Summer	-0.02	-0.17	-0.39	-0.23	-3.04	-2.79	-1.06	-2.81	179	-
Indus	14	Summer	-0.05	-0.19	-0.43	-0.27	-3.03	-2.85	-1.03	-2.80	407	105
Indus	15	Summer	0.25	0.11	0.09	-1.15	-3.20	-3.20	-0.67	-2.99	558	109
Indus	16	Summer	-0.18	-0.32	-0.72	-0.45	-2.73	-3.41	-1.10	-2.51	818	
Indus	17	Summer	0.26	0.12	0.09	-0.48	-2.81	-2.88	-0.61	-2.61	519	87
Indus	18	Summer	0.08	-0.06	-0.26	-0.48	-2.78	-3.09	-0.79	-2.58	637	89
Indus	19	Summer	0.18	0.04	-0.08	-0.51	-2.75	-3.03	-0.66	-2.55	613	94
Indus	20	Summer	0.21	0.07	-0.05	-0.45	-2.79	-2.90	-0.64	-2.60	869	91
Indus	21	Summer	-0.01	-0.15	-0.49	-0.48	-2.74	-3.20	-0.88	-2.55	1907	62
Indus	22	Summer	0.21	0.07	-0.03	-0.45	-2.69	-2.99	-0.60	-2.50	842	89
Indus	23	Summer	0.28	0.14	0.11	-0.45	-2.67	-2.93	-0.52	-2.49	966	80
Indus	24	Summer	0.12	-0.02	-0.16	-0.42	-2.66	-3.09	-0.68	-2.47	1689	-
Indus	25	Summer	0.37	0.23	0.38	-0.20	-2.51	-2.79	-0.41	-2.31	882	80
Tributary	26	Summer	-0.49	-0.64	-1.15	-0.66	-2.88	-3.95	-1.66	-2.62	390	116
Tributary	27	Summer	-0.04	-0.19	-0.19	-0.38	-2.54	-3.56	-1.11	-2.29	386	111
Tributary	28	Summer	-0.06	-0.22	-0.30	-0.46	-2.50	-3.71	-1.23	-2.24	334	110
Tributary	29	Summer	-0.63	-0.78	-1.68	-0.34	-2.15	-4.52	-2.06	-1.89	298	112

185

Table B2. Saturation indices, pCO_2, and oxygen saturation for the Indus River Basin.

River	No.	Season	Calcite	Aragonite	Dolomite	Barite	Anhydrite	Witherite	Magnesite	Gypsum	pCO_2 ppmv	O_2 sat. %
Tributary	30	Summer	-1.44	-1.59	-3.35	-1.36	-3.33	-5.14	-2.86	-3.08	212	111
Tributary	31	Summer	-0.43	-0.58	-0.79	-0.47	-2.72	-3.85	-1.29	-2.47	605	113
Tributary	32	Summer	-0.42	-0.57	-0.84	-0.49	-2.72	-3.85	-1.36	-2.47	366	102
Tributary	33	Summer	-0.17	-0.32	-0.29	-0.42	-2.40	-3.88	-1.13	-2.14	537	100
Tributary	34	Summer	-0.30	-0.45	-0.75	-0.71	-2.71	-3.96	-1.33	-2.46	874	86
Tributary	35	Summer	-0.85	-1.01	-2.01	-0.58	-2.93	-4.20	-2.22	-2.67	326	95
Tributary	36	Summer	-0.55	-0.70	-1.51	-0.58	-2.53	-4.26	-1.86	-2.27	405	94
Tributary	37	Summer	-1.54	-1.69	-3.64	-1.57	-3.72	-5.02	-2.95	-3.47	630	101
Tributary	38	Summer	-2.13	-2.28	-4.61	-2.17	-4.42	-5.53	-3.35	-4.17	173	116
Tributary	39	Summer	-	-	-	-	-	-	-	-	237	100
Tributary	40	Summer	0.27	0.13	0.29	-0.93	-2.87	-3.40	-0.75	-2.63	370	95
Tributary	41	Summer	0.19	0.04	-0.02	-1.33	-2.95	-3.76	-0.86	-2.72	289	98
Tributary	44	Summer	0.16	0.02	0.04	-0.94	-2.80	-3.50	-0.66	-2.58	574	96
Tributary	45	Summer	0.83	0.70	1.23	-0.24	-2.60	-2.23	0.08	-2.42	1321	97
Tributary	46	Summer	0.47	0.33	0.91	0.18	-1.92	-2.86	0.11	-1.74	977	88
Tributary	47	Summer	0.30	0.16	0.37	0.49	-1.53	-3.17	-0.41	-1.32	583	96
Tributary	48	Summer	-0.03	-0.16	-0.56	0.58	-1.00	-3.83	-0.76	-0.83	263	95
Tributary	49	Summer	0.13	-0.01	-0.22	-0.42	-2.80	-2.95	-0.76	-2.61	773	84
Tributary	49	Summer	0.05	-0.10	-0.32	-0.22	-2.62	-3.04	-0.85	-2.42	1509	75
Tributary	50	Summer	0.28	0.14	0.01	-1.13	-3.08	-3.29	-0.80	-2.86	495	91
Tributary	51	Summer	-0.58	-0.72	-1.71	-0.87	-3.05	-3.90	-1.61	-2.84	3400	94
Tributary	52	Summer	0.19	0.05	-0.18	-0.91	-2.99	-3.21	-0.81	-2.78	624	87
Tributary	53	Summer	-0.28	-0.42	-1.05	-0.57	-2.64	-3.66	-1.15	-2.45	2557	86
Tributary	54	Summer	0.27	0.13	0.08	-0.84	-2.89	-3.22	-0.77	-2.66	490	80
Tributary	55	Summer	-0.10	-0.24	-0.75	-0.86	-2.90	-3.55	-1.11	-2.69	418	101
Tributary	56	Summer	-0.40	-0.54	-1.34	-0.71	-2.80	-3.79	-1.38	-2.59	1790	89
Tributary	57	Summer	0.35	0.21	0.15	-0.66	-2.74	-3.04	-0.61	-2.54	394	83
Tributary	58	Summer	0.41	0.27	0.30	-0.18	-2.93	-2.36	-0.65	-2.71	482	84

Table B2. Saturation indices, pCO_2, and oxygen saturation for the Indus River Basin.

River	No.	Season	Calcite	Aragonite	Dolomite	Barite	Anhydrite	Witherite	Magnesite	Gypsum	pCO_2 ppmv	O_2 sat. %
Tributary	59	Summer	0.12	-0.02	-0.30	-0.70	-2.91	-3.16	-0.89	-2.71	989	72
Tributary	60	Summer	0.29	0.15	0.06	-0.49	-2.83	-2.86	-0.72	-2.62	1014	68
Tributary	61	Summer	0.42	0.28	0.30	-0.48	-2.81	-2.74	-0.59	-2.61	560	83
Tributary	62	Summer	0.25	0.11	0.08	-0.37	-2.77	-2.90	-0.79	-2.55	831	65
Tributary	63	Summer	-0.01	-0.15	-0.48	-0.34	-2.71	-3.15	-1.00	-2.50	1933	73
Tributary	64	Summer	0.27	0.13	0.01	-0.39	-2.60	-2.96	-0.62	-2.41	1272	97
Tributary	65	Summer	0.20	0.06	-0.11	-0.54	-2.65	-3.15	-0.69	-2.45	1037	87
Tributary	66	Summer	0.18	0.03	-0.07	-0.71	-3.12	-2.94	-0.81	-2.90	727	70
Tributary	67	Summer	-0.35	-0.49	-1.08	-0.42	-2.83	-3.47	-1.30	-2.61	3022	70
Tributary	68	Summer	0.17	0.03	-0.01	-0.24	-2.71	-2.87	-0.72	-2.50	863	81
Tributary	69	Summer	0.32	0.18	0.22	-0.23	-2.61	-2.77	-0.55	-2.41	922	80
Indus	2	Winter	-0.24	-0.40	-0.40	-0.15	-2.36	-3.78	-1.39	-2.11	458	102
Indus	3	Winter	0.18	0.02	0.44	-0.08	-2.38	-3.26	-0.96	-2.13	151	92
Indus	4	Winter	0.00	-0.17	0.05	-0.08	-2.33	-3.49	-1.12	-2.07	537	97
Indus	6	Winter	0.09	-0.07	0.17	-0.11	-2.30	-3.45	-1.03	-2.04	497	95
Indus	7	Winter	-0.22	-0.37	-0.41	-0.09	-2.23	-3.78	-1.24	-1.97	972	94
Indus	8	Winter	0.06	-0.10	0.14	-0.21	-2.32	-3.54	-1.00	-2.06	440	93
Indus	9	Winter	-0.29	-0.44	-0.56	-0.20	-2.37	-3.83	-1.34	-2.11	795	97
Indus	10	Winter	0.09	-0.07	0.06	0.36	-2.44	-2.79	-0.97	-2.18	442	94
Indus	11	Winter	0.05	-0.10	0.06	-0.02	-2.45	-3.20	-0.94	-2.20	628	92
Indus	13	Winter	-0.14	-0.29	-0.30	0.16	-2.42	-3.22	-1.10	-2.17	1125	95
Indus	14	Winter	0.17	0.01	0.31	0.17	-2.42	-2.91	-0.76	-2.16	660	95
Indus	15	Winter	0.07	-0.09	0.15	0.22	-2.38	-3.00	-0.85	-2.13	764	95
Indus	16	Winter	0.47	0.31	0.94	0.19	-2.37	-2.65	-0.46	-2.12	321	93
Indus	17	Winter	0.52	0.37	1.01	0.08	-2.38	-2.67	-0.37	-2.13	371	96
Indus	18	Winter	0.33	0.18	0.59	0.05	-2.38	-2.87	-0.54	-2.13	542	99
Indus	19	Winter	0.36	0.22	0.65	0.08	-2.35	-2.83	-0.49	-2.10	504	107
Indus	20	Winter	0.51	0.36	0.92	0.15	-2.34	-2.61	-0.33	-2.10	412	-

187

Table B2. Saturation indices, pCO_2, and oxygen saturation for the Indus River Basin.

River	No.	Season	Calcite	Aragonite	Dolomite	Barite	Anhydrite	Witherite	Magnesite	Gypsum	pCO_2 ppmv	O_2 sat. %
Indus	21	Winter	0.67	0.52	1.25	0.10	-2.36	-2.48	-0.19	-2.11	298	94
Indus	22	Winter	0.63	0.48	1.14	0.19	-2.28	-2.49	-0.21	-2.04	538	89
Indus	23	Winter	0.85	0.70	1.52	0.19	-2.26	-2.25	0.07	-2.03	607	85
Indus	24	Winter	0.80	0.66	1.51	0.21	-2.23	-2.33	0.03	-1.99	508	73
Tributary	27	Winter	0.22	0.05	0.48	0.14	-2.23	-3.16	-0.93	-1.97	219	102
Tributary	28	Winter	0.28	0.12	0.68	0.20	-1.98	-3.28	-0.83	-1.73	604	89
Tributary	33	Winter	0.25	0.09	0.70	0.10	-1.94	-3.43	-0.66	-1.68	405	95
Tributary	34	Winter	0.09	-0.07	0.26	-0.40	-2.48	-3.55	-0.93	-2.22	331	96
Tributary	43	Winter	0.55	0.40	1.25	0.10	-2.26	-2.75	-0.15	-2.01	689	106
Tributary	42	Winter	0.33	0.18	0.58	-0.43	-2.73	-3.03	-0.66	-2.48	701	91
Tributary	44	Winter	0.45	0.30	1.04	-0.17	-2.33	-3.02	-0.25	-2.08	1151	90
Tributary	45	Winter	1.19	1.04	2.42	0.46	-2.34	-1.65	0.39	-2.09	525	91
Tributary	46	Winter	1.03	0.88	2.66	0.80	-1.69	-2.15	0.71	-1.44	655	-
Tributary	49	Winter	0.70	0.55	1.43	0.35	-2.27	-2.30	-0.06	-2.03	298	108
Tributary	50	Winter	0.12	-0.03	-0.05	0.01	-2.64	-2.86	-0.96	-2.39	1207	90
Tributary	52	Winter	0.43	0.28	0.48	-0.35	-2.69	-2.79	-0.59	-2.46	724	98
Tributary	54	Winter	0.14	0.00	-0.04	-0.11	-2.64	-2.89	-0.83	-2.41	410	96
Tributary	57	Winter	0.82	0.68	1.46	-0.17	-2.34	-2.46	0.25	-2.15	670	115
Tributary	58	Winter	0.34	0.20	0.38	0.01	-2.47	-2.76	-0.66	-2.24	493	92
Tributary	60	Winter	-0.43	-0.57	-1.17	0.13	-2.48	-3.37	-1.34	-2.25	4099	55
Tributary	61	Winter	-0.32	-0.47	-0.96	0.12	-2.54	-3.25	-1.33	-2.30	4091	83
Tributary	63	Winter	1.01	0.86	2.20	0.83	-1.82	-1.89	0.58	-1.59	2064	58
Tributary	65	Winter	0.64	0.50	1.24	0.29	-2.24	-2.37	0.02	-2.02	342	101
Tributary	66	Winter	0.57	0.43	0.92	-0.40	-3.04	-2.32	-0.20	-2.82	402	106
Tributary	67	Winter	0.01	-0.14	-0.33	0.02	-2.48	-3.04	-0.95	-2.26	1860	84
Tributary	68	Winter	0.43	0.29	0.50	-0.01	-2.46	-2.57	-0.32	-2.26	999	104

Table B2. Saturation indices, pCO_2, and oxygen saturation for the Indus River Basin.

River	No.	Month	Calcite	Aragonite	Dolomite	Barite	Anhydrite	Witherite	Magnesite	Gypsum	pCO_2 ppmv	O_2 sat. %
Indus	22	Mar-94	0.63	0.48	1.14	0.19	-2.28	-2.49	-0.21	-2.04	538	89
Indus	22	Apr-94	0.09	-0.05	-0.09	0.94	-2.42	-2.02	-0.63	-2.22	2143	114
Indus	22	May-94	0.53	0.39	0.76	-0.09	-2.44	-2.60	-0.21	-2.24	434	105
Indus	22	Jun-94	-0.41	-0.55	-1.21	-0.17	-2.76	-3.27	-1.19	-2.57	1709	106
Indus	22	Jul-94	-0.59	-0.74	-1.42	0.11	-2.62	-3.45	-1.54	-2.38	2036	91
Indus	22	Aug-94	0.21	0.07	-0.03	-0.45	-2.69	-2.99	-0.60	-2.50	842	90
Indus	22	Sep-94	0.15	0.01	-0.13	-0.46	-2.70	-3.06	-0.66	-2.50	1000	91
Indus	22	Oct-94	0.28	0.14	0.19	-0.37	-2.55	-3.02	-0.55	-2.35	733	101
Indus	22	Nov-94	0.20	0.06	0.17	0.58	-2.44	-2.34	-0.67	-2.21	475	89
Indus	22	Dec-94	-0.12	-0.27	-0.36	0.47	-2.43	-2.84	-1.07	-2.19	1811	96
Indus	22	Jan-95	0.56	0.41	0.01	0.00	-2.40	-2.67	-1.36	-2.15	371	105
Indus	22	Feb-95	0.67	0.52	1.19	0.04	-2.36	-2.54	-0.25	-2.12	348	-

Table B3. Trace element chemistry for the Indus River Basin. No. refers to sample locations on Fig. 3.1.

River	No.	Season	Li	F	Al	Fe	Ti	Cr	Mn	Ni	As	Rb	Sr	Sb	Ba	Pb	U
				µmolesL⁻¹							nmolesL⁻¹						
Indus	1	Summer	5.976	10.7	0.59	0.13	31	25	17	12	115	27.6	4538	1.8	96	<0.5	8.68
Indus	2	Summer	-	13.7	-	-	-	-	-	-	-	-	-	-	-	-	-
Indus	4	Summer	3.550	10.1	1.33	0.16	32	22	64	12	42	47.4	2395	1.1	94	<0.5	14.82
Indus	5	Summer	2.836	11.3	1.33	<0.09	29	21	48	13	40	47.6	2409	1.2	93	<0.5	13.67
Indus	6	Summer	3.225	10.6	7.52	2.88	260	19	92	16	35	56.2	2188	1.0	104	1.0	13.82
Indus	7	Summer	1.886	9.7	7.93	3.83	374	17	158	15	35	58.5	1780	1.5	113	1.0	12.93
Indus	8	Summer	1.825	19.2	1.74	0.09	26	13	57	8	31	55.6	1763	1.3	87	<0.5	12.21
Indus	9	Summer	1.573	8.8	2.11	0.29	38	14	69	10	23	53.6	1544	1.3	88	0.8	10.34
Indus	10	Summer	0.919	8.4	3.11	0.18	25	12	17	3	21	64.8	1120	1.3	82	<0.5	7.48
Indus	11	Summer	0.583	8.4	2.11	0.16	18	8	8	6	17	28.7	814	0.8	49	<0.5	4.14
Indus	12	Summer	0.970	8.2	1.89	0.09	24	12	5	6	20	48.0	1383	1.4	155	<0.5	6.98
Indus	13	Summer	0.766	20.3	2.33	0.35	32	12	13	7	21	43.7	1311	1.4	543	0.9	6.72
Indus	14	Summer	0.827	7.8	1.59	0.24	29	15	8	9	23	33.0	1812	1.4	558	0.6	6.75
Indus	15	Summer	0.780	7.1	1.56	0.41	31	11	31	7	29	39.2	1666	1.5	173	1.0	7.86
Indus	16	Summer	0.839	7.5	1.78	0.26	32	10	17	9	19	34.4	1921	1.6	253	0.7	7.64
Indus	17	Summer	0.932	8.0	1.78	0.36	34	11	22	11	21	26.9	1997	2.2	363	1.5	9.74
Indus	18	Summer	0.923	8.9	1.56	0.35	34	12	11	6	15	26.7	2223	2.3	333	0.8	9.57
Indus	19	Summer	0.972	8.7	1.70	0.13	26	12	7	4	16	26.1	2328	2.6	331	0.5	10.17
Indus	20	Summer	0.743	9.5	0.78	0.16	35	14	9	3	20	12.0	2281	2.9	452	<0.5	10.91
Indus	21	Summer	0.744	9.5	1.45	0.58	36	12	22	7	16	14.2	2393	2.7	398	0.5	10.36
Indus	22	Summer	0.908	9.5	1.07	0.41	38	12	18	5	32	15.2	2755	2.8	390	0.6	11.79
Indus	23	Summer	1.030	10.0	1.22	0.45	45	13	15	7	13	13.0	2863	3.0	392	1.0	12.49
Indus	24	Summer	0.976	10.0	0.67	0.17	34	17	7	7	9	10.2	3179	3.1	398	<0.5	12.36
Indus	25	Summer	1.205	10.0	0.74	0.25	41	15	13	5	16	12.3	3665	3.1	482	0.6	12.52
Tributary	26	Summer	0.241	6.5	1.37	0.32	41	25	30	15	11	17.4	2135	0.5	104	1.5	2.37
Tributary	27	Summer	5.060	11.6	7.97	4.25	242	24	148	40	42	62.3	1980	1.0	121	1.6	22.53

Table B3. Trace element chemistry for the Indus River Basin.

River	No.	Season	Li	F	Al	Fe	Ti	Cr	Mn	Ni	As	Rb	Sr	Sb	Ba	Pb	U
				μ molesL^{-1}								nmolesL^{-1}					
Tributary	28	Summer	1.239	19.8	2.22	0.44	53	21	272	30	14	60.7	1498	0.9	98	1.0	16.24
Tributary	29	Summer	1.844	22.6	0.74	0.09	35	17	282	91	1	52.0	962	0.3	55	<0.5	6.91
Tributary	30	Summer	0.450	45.0	8.19	4.54	492	29	59	22	8	37.9	209	0.1	26	0.6	36.40
Tributary	31	Summer	0.537	27.3	11.64	8.46	384	88	177	165	166	38.2	591	0.2	123	0.7	7.78
Tributary	32	Summer	0.485	22.6	2.59	1.32	98	31	43	35	172	33.6	603	0.2	115	1.1	7.29
Tributary	33	Summer	1.324	19.7	5.23	2.80	204	17	223	17	80	54.0	1968	3.0	80	1.0	19.72
Tributary	34	Summer	0.743	5.9	1.78	0.81	87	14	41	6	40	42.1	1339	1.0	93	<0.5	9.08
Tributary	35	Summer	0.075	2.6	0.93	0.21	33	14	35	9	1	23.8	460	0.1	101	2.7	2.03
Tributary	36	Summer	0.856	29.6	9.78	3.81	397	18	87	14	358	48.0	2130	1.5	74	0.6	21.74
Tributary	37	Summer	0.142	2.6	1.11	0.21	26	13	20	10	27	14.9	337	0.5	53	7.9	0.63
Tributary	38	Summer	0.010	2.6	0.67	0.23	21	14	10	7	8	6.0	109	0.1	30	<0.5	0.04
Tributary	39	Summer	0.045	2.6	1.04	0.32	24	16	15	13	28	4.7	170	0.4	97	1.2	0.81
Tributary	40	Summer	0.232	7.4	0.70	0.09	36	20	55	11	9	20.8	1116	0.4	101	<0.5	1.65
Tributary	41	Summer	0.227	7.4	1.00	0.16	39	17	19	7	6	24.3	922	0.5	54	<0.5	2.82
Tributary	44	Summer	0.752	8.7	1.78	0.09	31	13	14	6	18	44.7	1542	1.9	111	<0.5	10.22
Tributary	45	Summer	0.453	11.1	0.82	0.65	53	12	12	16	21	6.5	5291	1.5	785	2.0	10.47
Tributary	46	Summer	1.815	2.6	1.30	0.40	47	15	18	24	11	14.7	10073	1.3	315	1.1	6.52
Tributary	47	Summer	1.731	2.6	0.70	0.09	33	12	13	3	9	27.4	10283	1.2	327	1.0	5.92
Tributary	48	Summer	3.637	2.6	0.96	0.09	67	13	100	2	1	35.6	44528	0.6	357	<0.5	4.23
Tributary	49	Summer	0.601	10.0	1.96	0.83	49	44	42	24	23	10.9	1972	2.8	505	2.0	11.22
Tributary	49	Summer	0.670	4.5	1.47	0.69	33	<2	27	4	32	10.1	2480	3.3	532	3.2	14.37
Tributary	50	Summer	0.199	2.3	1.65	0.35	16	2	47	10	16	29.1	2062	1.1	144	0.6	3.10
Tributary	51	Summer	0.202	1.7	1.03	0.36	17	2	25	<3	13	13.0	2045	1.0	281	0.6	2.85
Tributary	52	Summer	0.227	1.8	1.44	0.66	31	2	39	6	13	10.3	2190	1.0	249	1.3	3.04
Tributary	53	Summer	0.323	2.1	0.54	0.15	13	<2	8	<3	15	9.8	2939	1.1	295	<0.5	4.08
Tributary	54	Summer	0.363	3.7	1.51	0.28	17	2	116	9	21	45.3	1405	1.2	173	<0.5	5.42

Table B3. Trace element chemistry for the Indus River Basin. No. for the springs refer to the closest river sample on Fig. 3.1.

River	No.	Season	Li	F	Al	Fe	Ti	Cr	Mn	Ni	As	Rb	Sr	Sb	Ba	Pb	U
				$\mu\,molesL^{-1}$							$nmolesL^{-1}$						
Tributary	55	Summer	0.393	2.5	2.30	0.66	40	<2	69	<3	20	41.6	1091	1.3	182	1.2	5.66
Tributary	56	Summer	0.443	4.2	2.02	0.55	31	<2	22	4	23	30.1	1312	1.5	228	1.0	7.74
Tributary	57	Summer	0.507	4.5	1.20	0.29	20	<2	13	<3	25	20.3	1433	1.9	238	<0.5	9.21
Tributary	58	Summer	0.263	3.9	0.93	0.41	13	2	32	7	36	18.6	1327	4.0	983	<0.5	5.96
Tributary	59	Summer	0.290	3.0	0.81	0.29	18	<2	132	6	48	25.1	1339	2.5	328	<0.5	6.41
Tributary	60	Summer	0.330	3.8	1.07	0.39	21	<2	75	45	50	22.2	1454	2.9	468	0.7	7.91
Tributary	61	Summer	0.346	4.4	0.86	0.29	15	<2	26	17	61	24.9	1396	3.3	442	<0.5	8.84
Tributary	62	Summer	0.399	3.9	1.00	0.45	20	<2	41	8	44	20.1	1655	4.0	431	<0.5	10.48
Tributary	63	Summer	0.430	5.4	2.04	1.11	44	<2	40	4	40	15.2	1952	4.3	468	0.6	12.48
Tributary	64	Summer	0.503	5.9	1.00	0.45	23	<2	29	9	41	13.5	1973	4.6	435	0.5	14.05
Tributary	65	Summer	0.481	3.3	0.70	0.21	18	<2	8	<3	30	9.8	2402	2.5	301	<0.5	9.50
Tributary	66	Summer	0.524	3.2	1.44	0.58	29	2	27	4	40	15.5	1453	2.6	430	0.5	8.43
Tributary	67	Summer	0.560	4.4	1.46	0.64	33	<2	182	8	56	18.1	1746	2.4	428	0.5	10.60
Tributary	68	Summer	0.695	5.8	0.96	0.37	19	<2	29	<3	38	12.2	2296	3.3	521	0.6	15.83
Tributary	69	Summer	0.762	5.2	2.00	1.08	79	9	27	6	33	10.7	2450	3.5	534	1.0	16.97
Spring	G1	Summer	0.000	5.4	-	-	-	-	-	-	-	-	-	-	-	-	-
Spring	G4	Summer	0.396	5.2	0.93	0.36	49	56	15	19	28	5.3	1366	0.7	127	0.8	15.16
Hot Spring	G36	Summer	109.350	1262.2	7.08	2.44	277	12	55	45	7	897.7	552	24.2	10	<0.5	0.10
Spring	G7	Summer	0.461	5.5	1.33	0.34	73	17	22	9	30	16.6	1523	0.2	104	16.3	12.13
Spring	G9	Summer	3.284	16.9	0.74	<0.09	71	17	17	<3	2	8.8	2375	0.1	154	<0.5	126.20
Indus	2	Winter	3.958	11.2	0.33	-	-	8	15	-	52	29.6	4356	1.4	95	-	8.83
Indus	3	Winter	4.737	18.1	0.37	-	-	6	13	-	44	37.6	3797	1.5	128	-	17.94
Indus	4	Winter	4.339	14.9	0.33	-	-	6	40	-	39	43.8	3578	1.3	130	-	20.45
Indus	6	Winter	4.400	16.2	0.37	-	-	6	33	-	39	48.9	3426	1.4	130	-	21.62
Indus	7	Winter	3.410	16.7	0.48	-	-	6	18	-	36	43.1	3136	2.0	133	-	23.38
Indus	8	Winter	3.255	15.8	0.44	-	-	6	16	-	39	41.9	2865	1.8	110	-	20.48

Table B3. Trace element chemistry for the Indus River Basin.

River	No.	Season	Li	F	Al	Fe	Ti	Cr	Mn	Ni	As	Rb	Sr	Sb	Ba	Pb	U
				μ molesL^{-1}							nmolesL^{-1}						
Indus	9	Winter	2.900	15.1	0.41	-	-	6	22	-	31	42.7	2521	1.6	117	-	18.91
Indus	10	Winter	1.815	14.4	0.48	-	-	2	275	-	43	49.1	2189	2.1	605	-	18.51
Indus	11	Winter	1.991	14.2	0.41	-	-	2	98	-	31	47.2	2466	2.0	269	-	18.51
Indus	13	Winter	2.644	14.2	0.41	-	-	3	21	-	32	46.7	2712	2.0	414	-	18.44
Indus	14	Winter	2.750	11.7	0.52	-	-	5	14	-	36	48.1	2868	2.0	439	-	17.59
Indus	15	Winter	2.628	10.9	0.30	-	-	4	9	-	29	40.4	2978	1.8	455	-	17.52
Indus	16	Winter	2.418	11.4	0.44	-	-	3	16	-	31	41.8	3221	2.2	401	-	19.12
Indus	17	Winter	1.963	12.1	0.52	-	-	3	13	-	20	34.2	3114	2.6	351	-	19.80
Indus	18	Winter	1.939	12.5	0.59	-	-	5	19	-	18	30.7	3264	6.0	364	-	20.58
Indus	19	Winter	1.909	14.1	0.67	-	-	3	28	-	21	25.5	3318	3.1	376	-	20.53
Indus	20	Winter	2.540	14.3	1.07	-	-	5	59	-	21	20.6	3424	2.2	469	-	20.60
Indus	21	Winter	1.991	14.5	0.78	-	-	4	9	-	15	16.4	3173	2.0	427	-	19.86
Indus	22	Winter	2.084	2.6	1.19	-	-	5	11	-	29	16.3	3875	2.2	517	-	23.19
Indus	23	Winter	1.909	11.3	0.30	-	-	2	5	-	31	15.3	4836	1.9	676	-	27.85
Indus	24	Winter	1.831	2.6	0.37	-	-	3	7	-	32	10.9	4907	1.9	564	-	27.83
Tributary	27	Winter	5.898	20.6	0.82	-	-	6	15	-	25	47.7	2963	0.9	178	-	32.67
Tributary	28	Winter	2.991	14.3	0.56	-	-	2	284	-	9	76.2	2999	1.4	151	-	37.01
Tributary	33	Winter	3.744	10.2	0.82	-	-	4	62	-	84	65.8	3463	4.6	119	-	40.47
Tributary	34	Winter	1.310	17.0	0.19	-	-	8	5	-	41	21.8	1748	1.0	90	-	13.44
Tributary	43	Winter	6.175	17.9	0.41	-	-	10	44	-	28	53.5	4560	1.9	340	-	25.15
Tributary	42	Winter	0.194	8.7	0.19	-	-	32	216	-	10	7.0	2019	0.3	262	-	4.09
Tributary	44	Winter	3.386	13.1	0.26	-	-	10	38	-	20	33.6	4032	1.6	226	-	18.77
Tributary	45	Winter	0.746	11.3	0.19	-	-	2	18	-	80	13.5	8427	1.0	1145	-	13.74
Tributary	46	Winter	3.594	2.6	0.26	-	-	31	3	-	14	10.9	19278	0.8	521	-	16.53
Tributary	49	Winter	1.533	2.6	0.44	-	-	5	8	-	29	10.8	4356	2.7	589	-	18.41
Tributary	50	Winter	0.302	2.6	0.78	-	-	2	806	-	43	21.4	3164	3.1	682	-	6.82

Table B3. Trace element chemistry for the Indus River Basin.

River	No.	Season/month	Li	F	Al	Fe	Ti	Cr	Mn	Ni	As	Rb	Sr	Sb	Ba	Pb	U
			μ molesL^{-1}								nmolesL^{-1}						
Tributary	52	Winter	0.257	5.3	0.41	-	-	<2	9	-	27	10.4	2964	2.9	402	-	6.38
Tributary	54	Winter	0.945	2.6	0.67	-	-	2	36	-	33	43.2	1587	0.9	472	-	5.77
Tributary	57	Winter	1.039	11.2	0.41	-	-	10	9	-	68	38.1	3971	4.5	385	-	23.35
Tributary	58	Winter	0.641	12.4	0.44	-	-	<2	18	-	56	24.1	1629	1.8	459	-	6.38
Tributary	60	Winter	0.850	12.5	0.82	-	-	6	538	-	107	42.4	1931	3.0	721	-	7.08
Tributary	61	Winter	0.453	6.3	0.56	-	-	3	99	-	52	34.8	2844	2.8	784	-	7.83
Tributary	63	Winter	3.237	7.4	0.56	-	-	12	461	-	158	44.3	7555	15.3	963	-	115.72
Tributary	65	Winter	1.445	24.7	0.48	-	-	4	11	-	143	19.3	4794	1.8	620	-	17.84
Tributary	66	Winter	0.759	10.0	0.41	-	-	3	7	-	91	20.5	1642	1.1	664	-	9.19
Tributary	67	Winter	0.561	9.5	0.63	-	-	4	240	-	83	37.5	2652	3.1	614	-	9.16
Tributary	68	Winter	0.527	4.2	0.41	-	-	3	20	-	62	21.8	2990	2.9	690	-	11.73
Indus	22	Mar-94	2.084	2.6	1.19	0.35	45	5	11	2	29	16.3	3875	2.2	517	1.9	23.19
Indus	22	Apr-94	1.998	14.1	1.56	0.53	52	5	22	7	45	22.7	3598	2.9	5705	1.0	23.87
Indus	22	May-94	1.834	9.5	3.82	1.89	97	9	48	2	46	21.4	3185	3.1	500	1.8	20.08
Indus	22	Jun-94	1.144	10.1	3.67	2.02	77	6	56	5	26	17.8	2190	3.2	702	0.5	9.20
Indus	22	Jul-94	1.092	11.0	3.63	1.58	69	3	42	7	25	18.5	2482	3.4	663	2.9	8.92
Indus	22	Aug-94	0.908	9.5	1.07	0.41	38	12	20	5	32	15.2	2755	2.8	390	0.6	11.79
Indus	22	Sep-94	0.920	10.0	9.23	5.75	97	19	145	21	24	20.6	2582	2.5	376	2.1	12.73
Indus	22	Oct-94	1.266	11.6	0.63	0.14	33	12	8	5	26	14.1	2658	2.5	312	<0.5	16.22
Indus	22	Nov-94	1.513	13.1	0.56	0.12	38	4	11	12	27	14.8	3343	2.0	1849	0.7	20.05
Indus	22	Dec-94	1.709	4.7	0.65	0.26	19	4	18	8	19	12.4	3428	3.3	1141	2.2	17.56
Indus	22	Jan-95	0.215	4.1	0.63	0.24	10	<2	15	7	2	2.7	484	9.3	466	1.8	1.44
Indus	22	Feb-95	1.486	4.2	4.19	2.35	72	8	58	18	26	19.2	5090	2.0	466	1.5	21.75

Table B4. Isotope chemistry for the Indus River Basin. No. refers to sample locations on Fig. 3.1, d is deuterium excess.

River	No.	Season	$\delta^{13}C$	$\delta^{34}S$	$\delta^{18}O$ ‰	δD	d	$^{87}Sr/^{86}Sr$
Indus	1	Summer	-2.5	-5.2	-14.9	-103	17	-
Indus	2	Summer	-2.0	-5.7	-14.4	-101	14	-
Indus	4	Summer	-1.2	-0.4	-15.4	-101	22	-
Indus	5	Summer	-1.0	0.5	-14.7	-103	15	-
Indus	6	Summer	-2.3	-0.2	-15.1	-104	17	-
Indus	7	Summer	-2.1	-0.7	-14.3	-98	16	-
Indus	8	Summer	-2.4	-1.0	-14.2	-96	18	-
Indus	9	Summer	-1.6	-0.5	-14.0	-93	18	-
Indus	10	Summer	-3.9	0.1	-13.6	-89	20	-
Indus	11	Summer	-3.4	0.6	-13.2	-86	20	-
Indus	12	Summer	-4.1	0.7	-13.1	-86	18	-
Indus	13	Summer	-4.2	0.7	-12.8	-85	18	-
Indus	14	Summer	-4.4	2.7	-12.0	-79	17	-
Indus	15	Summer	-4.6	2.7	-12.4	-81	18	-
Indus	16	Summer	-4.7	-1.4	-12.6	-82	18	-
Indus	17	Summer	-5.1	0.9	-12.2	-80	18	-
Indus	18	Summer	-4.9	0.2	-12.4	-81	18	-
Indus	19	Summer	-4.9	0.4	-12.2	-80	18	-
Indus	20	Summer	-5.7	3.2	-9.4	-58	17	-
Indus	21	Summer	-5.6	2.2	-9.9	-60	19	-
Indus	22	Summer	-5.7	0.7	-11.0	-67	20	-
Indus	23	Summer	-5.5	0.2	-10.9	-68	20	-
Indus	24	Summer	-6.1	0.5	-10.6	-67	18	-
Indus	25	Summer	-6.2	0.8	-10.5	-66	18	-
Tributary	26	Summer	-3.4	-3.4	-13.4	-88	19	0.709409
Tributary	27	Summer	-1.6	1.7	-15.7	-111	15	0.710999
Tributary	28	Summer	-1.3	5.4	-14.6	-95	22	0.713704
Tributary	29	Summer	0.0	10.4	-12.7	-80	21	0.730615

Table B4. Isotope chemistry for the Indus River Basin.

River	No.	Season	δ¹³C	δ³⁴S	δ¹⁸O	δD	d	⁸⁷Sr/⁸⁶Sr
					‰			
Tributary	30	Summer	-3.0	9.6	-11.1	-71	18	0.822361
Tributary	31	Summer	-2.3	4.7	-11.2	-73	17	0.713957
Tributary	32	Summer	-1.9	4.4	-11.3	-72	18	0.713430
Tributary	33	Summer	-2.3	-1.8	-14.5	-93	23	0.712654
Tributary	34	Summer	-5.1	0.7	-12.9	-84	19	-
Tributary	35	Summer	-3.4	2.0	-10.7	-66	20	0.708295
Tributary	36	Summer	-0.9	6.8	-12.1	-77	20	0.716579
Tributary	37	Summer	-2.8	-	-11.2	-72	17	0.709750
Tributary	38	Summer	-1.7	-	-8.1	-41	24	0.708931
Tributary	39	Summer	-3.4	-	-8.5	-47	21	0.712270
Tributary	40	Summer	-4.5	6.6	-6.9	-35	20	0.715834
Tributary	41	Summer	-3.3	2.9	-7.0	-36	20	0.714337
Tributary	44	Summer	-5.4	1.8	-11.7	-73	20	0.712535
Tributary	45	Summer	-6.0	0.0	-6.9	-41	14	0.709933
Tributary	46	Summer	-6.2	-3.8	-3.4	-18	10	-
Tributary	47	Summer	-5.2	-5.3	-9.3	-59	15	0.709600
Tributary	48	Summer	-3.1	-5.5	-2.4	-12	7	0.708228
Tributary	49	Summer	-5.6	5.2	-8.4	-49	18	-
Tributary	49	Summer	-0.5	-	-10.6	-70	15	-
Tributary	50	Summer	0.2	5.5	-10.3	-67	16	0.712672
Tributary	51	Summer	-0.5	-	-9.8	-61	18	-
Tributary	52	Summer	-	-	-9.7	-67	11	-
Tributary	53	Summer	-0.8	-	-10.0	-60	20	-
Tributary	54	Summer	-2.8	6.2	-12.8	-86	16	0.721097
Tributary	55	Summer	-3.5	-	-12.3	-83	15	-
Tributary	56	Summer	-0.2	-	-11.6	-77	16	-
Tributary	57	Summer	-2.3	-	-12.6	-82	18	-

Table B4. Isotope chemistry for the Indus River Basin. No. for the springs refer to the closest river sample on Fig. 3.1.

River	No.	Season	δ¹³C	δ³⁴S	δ¹⁸O ‰	δD	d	⁸⁷Sr/⁸⁶Sr
Tributary	58	Summer	-3.1	4.0	-11.2	-77	13	0.729120
Tributary	59	Summer	-1.1	-	-11.3	-78	12	-
Tributary	60	Summer	-0.6	-	-11.2	-76	13	-
Tributary	61	Summer	-1.4	-	-11.4	-76	15	-
Tributary	62	Summer	-1.1	-	-11.3	-78	13	-
Tributary	63	Summer	-1.1	-	-11.0	-74	13	-
Tributary	64	Summer	-1.0	-	-10.8	-73	13	-
Tributary	65	Summer	-2.7	-	-11.0	-76	12	-
Tributary	66	Summer	-4.0	4.6	-11.5	-78	14	0.721757
Tributary	67	Summer	-1.2	-	-11.5	-78	14	-
Tributary	68	Summer	-1.0	-	-10.9	-79	8	-
Tributary	69	Summer	-0.8	-	-10.5	-74	10	-
Spring	G1	Summer	-8.1	-	-14.2	-100	14	-
Spring	G4	Summer	-5.0	-	-13.2	-89	17	-
Hot Spring	G36	Summer	0.6	13.5	-10.4	-71	13	-
Spring	G7	Summer	-9.6	-	-11.1	-72	17	-
Spring	G9	Summer	-8.2	-	-7.6	-45	16	-
Indus	2	Winter	-3.1	-2.7	-14.8	-103	16	0.709764
Indus	3	Winter	-2.6	-0.3	-14.9	-107	12	0.709951
Indus	4	Winter	-2.1	1.2	-14.8	-105	13	0.710437
Indus	6	Winter	-1.8	1.9	-14.4	-101	14	0.710874
Indus	7	Winter	-1.9	1.5	-13.8	-94	16	0.711593
Indus	8	Winter	-1.9	1.2	-13.3	-93	14	0.711353
Indus	9	Winter	-1.1	1.4	-12.6	-86	15	0.711726
Indus	10	Winter	-3.0	2.0	-12.0	-84	12	0.711990
Indus	11	Winter	-3.3	2.6	-12.0	-80	16	0.711949
Indus	13	Winter	-3.9	2.1	-11.9	-81	15	0.711807

197

Table B4. Isotope chemistry for the Indus River Basin.

River	No.	Season	$\delta^{13}C$	$\delta^{34}S$	$\delta^{18}O$	δD	d	$^{87}Sr/^{86}Sr$
			‰					
Indus	14	Winter	-4.1	2.7	-11.4	-78	14	0.711909
Indus	15	Winter	-4.2	2.1	-11.6	-75	18	0.711447
Indus	16	Winter	-4.1	1.7	-11.5	-76	16	0.711374
Indus	17	Winter	-3.9	1.9	-11.4	-75	16	0.711351
Indus	18	Winter	-4.0	1.9	-11.3	-74	16	0.711277
Indus	19	Winter	-3.5	2.0	-11.3	-80	11	0.711210
Indus	20	Winter	-3.6	2.2	-11.2	-75	15	0.711434
Indus	21	Winter	-3.6	2.2	-11.1	-74	14	0.711492
Indus	22	Winter	-3.6	3.0	-10.3	-67	15	0.711590
Indus	23	Winter	-6.3	3.8	-9.7	-65	13	0.711780
Indus	24	Winter	-5.6	3.8	-9.1	-62	11	0.711718
Tributary	27	Winter	-0.5	3.1	-15.3	-108	15	0.710487
Tributary	28	Winter	-0.8	4.9	-14.0	-96	16	0.713613
Tributary	33	Winter	-1.4	-1.3	-13.5	-93	15	0.712542
Tributary	34	Winter	-3.1	1.0	-13.0	-91	13	0.712211
Tributary	43	Winter	-4.7	4.3	-10.9	-73	14	0.713384
Tributary	42	Winter	-6.4	3.8	-7.6	-45	16	0.710560
Tributary	44	Winter	-5.7	4.0	-9.8	-63	15	0.712519
Tributary	45	Winter	-3.2	5.7	-2.6	-17	4	-
Tributary	46	Winter	-5.8	-1.3	-3.9	-19	13	0.709445
Tributary	49	Winter	-3.5	2.2	-8.9	-57	14	0.713036
Tributary	50	Winter	-7.1	5.7	-7.1	-39	18	0.712588
Tributary	52	Winter	-6.3	6.0	-6.8	-32	23	0.712201
Tributary	54	Winter	-4.0	6.2	-8.4	-46	20	0.724117
Tributary	57	Winter	-6.0	9.3	-6.2	-33	17	0.715551
Tributary	58	Winter	-4.8	4.9	-6.0	-40	8	0.730431

198

Table B4. Isotope chemistry for the Indus River Basin.

River	No.	Season/ month	$\delta^{13}C$	$\delta^{34}S$	$\delta^{18}O$ ‰	δD	d	$^{87}Sr/^{86}Sr$
Tributary	60	Winter	-5.6	5.8	-7.7	-45	17	-
Tributary	61	Winter	-6.2	5.5	-7.2	-39	19	-
Tributary	63	Winter	-8.4	7.2	-5.5	-40	4	0.718482
Tributary	65	Winter	-3.8	8.1	-7.9	-50	13	-
Tributary	66	Winter	-4.7	4.1	-5.1	-30	11	0.723574
Tributary	67	Winter	-6.9	5.9	-7.4	-31	28	-
Tributary	68	Winter	-5.1	4.0	-5.6	-33	12	0.716447
Indus	22	Mar-94	-3.6	3.0	-10.3	-67	15	0.711590
Indus	22	Apr-94	-3.6	3.1	-8.8	-53	17	-
Indus	22	May-94	-3.9	3.1	-8.2	-54	12	0.711378
Indus	22	Jun-94	-4.5	1.2	-11.1	-73	16	0.711516
Indus	22	Jul-94	-5.1	3.1	-11.1	-72	17	0.711435
Indus	22	Aug-94	-5.7	0.7	-11.0	-67	20	0.711767
Indus	22	Sep-94	-5.9	4.2	-11.5	-73	18	0.712130
Indus	22	Oct-94	-4.9	1.9	-11.9	-81	14	0.712150
Indus	22	Nov-94	-4.1	2.6	-11.1	-74	15	0.711507
Indus	22	Dec-94	-3.8	-	-11.8	-80	14	0.711405
Indus	22	Jan-95	-	-	-11.5	-76	16	0.711307
Indus	22	Feb-95	-5.0	-	-9.5	-61	16	0.712458

Appendix C

Spatial data

Table C1. Geographic location, mean altitude, drainage area and percentage of rock types exposed in each tributary basin. No. refers to sample location on Fig. 3.1.

No.	Mean latitude	Mean longitude	Elevation (m)	Area (km^2)	Granites	Metase-diments	Mafic-ultra-mafic rocks	Metabasalts	Alluvium	Sedimentary carbonates	Molasse sediments	Shales
26	34.463	75.857	4789	10826	44	45	5	0	2	4	0	0
27	34.835	77.585	5390	25016	39	34	0	13	0	13	0	0
28	35.832	75.814	5072	8824	19	80	0	0	1	0	0	0
29	35.771	75.047	4502	188	33	0	0	67	0	0	0	0
30	35.839	74.850	4865	36	94	0	0	6	0	0	0	0
31	35.908	74.831	4809	41	9	0	0	91	0	0	0	0
32	35.977	74.770	4937	95	98	2	0	0	0	0	0	0
33	36.526	74.733	4800	12954	41	59	0	0	0	0	0	0
34	36.242	73.424	4321	11199	58	42	0	0	0	0	0	0
35	35.737	74.350	4051	580	100	0	0	0	0	0	0	0
36	35.238	74.374	5114	460	48	12	3	27	10	0	0	0
37	35.611	72.996	3706	2745	48	2	50	0	0	0	0	0
38	35.292	73.043	3402	225	0	0	45	55	0	0	0	0
39	35.211	72.884	3270	486	0	3	42	55	0	0	0	0
40	34.987	72.686	2372	923	11	42	5	42	0	0	0	0
41	34.957	73.164	3787	666	0	14	4	82	0	0	0	0
44	35.408	72.043	3109	31006								
45	33.172	72.605	1021	10025	0	0	0	0	30	0	70	0
46	33.088	70.514	1400	16259	0	0	4	0	15	16	10	55
47	32.398	70.231	1121	5936	0	0	1	0	10	60	6	23
48	30.613	70.037	1336	6140	0	0	0	0	11	89	0	0
50	34.079	74.272	2862	33878	4	34	1	11	15	2	33	0
54	33.113	75.743	3353	31425	19	46	0	3	12	5	16	0
58	32.186	75.200	1537	20763	3	21	0	0	63	0	13	0
66	31.534	77.912	3375	88200	16	26	1	0	34	8	15	0

Table C2. Percentage of land use and population density classes in each tributary basin. No. refers to sample locations on Fig. 3.1.

No.	Land use			Population density			
	Desert	Cropland	Forest	Very Low	Low	Medium	High
26	100	0	0	72	28	0	0
27	100	0	0	90	10	0	0
28	100	0	0	83	17	0	0
29	100	0	0	48	52	0	0
30	100	0	0	67	33	0	0
31	100	0	0	100	0	0	0
32	100	0	0	100	0	0	0
33	100	0	0	48	52	0	0
34	100	0	0	18	82	0	0
35	99	0	1	0	100	0	0
36	92	0	8	1	99	0	0
37	100	0	0	0	99	1	0
38	100	0	0	0	16	84	0
39	100	0	0	0	78	22	0
40	100	0	0	0	81	20	0
41	100	0	0	0	0	100	0
44	80	19	1	18	7	75	0
45	0	90	10	0	3	89	8
46	63	34	3	0	26	70	5
47	77	14	9	0	76	24	0
48	71	29	0	0	92	8	0
50	75	17	8	2	20	78	0
54	70	20	10	12	24	48	16
58	26	71	3	2	25	18	54
66	63	31	6	48	19	24	9